THE PROCEEDINGS OF
THE PHYSICAL SOCIETY

Section A

VOL. 63, PART 5 1 May 1950 No. 365 A

Experimental Studies in Thermal Convection

BY A. O. RANKINE*

33rd Guthrie Lecture, delivered 21st March 1949

Mr. President, Ladies and Gentlemen,

I feel that I ought to begin this lecture with a confession. When it was proposed last year that we should celebrate the seventy-fifth anniversary of our Society I discouraged the idea. This was partly because the number 75 did not seem to me round enough to make a fuss about, but even more because I knew from experience how much work the arrangement of the event might involve. My recollections of the Society's Jubilee in 1924 were still vivid. At that time I had recently been appointed Business Secretary, and thus had to shoulder much of the responsibility of organizing the proceedings, which lasted several days and included a series of elaborate functions, the most notable of which was the Jubilee Dinner at which our present King was the principal guest of honour. So now, out of sympathy for the present Officers, whose routine duties are so much more onerous than in my day, I wanted to save them from the additional labour of another celebration, which I judged to be premature.

I thought that my views would be shared by most of the members of the Society, but it appears quite definitely that I was wrong, and, anyhow, I have been overruled. For modesty forbids me from flattering myself that this large gathering is assembled here today merely to hear me discourse, and I know that several hundred Fellows and their friends intend to participate in the Soireé later on this evening. I suppose the truth is that the younger members of our Society particularly, for whom this celebration is the first, welcome the opportunities it affords for social intercourse which has been missed so much during the dark days of the war and its aftermath. And even those of us who are older must agree with them in believing that today's functions, limited in scope though they be for reasons of economy, will help us to get to know one another better, and foster our united efforts to make our Society flourish still more in the years that lie ahead.

Now, as a sort of penance for my former reluctance, it falls to my lot to open the proceedings by giving the thirty-third Guthrie Lecture on this day exactly seventy-five years after our Society was founded through Guthrie's influence on 21st March 1874. We have therefore a double reason for remembering him afresh and paying tribute to the energy and foresight he exercised in our interests during the formative years. We do so now sincerely in the presence of several members of his family and other relatives, whom we welcome as on many former occasions, but with a note of deep regret that his daughter, Miss Hilda Guthrie, who has attended these lectures with great regularity and was present last year, has since died. We are especially pleased to be honoured again by the presence of another daughter, Miss Elfrida Guthrie, who has made a long journey to join us, in spite of her advancing age.

---

* This article also appeared in the April issue of *Proc. Phys. Soc.* B, p. 225.

This would seem also to be an appropriate occasion for reviewing our Society's development from its foundation until now, with special emphasis on the last twenty-five years—indeed to make this the subject of my lecture. But this would be what the theologians would call a work of supererogation. For such a review has been done comparatively recently, and by one whose ability to tell the story effectively and elegantly is far superior to my own. I refer to our former President, Professor Andrade, whose presidential address in 1945 on "The History and Future of the Physical Society" I have found so refreshing to read again that I recommend all of you to do likewise.

The subject which I have chosen instead is one which, on account of its largely experimental character, would, I think, have had Guthrie's approval. Yet I have some doubts as to whether it will be worthy of its place in the Guthrie Lecture series. I have attended most of these lectures since they were instituted, and I recognize both the eminence of my predecessors and the scientific importance of the matters they dealt with. I have indeed a suspicion that I have been chosen as the lecturer this year more in recognition of my long official connection with the Society than for my contributions to physics. If that be so, I appreciate all the more the honour conferred on me, and the opportunity it may provide for putting on record in the *Proceedings* of our Society some of the results of the most arduous piece of work I ever did in my life, and in which I myself feel a certain pride in having performed. It was done during the war in collaboration with several colleagues, of whom I desire to mention particularly Mr. C. R. Young and Mr. C. Bird, in connection with the operation of dissipating fog over airfields. The results comprise comprehensive data relating to certain aspects of thermal convection in the air, and are at present accessible only in the documents of the now defunct Petroleum Warfare Department. Some at least of them I think may be found to be of more general interest and applicability, and it will be for the Editing Committee to say how much of the contents of my final report might properly be published by the Society.

It is not my intention to deal now with the question of fog clearance, except incidentally. My main purpose is to direct attention to some experimental facts that emerged concerning the behaviour of air heated artificially, and to the means whereby the facts were discovered. But to provide a suitable background for describing the work, and to explain how these experiments came to be undertaken, I must first recall the way in which the problem of dissipating fog by artificial means presented itself for solution as a war-time operation.

Towards the end of 1942 Mr. Churchill charged the Petroleum Warfare Department with the duty of providing means of dissipating fog over airfields. The method chosen was to heat the air by burning petrol close to the ground. Such a scheme had already been contemplated before the war, and experiments had been carried out by the Royal Aircraft Establishment under the direction of the Meteorological Committee of the Air Ministry. The results then obtained provided useful guidance, and there were available also the important calculations made by Professor Brunt indicating the minimum fuel requirements, having regard to the fact that fog drifting across an airfield needs to be dissipated continually as it encroaches thereon.

The first step taken was to construct in the large unfinished reservoir at Staines a petrol-burning installation approximately on the required airfield scale. A similar installation with coke as the fuel was also laid out. Both these were used when atmospheric conditions were suitable to obtain data regarding the distribution of convective heat in the air, employing ordinary meteorological thermometers and anemometers for the purpose. But useful information was slow in accumulating, and it was decided to institute model experiments in which conditions would be under control. I was put in charge of this work and submitted my final report early in 1945.

What follows is mainly extracted from this report. As before indicated I have selected what appears to me likely to be of some general interest, not particularly in relation to the original problem. It being possible, however, that a few readers of this lecture may desire access to the whole report, I have deposited several copies of it in the Society's library where they will be available for perusal.

EXPERIMENTS IN THE EMPRESS HALL, EARL'S COURT, LONDON, ON THE DISTRIBUTION OF HEAT FROM LINE BURNERS, IN RELATION TO THE PROBLEM OF FOG CLEARANCE ON AIRFIELDS

Introduction

The process of clearing fog consists in establishing in the required regions conditions which lead to the re-evaporation of the water droplets constituting the fog. If the method employed is the thermal one the practical requirement is the delivery of heat in sufficient quantity to all those parts of the atmosphere from which the fog is to be removed by evaporation. In respect of airfields *rapid* fog clearance is also requisite, and this has in practice to be brought about by providing in general much more heat than is necessary merely to vaporize the water, so that, by sufficient drying of the atmosphere as well, the fog droplets vaporize quickly enough. Given the constitution of a particular fog—its temperature, its water content and the speed with which it is moving—the heat requirements for its rapid dissipation are easy to calculate.

A question obviously of fundamental importance is the manner in which the heat provided becomes distributed in the atmosphere. It has been held necessary to adhere strictly to certain conditions laid down by the air authorities, namely, that the sources of heat used—in practice lines of burning fuel—must be very close to the ground, and not nearer than 50 yards from the edge of the runway over which it is desired to clear fog. A further desideratum is that clearance should extend to a height of at least 100 feet above the centre of the runway. The problem thus became one of investigating the behaviour of the thermal convective jets originating in lines of burning fuel, under the influence of winds of various strengths and directions, including, of course, the special case of no natural wind at all.

In theory this problem could be solved by carrying out a large number of experiments in the open air on the actual scale of the proposed airfield installation. In practice, however, this would be a very lengthy and difficult process, as no control could be had over the atmospheric conditions, and observations would be restricted on the occasions when those conditions happened to be favourable. It appeared, therefore, that experiments might with advantage be carried out on a much diminished linear scale, under artificial conditions fully under control and capable of reproduction whenever required. There were, in fact, good reasons for believing that, with proper adjustments of the rate of heat emission from the burning line, and of the speed of the imposed wind, a pattern of heat flow, resembling the full-scale pattern, could be produced and investigated with a model installation, the linear dimensions of which were, say, one-thirtieth or one-sixtieth of that used in the field. The sequel will show that this belief has been fully justified.

A further word of explanation is necessary before proceeding to describe the model experiments. Strictly speaking, the measurements of heat flow, whether in the model or in the field, ought to be made under atmospheric conditions involving actually precipitated fog. But the results obtained are nearly enough correct in a clear atmosphere, and, if necessary, an appropriate allowance can be made. Consequently, in the model experiments the observations throughout have been made without the inconvenience of having to create and maintain artificial fogs.

Wind Tunnel for Model Experiments

The model work has been carried out in the Empress Hall during the period from April 1943 to December 1944. For the purpose of most of the experiments a wind tunnel was constructed within the hall, which is a very spacious enclosure about 200 ft. long, 150 ft. broad and 70 ft. high. The tunnel itself was constructed with the advice and collaboration of the National Physical Laboratory, especially of Mr. L. F. G. Simmons, of that laboratory. It was built on the concrete floor of what had been a skating rink, and the main part was 100 ft. long, 30 ft. wide and 12 ft. high, the sides and roof being composed of wooden boards. At one end the rectangular cross section was flared down in a distance of 30 ft. to a square cross section of 12 ft. side, and thereafter to a circular channel 10 ft. in diameter which housed a 27 H.P. electric fan lent by the London Passenger Transport Board. At 30 feet inside the tunnel from the open end a wire mesh partition (30 meshes to the inch) was inserted for the purpose of rendering regular the air flow created by the suction of the fan. Doors in the sides gave access to the tunnel between the wire screen and the fan. Photographs of the exterior and interior of the tunnel are shown in Figures 1 and 2 (see Plates).

Investigation of Wind Structure in Tunnel

The range of air speeds required was from zero to a few feet per second, so as to correspond, with due allowance for scaling, with the winds likely to be operative in fogs on airfields. Running at its normal speed the fan made the air in the tunnel move much too fast. It was necessary, therefore, to reduce this by appropriate resistance adjustments on the fan motor. Further reduction was secured, as necessary, by shutting a pair of perforated doors housed in the square part of the tunnel just in front of the fan. In this way a range of air-speeds from 0·5 to 5 feet per second could be produced and reproduced as required. On a 1/60 linear scale, on which a large part of the work was done, this range corresponds to full scale values from 2·65 to 26·5 miles per hour.

Preliminary tests with a meteorological cup anemometer showed that the general air movement was fairly uniform in the tunnel except near the floor, roof and walls. Such anemometers were, however, not accurate enough for

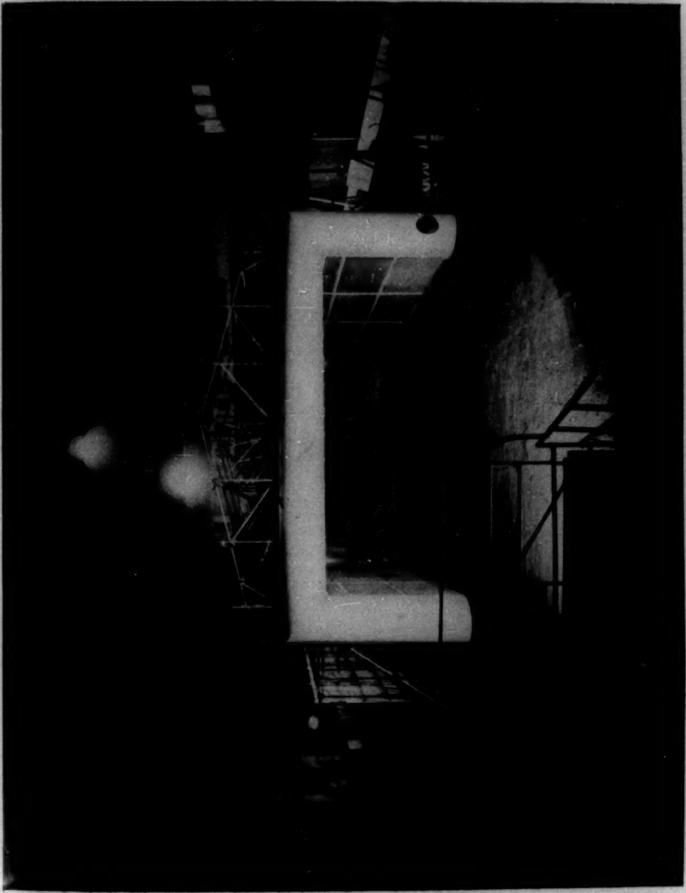

Figure 1. Exterior view of wind tunnel.

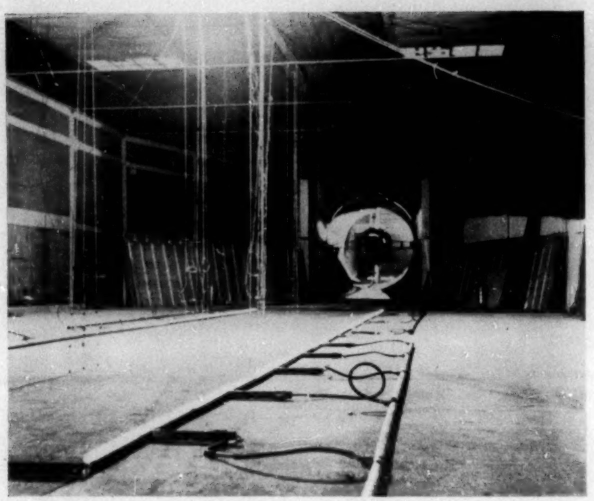

Figure 2. Interior view of wind tunnel showing fan and one arrangement of apparatus.

the purpose of measuring low wind speeds. Moreover, on the scale of the work they were too large, thereby interfering unduly with the air flow they would purport to measure. Recourse was had again to Mr. Simmons, who produced and made available about a dozen small electrical anemometers of a form which would not disturb appreciably the air currents under investigation. These anemometers will be described fully elsewhere. Here it must suffice to indicate that they depend on the principle that a thin wire electrically heated is cooled by air flowing past it to an extent which increases with the air speed, and that the cooling is measured electrically by thermocouple elements held close to the hot wires. These anemometers, besides being small and of suitable sensitivity, had the additional advantage of providing remote observation, so that the measuring operations could be performed outside the tunnel by means of instruments connected by thin wires to the anemometers disposed at suitable points inside.

Before being employed to investigate the wind structure in the tunnel under the various conditions of the experiments the anemometers had to be calibrated, so that the corresponding air speed could be derived from the measured electric potential of the thermocouple. In their original form the anemometers were calibrated at the National Physical Laboratory, but evidence soon accumulated that they changed sometimes in behaviour, so as to necessitate recalibration rather frequently. In order to do this without having to disconnect the anemometers and remove them from the tunnel—a somewhat laborious procedure also liable in itself to produce changes in them—a method was devised to re-calibrate them *in situ*. It consisted of establishing the air speeds along the centre of the tunnel, for various settings of the electric controls of the fan motor, by observing the times of passage between two fixed planes of almost weightless flakes of suitable material carried along by the air stream. The material used was the solid fuel known by the trade name of 'Meta', which is provided in small sticks. On touching a stick with a hot rod such as a soldering iron the material volatilizes and condenses again almost immediately in a form like snow flakes, but relatively much lighter. These fall very slowly, and in a horizontal air stream moving even as slowly as 0·5 foot per second, travel nearly horizontally. By releasing them in the tunnel and determining the average times of passage of many individual flakes between fixed planes 10, 20 or 30 feet apart, it proved possible to obtain reliable values of the air speed in the parts of the tunnel unaffected by the proximity of the floor, roof and sides. This was done for a range of air speeds from about 0·5 to 5 feet per second, and provided a convenient means of checking periodically the performance of the anemometers. Eventually Mr. Simmons modified the instruments into a form which was much more stable and reliable, but it was not until the later stages of the experiments that confidence could be placed on the results. The patterns of the wind structure were, in fact, re-determined in most cases by means of the anemometers in their final reliable form, the accuracy of measurement attained being a few per cent.

Measurement of Air Temperatures

Besides air speeds it was necessary to know the degree of heating of the air in order to define the complete pattern of the heat flow originating in the line burners. For this purpose electrical thermocouples were used so as to have again the advantage of remote observation outside the tunnel. Moreover, this kind of thermometer, consisting as it does of thin wires, could be disposed in the air stream without modifying appreciably its structure. The installation of these thermocouples was facilitated greatly in the early stages of the experiments by the cooperation of the General Electric Company, and in particular of Mr. Lait, who spent many days on the work. The thermocouples consisted of soldered junctions of 30 S.W.G. copper wire and 32 S.W.G. Eureka wire, and they were calibrated so that the temperatures of air passing them could be deduced from the electrical potentials measured on a Tinsley potentiometer. As in the case of the anemometers, suitable switchboards enabled measurements to be made in turn on the various thermocouples mounted on slender frames at the points of investigation in the tunnel. At first measurements of the actual temperatures (above 0° C.) were made in the heated air and at a point outside the influence of the burning lines, the temperature rise being deduced by subtraction. Later the more convenient method was adopted of disposing the two elements of the thermocouple, one in the heated air and the other where there was no heat flow, so that the temperature rise could be obtained from a single measurement of potential. The accuracy of temperature measurement attainable was about 0·1° C. or 0·2° F. Investigation showed that radiation from the burner lines did not affect the thermocouples appreciably, and that they in fact assumed quickly enough the actual temperature of the air surrounding them.

The Burning Lines, and Method of controlling Heat Emission

The fuel used for the burning lines was butane, provided in iron bottles supplied from Petroleum Warfare Research Station, Langhurst. This fuel is especially convenient for small scale work because, the normal boiling point being about 0° C., it usually develops in the bottles a vapour pressure somewhat above atmospheric, so that it is delivered as gas to the burners. Except occasionally on very cold days (when artificial warming of the bottles had to be resorted to) sufficient gas could be delivered to the burners at convenient pressures to provide the quantities of heat required, which, for the purpose in hand, had to range from zero up to a total value of about 5 therms per hour. The design and construction of suitable burners presented something of a problem. It was desired to burn the gas so that combustion was as complete as possible, for it was known that convective or sensible heat, as distinct from thermal radiation, was in fact the means whereby fog could be surely dissipated. Consequently, so-called non-luminous burning, such as occurs normally in a bunsen burner using coal gas, was aimed at. But ordinary bunsen burner nozzles and air inlets were not suitable, on account of the much greater (six times) calorific value of butane as compared with coal gas. New burners had to be made to meet the case, and, in the first instance, two pipes each 30 ft. long were provided from P.W.R.S., Langhurst, which through numerous orifices in the top about ½ in. apart gave lines of non-luminous flames reasonably uniform in size over the whole length, although the butane entered the pipe through a suitable nozzle, and past a variable air inlet at one end only. These burners were used extensively in the earlier part of the investigation, but their dimensions were too great for all purposes. When laid on the floor, for example, the flames originated about 4 in. high, which, on the basis of model work on 1/60 field scale, would correspond to 20 ft. high in the field, whereas in airfield installations they start a foot or even less from the ground. To avoid this dimensional discrepancy, which would have vitiated the application of scaling in the manner hereinafter described, the tunnel floor was in effect raised to the level of the flame orifices by boards mounted on blocks.

Later on a large number of smaller burners were made at the P.W.D. Experimental Station at Staines, some 10 ft. long and some 4 ft. long and all of 1 in. diameter, served by suitable nozzles obtained from the Physics Department of the Imperial College of Science and Technology. These burners proved to have a more uniform and quite satisfactory flame distribution, and, being relatively short, gave greater flexibility in constructing the various patterns of installation which had to be investigated. Moreover, on account of their small diameter, adjustment of floor level was not considered to be necessary. Another useful feature, as will appear presently, was that they could be altered, by means of the adjustable air inlet, so that the butane burnt luminously.

The various nozzles belonging to the burners were calibrated in relation to pressure above atmospheric and passage of butane. The pressure was measured by U-tube gauges, usually containing mercury, but occasionally water, and the rate of flow of butane was observed by a gas meter. With the nozzles thus calibrated serving any particular layout of burners, and the butane pressure being held constant by a control valve, any desired rate of delivery of butane per yard of burning line could be maintained. With the butane ignited, the calorific value being known, the corresponding gross heat emission rate per unit length could be deduced. The range in fact covered in the experiments was from 0·03 to 0·48 therms/yard.hour.

With the multiple burners sometimes used it was, of course, necessary to provide a system of service pipes connected with the bottles of butane and provided with sufficient taps to deliver gas to the individual burners. This was constructed as required out of 1 in. piping, and the connections to the burner nozzles were made with flexible rubber tubing. There was, however, no appreciable loss of pressure in the service system, the burner nozzles being so relatively small as to ensure that practically the whole pressure drop occurred across their orifices. Thus, with equal nozzles in burners of equal length, uniform heat output could be secured at a single pressure in all parts of the system.

Observational Procedure in Wind and Temperature Measurements

The procedure at first visualized was to lay out the particular type of burner system to be investigated, to instal the electrical anemometers and thermometers at suitable points, and then to make a few observations simultaneously of the air speeds and temperatures at these points both without and with the burners in operation. In practice this procedure had to be much modified in several respects. It was soon found that, owing to the turbulence of the air movement, the velocity and the temperature at a fixed point varied, sometimes very greatly, from moment to moment, and that, in order to be able to assign to the point reliable average values, a much larger number of readings would be necessary. Instead of a few readings usually fifty were taken, and the time occupied in thus dealing with every anemometer and thermocouple became much longer than had been anticipated. In all, several hundred thousand observations were made, each involving the manipulation of the appropriate potentiometer; and on some days more than two thousand data were added to the records. All these had to be corrected as necessary, classified and analysed before the final results emerged.

For reasons already mentioned, namely, the relative unreliability of the anemometers in their original form, it was not possible to carry out consistently the idea of simultaneous measurement of temperatures and air speeds. In some of the experiments for this reason no velocity measurements were made. In others, where a knowledge of velocities was more essential, they were re-determined during the latter stages of the investigation, when the improved anemometers became available. For example, what would naturally have been done first—the examination of variation of flow of the unheated air in the tunnel near the floor and sides—had to be thus postponed. Some of these vertical profiles of horizontal velocity are shown in Figure 3.

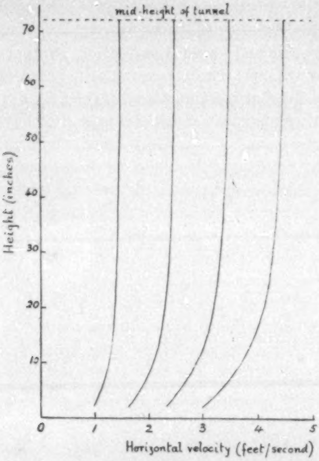

Figure 3. Vertical profiles of horizontal velocities of the air (unheated) in tunnel

Detailed Investigation of Convective Heat Flow produced by Winds across Burner Lines

The principal feature of the work in the tunnel was the systematic investigation of the pattern of heat flow downwind of a burning line across which imposed winds of various strengths were operating. This particular case, in its full scale realization, is probably the most important in relation to fog clearance over runways, for it may be expected to provide answers to the questions—how much heat should be provided in a burning line, and where should the line be placed relative to the axis of the runway in order that fog clearance may be achieved to adequate heights over the middle of the runway, even when the wind originally blowing across both line and runway attains so high a value as, perhaps, 25 miles per hour?

Previous field experience has shown that in such circumstances the convective heat from a burning line is very easily deflected from the nearly vertical flow which occurs in air originally stagnant. Quite a low wind—a few miles per hour—

causes the heated jet to engage the ground on the downwind side of the line, while the upper edge makes an angle with the ground which diminishes rapidly as the imposed wind increases. Above this edge no appreciable amount of heat is imparted to the air, so that no fog dissipation can be expected there. Near the ground the required heat supply is more than adequate for the purpose; it is higher up that deficiency is liable to occur, and the aim is to ensure that at the minimum specified height for fog clearance the heat supply is at least enough. In other words the heat flow pattern under the influence of naturally occurring winds is not ideal. Such winds help in transporting the heat in the right direction from the burning line, but they give rise to a distribution of the heat which compels considerable waste at low levels in order to have at least enough at, say, 100 feet high over the middle of the runway.

This was the problem now tackled with the model. A burner line was laid across the full width of the tunnel, usually about midway between the wire screen and the plane where the cross section began to flare down to the fan. Anemometers and thermo-elements were installed at suitable heights above the floor in the axial vertical plane of the tunnel at distances of 3 ft. 9 in., 7 ft. 6 in. and 15 ft. downwind of the burner line, and, as required, in the unheated upwind air as well. Systematic measurements of the temperatures and velocities of the moving air were carried out for a range of heat emissions from 0·03 to 0·48 therms/yard.hour, and of imposed winds from 1 to 5 feet per second at the mid-height (6 ft.) of the tunnel. Auxiliary measurements defined the vertical profiles of the various imposed winds when the air was unheated, as indicated in Figure 3, so that the changes caused by the burning operations could be determined. Also, traverses with anemometers and thermo-elements across the tunnel showed no appreciable variations except near the walls. Thus the results given for the axial vertical plane apply also to any parallel plane not too near the ends of the burning line.

These results have been analysed, interpolated and smoothed to remove evident errors in the customary manner, and are given in tabular form in the Appendix, with intervals small enough for it to be permissible to interpolate by proportional parts. A graphical method of representation which, *prima facie*, might have been deemed preferable, has been found too elaborate, on account of the multiplicity of the variations, since it would involve drawing some 380 graphs.

Discussion of Results for Winds across Burner Lines

It is, however, instructive to represent a few of the cases graphically, and the chief points are thus illustrated in Figures 4, 5, 6, 7 and 8. Figure 4 (*a*) shows the vertical profile of temperature rise of the air 7 ft. 6 in. downwind of the burning line when the gross heat emission is 0·24 therms/yard.hour, under the influence of an imposed wind of the magnitude 2 feet per second at the mid-height (72 in.) of the tunnel. This value implies a vertical profile of velocity of the type shown in Figure 3 for unheated air, and the particular profile in the present case appears in the dotted line in Figure 4 (*b*), which exhibits also, by the full line, the profile modified by the heating of the air. Figure 5 represents a similar case, except that the imposed wind here is higher, namely 3·5 feet per second, with corresponding different profiles both heated and unheated. It will be noticed by comparison of Figures 4 (*a*) and 5 (*a*) that increase of wind speed reduces the temperature rise at the higher levels and increases it at the lower levels. Also, inspection of Figures 4 (*b*) and 5 (*b*) shows, under burning conditions, that the original air-speed is enhanced considerably except at the higher levels, where there is little change. Figure 4 (*b*) in fact demonstrates that, for low speeds of the imposed wind, the enhancement due to heating may cause the speed at low levels to exceed that at points higher up. This phenomenon of wind enhancement has been found to be generally true, and to be emphasized both by a reduction of imposed wind speed and an increase in the degree of heating.

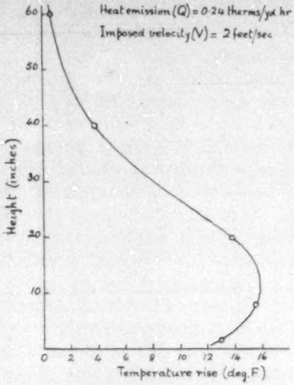

(*a*)

Figure 4 (*a*). Temperature pattern 7′ 6″ downwind of burner.

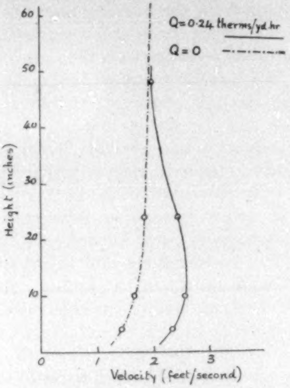

(*b*)

Figure 4 (*b*). Velocity pattern 7′ 6″ downwind of burner.

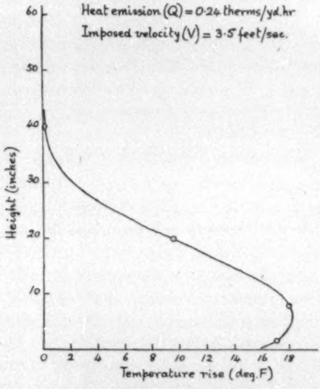

(*a*)

Figure 5 (*a*). Temperature pattern 7′ 6″ downwind of burner.

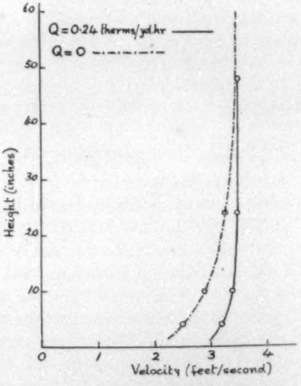

(*b*)

Figure 5 (*b*). Velocity pattern 7′ 6″ downwind of burner.

The effect on the temperature rise of increasing the heat emission from the burning line is shown in Figure 6. Under the same imposed wind the temperature rise becomes greater at all heights, although not in a proportional manner, the ratio increasing rapidly with height. The heat emission in fact exercises control over the shape of the temperature profile as well as its dimensions. Another set of curves (Figure 7) illustrates the way in which the temperature

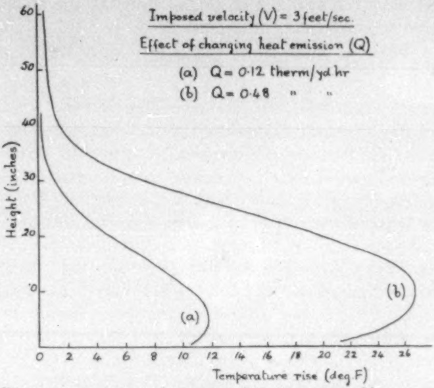

Figure 6. Temperature pattern 7′6″ downwind of burner.

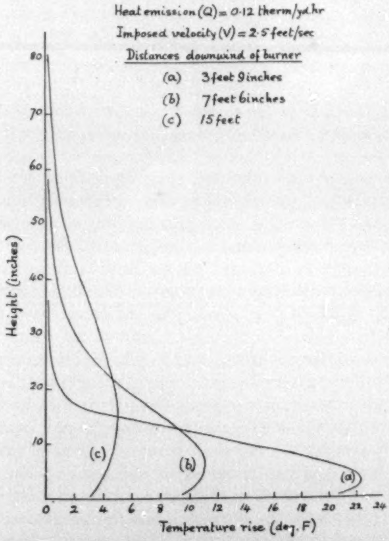

Figure 7. Temperature pattern downwind of burner.

profiles vary with distance downwind of the burning line, heat emission and imposed wind being constant. The most striking feature is the way in which the 'nose' of the curve (to which reference is made later) becomes blunted and elevated as the distance from the burning line increases.

Integration of Convective Heat Flow. Losses by Radiation and Ground Absorption

An important check can be made on the accuracy of the results by calculating the total quantity of convective heat passing downwind. This can be done when, as in most cases, the temperature rise is zero, or nearly so, at the maximum height of observation. The density and specific heat of air are known; the remaining factor involved in the determination is the product at all heights of the temperature rise and the wind speed, which is effectively horizontal. Figure 8 shows these products, plotted against height, for the data contained in Figures 4 and 5, and each of the two curves, for the same heat emission but different wind speeds, provide the means of graphical integration of the total convective heat flux, which is proportional to the area enclosed by the curve. The areas enclosed by the two curves are found to be nearly equal, implying that the convective heat flux is the same in the two cases. It is, however, considerably less than the gross thermal energy developed by combustion in the burning line. This is true, not merely for the two cases here considered, but quite generally. On the average only about 80 per cent of combustion heat has been found to cross any of the downwind planes of observation, in the form of convective heat, which alone could be effective in clearing fog.

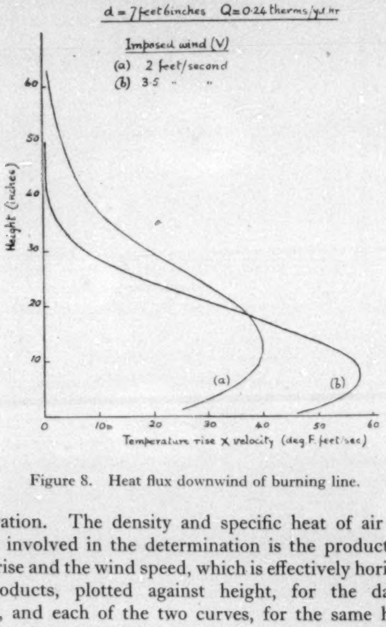

Figure 8. Heat flux downwind of burning line.

This loss of about 20 per cent is accounted for in two ways. Some is lost to the floor, as is evident from the shapes of the temperature profiles. Always the temperature of the air close to the floor is lower than that somewhat higher up, giving rise to the 'nose' of the profile. Moreover, the floor itself is always colder still, and this temperature gradient implies that the air does lose heat to the floor. The amount is not great; a fair estimate is about 5 per cent of the total thermal emission from the burning line, and most of this loss occurs closer to the burner line than 3 ft. 9 in., since there is no consistent evidence of variation of convective heat flux between this and greater distances downwind. It is probable that the ground of an airfield behaves in much the same way as the concrete floor of the tunnel with regard to transfer of heat from the air, so that the heat loss to the ground may also be taken as 5 per cent. It is fortunate that it is so small, and that most of the sensible heat remains in the air, where it is wanted for fog dissipation.

The remaining 15 per cent or so of the gross thermal energy of combustion, which does not appear as convective heat, is without doubt in the form of thermal radiation, including, of course, the small fraction of this which is luminous (even for so-called non-luminous flames). This is not appreciably absorbed by the air in the short distances (up to 15 ft.) over which measurements were made, and therefore does not become converted into sensible heat which would be registered by the thermometers. As regards full scale installations it may be reasonably assumed that the hydrocarbons constituting the petrol there used do not differ appreciably from the particular hydrocarbon butane in respect of radiation from flames. So that here also, unless the radiation is converted by absorption into heat capable of evaporating fog, it must be written off as a loss. The degree of this absorption is not known, but it may be said that conditions are somewhat more favourable in the full scale installation than in the model, owing mainly to the greater distances involved, and also to the fact that the constituents of a fog-laden atmosphere have a greater absorbing power than the clear unsaturated atmosphere in the tunnel, in respect of the specific radiation emitted by hydrocarbons burning non-luminously.

Radiation from Luminous and Non-luminous Flames—Experimental Comparison

This question of radiation was under constant discussion during the course of the model work at Empress Hall, and is the basis of the additional experiments now to be described. In the airfield installations the petrol has not been burnt non-luminously, but with less than the requisite supply of air for complete combustion, so that the flames have been highly luminous, and often near to being smoky. In this respect the burning lines have been different from the non-luminous (blue) flames of the butane ordinarily used in the model work. As mentioned earlier, however, it was possible, by restricting the air supply, to make the butane burn with luminous yellow flames more nearly similar to the petrol flames in the field. With this arrangement many measurements were made of the convective heat flux, for comparison with the corresponding flux for non-luminous burning. The results were of considerable significance. Generally, with equal rates of supply of butane to the burning line, the convective heat derived from luminous burning was found to be only about 80 per cent of that derived from non-luminous burning, i.e. 64 per cent of the gross amount calculated from the calorific value of the fuel. It appeared, therefore, that the loss by radiation was increased by a further 16 per cent if luminous burning was employed, making a total of about twice that for non-luminous burning.

This result was confirmed subsequently by direct comparisons made between the amount of radiation emitted by luminous and non-luminous flames consuming equal quantities of butane, the same fraction of the total radiation from a line burner being received on a thermopile suitably disposed. With a butane consumption rate per yard equal to that in the former measurements of heat flux, the ratio of the total radiation from the flames when luminous to that for non-luminous combustion was found in a long series of observations to be 1·8, compared with the ratio 2 estimated indirectly as indicated in the previous paragraph. It was observed also that this radiation ratio depended upon the size of the flames, increasing as the flames were made larger by raising the fuel consumption rate. At the highest rate employed, when the flames were still only about 3 inches long, the radiation ratio was 2·4. This would imply, allowing also for the 5 per cent loss of heat to the ground, that the available convective heat is rather less than 60 per cent of the gross thermal emission. Compare this with the 80 per cent that can be obtained with non-luminous burning.

As regards the implications in full-scale petrol burning installations much the same conditions are likely to apply, or they may be even worse. The flames are much larger, perhaps two feet long, with a tendency to be smoky, consequently the degree of radiation from them will be even larger than in the model. Moreover, the additional radiation associated with their luminosity, occurring as it does in the near infra-red spectral region, is absorbed very little by any of the constituents of foggy air. Its transformation in the regions required to the only form of heat capable of dissipating fog, namely, convective or sensible heat, cannot, therefore, be relied upon to a useful extent. In fact, it is most unlikely that, with the petrol burners usually employed, the useful heat for purposes of fog clearance exceeds 60 per cent of the total calorific value of the petrol; it is probably considerably less when the burners are on the point of smoking.

The implication is clear. The petrol should be burnt non-luminously, in which case somewhat more than 80 per cent of the gross heat supply will be available for fog dissipation. An economic saving of 25 per cent of the petrol consumption could be achieved in this way.

Comparison of Model with full-scale Installation. Application of Principles of Dimensional Scaling

The measurements embodied in the tables of the Appendix provided the means of carrying out the crucial test as to whether, by the proper application of the principles of scaling (or dynamical similarity), the model results could be used to predict the behaviour of full-size installations, and thereby to specify the field requirements for the successful dissipation of fog. For this test some full-scale observations were necessary, and certain data of this character were available from field work at Staines.

Without going into the reasons thereof, the principles of scaling believed to be applicable may be simply stated as follows. Denote by L_m any particular length in the model (such as the distance of an observation point from the burning line) and by L_f the corresponding full-scale length. Similarly, V_m denotes the air speed at any point in the model, and V_f that at the corresponding point in the full-size installation. If also θ_m and θ_f are in like manner the corresponding temperature rises of the air, then

$$\frac{V_m^2}{L_m\theta_m} = \frac{V_f^2}{L_f\theta_f}$$

for all points. It is to be noted that this relation approximates to the truth only when θ_m and θ_f are small compared with the absolute temperature of the air, and this limitation must therefore be observed in applying it. The special application of the equation to the present argument deals with the case when

$$\frac{V_m^2}{L_m}=\frac{V_f^2}{L_f} \quad \text{or} \quad \frac{V_f^2}{V_m^2}=\frac{L_f}{L_m},$$

in which case $\theta_m=\theta_f$ or the temperature rises at corresponding points in the full-size installation and its linearly scaled model are the same. To realize this, having chosen the linear scale ratio L_m/L_f to be r, say, it is necessary to arrange that $V_m^2/V_f^2=r$, or $V_m/V_f=\sqrt{r}$. We have control over the air velocities in the model in two respects, namely, the speed of the artificially produced wind across the burner, and the convective velocity of the thermal jet originating in the burner itself. As regards the latter, theoretical considerations * have shown that the velocities produced in the air by convective action are proportional to the cube root of the heat per unit length, H, of a long line source, which issues in convective form. Thus, to make the convective emission tally as between the full-scale installation and the model, the condition

$$H_m/H_f=V_m^3/V_f^3=r\sqrt{r}$$

must be fulfilled in making comparisons.

The question then is this. If we take a series of measurements on full scale at Staines when a natural wind was blowing across a burning line, and select by the above rules corresponding observation points, imposed wind speeds and convective heat flux in the tables of the Appendix, do we in fact find in the model temperature rises equal to those of similarly placed points at Staines? This has been answered affirmatively by several comparisons carried out in the manner indicated, using data from Staines which appeared to be self-consistent and reliable. Figure 9, for example, relates to a petrol burning at Staines in which observations of temperature rise were made at several heights 75 yards downwind opposite the middle of a burning line 600 yards long. The scope of the model measurements was great enough to permit predictions by scaling for three different values of r, namely 1/60, 1/30, and 1/15. It will be observed that these predictions are reasonably consistent among themselves, indicating that internal scaling, i.e. within the range covered by the model investigation, is applicable. The curve represents the mean predicted temperature profile, and the closeness of the Staines observations to it is striking evidence of the validity of the scaling principles employed, even up to full scale.

Another result of the same kind is shown in Figure 10, which relates to a coke burning at Staines under like conditions as regard the relative positions of the observation points and the burning line. Here only two predictions from the model are possible, but they are fairly consistent, and the mean profile is again close to the actual Staines observations. It will be noticed that in both cases the temperature rises are small, the maximum value being 13·5° F., which is less than 3 per cent of the absolute temperature, so that the condition for the constancy of $V^2/L\theta$ is not violated. The difference between the predicted and actual values of the temperature rises nowhere exceeds 0·8° F., and this is well within the accuracy of measurement, having regard to the errors to which both field and tunnel observations were liable.

---

* Sir Geoffrey Taylor drew attention in 1943 to the work of W. Schmidt published in November 1941 in the *Zeitschrift für angewandte Mathematik u. Mechanik*, and himself contributed valuable notes on the subject of thermal and forced jets.

On the basis of these and other similar satisfactory comparisons it seems reasonable to conclude that the principles of comparison described are of general validity even for linear ratios as great as 60 : 1. In particular, the data contained in the Appendix may be confidently used in this way to discover the nature of the convective heat flow from a field burning line for all the higher cross-wind speeds likely in fog-clearing practice to be encountered, and for all heat emissions within reasonable practical attainment. Conversely, the requirements as to the position and heat emission of the burning line can be specified so as to ensure fog clearance over a runway to any requisite height.

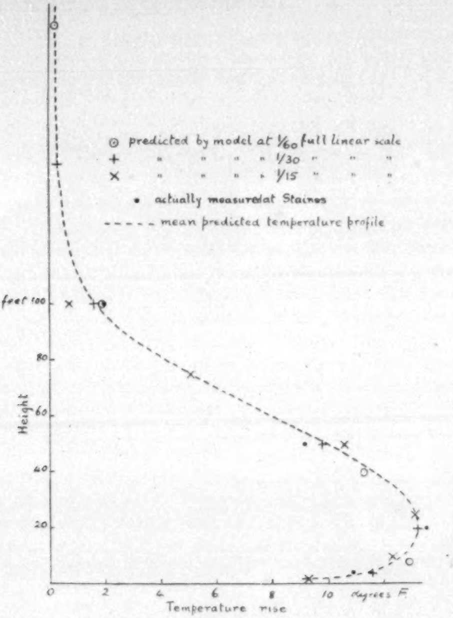

Figure 9.

Petrol burning, Staines, 14.12.42. Wind speed normal to burning line 8½ m.p.h.; convective heat flux 22·4 therms/yd.hr.

Comparison of predictions from model observations with field results, using principles of dynamical similarity.

Limitation of Use of Tunnel in respect of Low Wind Speeds

Soon after the tunnel had been constructed early in 1943 Sir Geoffrey Taylor pointed out that its utility would be restricted, possibly seriously, by the existence of the roof, which would have no counterpart in the open atmosphere. He suggested modifications to transform the tunnel into what may be called a channel by removing the roof, and, by reversing the fan motion, to create the artificial wind by blowing instead of sucking. His proposals also contained other ancillary measures to render the velocity profiles suitable.

It turned out to be impracticable to implement these modifications, although, later, a separate channel was constructed and used, as described presently. The restrictions on the use of the tunnel had, therefore, to be examined and assessed.

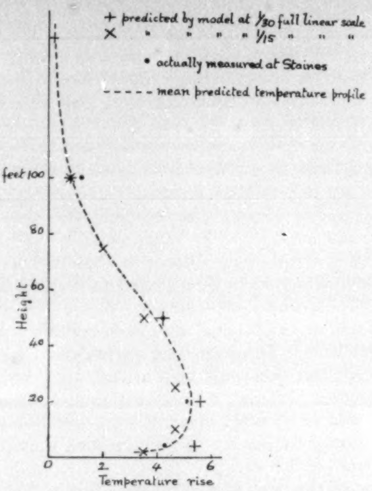

Figure 10.

Coke burning, Staines, 18.1.43. Wind speed normal to burning line 5 m.p.h.; convective heat flux 5·9 therms/yd. hr.

Comparison of predictions from model observations with field results, using principles of dynamical similarity.

Clearly, it would not permit the simulation of full-scale burning lines in calm atmospheres; for the heated air jet, rising vertically and reaching the roof, would be forced to spread out in *both* directions along the tunnel, in a manner which would not occur in the open atmosphere. The same would be true when the jet became deflected from the vertical by low-speed imposed winds; there would still be reversed air flow near the roof which would vitiate simulation of full-scale operations. The question to be decided was at what imposed wind speed this reversal, or re-circulation, ceased, owing to the thermal jet being depressed sufficiently not to engage the roof. This occurrence of re-circulation was tested both by observing visually the flight of meta flakes, and by observations with anemometers suitably disposed between roof and floor. If there is re-circulation the reversal near the roof is accompanied by increased velocity in the original direction near the floor, with a zero speed somewhere in between.

The result of these tests was to show that re-circulation was more liable to occur with the higher values of the heat emissions employed, as would be expected. Even with these heat ratings, however, it ceased to be noticeable for imposed wind speeds somewhat in excess of 1 foot per second. Consequently, the application of the tunnel experiments to predict open-air results has been limited in this sense, and the tables in the Appendix have been deliberately restricted at the lower limits of V. To be on the safe side the lowest value of V included for the range up to $Q=0{\cdot}20$ therms/yard.hour is 1·5 feet per second, and for the range of Q from 0·24 to 0·48 therms/yard.hour to 2 feet per second.

This completes the description of the part of the work at Earl's Court which I deem to be suitable for publication in the *Proceedings*. For the rest, reference must be made to the full report, copies of which, as already stated, have been deposited in the Society's library. But I would like to indicate briefly here two aspects of this additional work which may find application in other directions in the future.

The first relates to the channel already mentioned as having been constructed with no roof in an attempt to realize conditions comparable with the open air. The difficulty here was to produce a reasonably uniform horizontal flow of air along the channel. Motor blowers directed along the channel proved to be abortive. Consideration was given to other possible methods, in particular that of using across one end of the channel a thermal line jet which, by its sideways entrainment of air, might be expected to create a horizontal wind of good uniformity. Theoretically, according to Schmidt, the entrainment speed would be independent of height, and, over a considerable distance along the channel, would vary little. This promising system could not be used because it required much more fuel than could be provided, but it remains one I should like to see implemented. Instead, a somewhat similar system was employed. Motor blowers of cold air directed upwards were installed at one end of the channel so as to constitute a line jet, thereby creating a horizontal drift of the air eventually entrained in this jet.

The other aspect of the work to which I wish finally to refer is the use of a device proposed and demonstrated early in 1944 by the General Electric Company's staff (Mr. Ryde in particular) to study visually the behaviour of thermal jets. This device, which has been called the 'Shadowgraph', consists of projecting through the jet a beam of light, originating in a small but very brilliant source, on to a white screen suitably situated beyond the jet. The result is that a pattern of fluctuating lights and shades appears on the screen, due to the point to point changes of the refractivity of the heated air. This pattern is very instructive, for, while not a complete substitute for the systematic investigation of the temperature and velocity structure of the jet, it does provide a quick means of getting a general picture of the movements of the heated air associated with various arrangements of burning lines. Through the courtesy of the General Electric Company the shadowgraph was used extensively during the later stages of the investigation. Had it been available earlier the planning of the work would have been greatly facilitated.

It proved to be possible to make some motion picture films of the patterns appearing on the shadowgraph screen in the tunnel. These, although by no means so brilliant as the originals, are reasonably good. By the nature of things, they cannot be included in this publication, and I am therefore glad to have been able to exhibit them, during the course of this lecture, through the courtesy of the Ministry of Supply.

REFERENCES

Andrade, E. N. da C., 1945, *Proc. Phys. Soc.*, **57**, xxi.
Brunt, D., 1936, *Trans. Faraday Soc.*, **32**, 1264; 1939, *J. Sci. Instrum.*, **16**, 137.
Simmons, L. F. G. 1949, *J. Sci. Instrum.*, **26**, 407.

APPENDIX

EXPERIMENTS IN THE WIND TUNNEL AT EMPRESS HALL

Structure of convective air jets, originating in a burning line of non-luminous butane flames, under the influence of winds blowing normally across the line, as derived from observations of velocities and temperatures of the flowing air.

V denotes the air speed at the mid-height of the tunnel (72 in.) when no heat is being injected. This defines the structure of the air current imposed on the thermal jet emerging from the burning line.

Q denotes the thermal emission rate per unit length of the burning line, calculated from the calorific value of the butane.

h denotes the height of the point of observation above the floor.

d denotes the horizontal distance downwind of the burning line.

θ denotes the excess of temperature of the air in the thermal jet at the point indicated over that of the air upwind of the burning line.

v denotes the local horizontal air speed. The values of v in relation to those of h for $Q=0$ show the initial vertical velocity profile of the unheated air current. The heat-modified velocity profiles are derived similarly for the corresponding Q values.

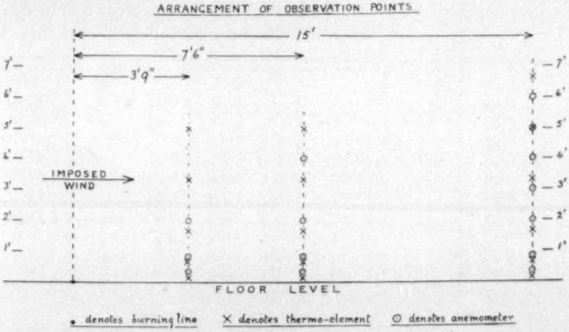

The data given are derived from the averages of multiple observations, of which there were at least 50 for each experimental point. The temperature rises recorded are believed to be accurate to within 0·5° F., or 5 per cent, whichever is the greater. The errors of the velocities shown are estimated not to exceed ±5 per cent.

The chief purpose of the tabulated data of these model experiments is to provide means of predicting the conditions applicable to installations on other scales, by use of the accepted principles of dynamical similarity, namely, the constancy of the dimensional ratio $[V^2/L\theta]$, when θ is small, with the further relation that the fraction H of Q which is in the form of convective heat is proportional to V^3. For these tables $H=0{\cdot}8Q$, for the reasons given in the text relating to losses by radiation and ground absorption.

An apology is perhaps due for the units employed; the C.G.S. system would probably be preferred in some aspects of possible future use of the tables. The choice was determined by the fact that the data were required primarily for comparison with results obtained in the field, where British units had already been adopted for the full-scale work.

Tables of θ (in °F.) for various values of d

(Q in therms/yard.hour)

d=3 ft. 9 in.

h=60 inches

Q	V in feet per second							
	1·5	2·0	2·5	3·0	3·5	4·0	4·5	5·0
0·00	0·0							
0·04	0·0							
0·08	0·1	0·0						
0·12	0·2	0·1	0·0					
0·16	0·4	0·2	0·0					
0·20	0·6	0·3	0·1	0·0				
0·24		0·5	0·2	0·1	0·0			
0·28		0·6	0·3	0·2	0·1			
0·32		0·7	0·4	0·3	0·2	0·0		
0·36		0·8	0·5	0·4	0·3	0·1	0·0	
0·40		1·0	0·7	0·5	0·4	0·2	0·1	0·0

h=40 inches

Q	V in feet per second							
	1·5	2·0	2·5	3·0	3·5	4·0	4·5	5·0
0·00	0·0	0·0						
0·04	0·1	0·0						
0·08	0·3	0·1	0·0					
0·12	0·5	0·2	0·1					
0·16	0·8	0·4	0·2	0·0				
0·20	1·1	0·6	0·3	0·1	0·0			
0·24		0·8	0·5	0·2	0·1	0·0	0·0	
0·28		1·0	0·7	0·4	0·2	0·1	0·1	0·0
0·32		1·3	0·9	0·6	0·4	0·3	0·2	0·1
0·36		1·6	1·2	0·8	0·6	0·5	0·4	0·3
0·40		2·0	1·5	1·1	0·9	0·7	0·6	0·5

h=20 inches

Q	V in feet per second							
	1·5	2·0	2·5	3·0	3·5	4·0	4·5	5·0
0·00	0·0	0·0	0·0	0·0				
0·04	1·1	0·8	0·4	0·0				
0·08	3·0	1·8	0·7	0·1				
0·12	4·9	2·9	1·1	0·2	0·0			
0·16	6·9	3·9	1·6	0·5	0·2	0·0	0·0	
0·20	8·9	5·0	2·2	1·0	0·5	0·2	0·1	0·0
0·24		6·1	3·0	1·5	0·8	0·4	0·3	0·2
0·28		7·3	3·9	2·0	1·1	0·6	0·5	0·3
0·32		8·7	5·0	2·6	1·3	0·9	0·7	0·5
0·36		10·4	6·2	3·1	1·5	1·1	0·8	0·6
0·40		13·0	7·7	3·6	1·8	1·3	0·9	0·7

Tables of θ (in °F.) for various values of d (*cont.*)

(Q in therms/yard.hour)

$d=3$ ft. 9 in.

$h=8$ inches

Q	V in feet per second							
	1·5	2·0	2·5	3·0	3·5	4·0	4·5	5·0
0·00	0·0	0·0	0·0	0·0				
0·04	8·4	7·0	5·6	4·1				
0·08	14·1	13·1	11·6	9·6	7·5			
0·12	18·8	18·1	16·6	15·0	13·9			
0·16	23·0	21·8	20·3	18·4	16·9			
0·20	26·7	25·5	24·1	22·0	20·0			
0·24		29·4	28·0	25·7	23·2			
0·28		33·4	32·0	29·3	26·5	24·6	23·0	21·6
0·32		37·5	35·8	32·8	30·0	28·0	26·3	25·0
0·36		41·7	39·5	36·3	33·6	31·4	29·6	28·4
0·40		45·9	43·1	39·7	37·2	34·8	32·9	31·8

$h=1·6$ inches

Q	V in feet per second							
	1·5	2·0	2·5	3·0	3·5	4·0	4·5	5·0
0·00	0·0	0·0	0·0	0·0				
0·04	9·8	10·2	10·6	11·0				
0·08	15·0	16·3	17·5	18·8	20·0			
0·12	19·5	20·8	21·9	22·9	23·7			
0·16	23·1	24·2	25·4	26·3	27·1			
0·20	26·3	27·6	28·9	29·8	30·6			
0·24		31·1	32·4	33·2	34·0			
0·28		34·7	36·0	36·7	37·5	38·3	39·1	39·9
0·32		38·1	39·6	40·3	41·1	41·9	42·7	43·6
0·36		41·3	43·1	43·8	44·6	45·4	46·3	47·3
0·40		44·5	46·3	47·3	48·1	49·0	49·9	50·6

$d=7$ ft. 6 in.

$h=60$ inches

Q	V in feet per second							
	1·5	2·0	2·5	3·0	3·5	4·0	4·5	5·0
0·00	0·0	0·0						
0·04	0·2	0·1						
0·08	0·4	0·2	0·0					
0·12	0·6	0·3	0·1	0·0				
0·16	1·0	0·4	0·2	0·1				
0·20	1·4	0·5	0·3	0·2	0·0			
0·24		0·6	0·4	0·2	0·1			
0·28		0·7	0·5	0·3	0·1			
0·32		0·8	0·6	0·3	0·1			
0·36		1·0	0·7	0·4	0·2	0·0		
0·40		1·1	0·8	0·4	0·2	0·1		
0·44		1·2	0·8	0·5	0·3	0·1	0·0	
0·48		1·4	0·9	0·5	0·3	0·2	0·1	0·0

Tables of θ (in °F.) for various values of d (*cont.*)

(Q in therms/yard.hour)

d=7 ft. 6 in.

h=40 inches

Q	V in feet per second							
	1·5	2·0	2·5	3·0	3·5	4·0	4·5	5·0
0·00	0·0	0·0	0·0	0·0				
0·04	0·6	0·3	0·1	0·1				
0·08	1·4	0·7	0·4	0·2				
0·12	2·4	1·1	0·8	0·2				
0·16	3·6	1·7	1·0	0·3	0·0			
0·20	5·5	2·8	1·2	0·3	0·1			
0·24		3·8	1·5	0·4	0·1	0·0		
0·28		4·8	1·9	0·5	0·2	0·1	0·0	
0·32		5·7	2·3	0·7	0·4	0·2	0·1	0·0
0·36		6·6	2·8	0·9	0·6	0·3	0·2	0·1
0·40		7·6	3·3	1·1	0·8	0·5	0·4	0·3
0·44		8·6	3·8	1·4	1·0	0·7	0·6	0·5
0·48		9·6	4·3	1·8	1·2	0·9	0·8	0·7

h=20 inches

Q	V in feet per second							
	1·5	2·0	2·5	3·0	3·5	4·0	4·5	5·0
0·00	0·0	0·0	0·0	0·0				
0·04	3·5	2·6	1·7	0·8				
0·08	6·5	5·2	4·1	2·9	1·7			
0·12	8·4	7·9	6·5	5·0	3·6			
0·16	10·3	9·9	8·4	7·0	5·8			
0·20	12·0	11·9	10·2	9·0	7·8	6·3	4·9	3·5
0·24		13·8	12·0	10·6	9·6	8·1	6·6	5·0
0·28		15·5	13·9	12·5	11·3	10·0	8·4	6·5
0·32		17·5	15·5	14·2	12·8	11·5	9·9	8·0
0·36		19·0	17·3	15·9	14·3	12·9	11·1	9·4
0·40		20·7	18·9	17·4	15·6	14·1	12·5	10·9
0·44		22·3	20·5	18·8	17·0	15·4	13·7	12·2
0·48		23·9	22·0	20·0	18·1	16·5	14·9	13·5

h=8 inches

Q	V in feet per second							
	1·5	2·0	2·5	3·0	3·5	4·0	4·5	5·0
0·00	0·0	0·0	0·0	0·0				
0·04	5·1	4·9	4·6	4·2				
0·08	8·0	7·5	7·9	8·3	8·5			
0·12	10·4	9·8	10·9	11·4	11·5			
0·16	12·0	11·8	13·0	13·5	13·7			
0·20	13·4	13·6	15·0	15·5	16·0			
0·24		15·5	17·0	17·5	18·0			
0·28		17·4	18·7	19·4	20·0	20·0	19·8	19·6
0·32		19·0	20·4	21·0	21·5	21·4	21·2	21·0
0·36		20·5	21·9	22·5	23·0	23·2	23·3	23·1
0·40		22·0	23·1	24·0	24·5	24·7	24·8	24·6
0·44		23·4	24·5	25·3	25·7	25·9	26·0	25·8
0·48		24·6	25·7	26·5	27·0	27·2	27·2	26·9

Tables of θ (in °F.) for various values of d (*cont.*)

(Q in therms/yard.hour)

d=7 ft. 6 in.

h=1·6 inches

Q	V in feet per second 1·5	2·0	2·5	3·0	3·5	4·0	4·5	5·0
0·00	0·0	0·0	0·0	0·0				
0·04	4·9	4·4	5·1	6·2				
0·08	7·0	6·7	8·4	9·1	10·8			
0·12	8·5	8·4	10·0	11·1	11·9			
0·16	9·9	10·0	11·6	13·0	13·7			
0·20	11·0	11·5	13·4	14·8	15·5			
0·24		13·0	14·9	16·4	17·1			
0·28		14·5	16·1	17·7	18·7	19·5	20·0	20·5
0·32		15·6	17·3	19·0	20·0	20·8	21·4	22·9
0·36		16·8	18·3	20·0	21·1	21·9	22·5	23·1
0·40		17·6	19·1	20·9	22·0	22·8	23·5	24·0
0·44		18·5	20·0	21·5	22·7	23·6	24·3	24·9
0·48		19·1	20·5	22·1	23·4	24·2	24·9	25·4

d=15 ft.

h=80 inches

Q	V in feet per second 1·5	2·0	2·5	3·0	3·5	4·0	4·5	5·0
0·00	0·0	0·0	0·0					
0·04	0·3	0·1	0·0					
0·08	0·7	0·3	0·1	0·0				
0·12	1·3	0·5	0·2	0·1	0·0			
0·16	2·0	1·0	0·4	0·2	0·0			
0·20	3·0	1·5	0·6	0·3	0·1	0·0		
0·24		2·0	0·8	0·4	0·2	0·0		
0·28		2·5	1·1	0·5	0·2	0·0		
0·32		2·9	1·5	0·6	0·3	0·1	0·0	
0·36		3·4	1·9	0·7	0·3	0·1	0·0	
0·40		3·9	2·3	0·8	0·4	0·1	0·0	
0·44		4·4	2·7	1·0	0·4	0·2	0·0	
0·48		5·0	3·1	1·1	0·5	0·2	0·0	

h=60 inches

Q	V in feet per second 1·5	2·0	2·5	3·0	3·5	4·0	4·5	5·0
0·00	0·0	0·0	0·0					
0·04	0·7	0·3	0·1	0·0				
0·08	1·7	0·7	0·3	0·1	0·0			
0·12	2·7	1·5	0·7	0·3	0·1	0·0		
0·16	3·8	2·5	1·2	0·5	0·3	0·1		
0·20	4·8	3·5	1·9	0·9	0·5	0·2	0·0	
0·24		4·5	2·5	1·4	0·7	0·4	0·1	0·0
0·28		5·5	3·4	1·9	1·0	0·6	0·2	0·1
0·32		6·2	4·1	2·4	1·4	0·9	0·4	0·2
0·36		6·8	4·9	3·1	1·9	1·2	0·6	0·3
0·40		7·5	5·8	3·9	2·4	1·6	0·9	0·4
0·44		8·2	6·7	4·6	3·0	2·0	1·2	0·5
0·48		8·9	7·7	5·6	3·8	2·6	1·6	0·7

Tables of θ (in °F.) for various values of d (*cont.*)

(Q in therms/yard.hour)

d=15 ft.

h=40 inches

Q	V in feet per second							
	1·5	2·0	2·5	3·0	3·5	4·0	4·5	5·0
0·00	0·0	0·0	0·0	0·0				
0·04	1·6	1·2	0·8	0·4				
0·08	2·9	2·3	1·7	1·1				
0·12	4·0	3·1	2·4	1·7	0·9			
0·16	5·0	4·2	3·3	2·6	1·6			
0·20	5·9	5·1	4·2	3·5	2·6			
0·24		6·1	5·1	4·5	3·7			
0·28		6·9	6·1	5·5	4·6	3·9	3·1	2·3
0·32		7·5	7·1	6·5	5·6	4·8	4·0	3·1
0·36		8·2	8·1	7·6	6·5	5·6	4·9	4·1
0·40		8·9	9·1	8·7	7·5	6·5	5·7	4·9
0·44		9·6	10·0	9·9	8·4	7·2	6·5	5·6
0·48		10·2	11·0	11·2	9·3	8·0	7·1	6·4

h=20 inches

Q	V in feet per second							
	1·5	2·0	2·5	3·0	3·5	4·0	4·5	5·0
0·00	0·0	0·0	0·0	0·0				
0·04	2·5	2·5	2·5	2·4				
0·08	4·0	3·8	3·9	3·9				
0·12	4·9	4·4	4·8	4·9	5·0			
0·16	5·6	5·1	5·5	5·7	5·8			
0·20	6·3	5·9	6·4	6·6	6·6			
0·24		6·7	7·1	7·5	7·5			
0·28		7·5	8·0	8·4	8·5	8·5	8·5	8·5
0·32		8·3	8·9	9·3	9·5	9·5	9·5	9·5
0·36		8·9	9·6	10·1	10·4	10·4	10·4	10·4
0·40		9·5	10·4	11·0	11·2	11·2	11·2	11·2
0·44		10·2	11·1	11·9	12·0	12·0	12·0	12·0
0·48		10·9	12·0	12·7	12·7	12·7	12·7	12·7

h=8 inches

Q	V in feet per second							
	1·5	2·0	2·5	3·0	3·5	4·0	4·5	5·0
0·00	0·0	0·0	0·0	0·0				
0·04	2·6	2·3	2·4	2·6				
0·08	4·0	3·5	3·7	4·0				
0·12	4·9	4·4	4·6	5·0	5·4			
0·16	5·4	5·1	5·5	5·8	6·1			
0·20	5·6	5·9	6·2	6·5	7·0			
0·24		6·5	6·9	7·2	7·8			
0·28		7·0	7·5	7·9	8·5	9·1	9·7	10·3
0·32		7·5	8·0	8·6	9·3	9·9	10·5	11·1
0·36		8·1	8·6	9·4	10·0	10·5	11·2	11·9
0·40		8·6	9·2	10·0	10·6	11·2	12·0	12·5
0·44		9·1	9·9	10·7	11·4	12·0	12·7	13·4
0·48		9·9	10·9	11·7	12·4	13·2	13·9	14·5

Tables of θ (in °F.) for various values of d (*cont.*)

(Q in therms/yard.hour)

d=15 ft.

h=1·6 inches

Q	V in feet per second							
	1·5	2·0	2·5	3·0	3·5	4·0	4·5	5·0
0·00	0·0	0·0	0·0	0·0				
0·04	2·0	1·7	1·8	2·0				
0·08	3·0	2·6	2·8	3·1				
0·12	3·4	3·3	3·5	4·0	4·3			
0·16	3·7	4·0	4·1	4·5	5·0			
0·20	4·0	4·5	4·6	5·0	5·5			
0·24		4·9	5·1	5·6	6·1			
0·28		5·3	5·5	6·1	6·7	7·2	7·6	7·9
0·32		5·6	6·0	6·6	7·2	7·8	8·2	8·6
0·36		6·0	6·5	7·1	7·8	8·3	8·7	9·1
0·40		6·5	7·0	7·6	8·4	8·9	9·4	9·9
0·44		6·9	7·5	8·2	8·9	9·5	10·0	10·5
0·48		7·3	8·0	8·8	9·5	10·1	10·7	11·2

Tables of v (in ft/sec.) for various values of d

(Q in therms/yard.hour)

d=3 ft. 9 in.

h=24 inches

Q	V in feet per second							
	1·5	2·0	2·5	3·0	3·5	4·0	4·5	5·0
0·00	1·40	1·87	2·35	2·80	3·27	3·74	4·20	4·66
0·04	1·45	1·90	2·38	2·84	3·31	3·80	4·26	4·73
0·08	1·49	1·94	2·42	2·87	3·35	3·85	4·32	4·79
0·12	1·54	1·98	2·45	2·90	3·39	3·89	4·36	4·83
0·16	1·59	2·02	2·49	2·93	3·43	3·91	4·39	4·86
0·20	1·63	2·07	2·52	2·96	3·45	3·90	4·37	4·83
0·24		2·12	2·56	2·99	3·45	3·89	4·33	4·79
0·28		2·19	2·59	3·02	3·45	3·88	4·30	4·73
0·32		2·26	2·63	3·05	3·45	3·87	4·27	4·67
0·36		2·34	2·66	3·08	3·45	3·89	4·24	4·60

h=10 inches

Q	V in feet per second							
	1·5	2·0	2·5	3·0	3·5	4·0	4·5	5·0
0·00	1·25	1·68	2·08	2·50	2·89	3·28	3·68	4·08
0·04	1·49	1·83	2·22	2·66	3·06	3·45	3·85	4·23
0·08	1·72	1·98	2·36	2·81	3·22	3·59	3·98	4·36
0·12	1·90	2·14	2·50	2·95	3·37	3·72	4·10	4·48
0·16	2·06	2·29	2·64	3·08	3·50	3·84	4·21	4·57
0·20	2·17	2·44	2·78	3·20	3·61	3·94	4·30	4·63
0·24		2·59	2·92	3·31	3·70	4·02	4·36	4·68
0·28		2·74	3·06	3·41	3·77	4·08	4·40	4·71
0·32		2·89	3·20	3·50	3·82	4·12	4·43	4·73
0·36		3·04	3·34	3·58	3·85	4·14	4·45	4·74

Tables of v (in ft/sec.) for various values of d (*cont.*)

(Q in therms/yard.hour)

d=3 ft. 9 in. h=4 inches

Q	V in feet per second 1·5	2·0	2·5	3·0	3·5	4·0	4·5	5·0
0·00	1·07	1·43	1·78	2·14	2·49	2·86	3·20	3·55
0·04	1·41	1·73	2·05	2·37	2·71	3·05	3·39	3·71
0·08	1·64	1·93	2·24	2·54	2·87	3·18	3·51	3·80
0·12	1·84	2·04	2·36	2·65	2·97	3·26	3·57	3·86
0·16	2·01	2·12	2·42	2·71	3·02	3·30	3·59	3·88
0·20	2·12	2·19	2·47	2·75	3·03	3·31	3·60	3·87
0·24		2·26	2·51	2·77	3·03	3·30	3·56	3·81
0·28		2·33	2·54	2·79	3·02	3·27	3·51	3·76
0·32		2·40	2·57	2·80	3·00	3·22	3·46	3·70
0·36		2·46	2·59	2·80	2·98	3·17	3·39	3·63

d=7 ft. 6 in. h=48 inches

Q	V in feet per second 1·5	2·0	2·5	3·0	3·5	4·0	4·5	5·0
0·00	1·46	1·96	2·46	2·96	3·44	3·93	4·42	4·90
0·04	1·48	1·96	2·47	2·97	3·46	3·95	4·45	4·95
0·08	1·49	1·97	2·48	2·98	3·48	3·97	4·47	4·98
0·12	1·50	1·98	2·49	2·99	3·49	3·99	4·49	4·99
0·16	1·51	1·99	2·50	3·00	3·50	4·00	4·50	5·00
0·20	1·52	2·00	2·49	2·99	3·49	3·99	4·49	4·99
0·24		2·01	2·48	2·98	3·48	3·97	4·48	4·98
0·28		2·02	2·47	2·97	3·47	3·95	4·46	4·96
0·32		2·03	2·46	2·96	3·45	3·93	4·44	4·94
0·36		2·04	2·45	2·95	3·43	3·91	4·42	4·92

h=24 inches

Q	V in feet per second 1·5	2·0	2·5	3·0	3·5	4·0	4·5	5·0
0·00	1·40	1·87	2·35	2·80	3·27	3·74	4·20	4·66
0·04	1·58	1·97	2·43	2·86	3·32	3·77	4·21	4·66
0·08	1·75	2·07	2·51	2·92	3·36	3·80	4·22	4·66
0·12	1·90	2·17	2·59	2·98	3·40	3·83	4·24	4·66
0·16	2·03	2·27	2·67	3·04	3·44	3·86	4·26	4·65
0·20	2·15	2·37	2·74	3·10	3·48	3·88	4·27	4·64
0·24		2·46	2·81	3·16	3·52	3·90	4·27	4·63
0·28		2·55	2·88	3·22	3·55	3·92	4·27	4·61
0·32		2·63	2·95	3·27	3·58	3·93	4·27	4·59
0·36		2·71	3·02	3·33	3·61	3·94	4·26	4·57

Tables of *v* (in ft/sec.) for various values of *d* (*cont.*)

(*Q* in therms/yard.hour)

d=7 ft. 6 in.

h=10 inches

Q	*V* in feet per second							
	1·5	2·0	2·5	3·0	3·5	4·0	4·5	5·0
0·00	1·25	1·68	2·08	2·50	2·89	3·28	3·68	4·08
0·04	1·52	1·91	2·24	2·63	3·00	3·40	3·76	4·15
0·08	1·73	2·09	2·38	2·74	3·09	3·48	3·82	4·19
0·12	1·92	2·23	2·51	2·84	3·17	3·54	3·88	4·23
0·16	2·07	2·35	2·62	2·93	3·25	3·60	3·94	4·27
0·20	2·20	2·46	2·72	3·01	3·32	3·65	3·98	4·30
0·24		2·57	2·81	3·08	3·38	3·70	4·02	4·32
0·28		2·67	2·89	3·14	3·43	3·75	4·05	4·34
0·32		2·77	2·96	3·20	3·48	3·79	4·08	4·36
0·36		2·87	3·02	3·25	3·52	3·83	4·10	4·38

h=4 inches

Q	*V* in feet per second							
	1·5	2·0	2·5	3·0	3·5	4·0	4·5	5·0
0·00	1·07	1·43	1·78	2·14	2·49	2·86	3·20	3·55
0·04	1·39	1·76	2·10	2·45	2·79	3·13	3·49	3·82
0·08	1·63	1·97	2·30	2·62	2·96	3·29	3·61	3·95
0·12	1·80	2·10	2·43	2·74	3·06	3·39	3·70	4·02
0·16	1·94	2·19	2·52	2·81	3·12	3·43	3·75	4·06
0·20	2·04	2·26	2·59	2·86	3·16	3·45	3·78	4·06
0·24		2·32	2·64	2·90	3·19	3·47	3·77	4·04
0·28		2·38	2·67	2·93	3·21	3·48	3·76	4·02
0·32		2·43	2·69	2·95	3·23	3·48	3·75	4·01
0·36		2·48	2·71	2·96	3·24	3·48	3·74	4·00

d=15 ft.

h=72 inches

Q	*V* in feet per second			
	2·0	2·5	3·0	3·5
0·00	2·00	2·50	3·00	3·50
0·12	2·00	2·49	2·99	3·50

h=60 inches

Q	*V* in feet per second			
	2·0	2·5	3·0	3·5
0·00	1·98	2·48	2·98	3·47
0·12	2·08	2·51	2·99	3·47

h=48 inches

Q	*V* in feet per second			
	2·0	2·5	3·0	3·5
0·00	1·96	2·46	2·96	3·44
0·12	2·16	2·56	3·01	3·49

h=36 inches

Q	*V* in feet per second			
	2·0	2·5	3·0	3·5
0·00	1·92	2·42	2·90	3·39
0·12	2·23	2·60	3·00	3·46

h=24 inches

Q	*V* in feet per second			
	2·0	2·5	3·0	3·5
0·00	1·87	2·35	2·80	3·27
0·12	2·27	2·60	2·97	3·42

h=10 inches

Q	*V* in feet per second			
	2·0	2·5	3·0	3·5
0·00	1·68	2·08	2·50	2·89
0·12	2·14	2·49	2·91	3·35

h=4 inches

Q	*V* in feet per second			
	2·0	2·5	3·0	3·5
0·00	1·43	1·78	2·14	2·49
0·12	1·99	2·39	2·84	3·31

The Surface Tension of Solids

By R. SHUTTLEWORTH*

H. H. Wills Physical Laboratory, University of Bristol

Communicated by N. F. Mott; MS. received 3rd May 1949, and in amended form 11th September 1949

ABSTRACT. A distinction is made between the surface Helmholtz free energy F, and the surface tension γ. The surface energy is the work necessary to form unit area of surface by a process of division: the surface tension is the tangential stress (force per unit length) in the surface layer; this stress must be balanced either by external forces or by volume stresses in the body.

The surface tension of a crystal face is related to the surface free energy by the relation

$$\gamma = F + A(dF/dA),$$

where A is the area of the surface. For a one-component liquid, surface free energy and tension are equal. For crystals the surface tension is not equal to the surface energy. The standard thermodynamic formulae of surface physics are reviewed, and it is found that the surface free energy appears in the expression for the equilibrium contact angle, and in the Kelvin expression for the excess vapour pressure of small drops, but that the surface tension appears in the expression for the difference in pressure between the two sides of a curved surface.

The surface tensions of inert-gas and alkali-halide crystals are calculated from expressions for their surface energies and are found to be negative. The surface tensions of homopolar crystals are zero if it is possible to neglect the interaction between atoms that are not nearest neighbours.

§ 1. FUNDAMENTAL CONCEPTS

In the study of capillarity the two concepts of surface tension and surface free energy are used. According to Millington (1945, 1947) the concept of surface tension was introduced by Cabeo (1629) and was stated more explicitly by Segner (1751). Theories that explain the surface tensions of liquids in terms of molecular forces have been advanced by Young (1805), Laplace (1806), Poisson (1830), Worthington (1884), Bakker (1928), Brown (1947), and Prandtl (1947). The concept of surface energy is more recent and was introduced by Gauss (1830). Rayleigh (1890) has shown that for the Laplace model of a liquid the surface tension and energy are numerically equal. Dupré (1869) by a general argument has shown that for a one-component liquid the surface tension and surface free energy must be equal.

Because the surface tension and surface free energy of a one-component liquid are numerically equal the two terms have tended to become confused and are often regarded as equivalent: this is not correct. Gibbs (1876) pointed out that for a solid they are not equal, and that the value of the surface tension in a particular crystal face can vary with direction. Recently Orowan (1950) and Nicolson (1950) have discussed the surface tensions of solids in detail, and Nicolson has calculated the surface tensions of some ionic crystals from the force constants of their ions.

In this paper the surface tension and the surface Helmholtz free energy are defined, and a thermodynamic relation between them is derived. The standard thermodynamic formulae of surface physics are reviewed, and it is found that the surface free energy appears in the expression for the excess vapour pressure of small crystals, and in the expression for the equilibrium contact angle between liquid and solid, but that the surface tension appears in the expression for the difference in pressure between the two sides of a curved surface. Surface energy is always positive: calculation shows that the surface tensions of inert-gas and alkali-halide crystals are negative whilst for homopolar crystals, for which it is possible to neglect the interaction between atoms that are not nearest neighbours, the tension is zero.

---

* Now at Physics Department, University of Illinois, Urbana, U.S.A.

(i) *Surface Free Energy*

Consider a large one-component crystal in equilibrium with its vapour in a constant volume enclosure that is maintained at a constant temperature. If this crystal is divided into two parts by a plane whose indices are p and the two parts are then separated, the Helmholtz free energy of the system increases by an amount A_pF_p, where A_p is the increase in surface area, and F_p is defined as the surface Helmholtz free energy per unit area. During this process there will be no change in the number of atoms in each of the two phases, and if the separation is made by a reversible process the external work that is needed will equal the increase in the total free energy of the system.

When a crystal is large compared with atomic dimensions it is possible to neglect the edge and corner energies, and the total free energy of a system consisting of a crystal in equilibrium with its vapour is $N_1F_1+N_2F_2+\Sigma A_pF_p$, where N_1 and N_2 are respectively the number of moles in the crystal and the vapour (N_1+N_2 is the total number of moles in the system), F_1 and F_2 are the free energies per mole of the crystal and vapour phases, and the summation is over all the crystal faces. The surface free energy is only a small correction to the total free energy of the system. For an isotropic material with a curved surface the surface free energy per unit area will be supposed independent of the curvature of the surface, in analogy with the neglect of the edge and corner energies of a crystal.

Although the densities of the two phases near the surface will vary from their value in the interior, the differences in density are small and occur only within a few interatomic distances of the surface, so that they may be neglected and N_1 and N_2 calculated from the volume of the phases on the assumption of constant density.

The surface free energy F_p will be a function of the volume strain of the crystal (e.g. strains produced by hydrostatic pressure). The free energy of the vapour F_2 will vary with the vapour pressure, and since the equilibrium vapour pressure of small crystals is greater than that of large crystals, F_2 will depend on crystal size. The free energy of the solid F_1 will vary with the volume strain in the crystal, and since the surface tension induces volume strains in the crystal (see (ii) below) F_1 will also depend upon crystal size. The variation of F_1 and F_2 is important only for small crystals.

Calculations of the surface energies of inert-gas and ionic crystals on the model of central forces between the atoms have been made by Shuttleworth (1949, to be referred to as I). Attempts to measure the surface free energy of mica were made by Obreimoff (1930) and Orowan (1933) based on the fact that mica can be split reversibly. A thin sheet of mica was partially split from a thicker piece by means of a wedge and the distance between the wedge and the line of bifurcation measured. For a constant height of the wedge the spreading of the crack reduced the elastic energy of the thin mica sheet but increased the surface free energy; the equilibrium depth occurred when the sum of the two energies was a minimum.

(ii) *Surface Tension*

A direct conclusion from the elementary experiments of capillarity is that a liquid surface is in a state of plane stress—this point has been emphasized by Brown (1947). The stress in a liquid surface is known as the surface tension; in the present paper an attempt is made to widen the concept so that it can be applied to crystal faces.

The surface stress is defined analogously to stress in elasticity. Suppose a cut is made perpendicular to the surface of a body and extending only a short distance into it; then in order that the surface remain in equilibrium and no additional stresses occur in the volume of the crystal, it is necessary to apply external forces to atoms near the surface of the cut. Equal and opposite forces, which are in the plane of the surface, must be applied to the atoms on the two sides of the cut; the total force per unit length of cut is the surface stress that existed across the line of the cut. These forces, which are over and above any due to a volume stress, need only be applied to atoms that are within a few atomic distances of the surface. Because two new surfaces have been created to form the cut, it is also necessary to apply forces that are perpendicular to the old surface in order to preserve the equilibrium of the atoms, but the sums of these forces on the atoms on each side of the cut are zero and so do not affect the definition of the surface stress. This surface stress can be balanced either by external forces, e.g. the forces that must be applied to the edges of a plane soap film, or by a volume stress in the material below the surface, e.g. the hydrostatic pressure inside a drop. When the surface stress is balanced by external forces some rearrangement will occur of those atoms that are within a few atomic distances of the point of application of the force, but the surface stress is regarded as a macroscopic concept and this local rearrangement does not affect the definition.

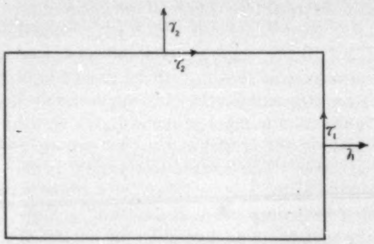

In an isotropic material, such as a liquid, the surface stress is perpendicular to every line in the surface. In a crystal face the surface stress will in general have a shear component; the Figure shows the forces per unit length on an arbitrary rectangle in a crystal face. The condition that there should be no resultant couple rotating the rectangle is that the shear components τ_1 and τ_2

should be equal (cf. elasticity theory). Thus, in general, three numbers are sufficient to specify the surface stress at a point: the normal components γ_1 and γ_2 across two perpendicular directions and the shear components τ parallel to these directions.

When the stresses across two directions in a crystal face are known, the stress across a third direction can be obtained by considering the mechanical equilibrium of a triangle in the face with sides parallel to the three directions. It is then readily shown (see, for example, Timoshenko 1934) that it is always possible to find two perpendicular directions across which the shear stresses are zero. These two directions and the normal stress components across them are referred to as the principal directions and the principal stresses. If there is a line of reflection symmetry in a crystal face the shear component across this line must be zero and therefore this will be one of the principal directions. From the expression for the stress across any arbitrary line it can be shown that the sum of the normal stress components in any two perpendicular directions is equal to the sum of the two principal stresses (see also § 3). The surface tension γ in a crystal face will be defined as half the sum of the two principal stresses, in analogy with elasticity where a third of the sum of the three principal stresses is defined as the hydrostatic pressure. The sign convention followed is in opposition to that for elasticity, and a tension stress will be taken as positive.

Since the surface stress must have at least the symmetry of the crystal face, one number (the surface tension) is sufficient to specify it when the face has a three-fold (or greater) axis of rotational symmetry. Then the normal stress components across all lines in the face are equal and all shear stresses are zero, so that the normal stress components are equal to the surface tension. This can be seen by considering any equilateral triangle in a face which has a three-fold axis of symmetry: by symmetry the stresses on each side must be equal and, since there must be no resultant couple to rotate the triangle, the stresses must be perpendicular to the sides (the same conclusion is reached for a four- or six-fold axis of symmetry by considering any square or regular hexagon in the surface). Now when the stresses across two directions in a crystal face are known the stress across any third direction is obtained from the equilibrium of a triangle whose sides are parallel to these three directions. Since the forces on two sides of this triangle are perpendicular to the sides and proportional to their length, the triangle of forces coincides with the triangle and the force on the third side is also perpendicular and proportional to its length. Hence the normal stress component is the same on all sides and the shear stresses are zero.

In a face-centred-cubic crystal the {111}, {100} and {110} faces have respectively six-, four- and two-fold axes of symmetry. The shear component of the surface stress will therefore be zero for the {111} and {100} faces, but not for the {110} faces.

A direct explanation of the surface tension of a liquid in terms of intermolecular forces is somewhat difficult. The conventional explanations (see, for example, Brown 1947) are based on the fact that the separations between the layers of atoms at the surface of a homopolar substance are greater than in the volume of the material (I). It is postulated that even in the surface layers the arrangement of the molecules of a liquid is isotropic, so that there is a corresponding increase in the separation of the atoms in directions parallel to the surface. This decrease in the density of molecules near the surface is equivalent to a negative pressure parallel to the surface; this negative pressure is identified as the surface tension.

A more immediate explanation of the origin of surface tension is possible for a crystal; for simplicity a crystal at 0° K. will be considered, and the forces between any two atoms will be supposed to depend only on their separation. If it is not possible to neglect the interaction between atoms that are not nearest neighbours, then the equilibrium separation of atoms in an isolated plane will be different from that in a three-dimensional lattice, since the number of non-nearest-neighbour atoms will be different in the two cases. The lattice constant of an isolated (100) plane of atoms of an inert-gas crystal is 0·643 % greater than that of the three dimensional crystal*. Lennard-Jones and Dent (1928) have shown that the lattice constant of an isolated (100) plane of ions of an alkali-halide crystal is about 5 % less than that of the three-dimensional crystal. In order that an isolated plane should have the same spacing as that of the crystal it is necessary to apply external forces to the edges of the plane and tangential to it: the forces are compression for inert-gas crystals and tension for alkali-halide crystals. If the stressed plane is now moved towards the crystal, until it becomes the surface plane, the external forces needed to keep it with the three-dimensional lattice constant will be reduced. When all the atoms are on the positions they would occupy if no surface existed and they were in the centre of the crystal, then the tangential force it is necessary to apply to the surface plane is reduced to half of that which must be applied to an isolated plane. This state is not stable, for in equilibrium the distance between the outermost plane of atoms and the next is different from that in the centre of the crystal (I); when the surface plane takes up its equilibrium position this movement causes a further change in the tangential force which must be applied.

Similar, but smaller, tangential forces must be applied to successive planes in the crystal surface. The surface tension is the total force per unit length that must be applied tangentially to the surface in order that the surface planes have the same lattice spacing as the underlying crystal.

It is possible that the energy of a crystal face would be reduced if, instead of the surface atoms being uniformly strained so as to fit the underlying lattice, faults such as dislocations occurred periodically; this would also change the surface stress. However, Frank and van der Merwe (1949) have shown that dislocations do not occur spontaneously in the surfaces of inert-gas crystals.

In a complete treatment it would also be necessary to consider the difference in the thermal vibrations of the surface and interior atoms.

Nicolson (1950) has measured the surface tension of sodium chloride and magnesium oxide crystals. By means of X-ray diffraction he measured the change in lattice constant which the surface tension causes in small crystals that have {100} faces. Although the surface tension induces non-uniform stresses in cubes, he makes the approximation that the change in lattice constant is the same as would occur in an isotropic sphere. From equations (4) and (5) of § 3,

$$\Delta R_1/R_1 = -2\beta\gamma/3R_1, \qquad \ldots\ldots (1)$$

where $2R_1$ is now the cube edge and β is the compressibility. The reduction in linear dimensions of the cube, $-\Delta R_1$, is independent of R_1, $\Delta R_1/R_1$ is strain which is measured by X-rays. He obtains positive values for the surface tension.

Udin, Shaler, and Wulff (1949) find that when copper is heated to near its melting point it behaves as a viscous fluid; a thin wire, radius R_1, shortens because of the surface tension forces. They balance this force of contraction by means of weight hung at the end of the wire; when the strain rate is zero the weight downwards is equal to the surface forces $\pi R_1\gamma$ upwards. They obtain a positive value (1,400 dyne/cm.) for the surface tension of solid copper. Since an infinitesimal stress causes plastic deformation the surface tension and surface free energy will be equal.

---

* The lattice sums of an isolated (100) plane of an inert-gas crystal are ${}_2A_6''=0{\cdot}5823$; ${}_2A_{12}''=0{\cdot}06350$ (see I for their method of calculation).

§ 2. THE RELATION BETWEEN SURFACE ENERGY AND SURFACE TENSION

A relation between the surface free energy and the surface tension of a crystal face can be obtained by an application of the principle of virtual work. Consider a crystal in which the surface tension is balanced entirely by external forces. If these are the only external forces that are applied to the crystal there will be neither stress nor strain in the volume of the crystal and any infinitesimal distortion will cause no change in the volume energy of the crystal; the work done by the external forces will be equal to the increase of surface energy. Suppose the crystal is deformed so that a square, of area A, in the crystal face is deformed into a rectangle whose sides are parallel to the square. An amount of work $\gamma_1\,dA_1+\gamma_2\,dA_2$ must be done against the surface stress, where γ_1 and γ_2 are the components of the surface stress perpendicular to the sides of the square, and dA_1 and dA_2 are the increases in area in these two directions (for this kind of deformation no work is done against any shear component of the surface stress). Provided the deformation is reversible and occurs at constant temperature, the additional work is equal to the increase in the surface free energy of the square

$$\gamma_1\,dA_1+\gamma_2\,dA_2=d(AF). \qquad \ldots\ldots (2)$$

For an isotropic substance, or for a crystal face with a three- (or greater) fold axis of symmetry, all normal components of the surface stress equal the surface tension and equation (2) reduces to

$$\gamma=d(AF)/dA=F+A(dF/dA), \qquad \ldots\ldots (3)$$

where dA is the total increase in area. For such faces no work is necessary to change the shape of the surface if there is no change in area, since the shear components of the surface stress are zero; equation (3) is therefore true no matter what the manner of deformation of the surface. If the crystal face has not such high symmetry suppose it to be deformed by an equal stretch in all directions, $dA_1=dA_2=\frac{1}{2}\,dA$, so that for this particular kind of deformation equation (3) is still true since $\gamma=(\gamma_1+\gamma_2)/2$.* The surface tension of any crystal face may therefore be defined as the work necessary to increase the area by unit amount by means of a reversible process of stretching which is the same in all directions. This work is additional to any which may be necessary to deform the volume of the crystal—if the initial volume strain in a crystal is not zero, work is necessary to deform the volume by even an infinitesimal amount.

In a solid, at least at low temperatures, the atoms are not mobile and after any deformation they preserve their relative positions: the total number of atoms in the surface remains constant and their separation changes. Then F is a function of area, the term dF/dA of equation (3) is not zero, and the surface tension and energy are not equal. As will be shown below, the terms F and $-A(dF/dA)$ are of the same magnitude.

---

* This proves the invariance of the sum of the normal stress components on any two perpendicular lines, since $d(AF)$ does not depend upon the orientation of the square.

In order to derive a value of dF/dA for a one-component liquid it is convenient to consider a deformation in which the increase of surface area is brought about by a change of the shape of the liquid without a change of volume. The molecules of a liquid are mobile, and in this deformation some are transferred from the centre of the liquid to form the new surface. Since there is no change of volume stress the configuration of the molecules at the surface is not changed. Thus F is not a function of area, dF/dA is zero and the surface energy is equal to the surface tension. This argument is a generalization of Dupré's who considered the work necessary to extend a film of liquid.

If a new surface is suddenly produced in a viscous liquid (say, by the rapid extension of a filament, or by a fracture) then the surface energy and tension will not be equal, but will become equal as rearrangement of molecules between the surface and interior occurs. The time for rearrangement will be greater the greater the viscosity. In the calculation of the rate of deformation of a viscous liquid by surface forces, it is only permissible to assume that surface energy and tension are equal when it can be shown that rearrangement of the molecules at the surface occurs much more rapidly than does the relaxation of the shear stress in the interior of the liquid.

Although surface tension and surface energy have the same physical dimensions, the convention of expressing surface tension in units of dyne/cm., and the surface energy in units of erg/cm^2, will be followed.

§ 3. THE THERMODYNAMICS OF SURFACES

(i) *Difference of Pressure between the two Sides of a Curved Surface*

When a surface has zero curvature the surface tension can be balanced by external forces applied at the periphery parallel to the surface. If, however, the surface is curved it is also necessary to apply normal pressures to each point of the surface. For an isotropic material, Δp the normal pressure at a point is readily calculable in terms of the radii of curvature at that point.

Consider the mechanical equilibrium of an infinitesimal curvilinear square, of side δ, drawn in the surface. Parallel sides of the square have the same curvature. The surface tension forces that act on the two pairs of sides of the square have components $\gamma\delta^2/R_1$ and $\gamma\delta^2/R_2$ parallel to the line drawn normal to the surface at the centre of the square; R_1 and R_2 are the radii of curvature of perpendicular sides. The components of the surface tension that act perpendicular to the normal are equal and opposite on parallel sides. The normal component of the pressure on the element of surface is $\Delta p\delta^2$; for equilibrium of the surface

$$\Delta p = \gamma(1/R_1 + 1/R_2). \qquad \ldots\ldots(4)$$

In the derivation of this formula it has been implicitly assumed that the radii of curvature are large compared with the depth to which the surface stress extends. Many textbooks obtain a similar formula, in which F replaces γ, by a method of virtual work, but they implicitly assume that dF/dA is zero.

The surface of a drop has no periphery and for equilibrium of the surface it is sufficient to apply a normal pressure Δp. In a spherical drop this normal pressure can be produced by a uniform volume dilatation

$$\Delta V/V_0 = 3\Delta R_1/R_1 = -\beta\Delta p, \qquad \ldots\ldots(5)$$

where β is the compressibility.

(ii) *Vapour Pressure of Small Crystals*

Because of the greater proportion of surface to volume the total free energy per mole of small crystals is greater than that of large crystals and, if in the same enclosure, they evaporate and condense on the large crystals. Thomson (1871) considered the equilibrium of a liquid in a capillary tube and derived an expression that connects the vapour pressure, surface tension, and the curvature of a surface; this proof is not appropriate to a solid as it depends on the fact that the shear stress in the liquid must be zero. The same expression can be derived (see, for example, Guggenheim 1933) if it is supposed that in equilibrium the chemical potentials of the liquid inside and the vapour outside a drop are equal; Gibbs (1876) has shown that this is not true for a solid. Helmholtz (1886) derives a similar expression in which the surface free energy appears instead of the surface tension; he neglects the effect of the compression of the liquid by the surface tension. Helmholtz's proof can be modified to apply to crystals.

Wulff (1901) and Wells (1946) have pointed out that the vapour pressure of a crystal depends on shape as well as size. The condition that the total surface energy, $\Sigma A_p F_p$, is a minimum predicts an equilibrium shape for the crystal. For this shape the vapour pressures of all those faces that appear are equal. If the surface energies of all crystal faces are nearly equal, large numbers of faces will appear in equilibrium and the shape will be approximately spherical. If, however, a particular face has a much lower surface energy than any other, only faces of this form will occur in the equilibrium shape, although the surface area will be larger than that of a sphere. A thermodynamic treatment is appropriate only to crystals of the equilibrium shape.

Consider a one-component crystal in equilibrium with its vapour in a constant volume enclosure. When the surface tensions in the crystal faces are produced by external forces there is no volume strain in the crystal and the free energy of the whole system is $N_1F_1+N_2F_2+\Sigma A_pF_p$ where N_1 and N_2 are the number of moles in the crystal and the vapour, and F_1 and F_2 are the free energies per mole of the unstrained crystal and the vapour. If the external forces are reduced to zero, the surface tensions are then balanced by elastic strains in the crystal. The energy of the system decreases by an amount equal to the work done against the external forces as they reversibly decrease to zero; the net decrease arises from a decrease in surface energy and an increase in volume strain energy. An accurate estimate of this decrease can be made only for an isotropic spherical drop, for which the external forces are equivalent to an excess hydrostatic pressure Δp; from equation (5) the decrease is seen to be

$$\int_{\Delta p=2\gamma/R_1}^{\Delta p=0} \Delta p\, dV = -\tfrac{4}{3}\beta\pi R_1^3 \int_{2\gamma/R_1}^{0} \Delta p\, d(\Delta p) = \tfrac{8}{3}\pi\beta\gamma^2 R_1. \quad \ldots\ldots (6)$$

The total free energy of the system then becomes

$$N_1F_1+N_2F_2+AF-\tfrac{8}{3}\pi\beta\gamma^2R_1. \quad \ldots\ldots (7)$$

Here, for simplicity, it is supposed that only crystal faces of one form occur; F is the surface free energy, γ is the surface tension, R_1 is the distance of a crystal face from the centre of symmetry.

When the crystal is in equilibrium with the vapour the change of free energy on the transfer of dN moles from crystal to vapour is zero. The corresponding decreases in volume, area, and radius of the crystals are

$$dV = M\,dN/w; \quad dA = 2\,dV/R_1; \quad dR_1 \simeq dV/4\pi R_1^2, \quad \ldots\ldots (8)$$

where w is the density of the crystal, and M is the molecular weight of the vapour. By equations (7) and (8) the equilibrium condition becomes

$$F_1 w/M + 2F/R_1 - 2\beta\gamma^2/3R_1^2 = w(\boldsymbol{R}T\ln p)/M. \qquad \ldots\ldots(9)$$

The vapour is assumed to be a perfect gas, so that F_2, the free energy per mole, is $\boldsymbol{R}T\ln p$ + terms that depend only on temperature, where T is the temperature and p is the pressure of the vapour. The ratio of the vapour pressure of a crystal with equivalent radius R_1 to that of an infinite crystal at the same temperature, is found by subtracting the corresponding equation from (9)

$$\frac{p}{p_\infty} = \exp\frac{2}{\boldsymbol{R}T}\frac{M}{w}\left(1 - \frac{\beta\gamma}{3R_1}\frac{\gamma}{F}\right)\frac{F}{R_1}. \qquad \ldots\ldots(10)$$

When the compressibility or the surface tension is small this reduces to Thomson's expression; even for the smallest crystals the correction will never be more than a few per cent.

(iii) *Contact Angle*

When three liquid surfaces meet at a line, the condition of equilibrium is that the particles that form the line should be in equilibrium when acted on by the three surface tensions—Neumann's triangle. It is clear that Neumann's triangle is still appropriate when there are different pressures in each of the three liquids; and hydrostatic stresses are the only stresses that can occur in stationary liquids.

This argument cannot be used to calculate the contact angle between liquid, solid, and vapour, because the solid can support a shear stress and this stress contributes to the equilibrium of the particles at the line of contact. Thus a sheet of stretched rubber, whose edge is fastened to the solid, can be in equilibrium at any angle. If, however, the solid is assumed undeformable and the liquid incompressible, the contact angle can be calculated in terms of the three interfacial free energies. Then the equilibrium contact angle occurs when an infinitesimal displacement of the line of contact along the solid causes no change in energy of the system. This (see, for example, Shuttleworth and Bailey 1948) leads to the expression

$$F_{\mathrm{SV}} = F_{\mathrm{SL}} + F_{\mathrm{LV}}\cos\theta, \qquad \ldots\ldots(11)$$

where θ is the equilibrium contact angle the liquid makes with the solid and F_{SV}, F_{SL} and F_{LV} are the surface energies of the three interfaces.

§4. THE SURFACE TENSION OF INERT-GAS CRYSTALS

In I the surface energies of inert-gas crystals at 0° K. were calculated on the assumption that the forces between any two atoms depended only on their separation. The potential between two atoms at a distance r apart was supposed to have the simple form

$$\epsilon(r) = \lambda r^{-s} - \mu r^{-t} \qquad \mathrm{s} > t, \qquad \ldots\ldots(12)$$

where the first term represents the short-range repulsive forces and the second term the longer-range attractive forces. U, the surface energy at 0° K., is entirely potential and for purposes of calculation was divided into two parts U' and U''; U' is the surface energy of a crystal face before any rearrangement of the surface atoms occurs, and while they occupy the same relative positions as they did when at the centre of the crystal. When the stress perpendicular to the surface is relieved by movement of the surface atoms in this direction, the surface energy decreases by an amount U'':

$$U = U' - U''. \qquad \ldots\ldots(13)$$

For a (100) face of an inert-gas crystal the surface plane of atoms are separated from the next by a distance 2·54% greater than normal, and this makes U'' about 1% of U'. Inert-gas crystals are face-centred-cubic and U' and U'' are given by

$$U_p' = \{-B_s''\lambda a^{-s} + B_t''\mu a^{-t}\}/2\omega_p a^2, \qquad \ldots\ldots(14)$$

$$U_p'' = \{\Delta C_s''\lambda a^{-s} - \Delta C_t''\mu a^{-t}\}/\omega_p a^2, \qquad \ldots\ldots(15)$$

where $2a$ is the lattice constant, $1/\omega_p a^2$ is the number of atoms per unit area in the surface plane, B_s'', B_t'', $\Delta C_s''$ and $\Delta C_t''$ are lattice sums whose values depend on the crystal face. Equations (14) and (15) are appropriate even when $2a$ is not the equilibrium lattice constant, provided the lattice has been distorted by a uniform dilatation. During uniform dilatation each face is stretched uniformly and its area is proportional to a^2. For such a distortion equation (3) enables the surface tension of a face at 0° K., γ_0, to be calculated from the surface energy:

$$\gamma_0 = \frac{d(AU)}{dA} = \frac{1}{2a}\frac{d(a^2U')}{da} - \frac{1}{2a}\frac{d(a^2U'')}{da}, \qquad \ldots\ldots(16)$$

$$\gamma_0 = \gamma_0' - \gamma_0''. \qquad \ldots\ldots(17)$$

From equations (14), (15), (16), and (17)

$$\gamma_0' = \{\tfrac{1}{2}sB_s''\lambda a_0^{-s} - \tfrac{1}{2}tB_t''\mu a_0^{-t}\}/2\omega a^2{}_0, \qquad \ldots\ldots(18)$$

$$\gamma_0'' = -\{s\Delta C_s''\lambda a_0^{-s} - t\Delta C_t''\mu a_0^{-t}\}/2\omega a_0^2, \qquad \ldots\ldots(19)$$

where $2a_0$ is the equilibrium lattice constant when the external pressure is zero; it is remembered (I) that $\Delta C_s''$ and $\Delta C_t''$ were derived from the condition

$$\left\{\frac{d(\Delta C_s'')}{da}\lambda a_0^{-s} - \frac{d(\Delta C_t'')}{da}\mu a_0^{-t}\right\}\frac{da}{dc} = 0, \qquad \ldots\ldots(20)$$

where ca_0 is the distances of the surface plane of atoms from the plane below. The heat of sublimation per atom of a crystal at 0° K. is

$$\epsilon = \{-A_s''\lambda a^{-s} + A_t''\mu a^{-t}\}/2, \qquad \ldots\ldots(21)$$

where A_s'' and A_t'' are lattice sums. When the crystal is unstrained ϵ is a minimum with respect to the variation of a at the value $a = a_0$, and

$$sA_s''\lambda a_0^{-s} = tA_t''\mu a_0^{-t}. \qquad \ldots\ldots(22)$$

When λa_0^{-s} and μa_0^{-t} are eliminated from equations (18) and (19) by equations (21) and (22)

$$\gamma_0' = +\frac{st}{s-t}\,\frac{B_s''/A_s'' - B_t''/A_t''}{2\omega}\,\frac{\epsilon_0}{a_0^2} = G'(s,t)\frac{\epsilon_0}{a_0^2}, \qquad \ldots\ldots(23)$$

$$\gamma_0'' = -\frac{st}{s-t}\,\frac{2\Delta C_s''/A_s'' - 2\Delta C_t''/A_t''}{2\omega}\,\frac{\epsilon_0}{a_0^2} = G''(s,t)\frac{\epsilon_0}{a_0^2}. \qquad \ldots\ldots(24)$$

The attractive forces between inert-gas atoms are of van der Waals type for which $t=6$. In Table 1, $G'(s,6)$ is given for $\{111\}$, $\{100\}$, $\{110\}$ faces and for values of s between 7 and infinity. Values of B_s'' and A_s'' for a range of s are given respectively in (1), and by Lennard-Jones and Ingham (1925). The tension γ_0' is negative in homopolar crystals and increases towards zero with increase in s (increase in hardness of the atoms).

The computation of $\Delta C_s''$ and $\Delta C_t''$ has been made (I) only for a (100) face for $s=12$, $t=6$; these values give $G''(12,6)=-0{\cdot}146$. For the $\{100\}$ faces of such a crystal

$$\gamma_0'=-0{\cdot}170\epsilon_0/a_0^2;\quad \gamma_0''=-0{\cdot}146\epsilon_0/a_0^2;\quad \gamma_0=-0{\cdot}024\epsilon_0/a_0^2. \qquad \ldots\ldots(25)$$

The surface distortion makes a large and positive contribution to the surface tension. Values of γ_0', γ_0'' and γ_0, for neon, argon, krypton, and xenon crystals were calculated from equation (25) and are given in Table 2; the surface energy of a (100) face at 0° K. is included for comparison.

Table 1. Variation of $G'(s,6)$ with Crystal Face and 'Hardness' of the Atoms

s	7	8	9	10	11	12	∞
$\{111\}$	$-0{\cdot}382$	$-0{\cdot}315$	$-0{\cdot}273$	$-0{\cdot}245$	$-0{\cdot}225$	$-0{\cdot}209$	$-0{\cdot}110$
$\{100\}$	$-0{\cdot}339$	$-0{\cdot}272$	$-0{\cdot}231$	$-0{\cdot}204$	$-0{\cdot}185$	$-0{\cdot}170$	$-0{\cdot}087$
$\{110\}$	$-0{\cdot}332$	$-0{\cdot}268$	$-0{\cdot}229$	$-0{\cdot}203$	$-0{\cdot}184$	$-0{\cdot}171$	$-0{\cdot}088$

Table 2. The Surface Tensions of the (100) Faces of Inert-Gas Crystals

	ϵ_0 (10^{-14} erg/atom)	a_0 (A.)	γ_0' (dyne/cm.)	γ_0'' (dyne/cm.)	γ_0 (dyne/cm.)	U (erg/cm^2)
Ne	4·08	2·26	−13·6	−11·7	−1·9	17·9
A	13·89	2·70	−32·4	−27·8	−4·6	42·7
Kr	19·23	2·79	−42·0	−36·1	−5·9	55·3
Xe	26·87	3·09	−47·8	−41·1	−6·7	63·0

From equation (2) the compressibility of a crystal at 0° K. is seen to be

$$\frac{1}{\beta_0}=V_0\left(\frac{d^2E}{dV^2}\right)_{V_0}, \qquad \ldots\ldots(26)$$

where E is the energy of a crystal volume V. For a face-centred-cubic crystal the volume and energy per atom are $2a^3$ and $-\epsilon$,

$$\frac{1}{\beta_0}=-\frac{1}{18a_0}\left(\frac{d^2\epsilon}{da^2}\right)_{a_0}. \qquad \ldots\ldots(27)$$

For inert-gas crystals, from equation (21),

$$1/\beta_0=\{s(s+1)A_s''\lambda a_0^{-s}-t(t+1)A_t''\mu a_0^{-t}\}/36a_0^3. \qquad \ldots\ldots(28)$$

The proportional change in lattice constant of an isotropic sphere due to a tension in the surface is given by equation (1). For a crystal whose faces are all of the same form an approximate value of the lattice change is obtained by using the equivalent radius of the crystal. From equations (1), (17), (18), (19), (22) and (28)

$$\frac{\Delta R_1}{R_1}=\frac{6}{\omega(s-t)}\left\{\frac{B_t''+2\Delta C_t''}{A_t''}-\frac{B_s''+2\Delta C_s''}{A_s''}\right\}\frac{a_0}{R_1} \qquad \ldots\ldots(29)$$

and from equations (23) and (24)

$$\frac{\Delta R_1}{R_1}=-\frac{12(G'-G'')}{st}\frac{a_0}{R_1}. \qquad \ldots\ldots(30)$$

As s and t increase, the dilatation caused by the surface tension tends to zero more quickly than does the tension. When the values $G'(6, 12)$ and $G''(6, 12)$ for a (100) face are used, the proportional increase in lattice constant is $\Delta R_1/R_1 = 0{\cdot}004a_0/R_1$; this is too small to be detected by X-rays, even in the smallest crystals. The increase in radius due to the volume dilatation is much smaller than the increase due to surface distortion ($0{\cdot}0254a_0$).

In a homopolar crystal in which it is possible to neglect the forces between atoms that are not nearest neighbours, all components of the surface stress are zero at zero temperature and pressure. This is because in such a crystal the attractive and repulsive forces between nearest neighbour atoms are equal and opposite, so that the net force between all pairs of atoms in the lattice is zero. It is, therefore, not necessary to apply external forces in order that the surface atoms remain in the same relative positions as they had in the centre of the crystal. That γ_0' is zero is also clear from equation (23) for, when only nearest neighbour interaction is considered, B_s''/A_s'' equals B_t''/A_t''. If, however, the simple model of central forces between the atoms is not adequate, and account must be taken of the electronic distortion of the surface atoms, then γ_0'' will not be zero (Gurney 1947).

§ 5. THE SURFACE TENSION OF ALKALI-HALIDE CRYSTALS

In crystals of the alkali-halides the alkali and halide ions are arranged on alternate points of a simple-cubic lattice. The interatomic forces are: electrostatic, dipole–dipole, dipole–quadrupole and short range repulsive forces. Mayer (1933), and Huggins and Mayer (1933) give numerical values for the force constants. In (I) it was shown that U', the surface energy of an undistorted face at 0° K., can be written

$$U' = \{2B_e'''\mathbf{e}^2a^{-1} + [B_6''(c_{++}+c_{--}) + 2B_6'c_{+-}]a^{-6} + [B_8''(d_{++}+d_{--}) + 2B_8'\,d_{+-}]a^{-8} \\ - N''(1{\cdot}25b_+^{\,2} + 0{\cdot}75b_-^{\,2})\exp(-\sqrt{2}a/\rho) - 2N'b_+b_-\exp(-a/\rho)\}/2\omega a^2, \qquad \ldots\ldots (31)$$

where a is the distance between adjacent alkali and halide ions. B and N are lattice sums given in I; c, b, d and ρ are the force constants. From equation (16)

$$\gamma_0' = -\{B_e'''\mathbf{e}^2a_0^{-1} + 3[B_6''(c_{++}+c_{--}) + 2B_6'c_{+-}]a_0^{-6} \\ + 4[B_8''(d_{++}+d_{--}) + 2B_8'\,d_{+-}]a_0^{-8} - (a_0/\sqrt{2}\rho)N''(1{\cdot}25b_+^{\,2} + 0{\cdot}75b_-^{\,2}) \\ \times\exp(-\sqrt{2}a_0/\rho) - (a_0/\rho)N'b_+b_-^{\,2}\exp(-a_0/\rho)\}/2\omega a_0^2. \qquad \ldots\ldots (32)$$

In Table 3 are given ${}_{100}\gamma_0'$ and ${}_{110}\gamma_0'$ the surface tensions of the {100} and {110} faces when there is no surface distortion; and the contributions of the various interatomic forces to ${}_{100}\gamma_0'$.

Table 3. The Contributions of the Various Forces to ${}_{100}\gamma_0'$ (dyne/cm.)

	NaF	NaCl	NaBr	NaI	KF	KCl	KBr	KI
Electrostatic	−309·0	−172·8	−144·9	−113·9	−198·3	−125·2	−107·9	−87·9
Dipole–dipole	−248·3	−238·7	--233·6	−228·5	−252·3	−209·3	−194·9	−181·8
Dipole–quadrupole	−35·3	−34·4	−33·4	−33·6	−33·3	−28·9	−26·4	−25·0
Repulsive	−1806·9	1087·3	946·0	794·6	1203·2	767·4	669·7	563·6
Total								
${}_{100}\gamma_0'$	1214	641	534	419	719	404	341	269
${}_{110}\gamma_0'$	1443	776	646	505	884	521	442	354

Dent (1929) has given numerical values of the contributions of the various forces to ${}_{100}\gamma_0''$ for sodium and potassium halides. Although her force constants are not the same as those used in this paper, her values have been used to calculate ${}_{100}\gamma_0''$ from equations (16) and (17). Since surface distortion is due almost entirely to the polarization of the surface ions in an electrostatic field that varies rapidly over their volume, the most important source of error is her assumption that the polarization of a surface ion is the same as it would be in a uniform field, whose value is equal to that at the centre of the ion. In Table 4 are given: ${}_{100}\gamma_0'$, ${}_{100}\gamma_0''$, ${}_{100}\gamma_0$, β (experimental) and ΔR_1 (from equation (1)) for sodium and potassium halides.

Table 4. The Surface Tensions of the {100} Crystal Faces (dyne/cm.)

	NaF	NaCl	NaBr	NaI	KF	KCl	KBr	KI
${}_{100}\gamma_0'$	1214	641	534	419	719	404	341	296
${}_{100}\gamma_0''$	1034	771	868	724	929	779	842	581
${}_{100}\gamma_0$	180	−130	−334	−305	−210	−375	−501	−312
β (10^{-12} bar^{-1})	2·11	4·26	5·08	7·0	3·31	5·63	6·70	8·54
ΔR_1 (A.)	−0·03	0·04	0·11	0·14	0·05	0·14	0·22	0·18

Except for sodium fluoride the calculated surface tensions are negative. However, the crude model used to calculate ${}_{100}\gamma_0''$ may have introduced considerable errors, so that the net surface tension ${}_{100}\gamma_0$ is uncertain even as to sign. The values obtained for ${}_{100}\gamma_0'$ are in fair agreement with those of Nicolson (1950); in his calculation of ${}_{100}\gamma_0''$ he took account of the polarization of the surface ions, but neglected the effect of their displacement, which procedure gives values of ${}_{100}\gamma_0''$ only half those of Table 4. Nicolson's experimental values of ${}_{100}\gamma_0$ were positive.

ACKNOWLEDGMENTS

I am indebted to Dr. M. M. Nicolson of the Physics Department of Leeds University, who has allowed me to read his paper on surface tension prior to publication, and to my colleagues Dr. K. Huang and Dr. G. G. Wiles, with whom I have had valuable discussions.

REFERENCES

Bakker, G., 1928, *Wien–Harms Handb. Exp. Phys.*, **6.**
Brown, R. C., 1947, *Proc. Phys. Soc.*, **59,** 429.
Cabeo, N., 1629, *Philosophia Magnetica, Ferrara*, lib. ii, cap. 20.
Dent, B. M., 1929, *Phil. Mag.*, **8,** 530.
Frank, F. C., and van der Merwe, J. H., 1949, *Proc. Roy. Soc.* A, **198,** 205.
Dupré, M. A., 1869, *Théorie mécanique de la chaleur* (Paris).
Gauss, C. F., 1830, *Werke*, **5,** 31.
Gibbs, J. W., 1876, *Collected Works*, **1,** 315 and 317 (London : Longmans and Green).
Guggenheim, E. A., 1933, *Modern Thermodynamics* (London : Methuen), 160.
Gurney, C., 1947, *Proc. Phys. Soc.*, **59,** 447.
Helmholtz, R., 1886, *Wied. Annalen*, **27,** 508.
Huggins, M. L., and Mayer, J. E., 1933, *J. Chem. Phys.*, **1,** 643.
Laplace, P. S., 1806, *Mécanique céleste*, **10.**
Lennard-Jones, J. E., and Dent, B. M., 1928, *Proc. Roy. Soc.* A, **121,** 247.
Lennard-Jones, J. E., and Ingham, A. E., 1925, *Proc. Roy. Soc.* A, **107,** 636.
Mayer, J. E., 1933, *J. Chem. Phys.*, **1,** 270.
Millington, E. C., 1945, *Annals of Science*, **5,** 253; 1947, *Ibid.*, **5,** 352.
Nicolson, M. M., 1950, to be published.

Obreimoff, J. W., 1930, *Proc. Roy. Soc.* A, **127**, 290.
Orowan, E., 1933, *Z. Phys.*, **82**, 239; 1950, to be published.
Poisson, S. D., 1830, *Memoirs de l'Academie des Sciences*, **9**.
Prandtl, L., 1947, *Ann. Phys., Lpz.*, **1**, 59.
Rayleigh, 3rd Lord, 1890, *Collected Works*, **3**, 397.
Segner, J. A., 1751, *Comment. Soc. Reg. Gött.*, **1**, 301.
Shuttleworth, R., 1949, *Proc. Phys. Soc.* A, **62**, 167.
Shuttleworth, R., and Bailey, G. L. J., 1948, *Discussion Faraday Soc.*, **3**, 16.
Thomson, W. (Lord Kelvin), 1871, *Phil. Mag.*, **42**, 448.
Timoshenko, S., 1934, *Theory of Elasticity* (New York: McGraw-Hill), p. 15.
Udin, H., Shaler, A. J., and Wulff, W., 1949, *J. Metals*, **1**, 186.
Wells, A. F., 1946, *Phil. Mag.*, **37**, 184.
Worthington, A. M., 1884, *Phil. Mag.*, **18**, 334.
Wulff, G., 1901, *Z. Kristallogr.*, **34**, 449.
Young, T., 1805, *Collected Works*, **1**, 418.

On the Temperature Dependence of Counter Characteristics in Self-quenching Geiger–Müller Counters

By OM PARKASH* and P. L. KAPUR†
* East Punjab University, Physics Department, Hoshiarpur (E. Punjab), India
† Delhi University, Physics Department, Delhi (India)

Communicated by E. N. da C. Andrade; MS. received 4*th November* 1949

ABSTRACT. The effect of temperature on the counting rate–voltage characteristics of self-quenching Geiger–Müller counters with internal and external cathodes (in this paper denoted as counters Nos. 1 and 2) has been investigated within the temperatures ranging from 8° to 60° c.

It is found that the average counting rate remains independent of temperature (within the statistical error limits), and this constancy is better in the case of the external cathode counter than with the other. As counter No. 1 shows a greater increase in slope at higher temperatures, the rate appears to be greater at higher applied potentials. Further, it is noticed that the plateau decreases and disappears at lower temperatures in the case of counter No. 1, while counter No. 2 does not show this effect. This is partly explained by the formation of semiconducting paths between the central wire and the cathode, the discharges along which give rise to spurious counts in the case of counter No. 1, and the absence of these in the case of counter No. 2.

It is also observed that the slope of the plateau increases and the width decreases with rise of temperature in both cases, though the increase in slope is more marked with counter No. 1 than with counter No. 2. The increase in slope is probably due to the presence of a greater number of multiple discharges or spurious counts at higher-temperatures, an important point which is under study.

The investigation also brings about the advantage of the external cathode in the construction and design of G–M counters, especially when reliable observations are desired with a counter under widely changing temperature conditions.

§1. INTRODUCTION

FROM the general considerations of the theory of discharge mechanism in Geiger–Müller counters developed by Rose and Korff (1941), Ramsey (1940), and Montgomery and Montgomery (1940) we find that the counters of the internally quenched type, first introduced by Trost (1937), must show some change in their characteristics with temperature. According to this theory, the organic vapour causes quenching of the discharge by absorbing the photons, thus causing conditions unfavourable for the continuation of the discharge. Under such conditions the number of vapour molecules, and consequently the effect of quenching, will depend on temperature; that is, at lower temperatures some of the vapour will condense out, with the result that (i) there may be insufficient quenching vapour left, and (ii) the liquid might condense near the electrodes in such a way as to form semiconducting paths across the insulating material between the wire and the cylinder. Leakage across such paths can manifest itself as multiple discharges or spurious counts. At higher temperatures, however, the number of molecules remains unaffected.

The authors have not come across any thorough investigation of these points, but there have been diverse views. It has been reported by Korff (1948) that self-quenching counters, usually employing argon or some other gas mixed with some organic vapour, show a temperature dependence of their counting rate which can sometimes be troublesome. Korff, Spatz and Hilberry (1942) during their experiments on argon–alcohol counters, found a marked dependence of the counting rate on temperature. They also found that the plateau disappeared at lower temperatures. Jánossy (1948) has stated that alcohol counters are temperature dependent and can be permanently spoiled if exposed to low temperatures. Putman (1948), in trying to eliminate variation of counting rate with temperature, found that there was a bodily shifting of the plateau towards higher operating potentials as the temperature was increased. In his case, however, when the plateau was flattened with an external quenching circuit, the counting rate became largely independent of temperature.

As the self-quenching counters using argon and alcohol are the most widely used in cosmic-ray and other experiments, any large temperature changes near the counters might lead to erroneous conclusions. It is, therefore, very necessary to know the nature of changes and the range of temperatures within which we can safely use the self-quenching G–M counters. The present investigation was undertaken with that in mind.

§ 2. APPARATUS AND EXPERIMENTAL PROCEDURE

Two G–M counters of the self-quenching type were chosen, one with internal (No. 1) and the other with external (No. 2) cathode. Counter No. 1 with internal cathode, prepared in this laboratory, is a usual type of glass-enveloped counter with a thin oxidized copper cylinder cathode, filled with commercial argon at 8·5 cm. and absolute alcohol (100% pure) at 1·5 cm. to a total pressure of 10 cm. of mercury, the temperature at the time of filling being 33–34° c. (Om Parkash and Sarna 1948). The second one is a thin-walled glass counter* of the self-quenching type with external cathode consisting of a thin layer of graphite on the outer surface of the glass cylinder. The details of construction are given in a paper by Maze (1946).

In order to vary the temperature of the counters a suitable brass enclosure was constructed (Figure 1). Inside the brass enclosure is placed another glass tube in three pieces, as shown, to insulate the counter electrically from the enclosure. The connecting leads to the axial wire and the cylinder pass through thick glass capillaries fixed in the side tubes attached to the enclosure. A thermometer is also inserted to record the temperature inside the enclosure.

---

* This counter was brought by Dr. P. S. Gill and given to Dr. H. R. Sarna of the East Punjab University. The authors are grateful to Dr. Sarna for lending the counter for the present investigation.

The counter is supported inside and the enclosure closed by means of a brass cap soldered to it; the whole is then made water-tight* and placed in a thermostatically controlled chamber. The temperatures were kept constant (in most cases to ±0·2° c.) during the time the whole plateau curve was plotted.

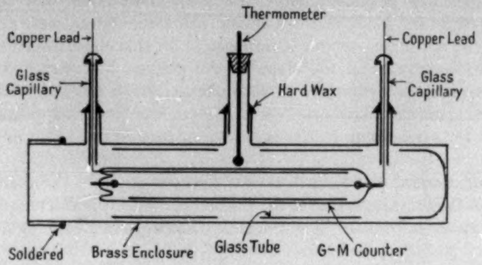

Figure 1.

The high tension, applied to the counters through a series resistance of 10^6 ohms, was obtained from 1,500 volt dry batteries packed into two units of 750 volts each, and could be changed by steps of approximately 24 volts. The electrical pulses were amplified and recorded mechanically in the normal manner.

One of the counters was placed in the enclosure and a number of counting rate–voltage curves were obtained with the counter at a series of constant temperatures. The experiment was repeated with the other counter. The total range of variation extended from 8° to 60° c. Observations were also taken at room temperature (33–35° c.) after heating or cooling the counters to see if there was any permanent effect of heating or cooling on the counter.

§ 3. RESULTS AND DISCUSSION

Figures 2 (*a*) and 2 (*b*) give the plateau curves at different temperatures for counters No. 1 and No. 2 respectively. In the case of counter No. 2 it is clear that there was practically no change in the counting rate within this temperature range, while with counter No. 1 there was a marked effect near the lower temperatures. In the latter case, also, the counting rate remains constant over the range 18–60° c.; below 18° c. the plateau decreased, and disappeared at about 9° c. Another important observation that is evident from the curves is that the plateau becomes flatter and wider at lower temperatures, though in the case of counter No. 1 it seems to disappear at still lower temperatures. It is also noticed that there is a definite increase in the slope (this is more prominent in the case of counter No. 1) and a decrease in overall width of the plateau at higher temperatures. Except for this, the two counters seem to exhibit similar characteristics. It may be remarked that within the temperature range investigated we do not find any bodily shifting of the plateau towards higher operating potentials at higher temperatures. This is so in both cases. The present observations do not show any bodily shifting of the plateau towards higher operating potentials, as experienced by Putman (1948).

---

* A small amount of CaCl is also introduced to absorb any water vapour inside, since at low temperatures condensation might occur on the outer surface of the counter, thus shorting the high tension.

The decrease in the plateau width and its disappearance at lower temperatures in the case of counter No. 1 might be explained on the supposition that some of the quenching vapour condenses, forming semiconducting paths between the cathodes and the central wire, the discharges across these giving rise to spurious counts. In the case of counter No. 2, however, there is no such possibility of conducting paths and hence no such effect. How far the decrease in the partial pressure of the quenching vapour is responsible for this effect has still to be seen.

It is also observed that the slope of the plateau increases and the width decreases at higher temperatures in both cases, though the increase in slope is more marked in the case of counter No. 1. In counter No. 2 it appears that below about 36° c. the slope seems to remain constant though the width of the plateau decreases.

Korff and Present (1944) have shown that the slope of the plateau in self-quenching G–M counters is due to the presence of multiple discharges which are recorded as spurious counts. The multiple discharges in a counter are produced either by photo-emission or by the positive ions striking the cathode. Quenching vapour has a dual rôle of neutralizing the positive ions and absorbing the photons, though Craggs and Jaffe (1947) have shown that the absorption of photons, capable of producing multiple pulses in self-quenching counters, is not complete. Also, at higher temperatures, the average energy and the number of positive ions being greater (Stever 1942), there is an increase in the number of ions reaching the cathode; this results in greater secondary emission and a corresponding increase in the frequency and multiplicity of the multiple pulses. The slope of the plateau is thus to be attributed to the increasing number of positive ions at higher temperature, though the absorption of photons might also be affected and thus contribute to the increase in slope (Putman 1948, Corson and Wilson 1948). Putman has further shown, from the study of the distribution of multiple pulses, that the spurious counts which are primarily responsible for the plateau slope in argon–alcohol counters are those produced by the positive ions.

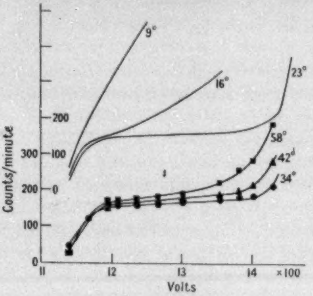

Figure 2 (*a*).

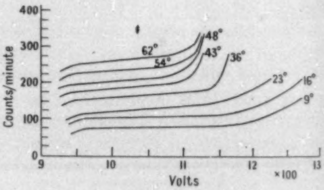

Figure 2 (*b*).

The increase in plateau slope observed in our case may be due both to the absorption of photons by the alcohol molecules and to the increased number of positive ions at higher temperatures, though in accordance with the above ideas of Stever, Putman and Wilson we suppose it to be more predominantly due to the latter. At higher temperatures the number of multiple pulses increases, giving a greater slope. As the number of alcohol molecules at higher temperatures remains unaffected, there being no condensation etc., photon absorption should not be greatly affected, but a greater number of positive ions reaching the cathode might be responsible for the observed effect. This point is still under investigation.

It is also observed that heating or cooling the counter within the range investigated does not produce any permanent effect on its characteristics as observed by Jánossy.

§ 4. CONCLUSION

The present investigation shows that in the usual type of argon–alcohol counters, with internal cathodes, the plateau decreases and disappears at lower temperatures, but that with the other counters such an effect is not observed within the range investigated. At higher temperatures there is an increase in the plateau slope and decrease in the width in both cases. The effect is more prominent with counter No. 1. Thus in using such counters large temperature changes in the vicinity should be avoided or satisfactory working at higher temperatures obtained by using some multivibrator or quenching circuits (Putman 1948) to suppress the multiple discharges. At lower temperatures, however, the nature of the effect is different and an external cathode counter is advantageous. Other gases and quenching vapours are being investigated and will be reported upon later.

ACKNOWLEDGMENTS

The authors are grateful to Dr. R. C. Majumdar and Dr. P. K. Kichlu of the Delhi University Physics Department for providing facilities for the present work, and to Dr. H. R. Sarna, Reader in Physics, East Punjab University, who has contributed useful discussion to this work. The investigation was financed partly by the senior author (O. P.) and partly by Delhi University Physics Department. We are particularly anxious to express our thanks to Dr. W. E. Duncanson of University College, London, for having read through the paper and having made several very helpful suggestions.

We are particularly thankful to Mr. S. K. Suri, M.Sc., formerly a student of the senior author, for showing keen interest while the work was in progress and for helping to set up the apparatus in the initial stages. We are also thankful to Mr. P. C. Bhatia, Head Mechanic, Physics Department, Delhi University, for help in constructing certain parts of the apparatus, and to Mr. Ram Narain, the glass blower, for his ready assistance.

REFERENCES

CORSON, D. R., and WILSON, R. R., 1948, *Rev. Sci. Instrum.*, **19,** 207.
CRAGGS, J. A., and JAFFE, A. A. ,1947, *Phys. Rev.*, **72,** 784.
JÁNOSSY, L., 1948, *Cosmic Rays and Nuclear Physics* (London : The Pilot Press).
KORFF, S. A., 1948, *Electron and Nuclear Counters* (New York : D. Van Nostrand and Co.).
KORFF, S. A., and PRESENT, R. D., 1944, *Phys. Rev.*, **65,** 274.
KORFF, S. A., SPATZ, W. D. B., and HILBERRY, N., 1942, *Rev. Sci. Instrum.*, **13,** 127.
MAZE, R., 1946, *J. Phys. Radium*, **7,** 164.
MONTGOMERY, C. G., and D. D., 1940, *Phys. Rev.*, **57,** 1030.
OM PARKASH and SARNA, H. R., 1948, *Indian J. Phys.*, **22,** 19.
PUTMAN, J. L., 1948, *Proc. Phys. Soc.*, **61,** 312.
RAMSEY, W. E., 1940, *Phys. Rev.*, **57,** 1022.
ROSE, M. E., and KORFF, S. A., 1941, *Phys. Rev.*, **59,** 850.
STEVER, H. G., 1942, *Phys. Rev.*, **61,** 38.
TROST, A., 1937, *Z. Phys.*, **59,** 850.

The Pressure Broadening of the Vibration Rotation Band of the HCN Molecule at 10380 A.*

By G. KORTÜM† and H. VERLEGER

National Physical Laboratory, South African Council for Scientific and
Industrial Research, Pretoria

Communicated by B. F. J. Schonland; MS. received 8th August 1949

ABSTRACT. The relation between the line-width of the 0–3 vibration–rotation band of HCN at 10380 A. and the pressure of the HCN gas, as well as the pressure resulting from the addition of different extraneous gases, was investigated. In the P and R branches of the band a relation was found between the half-line width and the rotational quantum number, *J*, which differs for the broadening due to self-pressure and the broadening resulting from pressure of extraneous gases. The results could be explained, according to London's theory, in the former case as an effect due to the combined action of rotational resonance alignment, and in the latter case to alignment alone. Measurements made with the addition of DCN suggest that the chain association of the hydrogen bridge bonds also has an effect on the half-width value.

§ 1. INTRODUCTION

WAVE mechanics yields infinitely sharp energy states for a molecule which is quite unperturbed. In spite of this, spectral lines of a finite width are obtained for transitions between such energy states, even when the highest spectroscopic resolving power is utilized. This *natural line width*, which has an order of magnitude of 10^{-4} A., is the result of the interaction of the molecule with the radiation field. This interaction is explained classically in terms of the harmonic oscillator as the result of the energy radiation and the accompanying vibration damping (radiation damping); quantum mechanically it is explained by means of Heisenberg's uncertainty relation because the limited time during which the molecule is in the excited state gives rise to a consequent lack of sharpness of the excited states (Weisskopf and Wigner 1930). The line width resulting from the radiation damping is independent of the wavelength. In the case of moving molecules the Doppler effect causes an additional line broadening which is dependent on the temperature and larger than the natural line width (order of magnitude 10^{-2} A. at room temperature). Because these effects are small, they can only be studied quantitatively under special experimental conditions.

The *pressure-dependent broadening* of the spectral lines is caused by the interaction of the molecules. It is, therefore, a perturbation effect which results from the intermolecular forces. It therefore allows one to draw some conclusions about this interaction. The degree of broadening is strongly dependent on the density of packing of the molecules and is, for instance, of such a magnitude in the cases of liquids and solids that the spectral lines overlap completely to form the well-known broad bands associated with liquids which offer no information about the forces of interaction. In the case of gases, however, the pressure-dependent line broadening can be investigated systematically by the variation of the pressure or the addition of various extraneous gases, so that such measurements may lead to conclusions about the intermolecular forces.

---

* See preliminary communication in *Naturwissenschaften*, 1943, **31**, 44.

† Institute of Physical Chemistry, University of Tübingen.

In the theory of the pressure broadening one usually distinguishes between two different considerations: at relatively low pressures ($p \leqslant 1$ atmosphere) the period during which an absorbing or emitting molecule is in the sphere of influence of a neighbouring molecule is short in comparison with the average time of free flight. One is therefore justified in limiting the discussion to the interaction of two molecules on one another. This interaction can be considered as an impact which causes a change of phase in the radiation. During the period between two collisions the vibrations take place unhindered. This change in phase, like the radiation damping, causes a broadening of the spectral lines which is known as *collision damping*. According to the theory of Lorentz, this line broadening is symmetrical and proportional to the number of collisions and, therefore, proportional to the pressure. Its order of magnitude is about 0·1 to 1·0 cm^{-1}, which corresponds to about 0·1 to 1·0 A. in the photographic infra-red.

At higher pressures the emitting or absorbing molecule is practically always in the sphere of influence of one or more neighbouring molecules. The approximate form of the spectral line can be determined statistically (Burkhardt 1940); it is usually asymmetrical, that is, besides the broadening, a displacement of the spectral lines takes place also. The statistical line width is, in general, much smaller than the width caused by collision damping and must be taken into consideration only at high pressures.

In the measurements which are considered below, no pressures greater than one atmosphere were employed, so that it is legitimate to consider only the collision damping effect of Lorentz.

A number of authors (Watson and Margenau 1937, Cornell 1937, Lindholm 1938, 1939, Margenau 1939) have tried to explain the dependence of the rotational quantum number J and the half-width in molecular spectra theoretically on the basis of London's (1930) quantum mechanical theory and the intermolecular forces. According to London the perturbation energy between two molecules, separated by a distance r, can be given as

$$E = a/r^3 + b/r^6.$$

The effective optical diameter ρ of the molecules at the time of collision can be derived from the perturbation energy, and hence, using Lorentz's formula for collision damping, the half-width of the lines can be derived as

$$\nu_{\frac{1}{2}} = \rho^2 \bar{v} N,$$

where $\bar{v}$ is the average relative velocity of the molecules and N the number of molecules per unit volume.

According to London's theory, one distinguishes in the molecular interaction between dispersion forces, induction forces and pole forces.

The most general action of the dispersion effect which occurs between molecules is based on a short-period mutual perturbation of the molecules caused by the movement of the electrons. In every case it contributes to the pressure broadening, in particular to the term in $1/r^6$. Clearly, however, it cannot cause a corresponding line broadening. The pressure broadening effect in the absorption spectra of non-polar molecules such as C_2H_2 (Herzberg, Patat and Verleger 1938) might, however, be accounted for by this dispersion effect.

The influence of the induction effect caused by the polarization of the individual molecules by the electrical field of the electrical moments is, according to London, very small and can be ignored even in the case of molecules with large dipole moments.

On the other hand the pole forces, due to the electrostatic potential of the electrical moments corresponding to the individual molecules, make a contribution to the $1/r^6$ as well as to the $1/r^3$ term of the perturbation energy. The contribution to the latter term is particularly important because of the much greater range of these forces. This pole effect of London corresponds to the alignment effect of the earlier theory studied by Keesom.

The contribution of the alignment effect to the $1/r^6$ term is, according to London, also J-dependent. The two lowest rotational states are particularly strongly influenced because the r^{-6} law goes over into a r^{-3} law for small distances r. This strong interaction corresponds more or less to a parallel orientation of the molecules, or the transformation of the rotation into an oscillation about the equilibrium position. One can therefore expect an exceptionally large half-width for the first lines in both the P and R branches.

The contribution to the $1/r^3$ term is based on a resonance effect of a double nature. Resonance occurs in the usual sense in which the total excitation energy at the transition to the higher vibrational state is carried over to the neighbouring molecule. This entails a marked shortening of the life-time and a corresponding broadening of the energy term, similar to the observed self-pressure broadening of the electronic terms in atomic spectra. The half-width is furthermore proportional to the transition probability of the corresponding line. This effect is generally small in the case of molecules because of the large number of possible rotational and vibrational states, so that this resonance effect has little influence and can usually be neglected. Added to the above effect there is the rotational resonance between neighbouring rotational terms in the same vibrational term. This effect is essentially limited to the ground vibrational state because at room temperature almost all the molecules are in this vibrational state. A J-dependence of the half-width for the rotational resonance may be expected, because the probability of a neighbouring molecule having a J-value differing by one is the largest when the J-value corresponds to the maximum of the intensity distribution. Therefore the lines which result from transitions between the most densely populated rotational states should show the strongest broadening.

A rotational resonance between two corresponding rotational terms in different vibrational states is also possible but can be neglected, because the energy differences in the two vibrational states are not equal on account of the different moments of inertia in the two vibrational states. The condition for effective rotational resonance is that the difference in the rotational quantum numbers of the two molecules should not be equal to ± 1.

It must, furthermore, be kept in mind that in the case of absorption measurements an apparent broadening of the lines can be observed in contrast with the case of emission lines. This results from the fact that in all parts of a line of finite width the intensity depends exponentially on the number of absorbing molecules, that is, it depends on the pressure p and the length of the absorbing path d according to the equation

$$I = I_0 \exp(-kpd),$$

where I_0 is the intensity of the incident light and k the absorption coefficient. In the case of emission lines, however, the line width is independent of the thickness of the emitting column, because with increasing thickness the intensity of the emission lines is increased equally in all the different parts of the lines, and the intensity is proportional to the number of radiating molecules. This means that in the case of emission spectra the half-width of the line remains constant whereas in absorption spectra the line width increases with the number of absorbing molecules, that is, increases with p and d; in other words it means that intense lines appear more strongly broadened than weak lines. In order to get the real pressure-broadening it is therefore necessary to measure the broadening at different absorbing path lengths and extrapolate to $d=0$, except in the case where the absorption effect is weak enough to be negligible.

Herzberg and Spinks (1934), followed by other authors (Herzberg and Verleger 1934, Cornell 1937, Lindholm 1938), investigated the self-pressure broadening of the rotational band lines in HCN. They found that the half-widths of the rotational lines in the P branch of the parallel bands, which result from the C–H valence vibration, are dependent on the rotational quantum number J. They also found that the lines belonging to the most densely populated rotational states, and therefore the lines near the intensity maximum ($J=8$) of the band, experienced the strongest broadening, and that the half-width values decreased for both increasing and decreasing J-values. In the case of the vibration–rotation bands of some other polyatomic molecules, such as NH_3, a definite increase in line width with increasing pressure of the absorbing gas was also observed, but no J-dependence of this line-broadening could be established. Other molecules (e.g. CH_4) gave sharp lines under similar conditions (Verleger 1937).

Measurements on the 0–3 rotation–vibration band at 10380 A. were repeated for pressures between 75 and 550 mm. Hg. These measurements were extended to include also the R branch of the band. Further, in order to obtain clearer information about the intermolecular action and its influence on the sharpness of the energy states, the influence of pressure of added extraneous gases with reference to their dipole moments was investigated. A pressure broadening of the rotational lines depending on J was also found. It is, however, of a different type from the broadening caused by the increase of self-pressure.

§ 2. EXPERIMENTAL

The spectra were photographed in the first order of a 6-metre grating on freshly sensitized infra-red plates. The dispersion was 2·6 A/mm. A 400-watt tungsten point source, used in conjunction with a Schott R.G. 8 filter, served as light source. The gas was enclosed in a steel tube 10 cm. in diameter, equipped with glass windows. The lengths of the absorbing paths were 5, 10 and 20 metres, the slit width 0·055 mm. and the exposure times varied from 12 to 24 hours.

The photometry of the plates was carried out on a Zeiss recording microphotometer which gave an enlargement ratio of ten times on the recording paper graduated in millimetres. The half-widths of all the lines in the spectrograms were determined. In both the P and R branches 22 lines could be measured with sufficient accuracy. In the cases where individual lines overlapped as a result of excessive broadening, it was assumed that the lines were completely symmetrical and that the densities fell on the linear part of the density curve. With these assumptions the intensity curves of the individual lines were constructed from the density measurements and the half-widths determined from these constructed curves. This procedure was necessary especially in the case of the R branch, where the lines are closely spaced.

The HCN was prepared from $K_4Fe(CN)_6$ and H_2SO_4, dried over $CaCl_2$ and P_2O_5, liquefied and fractionally distilled. The HCN was sealed in Jena glass flasks. It kept quite clear for months. Before the photographs were taken the HCN was distilled from the storing flasks into the evacuated absorption tube. The DCN was prepared by the triple exchange of equimolar mixtures of HCN with 99·8% D_2O. The HCN was separated after each exchange from the mixture by fractional distillation. The D content of the resulting mixture was determined, after the exposure, by burning the gas over CuO and measuring the index of refraction of the resulting water. The result indicated that the gas contained 50·5 mol. per cent DCN.

To determine the influence of the DCN on the half-width values of the HCN bands, it was assumed that the different broadening effects are additive. The self-pressure broadening effect of the additional HCN to the DCN was deducted and the resultant half-width value was calculated for a pressure of 475 mm. of DCN by interpolation. The other gases which were used as additional gases, viz. nitrogen, nitrous oxide, propylene, hydrogen sulphide, dimethyl ether, sulphur dioxide and ethyl chloride, were prepared in the usual ways, carefully purified and dried before adding to the HCN.

Control measurements at a constant product $p \times d$ have shown that the absorption was weak enough to waive the extrapolation to $d = 0$.

§ 3. RESULTS

The self-pressure broadening of the HCN bands over the pressure range 75 mm. Hg to 550 mm. Hg is shown in Figure 1, which is a reproduction of the original spectrogram (see Plate).

In Figure 2 are shown the obtained half-width values in relation to the rotational quantum number J for the P and R branches.

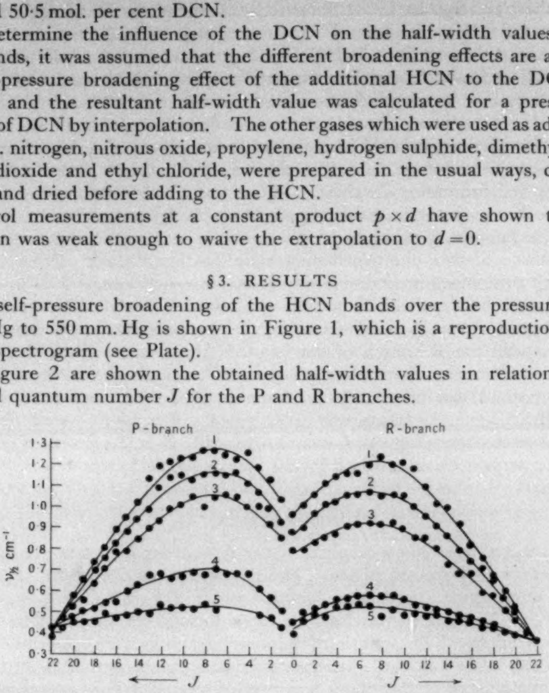

Figure 2. The half-width values of the absorption lines of the 0–3 band of HCN in relation to the rotational quantum number J of the P and R branch for different pressures of the absorbing gas.
1 : $p = 550$ mm. 2 : $p = 450$ mm. 3 : $p = 300$ mm. 4 : $p = 150$ mm. 5 : $p = 75$ mm.

The half-width values for both the branches reach a maximum in the density maximum of the band ($J \simeq 8$) and decrease with both decreasing and increasing quantum numbers. This is in agreement with earlier results. The rate of decrease in half-width for increasing J is, however, greater, especially for higher gas pressures. The absolute values of the half-widths for the R branch are, furthermore, always clearly smaller than those for the P branch. The half-width

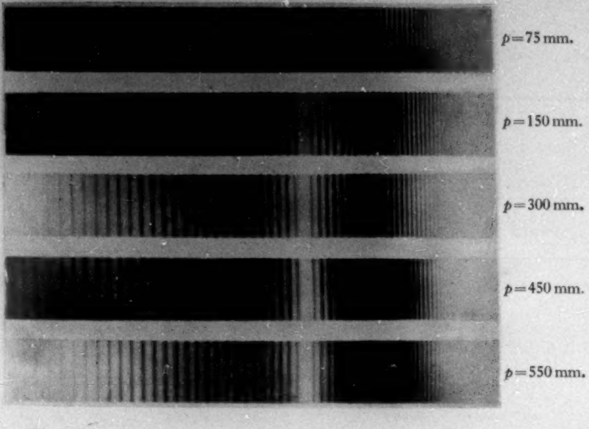
$p=75$ mm.
$p=150$ mm.
$p=300$ mm.
$p=450$ mm.
$p=550$ mm.

Figure 1. The 0–3 bands of the HCN molecules at different pressures of the absorbing HCN gas.*

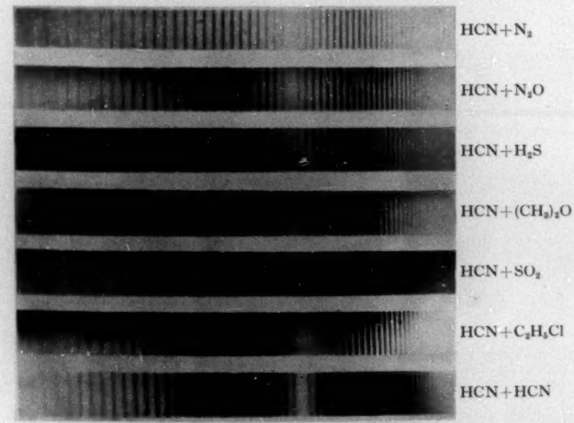
$HCN+N_2$
$HCN+N_2O$
$HCN+H_2S$
$HCN+(CH_3)_2O$
$HCN+SO_2$
$HCN+C_2H_5Cl$
HCN+HCN

Figure 4. The 0–3 band of HCN with the addition of various extraneous gases. p(HCN)=75 mm. Extraneous gas : $p=475$ mm.

---

* Figures 1 and 4 were reversed once only, so that the absorption lines appear as dark lines on a clear background.

values which have been averaged for all the band lines are strictly proportional to the pressure. This is shown in Figure 3.

In the measurement of the pressure-broadening of the HCN band by the addition of extraneous gases the HCN partial pressure was kept at 75 mm. and the total pressure at 550 mm. The results can therefore be compared with the self-pressure broadening of the HCN at 550 mm. of HCN. Figure 4 (see Plate) shows a reproduction of the original spectrograms, and in Figure 5 the half-width values deduced therefrom are plotted as a function of *J*.

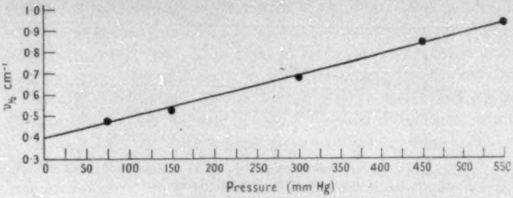

Figure 3. Mean values of the half-width values of all the rotational lines of a band in relation to the pressure of the absorbing HCN gas.

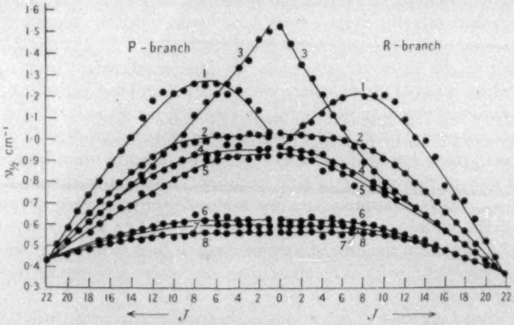

Figure 5. The half-width values of the absorption lines of the 0–3 band of HCN in relation to the rotational quantum numbers of the P and R branches when various extraneous gases are added. For the purpose of comparison the curve for p(HCN) = 550 mm. is also shown.*

1: $HCN + HCN$
2: $HCN + DCN$
3: $HCN + C_2H_5Cl$
4: $HCN + SO_2$
5: $HCN + (CH_3)_2O$
6: $HCN + H_2S$
7: $HCN + N_2O$
8: $HCN + N_2$

* The values of the dipole moments of the extraneous gases were, according to Debye: N_2, N_2O, C_3H_6, H_2S, $(CH_3)_2O$, SO_2, C_2H_5Cl, HCN = 0, 0·14, 0·35, 0·93, 1·32, 1·61, 2·05, 2·6 respectively.

The characteristic difference between the broadening effects of self-pressure and of extraneous gases is immediately apparent. In the case of the addition of extraneous gases, the half-width values are not greatest at intensity maximum of the band but reach a maximum for lines which result from transitions between energy states having low *J* values. The broadening decreases in both branches for increasing *J* values. This effect is particularly apparent in the case where ethyl chloride is added.

When a curve of the average half-width of all the lines of a band is drawn against the product of the dipole moments, μ(added gas) $\times \mu'$(HCN), the curve shown in Figure 6 is obtained. From the curve it follows that at first the half-width values change slowly for small μ. For $\mu > 0{\cdot}75$ ($\mu\mu' > 2$) the variation with the product of the dipole moments is almost linear.

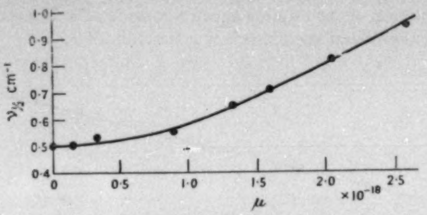

Figure 6. Averages of the half-width values of all the rotational lines drawn against the product of the dipole moments.

If one tries to explain the observed results according to London's theory, one must, firstly, remember that of the three possible active forces the dispersion and induction effects can only cause a small broadening of all the rotational lines but, secondly, cannot cause a J-dependent line-broadening. The strong J-dependent broadening of the lines can therefore be attributed solely to the alignment effect, to which is added the resonance effect in the case of self-pressure broadening.

If a rotational quantum number J_1 is assumed for an absorbing molecule in the ground vibrational state and a rotational quantum number J_2 for a neighbouring perturbing molecule, which is also in the ground vibrational state, then the difference in rotational quantum numbers, before absorption, is given by $\Delta J = J_2 - J_1$. After absorption, the first molecule is in a higher vibrational state and has, in the case where the transition resulted in a P line, the rotational quantum number $J_1 - 1$ and, in the case of a transition resulting in a R line, the rotational quantum number $J_1 + 1$. Therefore, the respective differences in rotational quantum after absorption will be $\Delta J + 1$ and $\Delta J - 1$.

If an absorbing molecule collides with such perturbing molecules so that $\Delta J \neq 0, \pm 1, \pm 2$, then the perturbations can be treated according to the alignment effect. If, however, the absorbing molecule collides with such disturbing molecules for which $\Delta J = \pm 1$, then a resonance effect is active before absorption and an alignment effect after absorption. In the case of $\Delta J = 0, \pm 2$, the alignment effect can be expected in the ground state and rotational resonance in the upper state. Because the moments of inertia in the upper and lower vibrational states differ, the collisions are termed 'diffuse degeneration' and 'diffuse resonance' respectively.

Lindholm (1938, 1939) calculated the influence of the alignment effect ($\Delta J \neq 0, \pm 1, \pm 2$) on the P lines of the HCN bands at 7952 A. and 8363 A. from London's formula. He found that the line width depends on J in such a manner that it reaches its maximum in the centre of the branch and decreases for both decreasing and increasing rotational quantum numbers. In the case of resonance ($\Delta J = \pm 1$) a curve is obtained with larger absolute values than those of the alignment effect and in which the J-dependence is more distinctly recognized. The same applied for the 'diffuse resonance' ($\Delta J = \pm 2$), where the differences in moments of inertia in the upper and lower states have an influence. These calculations were also made for both the branches of the vibration–rotation band of HCl at 9152 A., where the additional result was obtained that the curve for the P branch lies higher than the one for the R branch.

Comparing these qualitative results with the results obtained here, it is immediately clear that the effect of the self-pressure is actually at its strongest at $J \simeq 8$, and that the energy terms belonging to the most densely populated rotational states are the most strongly perturbed. The half-width values in the P and R branches decrease from this maximum value towards smaller and larger rotational quantum numbers. The rate of decrease in intensity towards the smaller rotational quantum numbers is a little slower than towards the larger numbers. The absolute values of the half-widths in the P branch are larger than the corresponding line widths in the R branch. This observation can actually be attributed to the superposed action of the alignment effect and the rotational resonance.

In the case of the addition of extraneous gases the resonance effect is reduced of course, so that the curve obtained there can actually be explained by the alignment effect. The distribution of the half-width values amongst the J-values in the presence of extraneous molecules shows such a J-dependence that the half-width values decrease faster with increasing J-values. The states having the smaller J-values are, as expected, strongly influenced by the addition of extraneous gases with increasing dipole moments. The curves for the P and R branches lie at the same height in the case of the addition of extraneous gases.

An exception is furnished by the case of the addition of DCN as extraneons gas, in so far as the curve does not lie above the curve for ethyl chloride in accordance with the larger dipole moment ($\mu(\mathrm{DCN}) \simeq \mu(\mathrm{HCN})$) but between ethyl chloride and sulphur dioxide. Possibly a predominant rôle is played by a hydrogen bond effect in addition to the alignment effect. Later measurements have shown the hydrogen bond effect to contribute to the strong chain association of the HCN molecules and the extraordinarily large dielectric constant of liquid HCN.* This effect occurs to the same extent for both HCN and DCN molecules.

---

* According to vapour density measurements of W. F. Giauque and R. A. Ruehrwein (*J. Amer. Chem. Soc.*, 1939, **61**, 2626), HCN consists of about 10% dimer, 2·7% trimer and 0·6% tetramer molecules at atmospheric pressure.

REFERENCES

Burkhardt, G., 1940, *Z. Phys.*, **115**, 592.
Cornell, S. D., 1937, *Phys. Rev.*, **51**, 739.
Herzberg, G., Patat, F., and Verleger, H., 1936, *Z. Phys.*, **102**, 1.
Herzberg, G., and Spinks, J. W. T., 1934, *Proc. Roy. Soc.* A, **147**, 434.
Herzberg, G., and Verleger, H., 1934, *Verh. dtsch. Phys. Ges.*, **15**, 17.
Lindholm, E., 1938, *Z. Phys.*, **109**, 223; 1939, *Ibid.*, **113**, 596.
London, F., 1930, *Z. Phys.*, **63**, 245.
Margenau, H., 1939, *Rev. Mod. Phys.*, **11**, 1.
Verleger, H., 1937, *Phys. Z.*, **38**, 83.
Watson, W. W., and Margenau, H., 1937, *Phys. Rev.*, **51**, 48.
Weisskopf, V., and Wigner, E., 1930, *Z. Phys.*, **63**, 54.

The Vibration–Rotation Bands of the Hydrogen Halides HF, $H^{35}Cl$, $H^{37}Cl$, $H^{79}Br$, $H^{81}Br$ and $H^{127}I$

By S. M. NAUDÉ and H. VERLEGER
National Physical Laboratory, South African Council for Scientific and Industrial Research, Pretoria, South Africa

Communicated by B. F. J. Schonland; MS. received 8th August 1949

ABSTRACT. The 2–0, 3–0 and 4–0 bands of $^1H^{19}F$, the 4–0 and 5–0 bands of $^1H^{35}Cl$ and $^1H^{37}Cl$, the 4–0 band of $^1H^{79}Br$ and $^1H^{81}Br$, and the 4–0 band of $^1H^{127}I$ were photographed under great dispersion in the infra-red. The molecular constants have been calculated and are summarized in a table.

§ 1. INTRODUCTION

In the course of a research programme on the structure of polyatomic molecules, whose vibration–rotation spectra in the photographic infra-red permit a definite interpretation of the geometric configuration of the individual atoms in the molecular system, we have also photographed a number of unknown harmonic bands of the diatomic molecules $^1H^{19}F$, $^1H^{35}Cl$, $^1H^{37}Cl$, $^1H^{79}Br$, $^1H^{81}Br$ and $^1H^{127}I$. It seemed valuable to us to calculate the constants of these molecules again from the new and improved data.

The bands were photographed in the first and partly also in the second order of a 6-metre grating on special re-sensitized infra-red plates. The dispersion was 2·6 A. in the first and 1·3 A. per mm. in the second order. The light-source was either a 1,000-watt pointolite or the sun, using a heliostat. A special mirror arrangement and an infra-red filter was used. A 12-metre long galvanized tube which consisted of several lengths which could be put together served as absorption tube. The light could be sent by mirrors backwards and forwards through the tube up to seven times, so that the maximum length of the absorption path was 84 metres.* The steel tube was closed at both ends by windows of Plexiglass which is very resistant to the hydrogen halides. The hydrogen halides diffuse a little into the surface of the windows but cause no fogging of the windows. Care had, however, to be taken that when the gases were changed the windows were either replaced or the plates cleaned. This was best accomplished by turning off the first few layers in a lathe and repolishing the surface. The exposures lasted up to 60 hours. The photographs were taken at room temperature (28° c.).

The wavelengths were determined by measuring the plates against iron standard lines photographed in the third or fourth orders of the grating. The accuracy of the determinations may have reached $\pm 0{\cdot}01\ \mathrm{cm}^{-1}$; the third decimal places are, however, given in the tables. It is difficult to draw definite conclusions about a possible temperature shift of the Fe lines (photographed at the start) relative to the absorption lines during the long exposure times. It is believed that this possible source of error is not important in this case.

---

* We are preparing a 25-m.-long absorption tube which will allow a light beam to traverse it up to 40 times. This will correspond to an absorption path of 1,000 m.

The atmospheric bands which lie in the photographic infra-red region were photographed separately. In this way these lines could be eliminated and a definite determination of the partly superposed absorption bands was greatly simplified.

The gases were prepared according to the usual methods and were purified by repeated re-distillation, and were finally distilled into an evacuated absorption tube.

The 2–0, 3–0 and 4–0 bands of the $^1H^{19}F$, the 4–0 and 5–0 bands of the $^1H^{35}Cl$ and $^1H^{37}Cl$, the 4–0 bands of the $^1H^{79}Br$ and $^1H^{81}Br$, and the 4–0 band of the $^1H^{127}I$ were photographed for the first time. On the other hand, the attempt to find the corresponding harmonic bands of CO failed.

For each molecule the wave-numbers of the new lines, the combination differences for the ground state of all known bands, which gives a measure of the accuracy of the measurements, the calculated vibration levels together with the results of previous investigations and a summary of the newly determined molecular constants are given in the tables.

The molecular constants are calculated with the new values of the fundamental constants according to Birge (1941). Values of wave-numbers are corrected to vacuum. It is believed that the results given here are in some cases more accurate than those published previously owing to the greater dispersion employed here.

§ 2. HYDROGEN FLUORIDE

Besides the vibration–rotation absorption spectra of the diatomic molecules $^1H^{35}Cl$ and $^1H^{37}Cl$, the spectrum of $^1H^{19}F$ has been investigated most thoroughly in the infra-red. The 1–0 band was measured by Imes (1919) and recalculated by Czerny (1927). Schaefer and Thomas (1923) found that the centre of the 2–0 band, which could not be resolved by them, lies at 1·27μ. There also exist analyses by Kirkpatrick and Salant (1935) of the 3–0 and 4–0 bands which lie in the photographic infra-red.

Our results for the 2–0, 3–0 and 4–0 bands are given in Tables 1, 2 and 3.

Table 1. 2–0 Band of $^1H^{19}F$

J	$R(J)$	$P(J)$
0	7789·730	—
1	7824·742	7710·824
2	7856·833	7666·526
3	7885·894	7619·486
4	7911·830	7569·704

Table 2. 3–0 Band of $^1H^{19}F$

J	$R(J)$	$P(J)$
0	11409·047	—
1	11441·206	11331·161
2	11468·679	11285·843
3	11491·449	11235·948
4	11509·490	11181·550
5	11522·781	11122·989
6	11531·282	11060·232
7	11534·920	—

Table 3. 4–0 Band of $^1H^{19}F$

J	$R(J)$	$P(J)$
0	14866·625	—
1	14895·680	14790·435
2	14918·894	14743·420
3	14935·820	14690·427
4	14946·702	14631·771
5	14951·654	14567·358

Table 4. Combination Differences for the Ground State, $v=0$, $^1H^{19}F$.
$\Delta_2F''(J)=R(J-1)-P(J+1)$

J	Naudé and Verleger			Kirkpatrick and Salant		Czerny and Imes
	2–0	3–0	4–0	3–0	4–0	1–0
1	123·204	123·204	123·205	123·21	123·20	122·92
2	205·256	205·258	205·253	205·25	205·24	205·21
3	287·129	287·129	287·123	286·95	287·06	286·08
4	—	368·460	368·462	368·27	368·32	366·50
5	—	449·258	449·269	449·57	—	446·78

Table 5. Position of the Vibration Levels, $^1H^{19}F$

v	Naudé and Verleger	Kirkpatrick and Salant	Czerny and Imes	Schaefer and Thomas
1	3962·960	—	3962·565	—
2	7751·766	—	—	7874·02
3	11372·574	11372·88	—	—
4	14831·550	14831·68	—	—

Table 6. Molecular Constants of $^1H^{19}F$

$B_0=20{\cdot}5352$ cm^{-1}
$B_1=19{\cdot}7870$
$B_2=19{\cdot}0249$
$B_3=18{\cdot}2876$
$B_4=17{\cdot}5609$
$B_e=20{\cdot}9093$
$D_e=0{\cdot}00108$
$\alpha_e=0{\cdot}7482$
$\beta_e=0{\cdot}0002$

$I_e=1{\cdot}3385\times10^{-40}$ gm.cm^2
$r_e=0{\cdot}9179\times10^{-8}$ cm.
$\omega_e=4143{\cdot}01$ cm^{-1}
$\omega_ex_e=91{\cdot}69$
$\omega_ey_e=1{\cdot}03$
$k_e=9{\cdot}68\times10^5$ dyne/cm.

$$\left.\begin{array}{l}\text{Dissoc. energy}\\ \text{(computed from}\\ \omega_e,\ \omega_ex_e)\end{array}\right\}\begin{array}{l}=133{\cdot}76\text{ kcal/mol.chem.}\\ =5{\cdot}8\text{ ev.}\end{array}$$

The discrepancy between the results of Schaefer and Thomas (1923) and ours for the 2–0 band can only be ascribed to the small sensitivity of the method of registration used by them.

§ 3. HYDROGEN CHLORIDE

The 1–0 and 2–0 bands of both isotope molecules in the thermal infra-red were measured by Meyer and Levin (1929). Herzberg and Spinks (1934) studied the 3–0 band in the photographic infra-red. This was the first vibration-rotation spectrum of a diatomic molecule to be thoroughly investigated in this region. Cleaves and Edwards (1935) announced in a short paper the photography of the 4–0 band, but gave no analysis. Lindholm (1942) investigated the pressure broadening of this band without giving detailed data about the molecular constants.

Table 7. 4–0 Band of $^1H^{35}Cl$

J	$R(J)$	$P(J)$
0	10941·276	—
1	10957·329	10901·918
2	10971·009	10878·608
3	10982·288	10852·957
4	10991·217	10824·972
5	10997·801	10794·691
6	(11002·001)	10762·103

Table 8. 5–0 Band of $^1H^{35}Cl$

J	$R(J)$	$P(J)$
0	13413·117	—
1	13427·969	13374·368
2	13439·830 s	13350·453
3	13448·721	13323·558
4	13454·632	13293·683
5	13457·586	13260·927

s = superposed.

Table 9. 4–0 Band of $^{1}H^{37}Cl$

J	$R(J)$	$P(J)$
0	10933·759	—
1	10949·804	10894·464
2	10963·451	10871·232
3	10974·738	10845·594
4	10983·664	10817·561
5	10990·220	10787·188

Table 10. 5–0 Band of $^{1}H^{37}Cl$

J	$R(J)$	$P(J)$
0	13404·128	—
1	13418·976	13365·472
2	13430·840	13341·608
3	13439·743 s	13313·777
4	13445·686	13285·005

s = superposed.

Table 11. Combination Differences for the Ground State, $v=0$, $^{1}H^{35}Cl$

	Naudé and Verleger		Herzberg and Spinks	Meyer and Levin	
J	4–0	5–0	3–0	1–0	2–0
1	62·668	62·664	62·626	62·69	63·00
2	104·372	104·411	104·311	104·29	104·16
3	146·037	146·147	145·994	146·03	146·04
4	187·597	187·794	187·507	187·45	187·61
5	229·114	—	228·994	228·87	228·84

Table 12. Combination Differences for the Ground State, $v=0$, $^{1}H^{37}Cl$

	Naudé and Verleger		Herzberg and Spinks	Mayer and Levin	
J	4–0	5–0	3–0	1–0	2–0
1	62·527	62·520	62·599	62·57	62·99
2	104·210	104·199	104·132	104·18	104·03
3	145·890	145·835	145·780	145·83	146·02
4	187·550	—	187·233	187·31	187·52

Table 13. Position of Vibration Levels, $^{1}H^{35}Cl$

v	Naudé and Verleger	Herzberg and Spinks	Meyer and Levin
1	2886·194	—	2885·88
2	5668·526	—	5667·96
3	8347·199	8347·200	—
4	10922·636	—	—
5	13395·204	—	—

Table 14. Position of Vibration Levels, $^{1}H^{37}Cl$

v	Naudé and Verleger	Herzberg and Spinks	Meyer and Levin
1	2883·473	—	2883·87
2	5663·881	—	5663·96
3	8341·182	8341·186	—
4	10915·332	—	—
5	13386·288	—	—

Both the isotope molecules $^{1}H^{35}Cl$ and $^{1}H^{37}Cl$, which differ in their masses but not in their atomic numbers, must have the same force constants and nuclear distances owing to the identity of the electron motions. On the other hand the vibrational frequencies and the rotational terms must be different as a result of their different masses.

In the case of the isotope effect observed here, one has to deal essentially with a vibrational isotope effect on which is superposed a much smaller rotational isotope effect.

By introducing a factor $\rho=\sqrt{(\mu/\mu_1)}$ the isotope shift due to the vibration can be calculated from

$$\Delta\nu_v=\nu_v^{1}-\nu_v=(\rho-1)\omega_e[(v'+\tfrac{1}{2})-(v''+\tfrac{1}{2})]-(\rho^2-1)\omega_e x_e[(v'+\tfrac{1}{2})^2-(v''+\tfrac{1}{2})^2],$$

where ν_v and ν_v^{1} indicate the frequency of the corresponding bands.

Table 15. Molecular Constants for $^1H^{35}Cl$ and $^1H^{37}Cl$

	$^1H^{35}Cl$	$^1H^{37}Cl$
B_0	10·4440 cm^{-1}	10·4204 cm^{-1}
B_1	10·1445	10·1213
B_2	9·8450	9·8221
B_3	9·5343	9·5230
B_4	9·2615	9·2275
B_5	8·9462	8·9197
B_e	10·5937	10·5700
D_e	0·000533	0·000532
α_e	0·2995	0·2992
β_e	0·000004	0·000004
I_e	$2·6409 \times 10^{-40}$ gm.cm^2	$2·6477 \times 10^{-40}$ gm.cm^2
r_e	$1·2744 \times 10^{-8}$ cm.	$1·2750 \times 10^{-8}$ cm.
ω_e	2990·57 cm^{-1}	2986·50 cm^{-1}
$\omega_e x_e$	52·26	51·50
$\omega_e y_e$	0·06	−0·01
k_e	$5·16 \times 10^5$ dyne/cm.	$5·15 \times 10^5$ dyne/cm.
Dissoc. energy	122·28 kcal/mol. chem.	123·75 kcal/mol. chem.
(from ω_e, $\omega_e x_e$)	5·30 ev.	5·37 ev.

For the rotational part of the isotope effect, which has the result that the isotope effect of corresponding band lines are not the same but are increasingly shifted, one gets

$$\Delta\nu_r = \nu_r^{\,i} - \nu_r = (\rho^2 - 1)[\nu_r - \tfrac{1}{2}\alpha\{(v' + \tfrac{1}{2})(J' + \tfrac{1}{2})^2 - (v'' + \tfrac{1}{2})(J'' + \tfrac{1}{2})^2\}$$
$$+ D_e\{(J' + \tfrac{1}{2})^4 - (J'' + \tfrac{1}{2})^4\}].$$

ν_r denotes the rotational portion of the wave number of a line.

The good agreement of the isotope shifts can be seen from the following table, where the average of the measured displacements for all the lines of the 1–0, 2–0, 3–0, 4–0 and 5–0 bands are compared with the theoretical displacements.

Table 16. Observed and Calculated Vibrational Isotope Shifts in the Infra-red Hydrogen Chloride Bands

Band	Observed	Calculated	Observer
1–0	2·01	2·105	Meyer and Levin
2–0	4·00	4·053	Meyer and Levin
3–0	5·834	5·854	Herzberg and Spinks
4–0	7·490	7·481	Naudé and Verleger
5–0	8·899	8·907	Naudé and Verleger

By determining the factor $\rho = \sqrt{(\mu/\mu_i)}$ it is possible to obtain an accurate value for the mass ratio of the participating molecules and to compare the value obtained with Aston's value. This determination can be made from the vibrational or the rotational isotope effect, but can also be found by comparison of the molecular constants, for we have, for example,

$$B_e^{\,i} = \rho^2 B_e\,; \qquad \alpha_e^{\,i} = \rho^3 B_e^{\,i}; \qquad D_e^{\,i} = \rho^4 D_e.$$

A simple computation shows that Aston's values are verified by the observed isotope effects and, furthermore, that his values are more accurate than assumed by him. Herzberg and Spinks (1934), as well as Jenkins and McKellar (1932), have pointed this out before.

We intend to investigate the isotope effects of the deuterium halides separately.

§4. HYDROGEN BROMIDE

Plyler and Barker (1933) have photographed and analysed the 1–0 and 2–0 bands of the HBr molecule most recently. The resolution of their arrangement did not, however, suffice to establish independent equations for the isotopic molecules $^1H^{79}Br$ and $^1H^{81}Br$.

The 4–0 band was the only one which we could photograph with the isotope effect clearly visible. Of the 3–0 band at 13500 A. only two to three lines of the R branch could be observed, and we could find no absorption of the 5–0 band which lies at 8130 A.

Table 17. 4–0 Band of $^1H^{79}Br$

J	$R(J)$	$P(J)$
0	9709·392	—
1	9722·501	9677·765
2	9733·817	9659·230
3	9743·351	9638·898

Table 18. 4–0 Band of $^1H^{79}Br$

J	$R(J)$	$P(J)$
0	9708·020	—
1	9721·123	9676·405
2	9732·484	9657·878
3	9742·048	9637·554

Table 19. Combination Differences for the Ground State $v=0$, $^1H^{79}Br$ and $^1H^{81}Br$

	Naudé and Verleger		Plyler and Barker	
J	4–0 ($^1H^{79}Br$)	4–0 ($^1H^{81}Br$)	1–0 ($^1H^{79,81}Br$)	2–0 ($^1H^{79,81}Br$)
1	50·162	50·142	50·04	49·97
2	83·603	83·569	83·37	83·30

Table 20. Molecular Constants of $^1H^{79}Br$ and $^1H^{81}Br$

	$^1H^{79}Br$	$^1H^{81}Br$
ν (4–0)	9694·495 cm^{-1}	9693·151 cm^{-1}
B_0	8·360	8·357
B_4	7·454	7·439
B_e	8·473	8·471
α_e	0·226	0·229
D_e	0·000372	0·000378
β_e	0·000002	0·000003
I_e	$3·303 \times 10^{-40}$ gm.cm^2	$3·304 \times 10^{-40}$ gm.cm^2
r_e	$1·414 \times 10^{-8}$ cm.	$1·414 \times 10^{-8}$ cm.

The ω_e, $\omega_e x_e$ and $\omega_e y_e$ values cannot be computed on the basis of these bands, because the data of Plyler and Barker (1933) for the 1–0 and 2–0 bands correspond to an average value for the two bromine isotopes. If one assumes $\omega_e = 2649·67$ and $\omega_e x_e = 45·21$ according to Plyler and Barker, one gets $\nu = 9694·5$ for the 4–0 band, which corresponds to the value found for $^1H^{79}Br$.

The computed vibrational isotope shift is 1·34 cm^{-1}, whereas the average taken over all the lines of the 4–0 band amounts to 1·35 cm^{-1}.

§5. HYDROGEN IODIDE

The 1–0 and 2–0 bands of $^1H^{127}I$ were investigated successfully by A. H. and H. H. Nielsen (1935). Just as in the case of the hydrogen bromides, only a few lines of the 4–0 band could be photographed on account of the strong decrease in the intensity of the harmonic bands. Together with the results of Nielsen and Nielsen they suffice, however, to carry out a calculation of the molecular constants.

Table 21. 4–0 Band of $^1H^{127}I$

J	$R(J)$	$P(J)$
0	8454·972	—
1	8464·976	8430·608
2	8473·514	8416·213
3	8480·608	8400·378

Table 22. Combination Differences for the Ground State $v=0$, $^1H^{127}I$

	Naudé and Verleger	Nielsen and Nielsen	
J	4–0	1–0	2–0
1	38·759	38·51	39·27
2	64·598	64·22	65·24

Table 23. Position of the Vibrational Levels, $^1H^{127}I$

v	Naudé and Verleger	Nielsen and Nielsen
1	2230·07	2230·08
2	4380·68	4380·71
3	6451·83	—
4	8443·52	—

Table 24. Molecular Constants of $^1H^{127}I$

$B_0=6{\cdot}460$ cm^{-1}
$B_4=5{\cdot}729$
$B_e=6{\cdot}551$
$\alpha_e=0{\cdot}183$
$D_e=0{\cdot}000213$
$\beta_e=0{\cdot}000003$

$I_e=4{\cdot}272=10^{-40}$ gm.cm^2
$r_e=1{\cdot}604\times10^{-8}$ cm.
$\omega_e=2309{\cdot}53$ cm^{-1}
$\omega_e x_e=39{\cdot}73$
$k=3{\cdot}14\times10^5$ dyne/cm.
$\left.\begin{array}{r}\text{Dissoc. energy}\\ \text{(from } \omega_e, \omega_e x_e\text{)}\end{array}\right\}\begin{array}{l}=95{\cdot}93 \text{ kcal/mol. chem.}\\ =4{\cdot}2 \text{ ev.}\end{array}$

According to theoretical considerations it could be expected that the intensities of the harmonic bands of HF would diminish increasingly as one proceeds successively to HCl, HBr and HI, and that the harmonic bands of the last molecule would not be observed in the region which we were able to photograph. Actually, however, it was possible to obtain plates also of the 4–0 band of HI.

An accurate comparison of the intensities of the four hydrogen halides of a given harmonic band has not been carried out. However, considering the fact that for $^1H^{35}Cl$, and even for $^1H^{37}Cl$, the highest harmonic vibrational bands were found and that their intensities were not so much less than could be expected according to theoretical considerations based on the intensity of the corresponding HF bands, it seems as if this missing intensity difference can be understood by an association of a part of the HF molecules to form double molecules. A band which would correspond to $(HF)_n$ could, however, not be observed with certainty. The 4–0 bands of HBr and HI are indeed substantially weaker than the corresponding bands of HCl and HF, but nevertheless, especially in the case of HI, not so weak as would be expected from the suspected approximate homopolar character of the bond of this molecule. The non-appearance of the CO bands in this spectral region remains completely inexplicable in this connection, for their intensities should have sufficed according to the above considerations.

After completing a larger absorption installation it is hoped to extend the above results and to continue the investigation of polyatomic molecules. By means of a shorter absorption tube we have already found new or additional absorption bands in the case of methyl cyanide ($H_3C–C{\equiv}N$), azomethane ($H_3C–N{=}N–CH_3$) and methyl acetylene ($H_3C–C{\equiv}CH$).

ACKNOWLEDGMENT

This paper is published with the permission of the South African Council for Scientific and Industrial Research.

REFERENCES

Birge, R. T., 1941, *Rev. Mod. Phys.*, **13**, 233.
Cleaves, A. R., and Edwards, C. W., 1935, *Phys. Rev.*, **48**, 850.
Czerny, M., 1927, *Z. Phys.*, **45**, 476.
Herzberg, C., and Spinks, J. W. T., 1934, *Z. Phys.*, **89**, 474.
Imes, E. S., 1919, *Astrophys. J.*, **50**, 251.
Jenkins, E. A., and McKellar, A., 1932, *Phys. Rev.*, **39**, 549.
Kirkpatrick, D. E., and Salant, E. O., 1935, *Phys. Rev.*, **48**, 945.
Lindholm, E., 1942, *Dissertation*, Stockholm.
Meyer, C. F., and Levin, A. D., 1929, *Phys. Rev.*, **34**, 44.
Nielsen, A. H., and Nielsen, H. H., 1935, *Phys. Rev.*, **47**, 585.
Plyler, E. K., and Barker, E. F., 1933, *Phys. Rev.*, **44**, 984.
Schaefer, Cl., and Thomas, M., 1923, *Z. Phys.*, **12**, 330.

Calculation of the Correction for Instrumental Broadening in X-ray Diffraction Lines

By M. S. PATERSON*
Cavendish Laboratory, Cambridge

Communicated by E. Orowan; MS. received 21st June 1949, *and in amended form 2nd November* 1949

ABSTRACT. A new numerical procedure, based on relaxation methods, for calculating the correction for instrumental broadening in x-ray diffraction lines has been evolved. The corrected integral breadth and the true line profile are obtained without restrictive assumptions. The calculations for a practical example are given.

§ 1. INTRODUCTION

In x-ray line-broadening studies, it is required to correct for the broadening due to 'instrumental' factors in the measured intensity distribution curve of the line; the line broadening obtained under similar geometrical conditions from an annealed specimen is often taken as a measure of this instrumental broadening. The problem has been clearly stated by Jones (1938) and involves solving the simple integral equation (1) given below. Recently, Stokes (1948) has published a method of solution, using Fourier analysis, which avoids the special assumptions regarding the form of the solution that have been made by previous workers. The present paper will describe briefly the numerical method that the author has used for solving the problem. It is very simple and direct, although in its present form it may take a slightly longer time than Stokes' method when means of rapid Fourier analysis are available. However, it may be of interest to describe it since it has the same general applicability, yielding the true line shape as well as its breadth.

---

* Now at Department of Supply and Development, Division of Aeronautics, Melbourne.

§ 2. DESCRIPTION OF THE METHOD

For the sake of uniformity, the notation will follow that of Jones (1938) in most respects. The shapes of the intensity distribution curves of x-ray diffraction lines with instrumental broadening, with intrinsic broadening (for example, that resulting purely from cold work), and with combined broadening (as measured on cold-worked metal) are represented respectively by the functions $f(x)$, $F(x)$, and $g(x)$ where the variable x represents, for example, distance along the x-ray film; these functions are assumed to have maximum values of unity. The integral breadths of the lines are then defined by

$$b=\int f(x)\,dx, \qquad \beta=\int F(x)\,dx, \qquad \text{and} \qquad B=\int g(x)\,dx,$$

respectively.

From Jones' analysis, it follows that the shape of the intensity distribution curve for a diffraction line with combined broadening is given by

$$g(\xi)=\frac{B}{b\beta}\int F(x)f(\xi-x)\,dx, \qquad \ldots\ldots(1)$$

ξ being used here for the variable in $g(x)$. The functions $g(x)$ and $f(x)$ are known, for example, from photometer measurements, so the problem is to solve the equation (1) for $F(x)$, which represents the true broadening. In order to do this, equation (1) may be approximated by the set of linear equations

$$g(\xi_j)=\sum_i 2l\frac{B}{b\beta}F_a(x_i)f_a(\xi_j-x_i), \qquad \ldots\ldots(2)$$

where $F_a(x_i)$ and $f_a(\xi_j-x_i)$ are then mean values of $F(x)$ and $f(x)$ over the intervals $x=x_i-l$ to x_i+l and $x=\xi_j-x_i-l$ to ξ_j-x_i+l, respectively, the distance between successive x_i being $2l$; the ξ_j are a discrete set of values of ξ, and the summation is taken over all values of i for which $F_a(x_i)$ and $f_a(\xi_j-x_i)$ have appreciable values. For any set of ξ_j and x_i, the values of $g(\xi_j)$ and $f_a(\xi_j-x_i)$ are known and the set of linear equations (2) can then be solved for $(B/b\beta)F_a(x_i)$. Since $g(x)$ and $f(x)$ are very small for large values of $|x|$, the range of values of ξ_j and x_i that need be considered is restricted.

As an example, suppose that the only non-zero values of $f_a(x_i)$ and $g(\xi_j)$ are $f_a(-1)$, $f_a(0)$, $f_a(1)$ and $g(-3)$, $g(-2)$, $g(-1)$, $g(0)$, $g(1)$, $g(2)$, $g(3)$, where x_i and ξ_j are chosen at the same, equal, intervals and the units are chosen so that $2l=1$. Then the set of equations (2) becomes

$$\left.\begin{array}{lr}
f_a(-1)F_a'(-2) & =g(-3)\\
f_a(0)F_a'(-2)+f_a(-1)F_a'(-1) & =g(-2)\\
f_a(1)F_a'(-2)+f_a(0)F_a'(-1)+f_a(-1)F_a'(0) & =g(-1)\\
\qquad f_a(1)F_a'(-1)+f_a(0)F_a'(0)+f_a(-1)F_a'(1) & =g(0)\\
\qquad\qquad f_a(1)F_a'(0)+f_a(0)F_a'(1)+f_a(-1)F_a'(2) & =g(1)\\
\qquad\qquad\qquad f_a(1)F_a'(1)+f_a(0)F_a'(2) & =g(2)\\
\qquad\qquad\qquad\qquad f_a(1)F_a'(2) & =g(3)
\end{array}\right\} \qquad \ldots\ldots(3)$$

(Here, $F_a'(x_i)\equiv(B/b\beta)F_a(x_i)$.) It is readily seen that $F_a'(x_i)$ must be zero for $|x_i|>2$, for if it were not, the $f(x)$ curve would be broadened to a curve $g(\xi)$ having non-zero values for $|\xi_j|>3$.

A direct method of dealing with the set of equations (2) would consist of solving the first equation for $F_a'(-2)$, then using this result to solve the second equation for $F_a'(-1)$, and so on. Such a procedure is very unsatisfactory, however, for the important values of $F_a'(x_i)$ near its maximum will be greatly influenced by the values of $f(x)$ and $g(x)$ at their extremities where the photometer curves are most unreliable. The method to be described permits the main attention to be given to the important values of $F_a'(x_i)$, yielding a solution of best fit which is not unduly influenced by small errors in the photometer measurements.

The simultaneous equations (2) are solved by the procedure of successive approximation which is the basis of the relaxation methods developed by Sir Richard Southwell and co-workers (Southwell 1940, 1946, Shaw 1946). Since the present application is a very simple one and its physical significance can readily be seen, a brief description will be given.

Consider the set of equations

$$\left.\begin{array}{ll}
g(-3)-(f_a(-1)F_a'(-2) &)=\mathrm{R}(-3)\\
g(-2)-(f_a(0)F_a'(-2)+f_a(-1)F_a'(-1) &)=\mathrm{R}(-2)\\
g(-1)-(f_a(1)F_a'(-2)+f_a(0)F_a'(-1)+f_a(-1)F_a'(0) &)=\mathrm{R}(-1)\\
g(0)\;-(\quad f_a(1)F_a'(-1)+f_a(0)F_a'(0)+f_a(-1)F_a'(1) &)=\mathrm{R}(0)\\
g(1)\;-(\quad f_a(1)F_a'(0)+f_a(0)F_a'(1)+f_a(-1)F_a'(2) &)=\mathrm{R}(1)\\
g(2)\;-(\quad f_a(1)F_a'(1)+f_a(0)F_a'(2) &)=\mathrm{R}(2)\\
g(3)\;-(\quad f_a(1)F_a'(2) &)=\mathrm{R}(3)
\end{array}\right\} \qquad \ldots\ldots(4)$$

The problem is now to find a set of values $F_a'(x_i)$ which reduces the 'residuals' $\mathrm{R}(\xi_j)$ as nearly as possible to zero. With this aim, successive increments are given in turn to the $F_a'(x_i)$, beginning with all $F_a'(x_i)$ equal to zero; each increment will reduce the values of some of the residuals. Finally, the individual increments for each of the $F_a'(x_i)$ are summed, giving the values of $F_a'(x_i)$ that form the solution of the problem.

A particular residual $\mathrm{R}(\xi_j)$ is most influenced by an increment of the $F_a'(x_i)$ having the largest coefficient in the corresponding equation. For example, if $f_a(0)$ is the largest of the $f_a(x_i)$, the residual $\mathrm{R}(-1)$ will be more influenced by an increment of $F_a'(-1)$ than by an equal increment of $F_a'(-2)$ or of $F_a'(0)$. Therefore, an increment of $F_a'(-1)$ would be used for reducing the residual $\mathrm{R}(-1)$ without influencing the neighbouring residuals more than necessary. Such considerations guide the computer in deciding to which of the $F_a'(x_i)$ an increment will be given at any stage during the calculations.

§ 3. A PRACTICAL EXAMPLE

The calculation of the broadening, due solely to cold work, of the (420) line from aluminium (obtained with cobalt K_α radiation) is reproduced in Tables 1A and 1B. Figure 1 shows the photometer curves for the x-ray lines from the metal after annealing and then after a plastic shear strain of 1·6 in torsion; from these curves the values of $f(x)$ and $g(x)$ are obtained, allowing for the background intensity.

The x_i and ξ_j are chosen at intervals of 0·2 mm., taken as unit length in the calculations. The values of $f_a(x_i)$ are given at the top of Table 1B and the values of $g(\xi_j)$ appear as the initial residuals in the main part of Table 1B. The increments given to $F_a'(x_i)$ at each step in the calculation are recorded in Table 1A, and the corresponding changes to the residuals are made in Table 1B.

The first steps aim at reducing the largest residuals and successive steps are directed systematically at the smaller residuals in turn. After step 18, it can be seen that more increments of $F_a'(x_i)$ with x_i near zero are needed for reducing residuals near $\xi_j=0$. Further increments of $F_a'(x_i)$ are used as dictated by the current values of the residuals, until all the residuals are sufficiently small. There is no point in trying to reduce the residuals to less than the probable errors in the $g(\xi_j)$ measurements, and so the relaxation process is stopped before all the residuals are zero.

If some increments of $F_a'(x_i)$ have been too large, so that residuals assume large negative values, then negative increments may be used to correct for this. Thus, in steps 44–46, negative increments have been applied to $F_a'(4)$, $F_a'(6)$ and $F_a'(7)$ where it has become apparent from the residuals that the initial increments were too large.

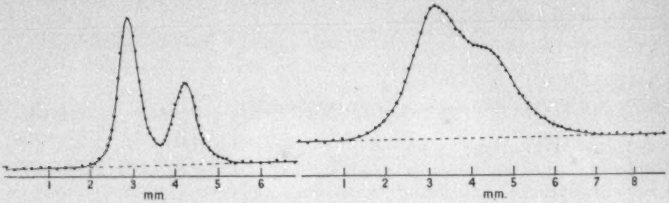

Figure 1.

(*a*) Annealed Al (420) line.

(*b*) Cold-worked Al (plastic shear strain 1·6) (420) line.

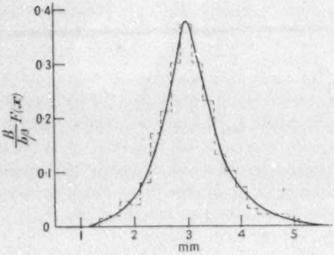

Figure 2.

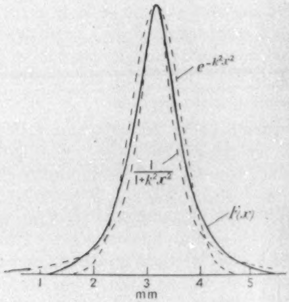

Figure 3.

The final solution, obtained by summing the columns of increments of each $F_a'(x_i)$, is given at the bottom of Table 1A and is plotted in Figure 2. The stepped curve indicates the quantities $(B/b\beta)F_a(x_i)$ that the calculation yields, and the smooth curve indicates the probable shape of the $(B/b\beta)F(x)$ curve to which the stepped curve is an approximation. The maximum of this curve must occur where $F(x)=1$, and therefore is equal to $B/b\beta$; from this, the true

Table 1A

Increments of $F_n'(x_i)$.

	x_i =	-8	-7	-6	-5	-4	-3	-2	-1	0	1	2	3	4	5	6	7	8	9	10
1										0·300										
2											0·200									
3									0·200											
4								0·100												
5							0·100													
6						0·050														
7					0·030															
8				0·030																
9			0·010																	
10												0·100								
11													0·100							
12														0·100						
13															0·050					
14																0·050				
15																	0·030			
16																		0·020		
17																			0·020	
18																				0·010
19									0·030											
20								0·050												
21							0·050													
22						0·030														
23					0·010															
24				0·010																
25			0·010																	
26		0·010																		
27											0·050									
28												0·050								
29													0·030							
30														0·020						
31															0·020					
32										0·030										
33									0·050											
34								0·050												
35							0·020													
36											0·030									
37												0·050								
38										0·020										
39									0·020											
40								0·010												
41				0·005																
42		0·005																		
43												0·030								
44																-0·020				
45																	-0·010			
46														-0·020						
47											0·020									
48										0·020										
$F_n(x_i)$ =		0·015	0·020	0·045	0·040	0·080	0·170	0·210	0·300	0·370	0·300	0·230	0·130	0·100	0·070	0·030	0·020	0·020	0·010	0·010

Table 1B

STEP						x_i = $f(x_i)$ =	-5 5	-4 30	-3 85	-2 230	-1 700	0 960	1 675	2 325	3 175	4 145	5 270	6 400	7 315	8 335	9 145	10 75	11 60	12 20	13 5							
	ξ_i = $g(\xi_i)$ =	-10 10	-9 30	-8 35	-7 90	-6 140	-5 225	-4 340	-3 515	-2 710	-1 920	0 1000	1 970	2 830	3 735	4 725	5 650	6 675	7 635	8 555	9 455	10 340	11 250	12 160	13 130	14 95	15 65	16 40	17 30	18 25	19 10	20
1							3 225	9 331	26 489	45 635	210 630	210 712	203 767	35 792	35 792	44 681	81 603	144 541	155 480	101 454	44 411	25 317	12 238	6 174	2 128							
2								330	6 485	17 618	50 640	140 572	192 575	135 637	65 677	35 646	25 580	34 477	56 384	103 351	67 344	25 285	15 223	8 166	4 124	1 36						
3						1 133	6 217	17 313	50 433	140 478	192 448	135 437	65 510	35 622	29 640	34 592	56 484	103 374	67 317	25 322	13 323	8 280	4 219	1 165								
4					1 89	3 136	9 208	25 288	70 363	56 392	68 380	33 404	18 392	15 607	27 621	48 544	32 432	34 340	15 302	8 314	4 325	2 278	1 218									
5				1 54	3 86	9 127	25 183	70 218	56 267	68 314	33 347	18 356	15 477	27 580	48 373	52 492	32 356	15 325	8 294	4 310	2 323	1 277										
6				2 52	4 82	13 114	35 146	48 170	34 233	16 258	9 338	7 379	14 463	24 556	28 547	17 475	7 391	4 321	2 292	1 309												
7			1 23	3 49	8 74	27 93	23 119	20 150	10 223	3 291	4 334	8 371	14 449	13 541	10 537	4 471	2 385	1 320	1 291													
8		1 9	3 26	8 41	21 53	25 64	20 93	10 140	3 218	4 289	8 326	14 357	13 434	10 531	4 533	2 469	1 388	1 319														
9		1 8	3 23	7 34	10 43	7 57	3 96	2 138	1 217	3 286	3 321	5 352	3 431	1 530	1 532																	
10									1 216	3 283	5 312	25 227	70 301	56 434	68 464	33 436	18 370	15 304	27 264	48 261	52 271	34 245	15 203	8 157	4 120	2 96	1 64					
11										1 282	3 309	9 318	25 326	70 364	56 368	68 308	33 337	18 286	15 249	27 234	48 223	52 191	34 169	15 142	8 112	4 88	2 62	1 39				
12											1 308	3 315	9 327	25 339	70 298	56 272	68 269	33 233	18 231	15 219	27 196	48 143	52 117	34 108	15 97	8 80	4 58	2 37	1 23			
13													2 325	4 335	13 285	35 237	48 221	34 219	18 215	9 210	7 189	14 129	24 93	26 82	17 80	7 71	4 54	2 45	1 44			
14														2 333	4 281	13 224	35 186	48 171	34 181	18 194	9 180	7 122	14 79	24 58	26 54	17 56	7 47	4 31	2 26	1 24		
15															1 200	3 221	8 174	21 150	29 152	20 174	10 170	5 117	4 75	8 50	14 40	13 41	10 37	4 27	2 24	1 23	1 9	
16																1 220	2 176	5 145	14 138	19 155	14 136	7 110	4 71	3 47	3 35	10 31	10 27	7 20	3 21	2 27	1 8	
17																	1 175	2 143	5 133	14 141	19 137	14 96	7 64	4 43	3 32	5 26	10 17	10 10	7 14	3 18	2 6	1 -1
18																			1 132	3 138	7 130	10 86	7 57	3 40	2 30	1 25	3 14	5 5	5 9	3 15	1 5	1 -2
19							1 95	3 135	8 208	21 261	29 279	20 295	10 315	5 328	4 276	8 212	14 161	15 128	10 122	4 134	2 128	1 85	1 56									
20						2 55	4 91	13 122	35 173	48 213	34 245	16 273	9 306	7 321	14 262	24 188	26 135	17 111	7 115	4 130	2 126	1 84										
21					2 41	4 51	13 78	35 87	48 125	34 179	16 229	9 270	7 299	14 307	24 238	26 162	17 118	7 104	4 111	2 128	1 125											
22				1 33	3 38	8 43	21 57	25 58	20 105	10 169	3 224	4 266	8 291	14 293	13 223	10 152	4 114	2 102	1 110	1 127												
23				1 32	3 35	7 36	10 47	7 51	3 102	2 167	1 223	3 263	5 286	3 288	3 220	1 151	1 113															
24			1 22	3 25	7 28	10 26	7 40	3 48	2 100	1 166	3 220	5 258	5 281	3 285	1 219	1 150																
25		1 7	3 15	7 22	10 18	7 13	3 37	2 46	1 99	3 163	5 215	5 253	3 278	1 284	1 218																	
26	1 -1	3 4	7 12	10 12	7 11	3 16	2 35	1 45	3 96	5 158	5 210	3 250	1 277	1 283																		
27									2 34	4 154	13 197	35 215	48 229	34 243	16 202	9 141	7 106	14 88	24 86	26 101	17 108	7 77	4 52	2 38	1 23							
28										2 152	4 191	13 202	35 154	48 201	34 168	16 125	9 97	7 81	14 72	24 77	26 84	17 60	7 45	4 34	2 27	1 24						
29											1 192	3 193	8 186	21 180	29 133	20 105	10 87	5 76	4 68	8 65	14 70	13 45	10 35	4 30	2 25	1 23	1 13					
30												1 190	2 184	5 175	14 125	19 86	14 73	7 69	4 64	3 66	5 65	10 35	10 25	7 23	3 22	2 21	1 12					
31													1 183	2 173	5 120	14 72	19 34	14 55	7 37	3 42	3 62	5 30	10 15	10 13	7 15	3 18	2 10	1 4				
32								1 44	3 91	8 144	21 171	29 165	20 163	10 163	5 115	4 68	8 46	14 41	15 42	10 52	4 50	2 21	1 14	1 12								
33							2 33	4 40	13 78	35 109	48 123	34 135	16 147	9 154	7 108	14 54	24 22	26 15	17 25	7 45	4 54	2 26	1 13									
34						2 14	4 22	13 27	35 43	48 61	34 89	16 113	9 138	7 147	14 94	24 30	26 -4	17 -2	7 18	4 41	2 32	1 25										
35					1 10	2 12	5 24	14 13	19 24	14 47	7 82	4 115	3 135	5 142	10 84	10 20	7 -11	3 -5	2 16	1 40												
36									1 23	3 44	8 74	21 34	29 106	20 122	10 74	3 13	4 -15	8 -13	14 2	15 25	10 42	4 21	2 11	1 11	1 14							
37										2 42	4 70	13 81	35 71	48 74	34 40	16 -1	3 -24	7 -20	14 -12	24 1	26 16	17 4	7 4	4 7	2 12	1 17						
38								1 12	2 21	5 37	14 56	19 62	14 57	7 67	4 36	3 -4	5 -29	10 -30	10 -22	7 -6	3 13	2 4	1 3									
39							1 23	2 10	5 16	14 23	19 37	14 48	7 50	4 63	3 33	3 -3	10 -39	10 -40	7 -22	3 -3	2 11	1 1										
40							1 22	3 7	7 9	10 13	7 30	3 45	2 48	1 62	1 30	3 -14	5 -44	3 -43	1 -30	1 -10												
41				1 11	4 6	3 7	3 19	2 5	1 8	1 12	1 23	2 43	43	3 60	1 23																	
42		1 3	4 8	5 8	3 3	2 3	1 18	1 4	1 7	2 10	2 26	2 47	1 44																			
43										1 9	3 23	8 33	21 23	29 31	20 9	10 -24	5 -49	4 -47	8 -38	14 -24	15 -4	10 -9	4 -1	2 3	1 11	1 16						
44														1 32	2 11	3 -19	14 -35	15 -28	14 -24	7 -17	4 0	3 -6	5 -4	10 15	10 21	7 23	3 13	2 6	1 8			
45																7 -18	3 -32	7 -21	10 -14	7 -10	3 -3	2 -4	1 5	3 14	5 29	5 28	3 16	1 7	1 9			
46												1 36	2 25	5 37	14 25	13 1	14 -18	7 -14	4 -10	3 -7	3 4	10 6	10 15	7 25	3 25	3 30	1 17					
47									1 6	2 7	5 18	14 20	19 6	14 22	7 18	4 -5	3 -21	5 -19	10 -20	10 -17	7 1	3 3	2 13	1 24								
48	-1	3	8	6	3	5	18	1 3	2 4	5 3	14 4	19 7	14 -8	7 16	4 14	3 -8	5 -26	10 -25	10 -30	7 -24	3 -2	2 7	1 12	24	29	30	17	7	9	15	5	-2

broadening β is readily obtained, since b and B are known. In the present case, $b = 1{\cdot}05$ mm. and $B = 2{\cdot}32$ mm.; then β is found to be

$$2{\cdot}32/1{\cdot}05 \times 0{\cdot}375 = 5{\cdot}90 \text{ units of } 0{\cdot}2 \text{ mm.} = 1{\cdot}18 \text{ mm.}$$

Thus we have found both the shape $F(x)$ of the true broadening curve and its integral breadth β.

It is interesting to compare the curve for $F(x)$ from this worked example with the functions $1/(1+k^2x^2)$ and $\exp(-k^2x^2)$ having the same integral breadths, as shown in Figure 3. Thus it is found in the case of cold-worked aluminium (and also in the case of cold-worked copper) that the true broadening curve falls between the curves corresponding to these two functions.

§ 4. REMARKS

The method can be made as accurate as required if the intervals $2l$ are chosen sufficiently small and the relaxation procedure is taken sufficiently far. However, in practice, excessive refinement of the calculation will reveal a great amount of detail in the $F(x)$ curve that has no physical meaning but is due to the experimental errors in the $f(x)$ and $g(x)$ curves.

Serious errors in the calculation are immediately apparent from anomalous values assumed by individual residuals. Another check on the calculation is provided by the fact that the sum $\Sigma_i F_a'(x_i)$ should be equal to B/b when the residuals have been reduced until their sum is zero.

It is convenient to choose the intervals for x_i and ξ_j to be the same, but this is not necessary; in some applications (for example, where one curve is much broader than the other) it may be advantageous to use different intervals of subdivision on the two curves. In other cases, finer subdivision may be used on portions of the curves (a common device in relaxation methods) if a more detailed study is being made of special features.

The method could also be extended to two or three dimensional problems but the amount of labour involved in the calculations would be, of course, much greater.

The physical meaning of the present method for deriving the true broadening curve from the measured curves is very simple and direct. The $f(x)$ curve is broadened step by step with such increments of $F(x)$ as appear necessary until the curve $g(x)$ has been constructed. The progress of this construction is followed by means of the residuals in Table 1B.

ACKNOWLEDGMENTS

The author is indebted to Mr. F. S. Shaw and Mr. J. P. O. Silberstein for helpful suggestions, which led to the use of this method of calculation. The work has been done at the Cavendish Laboratory, Cambridge, during the author's tenure of the Angas Engineering Scholarship (University of Adelaide) and an Australian Council for Scientific and Industrial Research Studentship.

REFERENCES

JONES, F. W., 1938, *Proc. Roy. Soc.* A, **166**, 16.

SHAW, F. S., 1946, *An Introduction to Relaxation Methods*, C.S.I.R. Div. of Aeronautics (Melbourne) Report S.M.78.

SOUTHWELL, R. V., 1940, *Relaxation Methods in Engineering Science* (Oxford: University Press); 1946, *Relaxation Methods in Theoretical Physics* (Oxford: University Press).

STOKES, A. R., 1948, *Proc. Phys. Soc.*, **61**, 382.

The Inversion Spectra of NH_3, CH_3Cl and CH_3Br at High Pressures

By B. BLEANEY and J. H. N. LOUBSER
Clarendon Laboratory, Oxford

Communicated by F. E. Simon; *MS. received* 19*th October* 1949

ABSTRACT. The absorption due to the inversion spectrum of ammonia has been studied at pressures up to 6 atmospheres between wavelengths of 8 cm. and 8 mm. The resonant frequency is found to shift downwards from $0{\cdot}78\ \text{cm}^{-1}$ as the pressure rises, becoming substantially zero above 2 atmospheres. The line width rises less rapidly than the pressure in the transition region, but ultimately becomes proportional to the pressure with an effective 'collision diameter' of 7·7 A. These effects are attributed to multiple collisions, which become dominant at the higher pressures; the resonant inversion is then destroyed by the molecular interaction.

In the methyl halides the inversion frequency is virtually zero owing to the low probability of tunnelling through the barrier, but the absorption line is spread out to the centimetre wave region by the collision process. The collision diameters are found to be 7·7 A. and 9·0 A. for methyl chloride and bromide respectively.

§1. INTRODUCTION

Collision broadening of the inversion spectrum of ammonia at pressures between 0·5 mm. and 60 cm. pressure has been studied previously by Bleaney and Penrose (1947 a, b). At the lowest pressures the rotational fine structure is resolved so that the frequencies and line breadths of the individual lines could be determined. Assuming that the line breadth varies linearly with the pressure, and using the Van Vleck–Weisskopf (1945) formula

$$\frac{\alpha}{\bar{\nu}^2} = \frac{4\pi^2}{3\boldsymbol{k}T}\sum_{J,K} N_{JK}|\mu^2_{JK}|\left\{\frac{\Delta\bar{\nu}_{JK}}{\Delta\bar{\nu}^2_{JK}+(\bar{\nu}_{JK}-\bar{\nu})^2}+\frac{\Delta\bar{\nu}_{JK}}{\Delta\bar{\nu}^2_{JK}+(\bar{\nu}_{JK}+\bar{\nu})^2}\right\} \qquad \ldots\ldots(1)$$

(where the symbols have their usual meanings) for the line shape, the absorption curve could be calculated for high pressures where the fine structure is not resolved. Comparison with the measured absorption curves showed that at 10 cm. Hg pressure the calculated and experimental curves were in close agreement, while at 60 cm. Hg the experimental curve showed a definite shift to lower frequencies. It seemed also that $\Delta\bar{\nu}$ was no longer increasing linearly with the pressure. In view of these results it seemed interesting to make a more extensive study of the absorption at high pressures. This involved the use of a much wider range of frequencies, since the absorption curve becomes very broad; in particular the use of low frequencies is important. This arises not only because of the shift of the resonance, but also because the second term in the bracket in equation (1) becomes relatively more important, and it might be possible to make an experimental check of the accuracy of the Van Vleck–Weisskopf formula. The measurements were extended also up to six atmospheres, being limited here by the vapour pressure at room temperature.

The phenomenon of inversion is not peculiar to ammonia, but should be present in all non-planar molecules. The inversion frequency is so low in other cases, however, as to be effectively zero as regards microwave measurements. For example, in PH_3, Sutherland, Lee and Wu (1939) have estimated it to be about 5 Mc/s.; in heavier molecules it will be orders of magnitude smaller again. Since the inversion is an allowed transition, such molecules possess an absorption line at $\bar{\nu}_{JK} \simeq 0$ which will be broadened by collisions. Putting $\bar{\nu}_{JK} = 0$ in equation (1) we have

$$\frac{\alpha}{\bar{\nu}^2} = \frac{8\pi^2}{3\boldsymbol{k}T}\left\{\sum_{J,K} N_{JK}|\mu_{JK}^2|\right\}\frac{\Delta\bar{\nu}}{\Delta\bar{\nu}^2 + \bar{\nu}^2}, \qquad \ldots\ldots(1\,a)$$

which is similar to a Debye curve for a liquid except that only part of the dipole moment contributes to the intensity. Walter and Hershberger (1946) found that a number of gases show absorption due to this effect at centimetre wavelengths at pressures such that $\Delta\bar{\nu} \simeq \bar{\nu}$. Methyl chloride and methyl bromide were selected on which to make measurements, as their rotational lines lie mainly at millimetre wavelengths, and the intensity of the inversion spectrum is amenable to simple calculation. Their vapour pressures are also fairly high (4 and 2 atmospheres respectively at room temperature).

§2. APPARATUS

In the measurements of Bleaney and Penrose (1947 b) at medium pressures (10 to 60 cm. Hg) an absorption cell consisting of one metre of waveguide was employed, closed at the ends by thin mica windows. The main experimental error was ascribed to interference between the small reflections from these windows; the optical path length between the two windows changed by over a quarter of a wavelength on introducing ammonia at 60 cm. pressure, and the change in the power reflected by the cell caused a scatter of about ± 4% in the points taken at this pressure. The discrepancy between these points and the calculated values was considerably greater than this, but it was thought worth while to repeat the measurements with a more refined technique of the same type before proceeding to a more extensive study of the absorption curve. For this purpose a rather longer cell (1·75 metres) was used, and efforts were made to design a more satisfactory window which might also be used at higher pressures. In addition a more sensitive type of bolometer was used as detector, which was shown by a D.C. calibration to follow an accurate linear relation between resistance and input power.

The results obtained with this apparatus showed a considerably smaller scatter than those of Bleaney and Penrose (1947 b) and lay approximately 2% higher. The anomalous behaviour of the spectrum was confirmed, and further measurements were undertaken.

For pressures higher than 90 cm. Hg the waveguide windows proved unsatisfactory owing to cracks or small leaks. Moreover, at longer wavelengths the attenuation α becomes small owing to the $\bar{\nu}^2$ factor in equation (1) and the fact that one is far from the resonance frequency. For example, at 8 cm. wavelength the calculated attenuation at 30 cm. pressure is only about 10 db/km. This would be difficult to measure accurately in a waveguide cell; the thickness of mica windows, for instance, required to withstand atmospheric pressure increases with a high power of the guide dimensions, and consequently their reflection coefficients would be considerably greater than at 1 cm. wavelength. For these reasons it was decided to use a resonator as the absorption cell; this has the following advantages:

(*a*) Power can be coupled into the cell by probes or small holes, which do not have to be reflectionless. The optical path length between input and output is a small fraction of a wavelength, and no interference effects arise. The diameter of the coupling holes is small and they can easily be covered to stand the pressure.

(*b*) In measuring small attenuations a resonator is equivalent to using a path length $(Q_0\lambda/\pi)$. Here Q_0 is the magnification factor of the resonator, which increases with $\lambda^{1/2}$ when the cavity dimensions are scaled in proportion to the wavelength. Thus the equivalent path length changes with $\lambda^{3/2}$, which almost balances the factor $\bar{\nu}^2$ in equation (2).

The resonator technique has been used by Bleaney and Penrose (1947 a, 1948) for measurements at pressures of the order of a millimetre Hg, a cavity resonant in the H_0 mode being employed to obtain the highest Q. This latter is unnecessary at high pressures where the attenuation due to the gas is large compared with other losses in the resonator. Moreover the H_0 mode resonator has the disadvantage that other modes of resonance can be present. Proper design of the coupling holes can prevent these modes being excited directly, but when the cavity length is such that an unwanted mode is simultaneously in resonance with the H_0 mode the Q of the cavity is strongly affected. On admission of a considerable pressure of gas, the change in the dielectric constant affects the two modes unequally owing to their different dispersions, and the Q changes up or down in a manner unrelated to, and by an amount often greater than, the effect due to absorption in the gas. To avoid this trouble a cylindrical cavity resonant in the lowest mode, H_1, was used, of such a diameter that it could resonate only in the H_1 mode. This mode is doubly degenerate owing to the two possible polarizations of the wave, and at the shorter wavelengths the probe coupling shifted one resonance slightly from the other. Since this would cause an error in measuring the Q, a thin wire was stretched across a diameter so that the resonance due to the mode polarized parallel to the wire was shifted far away from the other (perpendicular) mode.

Details of the four resonators used are given in Table 1. Q_0 refers to the empty resonator, while Q_1 is the magnification factor when filled with ammonia at 6 atmospheres.

Table 1

Wavelength range (cm.)	Diameter (cm.)	Q_0	NH_3 at $p=6$ atm.	
			Q_1	α (db/m.)
8–9	7·0	6000	860	0·4
3–3·5	2·1	4200	350	2·4
1·1–1·5	0·955	2500	160	13
0·8–0·95	0·625	2000	140	20

The figures given are of course only approximate, but they show how the ratio of Q_1 to Q_0 remains about 0·1, while the actual absorption in decibels per metre varies by a factor 50. The absorption coefficient per centimetre of path, α, is obtained from measurements of the magnification factors Q_0, Q_1 of the empty and filled cavity by the formula

$$\alpha = \frac{2\pi}{\lambda}\left(\frac{1}{Q_1} - \frac{1}{Q_0}\right).$$

The cavities were all of the transmission type, and were tuned by movement of a plunger driven by a micrometer head. To measure the Q the movement of the plunger required to travel from one half-power point of the resonance curve to the other was determined. The detectors used were crystal rectifiers, checked against a bolometer. A small correction was applied at higher levels for departure of the rectified current from exact proportionality with the input power.

At each wavelength the absorption was measured at a number of pressures and a curve of absorption against pressure constructed. Points were taken while the pressure was being increased and then again while it was being decreased in order to observe whether any irreversible effects occurred. This was necessary because immediately after more gas had been admitted the pressure was observed to fall slightly owing to adsorption of the gas on the walls. At high pressures where the attenuation due to the gas is practically independent of pressure no change in the Q of the cavity could be detected while the adsorption process was taking place. This shows that the gas adsorbed on the walls of the cavity did not cause any error in the measurements. Further evidence is provided by the comparison of waveguide and cavity measurements at the shorter wavelengths. These agree within 2%, though the ratio of wall area to volume is different by a factor of 100 or more.

§3. RESULTS FOR AMMONIA

In presenting the results, constant comparison with calculated values based on the Van Vleck–Weisskopf equation is required. It is convenient to outline in advance the method adopted of using this equation.

Already at 10 cm. Hg the resolution of the rotational fine structure is lost in the broadening due to collisions, and it becomes convenient to replace the summation over all the lines by a formula for a single line. In so doing average values of the intensity, the resonant frequency $\bar{\nu}_0$, and the line width $\Delta\bar{\nu}$ are required. The first of these is still accurately represented by that portion of the equation (1) not involving the frequency. The second, $\bar{\nu}_0$, may be taken as the centre of gravity of the absorption, $0{\cdot}78\ \mathrm{cm}^{-1}$. The question of line width is more difficult, owing to the complicated way in which $\Delta\bar{\nu}$ appears in (1), and the fact that it varies with J, K (Bleaney and Penrose 1948). A convenient average is obtained with the formula

$$\Delta\bar{\nu}=\frac{\sum\limits_{J,K} I_{JK}\Delta\bar{\nu}_{JK}}{\sum\limits_{J,K} I_{JK}}, \qquad \ldots\ldots\ldots(3)$$

where I_{JK} is the total intensity associated with the line J, K. Combining this with the assumption that $\Delta\bar{\nu}$ varies linearly with the pressure, one finds

$$\Delta\bar{\nu}/p=0{\cdot}62\ \mathrm{cm}^{-1}/\text{atmosphere}, \qquad \ldots\ldots(4)$$

where the empirical formula of Bleaney and Penrose (1948) for the variation of $\Delta\bar{\nu}$ with J, K has been used in obtaining the numerical value.

Two typical curves of 'reduced' absorption ($\alpha/\bar{\nu}^2$) against pressure are shown in Figure 1, the frequencies being $0{\cdot}749\ \mathrm{cm}^{-1}$ (curve A) and $0{\cdot}125\ \mathrm{cm}^{-1}$ (curve B). The former is practically at the centre of the absorption, where the absorption should be almost independent of pressure, except for the initial rise at very low pressures where the spread of the rotational fine structure is comparable with the line width. For $\bar{\nu}=\bar{\nu}_0$, the first term in (1) is a constant if $\Delta\bar{\nu}$ is proportional to

p (and hence to N), while the second term produces a slow rise as $\Delta\bar{\nu}$ becomes of the same order as $2\bar{\nu}_0$. The dotted curve, C, in Figure 1 shows the calculated absorption with this behaviour. After an initial attempt to flatten out in this way, the experimental curve rises above C at high pressures by an amount far outside any errors introduced by the approximations in the calculation. This cannot be explained by the overlapping of any other absorption lines, since the tails of the pure rotational lines at 20 cm^{-1} and higher are quite negligible. The rise must therefore be attributed to a fall in the value of $\Delta\nu/p$; that is, the line breadth ceases to increase linearly with the pressure.

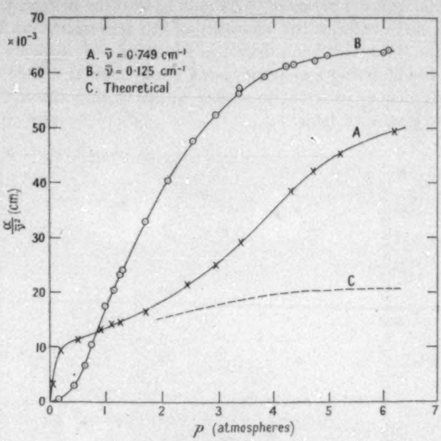

Figure 1. Variation of reduced absorption coefficient $\alpha/\bar{\nu}^2$ with pressure for ammonia at two frequencies.

Consideration of the Van Vleck–Weisskopf formula shows that for large values of $\Delta\bar{\nu}$, the absorption at low frequencies should approach that for $\bar{\nu}=\bar{\nu}_0$, but never surpass it. (In fact the calculated absorption for $\bar{\nu}=0{\cdot}125$ cm^{-1} for pressures above 2 atmos. practically coincides with the dotted line C of Figure 1 for $\bar{\nu}=0{\cdot}749$ cm^{-1}.) This deduction does not depend on how $\Delta\bar{\nu}$ varies with the pressure, so that the only result of the fall in $\Delta\bar{\nu}/p$ should be to raise the curve for 0·125 cm^{-1} up towards that for 0·749 cm^{-1}. The fact that experimentally it crosses the latter and becomes greater shows that, in addition, there must be a shift in the value of $\bar{\nu}_0$ from 0·78 cm^{-1} towards the lower frequencies as the pressure rises.

This shift is revealed directly in Figure 2, where experimental values of $\alpha/\bar{\nu}^2$ are plotted against $\bar{\nu}$ for various pressures. Already at 90 cm. Hg pressure the maximum has moved practically to zero frequency, and some displacement is visible at 30 cm. Hg. It is quite obvious that the line shape cannot be fitted by any choice of $\Delta\bar{\nu}$ for the Van Vleck–Weisskopf formula unless the value of $\bar{\nu}_0$ is also allowed to depart from that determined by the low pressure measurements.

To discover the values of $\Delta\bar{\nu}$ and $\bar{\nu}_0$ at these high pressures where the line is very broad it is necessary to make some assumption concerning the line shape.

We will therefore still employ the formula (1), which has the advantage that it includes the special case of $\bar{\nu}_0=0$. An attempt can then be made to fit the experimental absorption curves, using empirical values of $\Delta\bar{\nu}$ and $\bar{\nu}_0$, but retaining the total intensity identical with that calculated for the inversion spectrum, since this should be independent of the line structure. This restriction is equivalent to a relation between $\Delta\bar{\nu}$ and $\bar{\nu}_0$, since if the value of one of these is assumed, a single point on the experimental curve suffices to determine the other. Two points will therefore fix both the parameters $\Delta\bar{\nu}$ and $\bar{\nu}_0$, and the fit over the remainder of the absorption curve will test the adequacy of the representation by equation (1). On this basis the lines have been drawn in Figure 2. It appears that theoretical curves can be found giving a close fit to the experimental values at all pressures, except for some discrepancies at pressures of about one atmosphere; the cause of these will be discussed later.

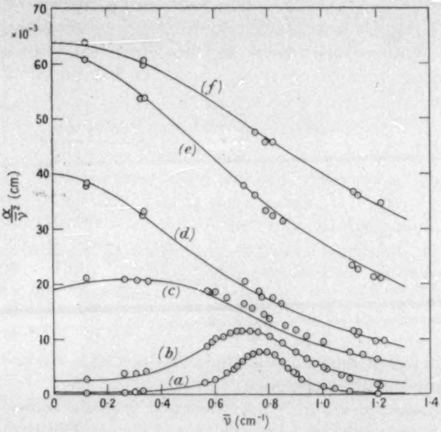

Figure 2. Variation of $\alpha/\bar{\nu}^2$ with frequency at various pressures for ammonia. Curve (a) 10 cm. Hg; (b) 30 cm. Hg; (c) 90 cm. Hg; (d) 2 atmospheres; (e) 4 atmospheres; (f) 6 atmospheres.

The values of $\bar{\nu}_0$ and $\Delta\bar{\nu}$ (divided by the pressure) used in drawing the curves shown in Figure 2 (and similar curves at intermediate pressures) are plotted as functions of the pressure in Figure 3. The value of $\bar{\nu}_0$ becomes substantially zero at pressures above 2 atmospheres, while $\Delta\bar{\nu}/p$ shows a steady initial fall, later becoming constant at a value of $0{\cdot}21_5\ \mathrm{cm}^{-1}$ per atmosphere. The values of $\Delta\bar{\nu}/p$ which have to be used at very low pressures in representing the absorption by a single line have, of course, fictitiously large values, since the rotational fine structure causes the line to be spread out. Thus at 10 cm. pressure the apparent line width $\Delta\bar{\nu}$ is $0{\cdot}115\ \mathrm{cm}^{-1}$, wher as the true width associated with pressure broadening is only $0{\cdot}082\ \mathrm{cm}^{-1}$. However the value of $\Delta\nu/p$ at ½ atmos. pressure has already fallen below the value calculated from low pressure measurements, showing that the region in which $\Delta\bar{\nu}/p$ is constant occupies a negligible portion of this diagram. Previous measurements (Bleaney and Penrose 1947 b) have shown the law $\Delta\bar{\nu}/p = \text{constant}$ is obeyed from 0·5 mm. up to 10 cm. pressure, and other workers have shown that, if saturation effects are avoided, the law holds down to about 10^{-3} mm. Hg, when the Doppler effect and other sources of broadening become important.

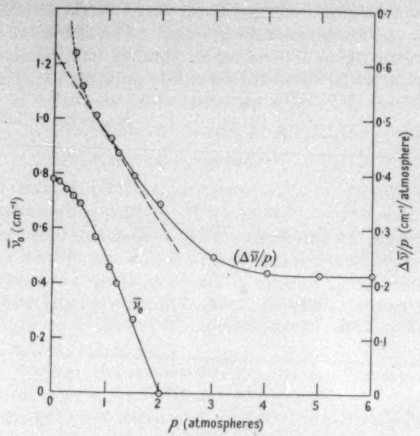

Figure 3. Variation with pressure of apparent inversion frequency, $\bar{\nu}_0$, and line width per atmosphere, $\Delta\bar{\nu}/p$, for ammonia.

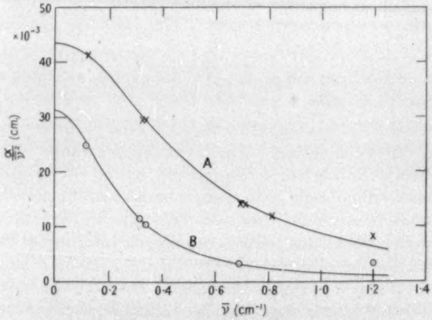

Figure 4. Reduced absorption coefficient plotted against frequency for: A, CH_3Cl at 4 atm pressure; B, CH_3Br at 2 atm. pressure.

RESULTS FOR METHYL CHLORIDE AND METHYL BROMIDE

Similar measurements were made for methyl chloride and bromide, and curves of $\alpha/\bar{\nu}^2$ against $\bar{\nu}$ are shown in Figure 4 for the highest pressures used in each case: 4 atmos. for the chloride and 2 atmos. for the bromide. The curves are calculated from equation (1 *a*), using the theoretical intensities given by Walter and

Hershberger (1946) and choosing the value of $\Delta\bar{\nu}$ to give the best fit. Since $\bar{\nu}_0$ is taken as zero, only one experimental point is required to determine $\Delta\bar{\nu}$. A good fit is obtained over the whole of the curve except at the high-frequency end, where the absorption is some 20% higher than that calculated for the chloride, while the discrepancy is still greater for the bromide. An additional absorption is to be expected from the pure rotational lines, whose fundamentals lie at 0·87 cm^{-1} for the chloride and 0·63 cm^{-1} for the bromide. The tails of the higher lines will also extend into the region of measurement, but the total contributions from the rotational lines cannot be calculated accurately until the line widths are known.

To fit the curves of Figure 4 the values of $\Delta\bar{\nu}$ were taken as

$$CH_3Cl: \quad p = 4 \text{ atmos.} \quad \Delta\bar{\nu} = 0{\cdot}49_5 \text{ cm}^{-1},$$

$$CH_3Br: \quad p = 2 \text{ atmos.} \quad \Delta\bar{\nu} = 0{\cdot}24_5 \text{ cm}^{-1}.$$

From similar curves at lower pressures it is found that $\Delta\bar{\nu}$ varies linearly with the pressure; a further check is provided by the variation of the absorption coefficient with pressure at a given frequency. From such a curve for $\bar{\nu} = 0{\cdot}322$ cm^{-1} for methyl bromide, for example, a value of $\Delta\bar{\nu}/p$ agreeing within 2% with that given above was obtained, and the shape of the curve followed equation (1 *a*) (assuming $\Delta\bar{\nu}$ proportional to the pressure) within the experimental error. From these results the data in Table 2 are obtained.

Table 2

Gas	$\Delta\bar{\nu}/p$ (cm^{-1}/atm.)	$\Delta\bar{\nu}$ at $p = 1$ mm. Hg (Mc/s.)	Collision diameter (A.)
CH_3Cl	0·124	4·9	7·7
CH_3Br	0·122	4·8	9·0

Here the value of $\Delta\bar{\nu}$ at a pressure of 1 mm. Hg has been calculated to facilitate comparison with other microwave data. The collision diameter σ has been obtained from the usual formula

$$\Delta\bar{\nu} = \frac{2N}{\mathbf{c}}\left(\frac{\boldsymbol{R}T}{\pi M}\right)^{1/2}\sigma^2.$$

The collision diameter comes out rather higher for the bromide owing to the lower average velocity of this molecule. The kinetic theory values of σ are 5·0 A. and 5·8 A. for the chloride and bromide respectively, so that the optical collision cross section is as usual rather larger than that for momentum collisions.

If the rotational lines are assumed to have the same width as the inversion lines, a simple calculation shows that there is insufficient intensity in the tails of these lines to account for the discrepancy between the measured and the calculated absorption at the higher frequency. In general, however, the widths of rotational lines are considerably greater than those here obtained in the inversion spectrum. Most of the measurements reported have been for linear molecules, but Gilliam, Edwards and Gordy (1949) give $\Delta\bar{\nu} = 20$ Mc/s. at $p = 1$ mm. for the fundamental rotation line of the very similar molecule CH_3F. If the rotational lines of CH_3Cl and CH_3Br have widths of this order the greater part of the discrepancy found here could be accounted for. The excess absorption increases roughly with the square of the pressure, as would be expected on this basis.

Some remark must be made here concerning the measurements of Walter and Hershberger (1946) using pressures up to 1 atmos. at the two frequencies 0·81 cm^{-1}

and 0·32 cm^{-1}. From these they deduced values of 0·22 cm^{-1}/atmos. and 0·21 cm^{-1}/atmos. for $\Delta\bar{\nu}/p$ for the methyl chloride and bromide respectively, but the total intensities thence deduced differ from the theoretical values by 30% or more. Comparison of their actual absorption coefficients with ours shows that they agree well at 0·32 cm^{-1} but are somewhat higher at 0·81 cm^{-1}. In calculating the values of $\Delta\bar{\nu}$ from the ratio of the absorption coefficients at these two frequencies a small change in this ratio will cause a large change in $\Delta\bar{\nu}$ because $(\Delta\bar{\nu})^2$ is small compared with $(\bar{\nu})^2$. The measurements described in this paper cover a larger range of frequency and pressure, including the region where $\Delta\bar{\nu}$ is of the same order as $\bar{\nu}$, and no disagreement between the theoretical and measured intensities is observed.

§ 5. DISCUSSION

Since this work was completed some measurements over a more limited range have been reported by other workers. D. F. Smith (1948) has described very briefly measurements on ammonia at 3·20 cm. and 4·43 cm. wavelength, which give values for the absorption coefficient rather higher than ours. The discrepancy amounts to about 8% at 4 atmospheres pressure and about 15% at 6 atmospheres; no estimate of the accuracy is given. Weingarten (1948) has used the technique of the large multiple mode cavity (Becker and Autler 1946) for measurements between 3 cm. and 0·8 cm. wavelength. Again at 3 cm. the results are considerably higher than ours, while at the shorter wavelengths they are somewhat lower. The cavity used was, however, only about 1/30 in volume of that of Becker and Autler, and the number of modes per unit bandwidth is correspondingly smaller. Considerable errors may therefore arise, especially at the longer wavelengths.

In these circumstances the most substantial confirmation of the accuracy of the work reported in this paper lies in its internal consistency. Although four separate sets of apparatus were used to cover the complete wavelength range, the scatter of the points on the curves of $(\alpha/\bar{\nu}^2)$ against $\bar{\nu}$ (Figures 2 and 4) is less than ± 3%. Further, for the methyl halides and the ammonia above 2 atmospheres, the one unknown parameter, $\Delta\bar{\nu}$, can be determined from the shape of the curve; the intensity is then fixed and agrees with the theoretical value within ± 3%. This seems convincing evidence for the accuracy claimed; it should be noted, however, that even if the errors were considerably greater the general conclusions concerning the shift of the ammonia line and the fall in $\Delta\bar{\nu}/p$ would still be valid.

In a preliminary report of these results for ammonia, it was pointed out that the probable cause of the line shift was the very strong electric dipole interaction between the ammonia molecules. From measurements of the line width at low pressures, the collision diameter is found to range from 10 A. to 14 A. with a mean value of 13·2 A. At two atmospheres pressure the mean distance between the molecules is only twice this, and it follows that the mutual interaction between the molecules will be, all the time, comparable with the splitting of the inversion doublet. Anderson (1949) and Margenau (1949) have since pointed out that a theoretical treatment can be carried out by taking a pair of ammonia molecules subject to a strong mutual dipole interaction. The selection rules are found to allow transitions between the energy levels of the pair only of low frequency, and consideration of the strength of the interaction required shows that the effects would be expected to appear at pressures of about one atmosphere.

The results shown in Figure 3 reveal that the transition to the strong interaction region is substantially complete at 2 atmospheres. At this pressure the empirical value of $\bar{\nu}_0$ is shown as zero, but naturally the curve of $\bar{\nu}_0$ against pressure should be rounded off. In practice it is impossible to evaluate $\bar{\nu}_0$ accurately in this region where $\bar{\nu}_0 \ll \Delta\bar{\nu}$, and it has therefore been taken to fall sharply to zero at 2 atmospheres. This approximation has little effect on the determination of $\Delta\bar{\nu}$, and $\Delta\bar{\nu}/p$ approaches a constant value gradually. Within the experimental error this constant value of $0{\cdot}21_5\ \mathrm{cm}^{-1}$/atm. is reached at 5 atmos. pressure. This is little over one-third of the value $0{\cdot}62\ \mathrm{cm}^{-1}$/atm. found at the low pressure limit, and corresponds to a collision diameter of 7·7 A. The latter concept has little meaning, however, when multiple collisions prevail, and, as Anderson has pointed out, the collision theory of line broadening has to be replaced by the statistical method. Anderson claims that his theory predicts a smaller value of $\Delta\bar{\nu}/p$ at high pressures, but the mechanism seems obscure.

Little can be said concerning the nature of the spectrum in the transition region at about one atmosphere pressure. From the electric dipole character of the molecular interaction one would expect the inversion lines for the different rotational states to be affected unequally, as was shown to be the case for the line breadths at low pressures. It is therefore not surprising that the attempt to represent the absorption curve as that due to a single line is a poor approximation, as can be seen from Figure 2 in the curve for 90 cm. Hg. On the other hand the authors (1948) have pointed out that the fall in $\Delta\bar{\nu}/p$ can be explained in a simple way. Since the collision diameter (13·2 A.) is considerably greater than the kinetic theory diameter (4·4 A.), an absorbing molecule A will have a colliding molecule B within its sphere of influence for a fraction $(4\pi/3)\sigma^3 N$ of the total time (where N is the number of molecules per cm^3). If another molecule C collides with A during this time, the collision is not effective in contributing to the line width, since the absorption of radiation was already interrupted. The line width therefore rises less rapidly than the pressure by a factor

$$(1-4\pi\sigma^3 N/3)=(1-0{\cdot}23p).$$

Experimentally the initial fall in $\Delta\bar{\nu}/p$ can be represented by the equation

$$\Delta\bar{\nu}/p=0{\cdot}62(1-0{\cdot}25p),$$

which is shown as a broken line in Figure 3. (The points at the lowest pressures lie too high owing to the contribution of the fine structure, as noted in § 3.)

In the methyl halides a similar effect should just be observable, though much smaller in magnitude. No such effect could be detected, however, indicating that there is probably no essential difference between the high and low pressure spectra when the latter is already centred on zero frequency.

§ 6. CONCLUSION

The work reported in this paper, initiated as a test of pressure broadening theory, has revealed a new phenomenon associated with the interaction of ammonia molecules at high pressures. Nevertheless, the Van Vleck–Weisskopf theory of the line shape is found to give a good approximation to the experimental absorption curves. The best test arises from measurement of the absorption in the wings of the line at low pressures, where the changes in $\Delta\bar{\nu}/p$ and $\bar{\nu}_0$ have not yet set in. At the low frequency end ($0{\cdot}125\ \mathrm{cm}^{-1}$), the absorption coefficient at 30 cm. Hg is definitely higher than the calculated value by a factor 2. However, the full absorption curve shows that molecular interactions have already affected the spectrum at this pressure. Unfortunately the measurements at lower pressures were not sufficiently accurate to determine whether an asymptotic approach to the theoretical value is achieved as the pressure is decreased.

At the other end of the spectrum, some measurements have since been made by one of us (J.H.N.L.) at Columbia University * at $\bar{\nu}=1{\cdot}6$, $2{\cdot}4$ and $5{\cdot}0\,\mathrm{cm}^{-1}$. At the two higher frequencies the absorption coefficients are practically identical for pressures up to 90 cm. Hg. This agrees with equation (1), which predicts that $\alpha/\bar{\nu}^2$ should fall away as $1/\bar{\nu}^2$ in the high frequency tail of a line, i.e. α should become constant. This behaviour is clearly revealed in Figure 5, where curves of the absorption coefficient against frequency are given for pressures of 90 cm. and 30 cm. Hg. It will be seen also that plotting α instead of $\alpha/\bar{\nu}^2$ produces little shift in the maximum at low pressures, but a very considerable shift and gross distortion at high pressures where the absorption is widely spread out. Reference to Figure 2 shows that the maximum of $\alpha/\bar{\nu}^2$ is in fact practically at zero frequency at 90 cm. pressure, and the maximum of α occurs, therefore, rather fortuitously near the centre of the low pressure resonant inversion.

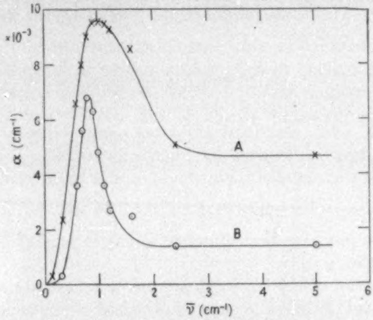

Figure 5. Absorption coefficient plotted against frequency for ammonia.
A : 90 cm. Hg; B : 30 cm. Hg.

REFERENCES

Anderson, P. W., 1949, *Phys. Rev.*, **75,** 1450.

Becker, G. E., and Autler, S. H., 1946, *Phys. Rev.*, **70,** 300.

Bleaney, B., and Loubser, J. H. N., 1948, *Nature, Lond.*, **116,** 522.

Bleaney, B., and Penrose, R. P., 1947 a, *Proc. Roy. Soc.* A, **189,** 358; 1947 b, *Proc. Phys. Soc.*, **59,** 418; 1948, *Ibid.*, **60,** 548.

Gilliam, O. R., Edwards, H. D., and Gordy, W., 1949, *Phys. Rev.*, **75,** 1014.

Margenau, H., 1949, *Phys. Rev.*, **76,** 121, and private communication.

Smith, D. F., 1948, *Phys. Rev.*, **74,** 506.

Sutherland, G. B. B. M., Lee, E., and Wu, C. K., 1939, *Trans. Faraday Soc.*, **35,** 1373.

Van Vleck, J. H., and Weisskopf, V. F., 1945, *Rev. Mod. Phys.*, **17,** 227.

Walters, J. E., and Hershberger, W. D., 1946, *J. Appl. Phys.*, **17,** 814.

Weingarten, I. R., 1948, *Thesis*, Columbia University, New York.

---

* We are indebted to Professor C. H. Townes for permission to quote these results.

The Neutrons Emitted in the Bombardment of ^{6}Li by Deuterons

By W. M. GIBSON * and L. L. GREEN †
Cavendish Laboratory, Cambridge

Communicated by C. F. Powell; MS. received 28th December 1949

ABSTRACT. The neutrons from deuteron bombardment of a separated ^{6}Li target have been studied by the photographic plate method. The energy release for the reaction

$$^6_3\text{Li}+{}^2_1\text{D}\longrightarrow{}^7_4\text{Be}+{}^1_0\text{n}$$

has been shown to be 3·40 ± 0·05 Mev., and evidence is given for the existence of a level in ^{7}Be at 450 ± 60 kev. This is identified with the level at 430 kev. found in work on the reaction $^{10}\text{B}(\text{p}\alpha)^7\text{Be}$.

§ 1. INTRODUCTION

A photographic plate study of the reactions from a normal lithium target has been described by Green and Gibson (1949). Tracks corresponding to neutrons of energy below 4·5 Mev. were neglected, since it was known that some of these would be due to the reaction

$$^6_3\text{Li}+{}^2_1\text{D}\longrightarrow{}^7_4\text{Be}+{}^1_0\text{n}+3\cdot34\ \text{Mev.} \qquad \ldots\ldots(1)$$

It would therefore not have been possible to assess accurately the contribution from the ^{7}Li isotope.

The disintegration of the ^{6}Li by deuterons was first studied by Rumbaugh, Roberts and Hafstad (1938), who showed the yield of neutrons from reaction (1) to be roughly equal to that from the reaction

$$^6_3\text{Li}+{}^2_1\text{D}\longrightarrow{}^4_2\text{He}+{}^3_2\text{He}+{}^1_0\text{n}+1\cdot72\ \text{Mev.} \qquad \ldots\ldots(2)$$

This reaction involves a three-body disintegration, however, and cannot therefore give a homogeneous group of neutrons.

An investigation has now been made of the neutrons from the above two reactions, the target being a separated specimen of the isotope ^{6}Li, which is present in ordinary lithium to the extent of about 7·5%. The photographic plate technique described by Powell (1940, 1943), Richards (1941), Peck (1948), and others was used, the exact procedure being similar to that given by Green and Gibson (1949).

A similar investigation, at one angle only, has been made recently by Mandeville, Swann and Snowdon (1949). Their results are in agreement with ours, but show no indication of the excited level in ^{7}Be at 430 kev. reported by Brown *et al.* (1950) and confirmed by Lauritsen and Thomas (1950), Burcham and Freeman (1950), and ourselves.

§ 2. EXPERIMENTAL TECHNIQUE

The thickness of the ^{6}Li specimen was estimated to be equivalent to an energy loss of 50 kev., from the known value of the total mass deposited in the electromagnetic separator. It was mounted on a water-cooled brass disc, and bombarded for 2½ hours with the 70 microampere deuteron beam from the

---

* Now at H. H. Wills Physics Laboratory, Bristol.
† Now at George Holt Physical Laboratory, Liverpool.

Cavendish Laboratory IMV equipment. The mean deuteron energy was 930 kev.; the exposure time necessary was estimated from the rough value of the neutron yield, as given by a high-pressure hydrogen-filled ionization chamber.

Ilford C2 plates, with $100\,\mu$ emulsions, were set to receive the neutrons emitted at 0° and 120° from the direction of the deuteron beam. The parts of the plates in which the measurements were made were at a mean distance of 9 cm. from the target.

The plates were processed in the ordinary way, and about 500 tracks were measured in each, by two observers using different magnifications. Every track seen which started within the area searched, had a knock-on angle of less than 19·5° and corresponded to a neutron energy of more than 1 MEV. was measured.

§ 3. NEUTRON SPECTRA

The energy of the neutron responsible for each track was calculated from its range and direction of the proton, as described by Gibson and Livesey (1948). The energy distribution obtained was corrected for the variation of neutron–proton scattering cross section (Sleator 1947), and of the escape factor (Gibson and Livesey 1948), with neutron energy. The resulting neutron spectra are shown in Figures 1 and 2, where each ordinate is proportional to the number of neutrons in an energy interval of 0·1 MEV. The scale has been chosen to make the ordinate equal to the number of proton tracks observed in the interval 3·15–3·25 MEV. At higher energies the ordinates are greater and at lower energies less than the numbers of tracks from which they are obtained.

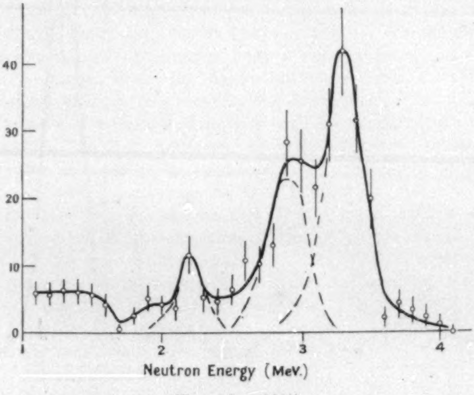

Figure 1. (120°).

In the 120° spectrum there are two partially resolved groups; the observed spectrum is made up of two Gaussian curves of half-width 0·3 MEV. and means at 3·30 MEV. and 2·92 MEV. (broken curves in Figure 1). There is also a small group at 2·2 MEV., with a half-width of about 0·25 MEV., and a continuous spectrum with no sign of a peak spreads from 1·6 MEV. downwards.

In the 0° spectrum there is a similar pair of partially resolved groups, again with half-widths 0·3 Mev., but with means at 4·20 ± 0·03 Mev. and 3·78 ± 0·05 Mev. There are other neutrons at various energies below 3·4 Mev.

§ 4. CALCULATION AND DISCUSSION

The ^{6}Li target thickness was equivalent to 50 kev. and the mean deuteron energy was 930 kev. The variation of excitation function between 880 kev. and 930 kev. would be expected to produce a negligible effect, so the observed energy distributions should be Gaussian, with means corresponding to a deuteron energy of 905 kev. If we assume that the main groups are due to the reaction (1), and use the masses quoted by Bethe (1947), we obtain values for the energy release Q of 3·48 ± 0·03 Mev. and 3·03 ± 0·05 Mev. from the 120° results; the 0° results give Q-values of 3·37 ± 0·03 Mev. and 2·93 ± 0·05 Mev. These values of the probable error refer only to the inaccuracy in estimating the mean of the observed groups.

The difference between the above figures, in so far as it is significant, may be due to the errors in the range–energy relation used (Lattes, Fowler and Cuer 1947). Results obtained by Rotblat (private communication) suggest that, while their curve is correct around 4·5 Mev., it may lead to over-estimation of energies by about 1·7% (i.e. 0·05 Mev.) around 3 Mev. We may therefore quote, as the Q-values for these two groups of neutrons, 3·40 ± 0·05 Mev. and 2·95 ± 0·06 Mev.; these probable errors include the uncertainty of the order of 0·04 Mev. in the range–energy relation.

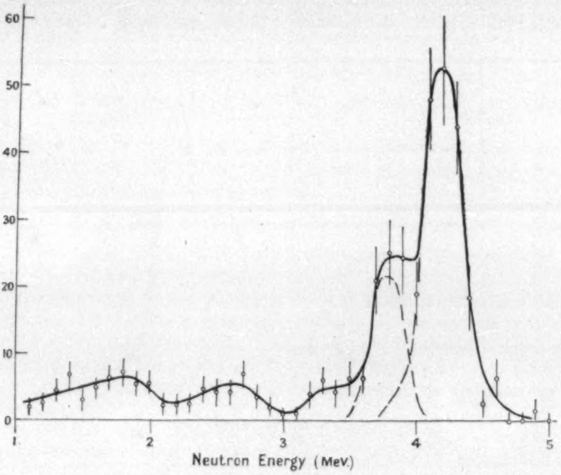

Figure 2. (0°).

The masses given by Bethe (1947) lead to an energy release of 3·34 Mev. in reaction (1). The results for the more abundant group are consistent with this value, but the second group shows the existence of an excited level in the ^{7}Be nucleus at 450 ± 60 kev. (inaccuracies in the range–energy relation leading to no appreciable error in the value for this difference). Since this work was done, it has been brought to our notice that studies of the α-particles from the reaction ^{10}B($p\alpha$)^{7}Be by Brown *et al.* (1950), and of the γ-rays by Lauritsen and Thomas (1950), have given conclusive proof of the existence of this level. Lauritsen and Thomas quote its energy as 429 ± 5 kev.

Reaction (2) should give distributions of neutrons up to maximum energies of 1·84 Mev. at 120° and 2·64 Mev. at 0°. These are in fact found in the 120° spectrum, but if there is a maximum energy in the 0° spectrum it would appear to be at about 3 Mev. We still have to consider, however, the effect of deuterium contamination of the target, and the consequent production of neutrons from the reaction

$$^2_1\mathrm{D} + ^2_1\mathrm{D} \longrightarrow ^3_2\mathrm{He} + ^1_0\mathrm{n} + 3{\cdot}23 \text{ Mev.}$$

This reaction has been considered in detail by Livesey and Wilkinson (1948). They have shown that at 120° the neutrons appear as a group of mean energy about 2·2 Mev., and of half-width determined almost entirely by straggling, since at this angle the 'thick-target' effect is slight. Our 120° spectrum shows exactly such a group. But at 0° D + D neutrons can appear at any energy between 2·5 Mev. and 4 Mev. Livesey and Wilkinson give the shape of spectrum to be expected with a thick and uniform target, but in our case the distribution of deuterium with depth will be far from uniform. We should expect to get a much higher proportion of neutrons in the 2·5–3 Mev. interval than was obtained from a uniform target, since the deuterium concentration will be greatest at the depth corresponding to the range of the deuterons. This will at least partly offset the decrease of excitation function with increasing depth (i.e. decreasing deuteron energy). In fact, however, we must regard all measurements at 0° between 2·5 Mev. and 4 Mev. as unreliable; we may attribute all the neutrons between 2·6 Mev. and 3·5 Mev. to the D + D reaction. Some of those between 3·5 Mev. and 4 Mev. may be due to D + D, and the 0° results alone cannot be regarded as giving reliable information on the *Q*-value of the lower group from the reaction (1), nor even on its existence. They should merely be considered as supplementing the much more reliable evidence contained in the 120° results, which are in no way affected by D + D neutrons.

We may therefore sum up our results as follows:

(i) The energy release in the reaction

$$^6_3\mathrm{Li} + ^2_1\mathrm{D} \longrightarrow ^7_4\mathrm{Be} + ^1_0\mathrm{n}$$

is 3·40 ± 0·05 Mev.

(ii) The nucleus ^{7}Be is found to have an excited state at 450 ± 60 kev. operative in this reaction; this state is identified with that found by Brown *et al.* (1950), Burcham (1950), and Lauritsen and Thomas (1950) to be excited in the reaction ^{10}B(pα)^{7}Be. Burcham and Freeman (1950) have obtained some evidence for the existence of this level.

ACKNOWLEDGMENTS

The authors' thanks are due to Dr. W. D. Allen, A.E.R.E., Harwell, for providing the ^{6}Li specimen, to Mr. G. H. Stafford for his assistance in estimating the necessary exposure times by the use of a high-pressure hydrogen ionization chamber, to Mr. W. Birtwhistle for attending the IMV equipment used, and to Dr. W. E. Burcham for his helpful criticism and advice. One of us (W.M.G.) is indebted to the Department of Scientific and Industrial Research for financial support.

REFERENCES

Bethe, H., 1947, *Elementary Nuclear Theory* (New York : John Wiley & Sons), p. 124.
Brown, A. B., Chao, C. Y., Fowler, W. A., and Lauritsen, C. C., 1950, *Phys. Rev.*, in course of publication.
Burcham, W. E., and Freeman, J. M., 1950, in course of publication.
Gibson, W. M., and Livesey, D. L., 1948, *Proc. Phys. Soc.*, **60,** 523.
Green, L. L., and Gibson, W. M., 1949, *Proc. Phys. Soc.* A, **62,** 407.
Lattes, C. M. G., Fowler, P. H., and Cuer, P., 1947, *Proc. Phys. Soc.*, **59,** 883.
Lauritsen, T., and Thomas, R. G., 1950, *Phys. Rev.*, in course of publication.
Livesey, D. L., and Wilkinson, D. H., 1948, *Proc. Roy. Soc.* A, **195,** 123.
Mandeville, C. E., Swann, C. P., and Snowdon, S. C., 1949, *Phys. Rev.*, **76,** 980.
Peck, R. A., 1948, *Phys. Rev.*, **73,** 947.
Powell, C. F., 1940, *Nature, Lond.*, **145,** 155; 1943, *Proc. Roy. Soc.* A, **181,** 344.
Richards, H. T., 1941, *Phys. Rev.*, **59,** 796.
Rumbaugh, L. H., Roberts, R. B., and Hafstad, L. R., 1938, *Phys. Rev.*, **54,** 657.
Sleator, W., 1947, *Phys. Rev.*, **72,** 207.

The Relationship between the Size of Nuclear Disintegration Stars and the Mean Energy of the Emitted Particles

By K. J. Le COUTEUR
Department of Theoretical Physics, Liverpool University

Communicated by H. Fröhlich; MS. received 7th December 1949

ABSTRACT. Nuclear evaporation theory predicts that the mean energy of the protons evaporated from disintegration stars should increase with star size. It is shown that the calculated rate of increase is in agreement with experimental results.

§ 1

The energy distribution of the charged particles emitted from nuclear disintegrations in photographic plates has been studied by Harding, Lattimore and Perkins (1949) and Page (1950). The results of H.L.P. (their figure 1, *a*, *b*, *c*, *d*) indicate that in the large stars the proportion of energetic particles is higher than in the small stars. The theoretical curves derived from evaporation theory (Le Couteur 1950, referred to as A) show the same tendency (A, figure 3) because the larger stars correspond to higher mean temperatures of the evaporating nucleus. Sufficient measurements are available to show a statistically significant increase of the mean energy of the emitted particles with increase of star size; in this note the experimental and theoretical results are evaluated and compared.

§ 2

The observed energy distribution contains a high energy tail which is not attributed to nuclear evaporation and so must be separated off empirically. Therefore, only the distribution of energies below 30 MeV. has been analysed. Two procedures are then possible: each star may be classified by either (i) n, the total number of visible prongs, or (ii) n', the number of prongs with energy below

30 MEV. The mean kinetic energy E of the particles of charge e and energy below 30 MEV. was determined for each star and the correlation of E against n or n' can be studied. At first sight it would seem more consistent to use n', but, since many of the prongs are due to α-particles of undetermined energy (because they pass out of the emulsion), in practice n' can only be approximated. The available data have been treated by both methods; the correlation coefficients r are

$$\text{(i) } r = 0{\cdot}74 \pm 0{\cdot}04, \qquad \text{(ii) } r = 0{\cdot}75 \pm 0{\cdot}04,$$

so that, on the grounds of internal consistency, there is nothing to choose between the two procedures. Since for protons the natural cut-off of the plates was 100 MEV. in the experiment of H.L.P. and only 40 MEV. in the experiment of Page, the difference between n and n' is always small.

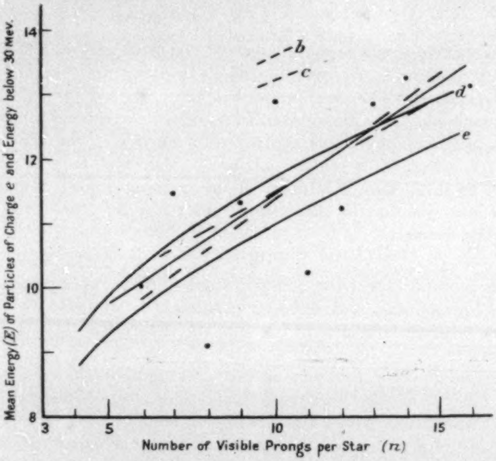

Theoretical and experimental results for the mean energy E of particles, of charge e and energy below 30 MEV., emitted from stars of n visible prongs.

The diagram shows the experimental points as treated by method (i). Each point represents the mean energy of all admissible tracks of charge e belonging to stars of size n. The sample contained 92 stars of from 6 to 16 prongs. The best straight line fitted to the weighted experimental points has slope 0·34 MEV/prong and the slope lies with 90% probability between the limits (0·34 ± 0·06) MEV/prong indicated by broken lines.

§ 3

The energy spectrum of evaporation is approximately (A, 79)

$$P(T)\,dT = \frac{T - V'}{\tau^2} \exp\{-(T - V')/\tau\}\,dT \quad \text{with} \quad \tau = \frac{2}{\Lambda}\sqrt{R}. \quad \ldots\ldots (1)$$

τ is the effective nuclear temperature and R, defined by (A, 60), is approximately equal to the excitation energy U of the nucleus. The relationship (1) between

τ and R corresponds to the Fermi gas model of the nucleus, Λ being a parameter, defined by (A, 39), which increases slowly with the mass number of the nucleus. The mean energy of emission is (A, 58)

$$\overline{T}=V'+\frac{4}{\Lambda}\sqrt{R}-\frac{6}{\Lambda^2}\simeq V'+2\tau, \qquad \ldots\ldots(2)$$

where V' represents the effective height of the potential barrier. For the present purpose this must be modified slightly because the spectrum (1) contains particles of energy above 30 MeV. The mean energy $\overline{T}_W$ of the particles evaporated with energy less than W is

$$\overline{T}_W=V'+k\left(\frac{2}{\Lambda}\sqrt{R}-\frac{3}{\Lambda^2}\right) \qquad \ldots\ldots(3)$$

with

$$k=2-x^2/(e^x-1-x) \quad \text{and} \quad x=W/\tau. \qquad \ldots\ldots(4)$$

For each value of the initial excitation energy, the mean energy E of these particles is obtained by averaging $\overline{T}_W$ over the whole evaporation process by numerical integration as in A. The calculation has been carried through for the four sets of parameters *b*, *c*, *d*, *e*, introduced in A, which correspond to different values of Λ and to different heights of the potential barrier. The results are shown in the Figure, where E is plotted against n, the total number of evaporated particles. The mean atomic number of the nucleus during evaporation is less for the large stars than for the small stars; since $\Lambda \propto A^{1/2}$, this is relevant and has been taken into account.

§ 4

As the evaporation spectrum contains some particles of energy above 30 MeV. ($\simeq 1$ for a 14-prong star) it is reasonable enough to compare the experimental (E, n) points, n being defined as in § 2, with the theoretical (E, n) curves, n being defined as in § 3.

The diagram shows that, taking all the stars together, curves *b* and *c* give too large a mean energy for the evaporated particles, and curves *d* and *e* give a correct value: this information, which was already contained in Figure 5 of A, supports the assumption of *d* and *e* that the potential barrier V is considerably reduced at high excitation energies. Apart from this, the agreement between the slopes of the theoretical curves and of the straight line fitted statistically to the experimental points provides independent evidence in support of the theory. Since the large stars involve much higher excitation energies than the small ones, equation (3) shows that this test of the theory amounts essentially to a check on the value of the parameter Λ.

The comparison of theory and experiment has also been carried through using the parameter n' introduced in § 2 instead of n. The experimental and theoretical curves are then a little steeper but the agreement between them remains.

§ 5

The energy distribution of the α-particles emitted from disintegration stars has been studied experimentally (H.L.P. 1949 and Page 1950) and theoretically (Le Couteur 1950). Unfortunately, there is not sufficient experimental material to determine the correlation between the mean α-particle energy and the star size. However, Perkins (1950) has pointed out that the lower limit of the energy spectrum of α-particles emitted from silver or bromine falls from about 10 Mev. for small stars of two or three prongs to about 2 Mev. for large stars of over twelve prongs. To describe this theoretically it was assumed in §4.1 of A that, as predicted by Bagge, the potential barrier is reduced at high excitation energies. This assumption is not in conflict with the fact that for the protons no such pronounced shift of the lower limit of the energy spectrum is observed. Because of the lower charge and greater probability of penetration, the effective potential barrier for the protons is only about 40% of that for the α-particles, and so varies only from about 3·5 Mev. to 0·8 Mev. over the range of excitation energies (0–600 Mev.) considered. This effect would, if taken by itself, imply a corresponding reduction of the lower limit of the proton spectrum with increase of star size. However, there is a competing decay process, described in §3.6 of A, for the emission of slow protons with energy below 3·5 Mev. This process completely masks the effect of the potential barrier in fixing the lower limit of the proton spectrum. Moreover, a study of Figure 1 of A shows that the contribution from the decay process is greatest when the initial excitation energy of the nucleus is about 150 Mev. (three-prong star) and falls slightly for larger stars; this partly compensates the increased emission of slow protons from large stars due to the assumed reduction in potential barrier. Thus, in agreement with observation, the theory does not predict any marked change with star size in the form of the lower end of the energy spectrum of the protons emitted in the disintegrations of silver and bromine.

ACKNOWLEDGMENTS

The author wishes to thank Dr. Page and Dr. Perkins for the trouble they have taken to supply him with full details of the experimental results. He is also indebted to Dr. Page for help with the reduction of the observations.

REFERENCES

Harding, J. B., Lattimore, S., and Perkins, D. H., 1949, *Proc. Roy. Soc.* A, **196,** 325.
Le Couteur, K. J., 1950, *Proc. Phys. Soc.* A, **63,** 259. (Referred to as A.)
Page, N., 1950, *Proc. Phys. Soc.* A, **63,** 250.
Perkins, D. H., 1950, *Phil. Mag.*, **41,** 138.

On the Scattering of Polarized Neutrons by Protons

By A. B. BHATIA*
Department of Theoretical Physics, The University, Liverpool

Communicated by H. Fröhlich; MS. received 22nd July 1949

ABSTRACT. The scattering and the consequent depolarization of a polarized beam of neutrons by an unpolarized proton gas is suggested as a means of obtaining information about the interaction potential between a neutron and a proton. It is found that the interaction, if it were spherically symmetrical, could be determined from a knowledge of the polarization and scattering differential cross sections. A similar analysis with non-central interaction has not yet been carried out. In this case, however, the polarization depends also on the azimuth ϕ of scattering. This dependence of polarization on ϕ is calculated for (*a*) very low energies, (*b*) very high energies. The maximum azimuthal variations for incident neutrons of energy 1 Mev. and 100 Mev. are about 1% and 50% respectively.

It is hoped that in future experimental techniques for the production and measurement of a polarized beam of fast neutrons will be developed, since these would give important information about the interaction potential between a neutron and a proton.

---

§ 1. INTRODUCTION

In spite of many attempts it has not been possible so far to develop a satisfactory theory of nuclear forces which accounts for all the properties of even the simplest system, a neutron and a proton. We shall, therefore, attempt to obtain the nuclear interaction empirically from various observed properties like the binding energy, the magnetic moment, the quadrupole moment of the deuteron etc., and the scattering of neutrons by protons. In this paper the use is suggested of an additional property, namely the depolarization of a polarized beam of neutrons on scattering by an unpolarized proton gas.

According to Wigner (1941) neutron–proton interaction must be of the form

$$V(r) = \begin{matrix} -\frac{1}{3}(\boldsymbol{\tau}_1 \cdot \boldsymbol{\tau}_2) \\ -\frac{1}{2}(1+\boldsymbol{\tau}_1 \cdot \boldsymbol{\tau}_2) \\ 1 \end{matrix} \left[\frac{3+\boldsymbol{\sigma}_1 \cdot \boldsymbol{\sigma}_2}{4} V_1(r) + \frac{1-\boldsymbol{\sigma}_1 \cdot \boldsymbol{\sigma}_2}{4} V_2(r) + \left(\frac{3(\boldsymbol{\sigma}_1 \cdot \mathbf{r})(\boldsymbol{\sigma}_2 \cdot \mathbf{r})}{r^2} - \boldsymbol{\sigma}_1 \cdot \boldsymbol{\sigma}_2 \right) V_3(r) \right], \quad \begin{matrix} \ldots\ldots(1\,\mathrm{A}) \\ \ldots\ldots(1\,\mathrm{B}) \\ \ldots\ldots(1\,\mathrm{C}) \end{matrix}$$

where $\boldsymbol{\sigma}_1, \boldsymbol{\sigma}_2$ and $\boldsymbol{\tau}_1, \boldsymbol{\tau}_2$ are the spin and isotopic spin coordinates of the two particles. The three $V_i(r)$'s, $(i=1,2,3)$ are arbitrary radial functions referring to triplet, singlet and non-central interactions. The three τ-terms give the possible forms of exchange interactions, related to the symmetrical, charged and neutral meson theories respectively. The first two, A and B, have the effect of making the interaction in the odd and even states different. A dynamic interaction will, of course, also exist. We shall assume here, however, that the static interaction terms are predominant.

The general problem is thus to decide from experiments whether the exchange nature of the interaction is given by one of the three cases A, B and C or is a linear combination of them and to find sufficient information about the radial functions $V_i(r)$. One of the main difficulties in this connection is due to the existence of the two spin states, singlet and triplet, which in scattering experiments appear always mixed up. In the following it will be first shown that separation can be made by using depolarization and scattering differential cross sections (§ 3), provided one assumes the non-central interaction, V_3, to vanish. The problem of finding V_1 and V_2, then becomes similar to the corresponding problem for spinless particles already considered by Fröberg (1948 a, b), Hylleraas (1948) and Bargmann (1949).

---

* Now at Physical Research Laboratory, Navrangpura, Ahmedabad 9, India.

It is known, however, from the magnitude of the quadrupole moment and the magnetic moment of the deuteron that the non-central interaction is of appreciable importance. In the presence of the latter, a qualitatively new feature appears in an azimuthal dependence of the polarization. In the following (§§ 4 and 5) it is found that the azimuthal dependence of the polarization in the scattering of a polarized beam of neutrons by a proton gas gives important information in this respect. It is hoped that in future it will be possible to show that the general problem of finding all the three V_i's can also be solved in this way.

It may be mentioned that so far it has not been possible to polarize a beam of fast neutrons. Recently, however, Schwinger (1948) suggested a means for polarizing neutrons of energies of the order of 1 Mev. One may hope that experimental techniques for the production and measurement of fast neutrons will be developed in the near future, as it would then be possible to obtain more information about the nature of the interaction between a neutron and a proton than is now possible.

§ 2. DEFINITION OF DEPOLARIZATION

The asymptotic behaviour of the wave function for the scattering problem is known to be of the form *

$$\psi=\Big(A_a\chi_a+\sum_{s=1}^{3}A_s\chi_s\Big)e^{ik(z=z_1-z_2)}+\frac{e^{ikr}}{r}\Big(B_a\chi_a+\sum_{s=1}^{3}B_s\chi_s\Big), \qquad \ldots\ldots(2)$$

in which the first term represents the incident wave of neutrons with momentum k along the z-axis in the centre of mass system and the second term the scattered wave. χ_a and χ_s, $(s=1,2,3)$ are the usual orthogonal spin functions, antisymmetric and symmetric respectively in the spin coordinates of the two particles:

$$\chi_1=v_+(1)v_+(2), \qquad \chi_2=v_-(1)v_-(2),$$

$$\chi_3=\frac{1}{\sqrt{2}}\{v_+(1)v_-(2)+v_-(1)v_+(2)\}, \qquad \chi_a=\frac{1}{\sqrt{2}}\{v_+(1)v_-(2)-v_-(1)v_+(2)\}.$$

The constants A in (2) are determined by the initial spin directions of the two particles in the incident beam, while the B's in the scattered wave contain A linearly and are functions of the angle θ and azimuth ϕ of scattering. Assuming the direction of quantization for the spin angular momentum to be fixed, the azimuth can be chosen so that the polar coordinates of the spin directions of the neutron and proton are $(\mu, 0)$ and (β, γ). The corresponding spin function of the two particles can be expressed as a sum of the four orthogonal χ-spin functions, by the identity

$$\Big(\cos\frac{\mu}{2}v_+(1)-\sin\frac{\mu}{2}v_-(1)\Big)\Big(\cos\frac{\beta}{2}v_+(2)-\sin\frac{\beta}{2}e^{i\gamma}v_-(2)\Big)\equiv A_a\chi_a+\sum_{s=1}^{3}A_s\chi_s, \qquad \ldots\ldots(3)$$

which determines the constants A in (2) and (3).

---

* This asymptotic form is quite general, even though it does not contain the isotopic spin coordinates explicitly, since the only effect of the presence of the latter in the interaction potential (1) is to make it different for states of odd and even orbital angular momentum (see Rosenfeld 1948, p. 98).

The scattering cross section $\sigma(\theta)$ is obtained from (2) in the usual manner, namely by taking the square modulus of the amplitude of the scattered wave and summing over all spin coordinates. Doing so, one obtains

$$\sigma(\theta)=B_a^* B_a+\sum_{s=1}^{3} B_s^* B_s. \qquad \ldots\ldots(4)$$

When either of the particles is unpolarized initially the right-hand side of (4) is to be averaged over all directions of the spin of that particle.

In this paper we shall be only concerned with the scattering and the depolarization on scattering of a polarized beam of neutrons by an unpolarized proton gas. The results of measurement on polarization can be conveniently expressed in terms of a polarization factor P, defined as the difference between the absolute probabilities that the spin of the scattered neutrons points parallel or antiparallel to the spin direction of the incident neutrons. $1-P$ will thus be a measure of the depolarization. Remembering that in our notation the latter direction makes an angle μ with the direction of quantization for spin angular momentum, one easily obtains the two probabilities in the usual way with the help of the operators

$$\tfrac{1}{2}[1+\sigma_1^{(3)}\cos\mu-\sigma_1^{(1)}\sin\mu] \quad \text{and} \quad \tfrac{1}{2}[1-\sigma_1^{(3)}\cos\mu+\sigma_1^{(1)}\sin\mu],$$

in which $\sigma_1^{(3)}$ and $\sigma_1^{(1)}$ are the spin operators for particle (1) (neutrons) and are given by the matrices $\begin{pmatrix}1 & 0\\ 0 & -1\end{pmatrix}$ and $\begin{pmatrix}0 & 1\\ 1 & 0\end{pmatrix}$ respectively. For P, one obtains the expression

$$P(\theta)=\Big[\cos\mu\{B_1^* B_1-B_2^* B_2+B_3^* B_a+B_a^* B_3\}-\frac{1}{\sqrt{2}}\sin\mu\,\{B_3^*(B_1+B_2)$$
$$+(B_1+B_2)^* B_3+B_a^*(B_2-B_1)+(B_2-B_1)^* B_a\}\Big]\Big/\Big\{\sigma(\theta)=\sum_{s=1}^{3} B_s^* B_s+B_a^* B_a\Big\}. \qquad \ldots\ldots(5)$$

If the direction of quantization is parallel to the spin direction of the incident neutrons ($\mu=0$), (5) reduces to the simple expression

$$P(\theta)=\{B_1^* B_1-B_2^* B_2+B_3^* B_a+B_a^* B_3\}/\sigma(\theta). \qquad \ldots\ldots(6)$$

In expressions (5) and (6) for $P(\theta)$, one has to average over all directions (β,γ) of the proton spin.

§ 3. INTERACTION POTENTIAL SPHERICALLY SYMMETRICAL

In this section we discuss some reciprocal relations between the phase shifts and the interaction potential on the one hand and $\sigma(\theta)$ and $P(\theta)$ on the other, for the case of spherically symmetrical interaction potential. From the well-known expression for the amplitude of the scattered wave for this case (see Rosenfeld 1948, p. 99), one has

$$\left.\begin{aligned} B_a&=\frac{1}{2ik}A_a\sum_{l=0}^{\infty}(2l+1)[\exp(2i\eta_l^a)-1]P_l(\cos\theta),\\ B_s&=\frac{1}{2ik}A_s\sum_{l=0}^{\infty}(2l+1)[\exp(2i\eta_l^s)-1]P_l(\cos\theta),\\ &(s=1,2,3 \text{ and } \eta_l^{(s)}=\eta_l^{(1)}=\eta_l^{(2)}=\eta_l^{(3)}),\end{aligned}\right\} \qquad \ldots\ldots(7)$$

in which A's are determined by the identity (3). With the help of the relations (3), (4), (5) and (7), one gets for $\sigma(\theta)$ and $P(\theta)$, after averaging over all directions (β, γ) of the proton spin, the expressions

$$\sigma(\theta)=k^{-2}\Big[\tfrac{1}{4}\sum_{m,n=0}^{\infty}(2m+1)(2n+1)\sin\eta_m^a\sin\eta_n^a\cos(\eta_m^a-\eta_n^a)P_m(\cos\theta)P_n(\cos\theta)$$
$$+\tfrac{3}{4}\sum_{m,n=0}^{\infty}(2m+1)(2n+1)\sin\eta_m^s\sin\eta_n^s\cos(\eta_m^s-\eta_n^s)P_m(\cos\theta)P_n(\cos\theta)\Big] \qquad \ldots\ldots(8)$$

and

$$P(\theta)=\frac{k^{-2}}{2\sigma(\theta)}\Big[\sum_{m,n=0}^{\infty}(2m+1)(2n+1)\sin\eta_m^s\sin\eta_n^s\cos(\eta_m^s-\eta_n^s)P_m(\cos\theta)P_n(\cos\theta)$$
$$+\sum_{m,n=0}^{\infty}(2m+1)(2n+1)\sin\eta_m^s\sin\eta_n^a\cos(\eta_m^s-\eta_n^a)P_m(\cos\theta)P_n(\cos\theta)\Big]. \qquad \ldots\ldots(9)$$

Since the interaction is spherically symmetrical and does not cause transitions between the various spin states, unlike the non-central interaction (see §4), expression (9) for $P(\theta)$ does not contain the angle μ which the spin direction of the incident neutrons makes with the incident direction.

In order to determine the phase shifts from an empirical knowledge of $\sigma(\theta)$ and $P(\theta)$, we use the well-known identity

$$P_m(\cos\theta)P_n(\cos\theta)=\sum_{r=0}^{\min(m,n)}\alpha_{mn,r}P_{m+n-2r}(\cos\theta), \qquad \ldots\ldots(10)$$

where

$$\alpha_{mn,r}=\alpha_{nm,r}=\frac{A_{m-r}A_rA_{n-r}}{A_{m+n-2r}}\cdot\frac{2m+2n-4r+1}{2m+2n-2r+1} \quad \text{and} \quad A_m=\frac{(2m)!}{2^m(m!)^2}.$$

Substituting (10) in (8) and (9) and putting

$$\lambda_{mn}^{a,s}=\lambda_{nm}^{a,s}=k^{-2}(2m+1)(2n+1)\sin\eta_m^{a,s}\sin\eta_n^{a,s}\cos(\eta_m^{a,s}-\eta_n^{a,s})$$

and

$$\mu_{mn}=\mu_{nm}=(2k^2)^{-1}(2m+1)(2n+1)[\sin\eta_m^s\sin\eta_n^a\cos(\eta_m^s-\eta_n^a)$$
$$+\sin\eta_n^s\sin\eta_m^a\cos(\eta_n^s-\eta_m^a)],$$

one obtains

$$\sigma(\theta)=\sum_{m,n=0}^{\infty}(\tfrac{1}{4}\lambda_{mn}^a+\tfrac{3}{4}\lambda_{mn}^s)\sum_{r=0}^{\min(m,n)}\alpha_{mn,r}P_{m+n-2r}(\cos\theta)\equiv\sum_t a_tP_t(\cos\theta) \qquad \ldots\ldots(11\,a)$$

and

$$\sigma(\theta)\times P(\theta)=\sum_{m,n=0}^{\infty}(\tfrac{1}{2}\lambda_{mn}^s+\tfrac{1}{2}\mu_{mn})\sum_{r=0}^{\min(m,n)}\alpha_{mn,r}P_{m+n-2r}(\cos\theta)\equiv\sum_t b_tP_t(\cos\theta), \qquad \ldots\ldots(11\,b)$$

with

$$a_t=\sum_{r=0}^{\infty}\sum_{m=r}^{r+t}(\tfrac{1}{4}\lambda^a+\tfrac{3}{4}\lambda^s)_{m,t+2r-m}\times\alpha_{m,t+2r-m,r}$$

and a similar expression for b_t. By using the orthogonality relations

$$\int_0^{\pi}P_m(\cos\theta)P_n(\cos\theta)\sin\theta\,d\theta=\frac{2\delta_{mn}}{2m+1},$$

the coefficients a_l and b_l are given by

$$a_l=\int_0^{\pi}\sigma(\theta)P_l(\cos\theta)\sin\theta\,d\theta \qquad \text{and} \qquad b_l=\int_0^{\pi}\sigma(\theta)P(\theta)P_l(\cos\theta)\sin\theta\,d\theta,$$

and hence become known if $\sigma(\theta)$ and $P(\theta)$ are known. Thus one obtains two sets of infinite numbers of equations involving the unknown singlet and triplet phase shifts. They are

$$\left.\begin{aligned}
a_0&=\tfrac{1}{4}\{\sin^2\eta_0^a+3\sin^2\eta_1^a+5\sin^2\eta_2^a+\ldots.\}\\
&\qquad\qquad+\tfrac{3}{4}\{\sin^2\eta_0^s+3\sin^2\eta_1^s+5\sin^2\eta_2^s+\ldots.\},\\
a_1&=\tfrac{1}{4}\{6\sin\eta_0^a\sin\eta_1^a\cos(\eta_0^a-\eta_1^a)+12\sin\eta_1^a\sin\eta_2^a\cos(\eta_1^a-\eta_2^a)+\ldots.\}\\
&\qquad+\tfrac{3}{4}\{6\sin\eta_2^s\sin\eta_1^s\cos(\eta_0^s-\eta_1^s)+12\sin\eta_1^s\sin\eta_2^s\cos(\eta_1^s-\eta_2^s)+\ldots.\},\\
a_2&=\tfrac{1}{4}\{6\sin^2\eta_1^a+10\sin\eta_0^a\sin\eta_2^a\cos(\eta_0^a-\eta_2^a)+\ldots.\}\\
&\qquad\qquad+\tfrac{3}{4}\{6\sin^2\eta_1^s+10\sin\eta_2^s\sin\eta_2^s\cos(\eta_0^s-\eta_2^s)+\ldots.\},
\end{aligned}\right\}\qquad\ldots\ldots(12)$$

and

$$\left.\begin{aligned}
b_0&=\tfrac{1}{2}\{\sin^2\eta_0^s+3\sin^2\eta_1^s+5\sin^2\eta_2^s+\ldots.\}+\tfrac{1}{2}\{\sin\eta_0^s\sin\eta_0^a\cos(\eta_0^s-\eta_0^a)\\
&\qquad+3\sin\eta_1^s\sin\eta_1^a\cos(\eta_1^s-\eta_1^a)+5\sin\eta_2^s\sin\eta_2^a\cos(\eta_2^s-\eta_2^a)+\ldots.\},\\
b_1&=\tfrac{1}{2}\{6\sin\eta_0^s\sin\eta_1^s\cos(\eta_0^s-\eta_1^s)+12\sin\eta_1^s\sin\eta_2^s\cos(\eta_1^s-\eta_2^s)+\ldots.\}\\
&\qquad+\tfrac{1}{2}\{3\sin\eta_1^s\sin\eta_0^a\cos(\eta_1^s-\eta_0^a)+3\sin\eta_0^s\sin\eta_1^a\cos(\eta_0^s-\eta_1^a)+\ldots.\}.
\end{aligned}\right\}\qquad\ldots\ldots(13)$$

For the case of spinless particles, where there is only one phase shift for each l, equations similar to (12) were first obtained and solved for the phase shifts by Fröberg (1948 b). Since here there are two phase shifts η_l^a and η_l^s for each l, equations (12) alone are not sufficient for their determination. However, one can obtain the phase shifts by solving both (12) and (13) up to any desired accuracy by successive approximations as follows. Assuming that $\eta_l^a\sim\eta_l^s$ (this is true except at very low energies of incident neutrons) and further $1\gg\eta_0\gg\eta_1\gg\eta_2$ etc., one obtains in the first approximation from the first equations of (12) and (13),

$$a_0=\tfrac{1}{4}\sin^2\eta_0^a+\tfrac{3}{4}\sin^2\eta_0^s, \qquad b_0=\tfrac{1}{2}\sin^2\eta_0^s+\tfrac{1}{2}\sin\eta_0^s\sin\eta_0^a,$$

which give

$$\sin^2\eta_0^s=\tfrac{1}{2}[a_0+b_0\pm\{(a_0+b_0)^2-4b_0^2\}^{\frac{1}{2}}], \qquad\ldots\ldots(14\,a)$$

$$\sin\eta_0^a=\frac{2(b_0-\frac{1}{2}\sin^2\eta_0^s)}{\sin\eta_0^s}. \qquad\ldots\ldots(14\,b)$$

Equation (14 *a*) gives for η_0^s four values. Let these be denoted by $\pm\eta_0^{s+}$, $\pm\eta_0^{s-}$ and the corresponding solutions for η_0^a by $\pm\eta_0^{a+}$, $\pm\eta_0^{a-}$. Assuming any one pair of the four to be the correct solution, all the other phase shifts η_l^s and η_l^a, $l>0$, are determined uniquely in the first approximation from equations of the first degree, derived from successive equations of (12) and (13). Determination of the phase shifts to a higher accuracy can be made by successive approximations using the values for the phase shifts obtained in the previous approximation.

The above results show that one can obtain all the phase shifts η_l^a, η_l^s $(l=0,1,2,\ldots.)$ uniquely from $\sigma(\theta)$ and $P(\theta)$, provided one can choose out of the four solutions $\pm\eta_0^{s\pm}$ and $\pm\eta_0^{a\pm}$ of (14) for the *s*-phase shifts, the correct pair. For the selection of the correct pair one has to use some additional properties of the neutron–proton system. Observed data on the binding energy of the deuteron and the scattering of thermal neutrons by protons and by ortho- and para-hydrogen indicate that both the singlet and triplet interactions are attractive, the former being the weaker of the two. Hence for high energy regions both the phase shifts must be of the same sign (positive) and $\eta_0^s > \eta_0^a$. This knowledge, as follows from the use of (14), is enough to fix the correct pair for this energy region. For very low energy incident neutrons η_0^a is negative since the singlet state of the deuteron is virtual. Here, then, one can either determine the phase shifts from some of the above mentioned properties or from a knowledge of P and σ (Rosenfeld 1948, pp.114–120).

The second part of the problem, namely the determination of the interaction potential from the phase shifts η^a's and η^s's thus known as a function of the energy of the incident neutrons, is exactly similar to the corresponding problem for spinless particles, except that, for each l state, one will get two interaction potentials V_1 and V_2 (the triplet and the singlet) as compared with only one for spinless particles. The latter case has been dealt with in detail by Fröberg (1948 a, b), Hylleraas (1948) and Bargmann (1949) and we shall not discuss it here.

§4. EXPRESSIONS FOR $P(\theta)$ WITH NON-CENTRAL INTERACTION

(i) *For incident neutrons of energies of the order of* 1 MeV.

The scattering problems in the presence of the non-central interaction $V_3(r)$ have been considered by several authors (see for example, for general expressions for ψ_{scat} in terms of phase shifts, Holmberg (1948) and Ashkin and Wu (1948), and for the low energy case (of the order of a few MeV.), Rarita and Schwinger (1941) and Hepner and Peierls (1942), the latter quoted in future as (HP)). Since $V_3(r)$ is effective only in triplet states, the usual method for central forces is modified only for these states. Here, the orbital angular momentum l, and the magnetic quantum numbers m_l and m_s are no longer constants of the collision. Instead the total angular momentum J, the magnetic quantum number J_z or M, the total spin $S=1$, are to be used.

For energies of the incident neutrons below a few MeV., only the $l=0$ state need be considered, except for the $D(l=2)$ state coupled with it. The coupled S-D state arises from the stationary state $J=1$. The remaining uncoupled state, $J=1$, $l=1$ can also be neglected. Following (HP) and taking the direction of quantization for spin and orbital angular momentum along the incident direction, the relevant portion of the incident wave in the JM scheme is

$$\psi_{\text{inc}} = \frac{1}{kr} \sum_{M=-1}^{1} [A^M \chi^M \sin kr - f\{A^M(\lambda_{l=2,\, m_s=M}^{J=1,\, M})\sqrt{10}\} F_{l=2}^{J=1,\, M}]. \quad \ldots\ldots(15)$$

In (15) $f = \left(\frac{\pi kr}{2}\right)^{\frac{1}{2}} J_{2+\frac{1}{2}}(kr) \xrightarrow{r\to\infty} \sin(kr-\pi)$ and $\lambda_{l,\, m_s}^{J,\, M}$ are the well-known matrix elements for the unitary transformation from $SlJM$ scheme to Slm_lm_s scheme, as given by Condon and Shortley (1935). They are shown in the Table for $J=1$, $l=2$. The coefficients A^M follow from the identity (3), the index M taking

	$M \backslash m_s$	1	0	-1
$\sqrt{10}\lambda_{2,\, m_s}^{1,\, M}$	1	1	$-\sqrt{3}$	$\sqrt{6}$
	0	$\sqrt{3}$	-2	$\sqrt{3}$
	-1	$\sqrt{6}$	$-\sqrt{3}$	1

the values 1, -1 and 0 respectively as s in A_s takes the values 1, 2 and 3. $F_l^{JM} \times \frac{1}{\sqrt{(2\pi)}}$ are the normalized spin-angular functions and are given by

$$F_l^{JM} = \sum_{m_s=-1}^{1} \lambda_{l,m_s}^{JM}\, Y_l^{M-m_s}(\theta)(\exp i(M-m_s)\phi)\chi_{ms}, \qquad \ldots\ldots(16)$$

where $Y_l^{M-m_s}$ are the normalized associated Legendre functions.

Now according to (HP) and the Appendix to this paper ψ_{scat} can be written in the form

$$\psi_{\text{scat}} = \frac{e^{ikr}}{r} \sum_{M=-1}^{1} [\{\alpha A^M - (\beta\sqrt{10} A^M \lambda_M^M)\}\chi^M + (-\gamma\lambda_M^M A^M \sqrt{10} + \delta A^M) F_2^M\ ], \qquad \ldots\ldots(17)$$

in which suffixes J and l which are 1 and 2 respectively, have been suppressed. α, β, γ and δ are certain constants independent of A^M and λ_M^M and can be expressed in terms of (ka) and its higher powers, provided the range a of the interaction is small $(ka \ll 1)$. From the appendix $\alpha \sim 1/(\epsilon_b + ik)$, $\gamma \ll \beta$ or δ and

$$|\beta| \simeq |\delta| \sim \tfrac{1}{10}(ka)^2 |\alpha|,$$

where $-\hbar^2\epsilon_b^2/M$ is the binding energy of the deuteron. In expression (17), γ is to be neglected, since this is the part of the scattered wave which comes from the pure D state included in $J=1$ and since we have already neglected quantities of the larger order than this such as the scattered amplitude from $J=1$, $l=1$ state. Writing the amplitude of the scattered wave in the singlet state as $A_a S_a$ and using the expression (16) for F_2^{1M}, we have for the coefficients B_s of (2):

$$B_a = A_a S_a,$$

$$B_s = B_{m_s} = \alpha A_{m_s} - \beta\sqrt{10}\lambda_{m_s}^{m_s} A_{m_s} + \delta \sum_{M=-1}^{1} A^M \lambda_{m_s}^M Y_2^{M-m_s}(\theta) \exp[i(M-m_s)\phi]$$

$$(s = 1, 2, 3 \text{ or } m_s = 1, -1, 0) \qquad \ldots\ldots(18)$$

Using (18), (3) and the Table in the expressions (4) and (5) for $\sigma(\theta)$ and $P(\theta)$ respectively and averaging over all directions (β, γ) of the proton spin, we have after some straightforward algebra

$$\sigma(\theta) = \tfrac{1}{4}|S_a|^2 + \tfrac{3}{4}\left[|\alpha|^2 + 2|\beta|^2 + \tfrac{1}{2}|\delta|^2 - \frac{2}{\sqrt{10}} Y_2^0(\theta)(\beta\delta^* + \beta^*\delta)\right] \qquad \ldots\ldots(19)$$

and

$$P(\theta) = \Big[\tfrac{1}{2}|\alpha|^2 + \tfrac{1}{4}(\alpha S_a^* + S_a\alpha^*) - \frac{1}{\sqrt{10}}[Y_2^0(\mu)\{\alpha\beta^* + \beta\alpha^* - (S_a\beta^* + S_a^*\beta)\}$$

$$- Y_2^0(\Theta)\{\alpha\delta^* + \alpha^*\delta - (S_a^*\delta + \delta^* S_a)\}] + O(|\beta|^2 \text{ or } |\delta|^2)\Big]\Big/\sigma(\theta), \qquad \ldots\ldots(20)$$

where Θ is the angle which the spin direction of the incident neutrons makes with the scattered direction.

(ii) *For incident neutrons of very high energies* (*greater than* 100 Mev.)

Here again the calculation for $\sigma(\theta)$ and $P(\theta)$ becomes easy, since one can use Born's approximation to calculate the scattered wave. This has been done by Ashkin and Wu (1948) and we first briefly outline their procedure. Denoting the triplet part of the interaction potential (1) by

$$V_{\mathrm{T}}(r) = V_1(r) + \left(\frac{3(\boldsymbol{\sigma}_1 \,.\, \mathbf{r})(\boldsymbol{\sigma}_2 \,.\, \mathbf{r})}{r^2} - \boldsymbol{\sigma}_1 \,.\, \boldsymbol{\sigma}_2\right) V_3(r),$$

the scattered wave in Born's approximation is given by

$$\frac{M}{4\pi\hbar^2}\frac{e^{ikr}}{r}\sum_{s'=1}^{3}\chi_{s'}\int \exp(-i\mathbf{k}' \,.\, \mathbf{r})\sum_{s=1}^{3}\langle\chi_{s'}V_{\mathrm{T}}(r)\chi_s\rangle A_s \exp(i\mathbf{k} \,.\, \mathbf{r})\,dV,$$

in which the integration is over the whole volume and $\langle\chi_{s'}V_{\mathrm{T}}(r)\chi_s\rangle$ are the matrix elements of the potential $V_{\mathrm{T}}(r)$.* The first term $V_1(r)$ in $V_{\mathrm{T}}(r)$ gives only diagonal terms. We put

$$\frac{M}{4\pi\hbar^2}\int \exp\{-i(\mathbf{k}'-\mathbf{k}) \,.\, \mathbf{r}\}V_1(r)\,dV = T(\theta). \qquad \ldots\ldots(21)$$

The second term in the potential will give non-diagonal matrix elements as well, corresponding to transitions from one triplet state to another, giving nine integrals in all. Regarding the spin vectors $\boldsymbol{\sigma}_1$ and $\boldsymbol{\sigma}_2$ as fixed while integrating over space, they can be easily seen to be of the form $C(\theta)\times\tau_{s's}$ where

$$C(\theta) = \frac{M}{4\pi\hbar^2}\int_0^\infty r^2 V_3(r)\left(\frac{\sin Kr}{Kr} - 3\frac{\sin Kr - Kr\cos Kr}{(Kr)^3}\right)dr, \qquad \ldots\ldots(22)$$

(with $K = |\mathbf{k}-\mathbf{k}'| = 2k\sin(\frac{1}{2}\theta)$) and

$$\begin{aligned}\tau_{s',s} &= \left\langle\chi_{s'}\left|\frac{3((\mathbf{k}-\mathbf{k}') \,.\, \boldsymbol{\sigma}_1)((\mathbf{k}-\mathbf{k}') \,.\, \boldsymbol{\sigma}_2)}{|\mathbf{k}-\mathbf{k}'|^2} - \boldsymbol{\sigma}_1 \,.\, \boldsymbol{\sigma}_2\right|\chi_s\right\rangle \\ &= \langle\chi_{s'}\,\tau\,\chi_s\rangle, \text{ say.}\end{aligned} \qquad \ldots\ldots(23)$$

If (lmn) are the direction cosines of the vector $\mathbf{k}-\mathbf{k}'$ and the direction of quantization for the spin angular momentum is chosen along $\mathbf{n}$ ($\sigma^{(n)}$ has the eigenvalues ± 1), then the matrix elements $\tau_{s's}$ are given by the equations:

$$\left.\begin{aligned}\tau\chi_1 &= (3n^2-1)\chi_1 + 3(l+im)^2\chi_2 + 3\sqrt{2}n(l+im)\chi_3,\\ \tau\chi_2 &= 3(l-im)^2\chi_1 + (3n^2-1)\chi_2 - 3\sqrt{2}n(l-im)\chi_3,\\ \tau\chi_3 &= 3\sqrt{2}n(l-im)\chi_1 - 3\sqrt{2}n(l+im)\chi_2 + (2-6n^2)\chi_3,\end{aligned}\right\} \qquad \ldots\ldots(24)$$

(cf. Ashkin and Wu 1948, p. 975, where $\mathbf{n}$ is parallel to $\mathbf{k}$).

Using the equations (21)–(24) and writing the amplitude of the scattered wave in the singlet state as $A_a S_a(\theta)$, the coefficients B_s in the scattered wave (see equation (2)) are

$$\left.\begin{aligned}B_1 &= A_1\{T(\theta)+(3n^2-1)C(\theta)\} + 3C(\theta)\{A_2(l-im)^2 + \sqrt{2}n(l-im)A_3\},\\ B_2 &= A_2\{T(\theta)+(3n^2-1)C(\theta)\} + 3C(\theta)\{A_1(l+im)^2 - \sqrt{2}n(l+im)A_3\},\\ B_3 &= A_3\{T(\theta)+(2-6n^2)C(\theta)\} + 3C(\theta)\{\sqrt{2}n(l+im)A_1 - \sqrt{2}n(l-im)A_2\},\\ B_a &= A_a S_a(\theta).\end{aligned}\right\} \qquad \ldots\ldots(25)$$

---

* For simplicity only ordinary forces are considered here. The effect of the exchange operator, however, is to change the ψ_{inc} from exp $(i\mathbf{k} \,.\, \mathbf{r})$ to exp $(-i\mathbf{k} \,.\, \mathbf{r})$ and hence the exchange nature of the force can be taken into account by changing the sign in ψ_{scat} and leaving ψ_{inc} alone.

The form of these expressions in terms of (lmn) is independent of the direction along which the $\mathbf{n}$ (direction of quantization) is chosen in space; (lmn) in terms of θ and ϕ will, of course, vary. One can, therefore, for simplicity, choose this direction along the spin direction of the incident neutrons (cf. §4 (i) where this direction was chosen along the incident direction). A's are now given by putting $\mu=0$ in (3) and replacing $\sigma(\theta)$ and $P(\theta)$ by expressions (4) and (6) respectively. Remembering that $C(\theta)$, $T(\theta)$ and $S_a(\theta)$ are all real, we have

$$\overline{B_1^*B_1}=\tfrac{1}{2}T^2+(3n^2-1)CT+\tfrac{1}{2}C^2(1+3n^2), \qquad \overline{B_2^*B_2}=\tfrac{1}{2}9C^2(1-n^2),$$

$$\overline{B_3^*B_3}=\tfrac{1}{4}T^2+CT(1-3n^2)+C^2(1+3n^2), \qquad \overline{B_a^*B_a}=\tfrac{1}{4}S_a^2(\theta),$$

and $\overline{B_3B_a^*}+\overline{B_aB^*}=\tfrac{1}{2}S_aT+(1-3n^2)CS_a$, from which

$$\sigma(\theta)=\tfrac{3}{4}T^2(\theta)+\tfrac{1}{4}S_a{}^2(\theta)+6C^2(\theta) \qquad \text{......(26)}$$

and

$$P(\theta)=\frac{1}{\sigma(\theta)}[\tfrac{1}{2}T^2(\theta)+C(\theta)\,(T(\theta)-S_a(\theta))(3n^2-1)+\tfrac{1}{2}S_a(\theta)T(\theta)+2C^2(\theta)(3n^2-2)]. \qquad \text{......(27)}$$

§ 5. DISCUSSION ON § 4

Since we have considered in the preceding section the scattering of polarized neutrons by an unpolarized proton gas, the expressions (19) and (26) for $\sigma(\theta)$ for the two energy regions are independent of the azimuth ϕ of scattering and the spin direction of incident neutrons.* $P(\theta)$, however, depends on both, since $\cos\Theta=\sin\mu\sin\theta\cos\phi+\cos\mu\cos\theta$ and $n=\sin\mu\cos\tfrac{1}{2}\theta\cos\phi+\cos\mu\sin\tfrac{1}{2}\theta$ in expressions (20) and (27) respectively (here θ denotes the angle between the incident direction and the spin direction of incident neutrons, cf. §4 (ii). It is obvious from (20) and (27) that the azimuthal variation of $P(\theta\phi)$ is greatest when $\mu=\pi/2$ i.e. when the spins of the incident neutrons are perpendicular to the incident direction; for $\mu=0$, $P(\theta\phi)$ is independent of ϕ. Taking the amplitude S_a of the scattered wave for the singlet state in the low energy region as $1/(\epsilon_a+ik)$ where $\hbar^2\epsilon_a{}^2/M$ is the eigenenergy of the deuteron in the singlet state and the values for α, β and δ given previously, expression (20) for the case $\mu=\pi/2$ reduces to

$$P(\theta)=\frac{1}{2(\epsilon_b^2+k^2)\sigma(\theta)}\left[1+\frac{\epsilon_a\epsilon_b+k^2}{\epsilon_a^2+k^2}+3x\sin^2\theta\cos^2\phi\left(1-\frac{\epsilon_a\epsilon_b+k^2}{\epsilon_a^2+k^2}\right)\right], \qquad \text{......(28)}$$

where $x=\beta/\alpha\sim(ka)^2/10$, while the expression (27) for $P(\theta)$ in the high energy region for $\mu=\pi/2$ reduces to

$$P(\theta)=\frac{1}{\sigma(\theta)}[\tfrac{1}{2}T^2(\theta)+C(\theta)(T(\theta)-S_a(\theta))(3\cos^2\tfrac{1}{2}\theta\cos^2\phi-1)$$
$$+\tfrac{1}{2}S_a(\theta)T(\theta)+2C^2(\theta)(3\cos^2\tfrac{1}{2}\theta\cos^2\phi-2)]. \qquad \text{......(29)}$$

Expression (28) shows that the anisotropy in $P(\theta)$ in the low energy regions is proportional to $(ka)^2$ as compared to the anisotropy in total scattering which is proportional to $(ka)^4$. For $\theta=\pi/2$ and for 1 Mev. incident neutrons, the maximum azimuthal variation in $P(P_{\max}=P_{\varphi=0}-P_{\varphi=\pi/2})$ is negative in sign and is about 0·7%. As the energy increases $|P_{\max}|$ increases and tends to a constant value of about 1·5%. However, formula (28) can hardly be regarded as valid beyond a few mega-electron volts. For the high energy region the values of $C(\theta)$, $T(\theta)$ and $S_a(\theta)$ have been given by Ashkin and Wu over a wide range of energies (from 0 to 200 Mev.) for the square-well potential. Using these values and formula (29) we have plotted in the Figure $P_{\max}$ for $\theta=\pi/2$, where

---

* *Note added in proof.*—The independence of $\sigma(\theta)$ on the azimuth of scattering ϕ in our expressions (19) and (26) is due to the approximations made in calculating the scattered amplitude. If one uses the correct phase shifts to evaluate the scattered amplitude, $\sigma(\theta)$ will depend on ϕ as well, unlike the case (expression (8)) when the interaction potential is spherically symmetrical (see Wolfenstein 1949).

$$P_{\max}(\pi/2)=3\{C(T-S_a)+2C^2)/\{2\sigma(\pi/2)\},$$

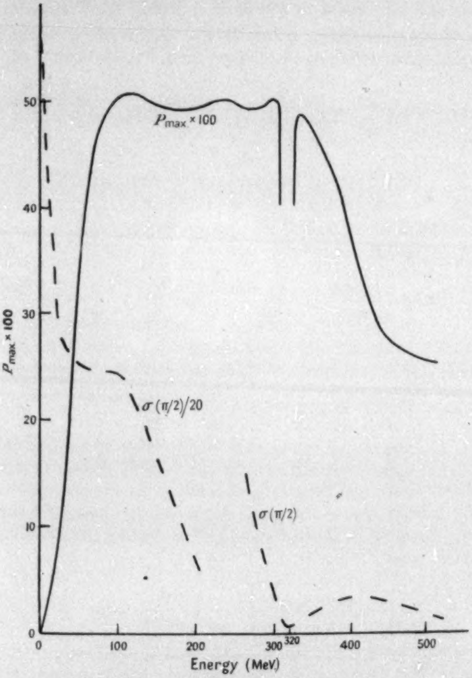

against the energy E of the incident neutrons. Though at low energies Born's approximation is certainly not correct, it gives at least a rough idea of the variation of $P_{\max}$ with E. Starting from zero at $E=0$, it is at first negative and at $E=2{\cdot}5$ Mev. is $-0{\cdot}3\%$. As E increases $P_{\max}$ becomes positive but at 10 Mev. it is only 0·2%; it then rises rapidly to about 40 to 50% at 70 Mev. and remains fairly constant over a wide range of energy. The sharp falling off of $P_{\max}$ at 320 Mev. is due to the fact that $C(\theta)$ vanishes at this energy. Beyond this energy $P_{\max}$ again rises and will show similar oscillations in the higher energy range. For comparison $\sigma(\pi/2)$ in arbitrary units is also plotted. The oscillatory behaviour of σ and $P_{\max}$ is due to the square-well potential and will smooth out for other radial forms of the interaction potential.

ACKNOWLEDGMENTS

The author wishes to thank Professor H. Fröhlich for kind encouragement and for many helpful discussions, and the Commissioners of the 1851 Exhibition for financial support.

APPENDIX

Evaluation of α, β, γ and δ as Functions of Energy of the Incident Neutrons

In this evaluation we follow closely (HP). Let u and w be the solutions of the two coupled radial differential equations for $J=1$, $l=0$ and $J=1$, $l=2$ states, which are

$$\left.\begin{aligned}\left(\frac{d^2}{dr^2}+k^2-\frac{M}{\hbar^2}V_1(r)\right)u&=\frac{M}{\hbar^2}2^{3/2}V_3(r)w\\ \text{and}\quad\left(\frac{d^2}{dr^2}-\frac{6}{r^2}+k^2-\frac{M}{\hbar^2}(V_1(r)-2V_3(r))\right)w&=\frac{M}{\hbar^2}2^{3/2}V_3(r)u.\end{aligned}\right\} \qquad \text{......(I)}$$

Outside the range of the potential, u and w are of the form

$$\left.\begin{aligned}u&=I_0\sin kr+S_0e^{ikr},\\ w&=I_2\left(-\sin kr-\frac{3\cos kr}{kr}+\frac{3\sin kr}{(kr)^2}\right)+S_2e^{ikr}\left(-1-\frac{3i}{kr}+\frac{3}{(kr)^2}\right),\end{aligned}\right\} \qquad \text{......(II)}$$

where I_0 and I_2 are the coefficients of $P_0(\theta)$ and $P_2(\theta)$ in the expansion (15) of the incident wave. S_0 and S_2 are then the two partial amplitudes of the scattered wave, to be determined. Now following (HP), at the boundary of the potential $r=a$ we can write

$$u_a'=Au+Bw, \qquad w_a'=Cw+(D=B)u, \qquad \text{......(III)}$$

where A, B and C are real constants, depending on the energy of the incident neutrons, but independent of the particular solutions chosen for the differential equations (I). Keeping A, B and C fixed and neglecting third and higher powers of ka, we obtain from (II) and (III)

$$S_0\left[(ik-A)\left\{\left(\frac{2}{a}+C\right)-\frac{1}{a}(ka)^2\right\}+B^2\right]$$
$$=I_0\left[ka\left\{A\left(\frac{2}{a}+C\right)-B^2\right\}-k\left\{\left(\frac{2}{a}+C\right)-2k^2a-\tfrac{1}{2}C(ka)^2\right\}\right]+\tfrac{1}{3}I_2Bk(ka)^2$$

or

$$S_0=\alpha I_0+\beta I_2, \quad \text{say,} \qquad \text{......(IV)}$$

and

$$S_2\left[(ik-A)\left\{\left(\frac{2}{a}+C\right)-\frac{1}{a}(ka)^2\right\}+B^2\right]=\tfrac{1}{3}I_0Bk(ka)^2+O(ka)^3I_2$$

or

$$S_2=(\delta=\beta)I_0, \quad \text{say.} \qquad \text{......(V)}$$

$$\beta/\alpha=\left\{\tfrac{1}{3}Bk(ka)^2\right\}\Big/\left[(ka)\left\{A\left(\frac{2}{a}+C\right)-B^2\right\}-k\left\{\left(\frac{2}{a}+C\right)-2k^2a-\tfrac{1}{2}C(ka)^2\right\}\right]. \qquad \text{......(VI)}$$

In order to evaluate β/α and α we have to know A, B and C. Now if u, w and u_0, w_0 are the solutions of the equations (I) for a low finite positive energy and binding energy $-\hbar^2\epsilon_b{}^2/M$ of the deuteron respectively, we have

$$\left(\frac{u'}{u}\right)_{r=a}=\left(\frac{u_0'}{u_0}\right)_{r=a}-\left(\frac{1}{u\,u_0}\right)_{r=a}\int_0^a(k^2+\epsilon_b{}^2)u\,u_0\,dr+\left(\frac{1}{u\,u_0}\right)_{r=a}2^{3/2}\int_0^a V_3(r)(w\,u_0-u\,w_0)\,dr$$

and

$$\left(\frac{w'}{w}\right)_{r=a}=\left(\frac{w_0'}{w_0}\right)_{r=a}-\left(\frac{1}{w\,w_0}\right)_{r=a}\int_0^a(k^2+\epsilon_b{}^2)w\,w_0\,dr+\left(\frac{1}{w\,w_0}\right)_{r=a}2^{3/2}\int_0^a V_3(r)(u\,w_0-w\,u_0)\,dr$$

or

$$u_a'=u_a\left[\left(\frac{u_0'}{u_0}\right)_{r=a}-\gamma(k^2+\epsilon_b{}^2)a-\left(\frac{1}{u\,u_0}\right)_{r=a}2^{3/2}\int_0^a V_3(r)u\,w_0\,dr\right]+\left(\frac{1}{u_0}\right)_{r=a}2^{3/2}\int_0^a V_3(r)w\,u_0\,dr \qquad \ldots\ldots(\text{VII}\,a)$$

and

$$w_a'=w_a\left[\left(\frac{w_0'}{w_0}\right)_{r=a}-\delta(k^2+\epsilon_b{}^2)a-\left(\frac{1}{w\,w_0}\right)_{r=a}2^{3/2}\int_0^a V_3(r)w\,u_0\,dr\right]+\left(\frac{1}{w_0}\right)_{r=a}2^{3/2}\int_0^a V_3(r)u\,w_0\,dr, \qquad \ldots\ldots(\text{VII}\,b)$$

where γ and δ are certain constants of the order of unity.*

If the range a of the potential is small, then within the range of the interaction, the difference between w and w_0 as well as between u and u_0 will be small, and the last of the terms in (VII a) and (VII b) can be written as $u_a\overline{V}_3a$ and $w_a\overline{V}_3a$ respectively; $\overline{V}_3$ is the average of $V_3(r)\times 2^{3/2}$ weighted by the function (u_0w) or $(u\,w_0)$. The two weighted averages are assumed to be the same in view of (III). The coefficients of u and w in (VII) then give the constants A, B and C in terms of ϵ_b, k and a. Now

$$u_0=ce^{-\epsilon_b r},\qquad w_0=de^{-\epsilon_b r}\left(\frac{1}{(\epsilon_b r)^2}+\frac{1}{\epsilon_b r}+\frac{1}{3}\right)\text{ for }r\geqslant a,$$

therefore

$$\left(\frac{u_0'}{u_0}\right)_{r=a}=-\epsilon_b,\qquad \left(\frac{w_0'}{w_0}\right)_{r=a}=-\frac{1}{a}\left(2+\frac{(\epsilon_b a)^2(1+\epsilon_b a)}{(\epsilon_b a)^2+3\epsilon_b a+3}\right),$$

and we have $\beta/\alpha=$ Numerator/Denominator, where the numerator is $\frac{1}{3}(\overline{V}_3a)k(ka)^2$ and the denominator is a long expression which is omitted here to save space. Since in general $\overline{V}_3$ is approximately the depth of the non-central potential, the highest term in the denominator is approximately $\{k(u_0/w_0)_{r=a}\overline{V}_3a\}$, the rest of the terms being of the order of (ka) or $(ka)^2$ times this. Hence if $\overline{V}_3$ is not zero, to a first approximation $\beta/\alpha=\frac{1}{3}(w_0/u_0)_{r=a}(ka)^2$. For $\epsilon_b a=\frac{1}{2}$, (HP) derive the value of

$$\left(\frac{w_0}{u_0}\right)_{r=a}=\frac{d}{c}\left(\frac{1}{(\epsilon_b a)^2}+\frac{1}{\epsilon_b a}+\frac{1}{3}\right)$$

---

* The constants γ and δ in (7) are not to be confused with those in the other expressions.

from the observed quadrupole moment of the deuteron as 0·3. Hence $\beta/\alpha \sim (ka)^2/10$. The value of α to this approximation in (ka) and $(\epsilon_b a)$ is a complicated one. Since, however, we are not interested in the absolute magnitudes of the scattering cross section, we have taken $\alpha \simeq 1/(\epsilon_b + ik)$ for simplicity, even though it is not strictly justified.

REFERENCES

ASHKIN, J., and WU, T., 1948, *Phys. Rev.*, **73,** 973.

BARGMANN, V., 1949, *Phys. Rev.*, **75,** 301.

CONDON, E. U., and SHORTLEY, G. H., 1935, *Theory of Atomic Spectra* (Cambridge: University Press), p. 76.

FRÖBERG, C., 1948 a, *Ark. Mat. Astr. Fys.*, **34,** No. 28; 1948 b, *Ibid.*, **36,** No. 11.

HEPNER, W., and PEIERLS, R., 1942, *Proc. Roy. Soc.* A, **181,** 43.

HOLMBERG, B., 1948, *Kungl Fysiografiska Süllskapets* I *Lund Handl.*, **18,** No. 7.

HYLLERAAS, E., 1948, *Phys. Rev.*, **74,** 48.

RARITA, W., and SCHWINGER, J., 1941, *Phys. Rev.*, **59,** 436.

ROSENFELD, L., 1948, *Nuclear Forces* (Amsterdam: North Holland Publishing Co.).

SCHWINGER, J., 1948, *Phys. Rev.*, **73,** 407.

WIGNER, E., 1941, *Proc. Nat. Acad. Sci., Wash.*, **27,** 282.

WOLFENSTEIN, L., 1949, *Phys. Rev.*, **76,** 541.

Interaction between Four Half-Spin Particles and the Decay of the μ-Meson

BY L. MICHEL
Physics Department, University of Manchester

Communicated by L. Rosenfeld; MS. received 28th September 1949

ABSTRACT. The general direct coupling between four fermions is studied. It is a linear combination of the five invariants used in β-decay theory. Altering the order of the particles in the Hamiltonian changes only the coefficients of the linear combination. The formalism of charge conjugation is used with the ordinary theory or the Majorana abbreviated theory for neutral particles. This is applied to the study of the decay of the μ-meson into an electron and two neutrinos.

§ 1. INTRODUCTION

THE purpose of this work is to study the most general contact interaction between four half-spin particles. The interaction Hamiltonian density used here consists of the most general linear combination of scalars which can be made up from four wave functions (or the conjugate of some of them). The interaction can be produced physically by an intermediary field; then the Hamiltonian only gives a phenomenological description.

Such an interaction between four fermions can give rise to $2^4 = 16$ kinds of processes, where i particles $(0 \leqslant i \leqslant 4)$ are absorbed $(\mathrm{M} = -1)$, and j particles $(j = 4 - i)$ are emitted $(\mathrm{M} = +1)$. M is a dichotomic variable having the values -1 and $+1$ for absorbed and emitted particles respectively. For example:

$i = 1$, β-decay: $N = P^+ + \epsilon^- + \nu$ with $\mathrm{M}_N = -1$, $\mathrm{M}_P = \mathrm{M}_\epsilon = \mathrm{M}_\nu = +1$;
$i = 2$, K-capture; scattering of fermions by fermions;
$i = 3$, pair annihilation near to an electron without emission of photons;
$i = 0$ or $i = 4$ (cf. Critchfield and Wigner 1941, Critchfield 1943).

The necessary energies for these processes can be supplied by external fields (e.g. $P^+ \rightarrow N + \epsilon^+ + \nu$).

The study of these processes will be restricted to the Schrödinger method of perturbation theory in which the Hamiltonian of the interaction does not contain the time explicitly.

I. INTERACTION BETWEEN FOUR HALF-SPIN PARTICLES

§1. FORMALISM OF THE CHARGE CONJUGATE THEORY

The charge conjugate formalism, which is preferable to Dirac's hole theory (see §9), has been developed by Majorana (1937) and later by Racah (1937) and Kramers (1937). Pauli's (1941) notation ($\hbar = c = 1$) will be followed here.

The most convenient representation of Dirac's matrices, which does not restrict the formalism, is that proposed by Majorana (1937).

$$(\gamma_\mu \partial_\mu + \kappa)\psi = 0 \qquad \ldots\ldots(1)$$

is the Dirac equation, where the γ_μ satisfy

$$\gamma_\mu \gamma_\nu + \gamma_\nu \gamma_\mu = 2\delta_{\mu\nu}. \qquad \ldots\ldots(2)$$

In the Majorana representation ($k = 1, 2, 3$)

$$\gamma_k^\dagger = \gamma_k = \tilde{\gamma}_k = \gamma_k^*; \qquad \gamma_4^\dagger = \gamma_4 = -\tilde{\gamma}_4 = -\gamma_4^*, \qquad \ldots\ldots(3)$$

or, with $\alpha_k = i\gamma_4\gamma_k$ and $\beta = \gamma_4$,

$$\alpha_k^\dagger = \alpha_k = \tilde{\alpha}_k = \alpha_k^*; \qquad \beta^\dagger = \beta = -\tilde{\beta} = -\beta^*. \qquad \ldots\ldots(3')$$

A solution of (1) can be split into plane waves normalized in a volume V:

$$\psi_\varrho = \frac{1}{(NV)^{\frac{1}{2}}} \sum_{\mathbf{k}\sigma} [u_+(\mathbf{k}, \sigma) a_\varrho(\mathbf{k}, \sigma) \exp\{i(\mathbf{k}\,.\,\mathbf{x} - k_0 x_0)\} + u_-^\dagger(\mathbf{k}, \sigma) b_\varrho(\mathbf{k}, \sigma)$$
$$\times \exp\{-i(\mathbf{k}\,.\,\mathbf{x} - k_0 x_0)\}] \qquad \ldots\ldots(4)$$

($N = \Sigma N_{\mathrm{L}}(\mathbf{k}, \sigma)$ is the total number of particles of this field, see equation (11)), and because of the Majorana representation

$$b_\varrho^*(\mathbf{k}, \sigma) = a_\varrho(\mathbf{k}, \sigma); \qquad \ldots\ldots(5)$$

where $\mathbf{k}$ is the momentum, $k_0 = (\mathbf{k}^2 + \kappa^2)^{\frac{1}{2}}$ and σ is a dichotomic variable for the two states of spin. Also

$$\left.\begin{aligned} \sum_\sigma a_\mu(\mathbf{k}, \sigma) a_\nu^*(\mathbf{k}, \sigma) &= \tfrac{1}{2}\left(1 + \frac{\boldsymbol{\alpha}\,.\,\mathbf{k} + \beta\kappa}{k_0}\right)_{\mu\nu} = [D(+)]_{\mu\nu} \\ \sum_\sigma b_\mu(\mathbf{k}, \sigma) b_\nu^*(\mathbf{k}, \sigma) &= \sum_\sigma a_\mu^* a_\nu = \tfrac{1}{2}\left(1 + \frac{\boldsymbol{\alpha}\,.\,\mathbf{k} - \beta\kappa}{k_0}\right)_{\mu\nu} = [D(-)]_{\mu\nu} = [\tilde{D}(+)]_{\mu\nu} \end{aligned}\right\} \qquad \ldots\ldots(6)$$

(there is a misprint of sign in Pauli's formula (1941, equation (86)).

It is assumed (without restricting the theory) that in (u) the indices

(a) + or − denotes for charged particles, the particle of charge $+e$ or $-e$ respectively (e being the charge of the positron);

(b) for neutral particles which have charge conjugate states, the indices + or − correspond to the sign of the magnetic moment (with respect to the spin direction);

(*c*) for neutral particles which have no different charge conjugate states, $u_+ \equiv u_-$ (this could be written u_0). These particles have no interaction with the electromagnetic field and cannot be described by Dirac's hole theory. They were first treated by Majorana (1937), and they will be referred to as 'Majorana neutral particles'.

Let us call

$$\left.\begin{array}{lll} \psi^{\mathrm{K}} = \psi, & u^{(\mathrm{K})} = u & \text{if } \mathrm{K} = -1 \\ \psi^{\mathrm{K}} = \psi^*, & u^{(\mathrm{K})} = u^\dagger & \text{if } \mathrm{K} = +1 \end{array}\right\}. \qquad \ldots\ldots (7)$$

The index L is either $+1$ or -1, and indicates either (*a*) the sign of the charge or (*b*) the sign of the magnetic moment, or (*c*) for Majorana neutral particles L is arbitrary (L or $-$L indicating the same state).

It is seen from (4) that ψ^* can be obtained from ψ by changing L into $-$L, so complex conjugation and charge conjugation are equivalent. Equations (4) and (6) can be written:

$$\psi_\varrho^{\mathrm{K}} = \frac{1}{(NV)^{\frac{1}{2}}} \sum_{\mathbf{k}\sigma} \sum_{\mathrm{L}} u_{\mathrm{L}}^{(\mathrm{LK})}(\mathbf{k}, \sigma) a_\varrho^{\mathrm{LK}}(\mathbf{k}, \sigma) \exp\{-\mathrm{LK} i(\mathbf{k}\,.\,\mathbf{x} - k_0 x_0)\} \quad \ldots\ldots (8)$$

and

$$\sum_\sigma a^{-\mathrm{K}}(\mathbf{k}, \sigma) a^{\mathrm{K}}(\mathbf{k}, \sigma) = D(\mathrm{K}). \qquad \ldots\ldots (9)$$

For Majorana neutral particles $\psi^{\mathrm{K}} = \psi^{-\mathrm{K}}$ (ψ is real). In formula (8) the upper index LK plays the part of the index K as defined by (7), its values being the product of the K and L occurring separately in (8).

The anti-commutation rules can be written

$$[u_{\mathrm{L}}^{(-\mathrm{K})}(\mathbf{k}, \sigma), u_{\mathrm{L}'}^{(\mathrm{K}')}(\mathbf{k}', \sigma')]_+ = \delta_{\mathrm{KK}'} \delta_{\mathrm{LL}'} \delta(\mathbf{k} - \mathbf{k}') \delta_{\sigma\sigma'} \qquad \ldots\ldots (10)$$

and

$$u_{\mathrm{L}}^{(\mathrm{K})}(\mathbf{k}, \sigma) u_{\mathrm{L}}^{(-\mathrm{K})}(\mathbf{k}, \sigma) = \left\{\begin{array}{ll} N_{\mathrm{L}}(\mathbf{k}, \sigma) & \text{if } \mathrm{K} = +1 \\ 1 - N_{\mathrm{L}}(\mathbf{k}, \sigma) & \text{if } \mathrm{K} = -1 \end{array}\right\}. \qquad \ldots\ldots (11)$$

The operator $N_{\mathrm{L}}(\mathbf{k}, \sigma)$ represents the number of particles in the state $\mathbf{k}, \sigma$, L; its eigenvalues are 0 or 1.

$u_{\mathrm{L}}^{(\mathrm{LK})}$ is an absorption operator if $\mathrm{LK} = \mathrm{M} = -1$, and

an emission operator if $\mathrm{LK} = \mathrm{M} = +1$; $\qquad \ldots\ldots (12)$

for a charged particle, of charge L*e*, it changes the total charge by an amount K*e*. All the dichotomic variables used here are listed in Table 3.

§ 2. PARTICLES OF DIFFERENT KINDS

If there are two different kinds S of particles, their amplitudes $v(S)$ commute:

$$[v^{(\mathrm{K})}(S, \mathrm{L}), v^{(\mathrm{K}')}(S', \mathrm{L}')]_- = 0 \quad \text{if} \quad S \neq S'. \qquad \ldots\ldots (13)$$

However, it is even possible to consider particles of different rest mass as like particles. For example, neutrons and protons are considered as nucleons, or electrons and neutrinos as leptons, by the formalism of isotopic spin, which is nothing other than writing the same v's in a more condensed form:

$$v(S) = \begin{pmatrix} v(1) \\ 0 \end{pmatrix} \text{ if } S = 1, \ v(S) = \begin{pmatrix} 0 \\ v(2) \end{pmatrix} \text{ if } S = 2 \text{ and } [v^{(\mathrm{K})}(1, \mathrm{L}), v^{(\mathrm{K}')}(2, \mathrm{L}')]_+ = 0,$$

since $v^{(\mathrm{K})}(1, \mathrm{L}) v^{(\mathrm{K}')}(2, \mathrm{L}') = 0$.

Another interesting extension which has been made is to consider a Majorana neutral particle and the two states of a charged particle as three conjugate states $(+, 0, -)$ of the same particle (Noma 1948).

Alternately there is a transformation, due to Klein (1938), which makes it possible always to have anti-commutation between the amplitudes of two like or unlike particles.

If the v's satisfy (13), putting $v^{(\mathrm{K})}(1, \mathrm{L}) = u^{(\mathrm{K})}(1, \mathrm{L})$ and $v^{(\mathrm{K})}(2, \mathrm{L}) = \zeta(1) u^{(\mathrm{K})}(2, \mathrm{L})$ with $\zeta(1) = \Pi[1 - 2N(1, \mathrm{L}, \mathbf{k}, \sigma)]$ (Π is taken over all the states $\mathrm{L}, \mathbf{k}, \sigma$) one gets $[u^{(\mathrm{K})}(1, \mathrm{L}), u^{(\mathrm{K}')}(2, \mathrm{L}')]_+ = 0$.

This can be extended to any number of kinds S of particles, so that one gets

$$[u^{(-\mathrm{K})}(S, \mathrm{L}, \mathbf{k}, \sigma),\ u^{(\mathrm{K}')}(S', \mathrm{L}', \mathbf{k}', \sigma')]_+ = \delta_{\mathrm{KK}'} \delta_{SS'} \delta_{\mathrm{LL}'} \delta(\mathbf{k} - \mathbf{k}') \delta_{\sigma\sigma'}. \qquad \ldots\ldots (14)$$

§ 3. SCALARS FORMED FROM FOUR ψ^{K}

The method of formation of such scalars is well known. Using only the relations (1) and (2), it has been demonstrated by Pauli (1936), corrected by Racah (1937). With the four γ_μ one can build 16 matrices $\gamma_A = \gamma_{[i, a]}$ ($A = 1$ to 16 or $i = 1$ to 5), viz.:

A	i	$a=1$	$a=2$	$a=3$	$a=4$	$a=5$	$a=6$
1	1	1					
2 to 5	2	γ_1	γ_2	γ_3	γ_4		
6 to 11	3	$i\gamma_2\gamma_3$	$i\gamma_3\gamma_1$	$i\gamma_1\gamma_2$	$i\gamma_1\gamma_4$	$i\gamma_2\gamma_4$	$i\gamma_3\gamma_4$
12 to 15	4	$i\gamma_2\gamma_3\gamma_4$	$i\gamma_3\gamma_1\gamma_4$	$i\gamma_1\gamma_2\gamma_4$	$-i\gamma_1\gamma_2\gamma_3$		
16	5	$\gamma_1\gamma_2\gamma_3\gamma_4$					

It is easily, the γ_μ satisfying (2) and (3), that $\gamma_A{}^2 = 1$ and $\gamma_A{}^\dagger = \gamma_A$. If

$$F_{ia} = \epsilon_{ia} \gamma_4 \gamma_{[i, a]} \qquad \ldots\ldots (15)$$

where ϵ_{ia} is such that $\epsilon_{ia}{}^2 = +,\ - - - +,\ + + + - - -,\ + + + -,\ -$, then

$$F_{ia}{}^\dagger = F_{ia} \qquad \ldots\ldots (16)$$

and

$$\sum_{\mu\nu} [\psi_S{}^{\mathrm{K}}(\mathbf{x}, x_0)]_\mu (F_{ia})_{\mu\nu} [\psi_{S'}{}^{\mathrm{K}'}(\mathbf{x}, x_0)]_\nu = \psi_S{}^{\mathrm{K}} F_{ia} \psi_{S'}{}^{\mathrm{K}'}$$

is a scalar for $i = 1$, the four components of a vector for $i = 2$, a skew tensor for $i = 3$, a pseudovector for $i = 4$ and a pseudoscalar for $i = 5$.

The scalars we require are $J_i(\kappa, P) =$ the scalar product of $\psi_1{}^{\mathrm{K}_1} F_{ia} \psi_2{}^{\mathrm{K}_2}$ and $\psi_3{}^{\mathrm{K}_3} F_{ia} \psi_4{}^{\mathrm{K}_4}$, i.e.

$$J_i(\kappa, P) = \sum_a \epsilon'_{ia} (\psi_1{}^{\mathrm{K}_1} F_{ia} \psi_2{}^{\mathrm{K}_2})(\psi_3{}^{\mathrm{K}_3} F_{ia} \psi_4{}^{\mathrm{K}_4}), \qquad \ldots\ldots (17)$$

where $\epsilon_{ia} = +,\ + + + -,\ + + + - - -,\ + + + -,\ +$, and (κ) is a contraction for $(\mathrm{K}_1, \mathrm{K}_2, \mathrm{K}_3, \mathrm{K}_4)$ and can have 16 different values; P indicates that the four ψ^{K} in $J_i(P)$ are in a definite order: 1, 2, 3, 4.

From (15), (16) and (3) it is found that

$$\widetilde{F}_{ia} = \theta_i F_{ia} \qquad \ldots\ldots (18)$$

with $\theta_i = -1, +1, +1, -1, -1$.

§ 4. THE MOST GENERAL HAMILTONIAN OF THE INTERACTION

We choose the Schrödinger picture for the operator H which then does not depend explicitly on the time, and have taken the same axes for the Heisenberg and Schrödinger pictures at time $x_0=0$. We therefore put $x_0=0$ in $J_i(\kappa, P)$, given by (17).

The most general Hamiltonian of the interaction, which must be Hermitian, can be written:

$$H=\int_V h(\mathbf{x})\,d\mathbf{x} \text{ with } h=\sum_{P=1}^{24}\sum_{\mathrm{K}=1}^{16}\sum_{i=1}^{5}\mathfrak{g}_i(\kappa, P)[J_i(\kappa, P)+J_i^\dagger(\kappa, P)]. \qquad \ldots\ldots (19)$$

The sum $\sum_P$ indicates a summation over all the twenty-four permutations of the four indices $S=1, 2, 3, 4$; the sum $\sum_{\mathrm{K}}$ indicates a summation over the 16 possible sign combinations of $\kappa=(\kappa_1, \kappa_2, \kappa_3, \kappa_4)$; and $\mathfrak{g}_i(\kappa, P)$ are real numbers called interaction constants.

For the following considerations we must exclude the transition in which two particles are absorbed and emitted again in their initial states: this would correspond to the self-energies of these particles due to this interaction.

We can then say that the ψ^{K} anti-commute, and from (16) it follows that

$$(\psi_S{}^{\mathrm{K}}F_{ia}\psi_{S'}{}^{\mathrm{K}'})^\dagger=-\psi_{S'}{}^{-\mathrm{K}'}F_{ia}\psi_S{}^{-\mathrm{K}}.$$

Therefore, if P_1 is the permutation (2143)

$$J_i^\dagger(\kappa, P)=J_i(-\kappa, P_1P). \qquad \ldots\ldots (20)$$

From (14) and (18) one gets

$$J_i^\dagger(\kappa, P_1P)=(-1)^2\theta_i^2J_i(\kappa, P)=J_i(\kappa, P). \qquad \ldots\ldots (21)$$

Therefore (20) can be written

$$J_i^\dagger(\kappa, P)=J_i(-\kappa, P)$$

and (19) becomes

$$h=\sum_P\sum_{\mathrm{K}}\sum_i\mathfrak{g}_i(\kappa, P)[J_i(\kappa, P)+J_i(-\kappa, P)]=\sum_P\sum_{\mathrm{K}}\sum_i[\mathfrak{g}_i(\kappa, P)+\mathfrak{g}_i(-\kappa, P)]J_i(\kappa, P)$$

or

$$h=\sum_P\sum_{\mathrm{K}}\sum_i\mathfrak{g}_i'(\kappa, P)J_i(\kappa, P) \qquad \ldots\ldots (22)$$

with

$$\mathfrak{g}_i'(\kappa, P)=\mathfrak{g}_i(\kappa, P)+\mathfrak{g}_i(-\kappa, P);$$

therefore one has

$$\mathfrak{g}_i'(\kappa, P)=\mathfrak{g}_i'(-\kappa, P). \qquad \ldots\ldots (23)$$

§ 5. ELIMINATION OF THE SUMMATION OVER THE TWENTY-FOUR PERMUTATIONS

It is well known (see for instance Speiser 1945) that the S_4 group (four object permutations) is soluble. All the permutations are given by the twenty-four terms of the symbolic expression: $(1+P_3)(1+P_3P_4+P_4P_3)(1+P_2)(1+P_1)$ with $P_1=(2143)$, $P_2=(3412)$, $P_3=(2134)$, $P_4=(1432)$. Each P is a product of the form

$$P=P_aP_b\ldots.P_k, \qquad \ldots\ldots (24)$$

where $a, b, \ldots. k=0$ to 4 and $P_0\equiv 1$. Let us write $(-1)^P=+1$ or -1 according as P is an even or an odd permutation.

We will now show that, for every P,

$$J_i(\kappa, PP_0)=\sum_j(-1)^PC_{ij}^PJ_j(\kappa, P_0), \qquad \ldots\ldots (25)$$

which means that under any permutation P of the four indices S, the J_i undergo a linear substitution; later on $J_i(\kappa, P)$ will simply be written $J_i(\kappa)$.

Indeed, for $P=P_1$, P_2 or P_3 we very easily find: $C_{ij}^{P_1}=\delta_{ij}$ (see (21)), $C_{ij}^{P_2}=\delta_{ij}$ (evident), $C_{ij}^{P_3}=\theta_i\delta_{ij}$ (see (18)). The case of $P=P_4$ has been studied by Fierz (1937), and the same method can be extended to the present choice of $F_{i\omega}$; it is found that

$$C_{ij}^{P_4}=\begin{pmatrix} \frac{1}{4} & -\frac{1}{4} & \frac{1}{4} & \frac{1}{4} & -\frac{1}{4} \\ -1 & -\frac{1}{2} & 0 & -\frac{1}{2} & -1 \\ \frac{3}{2} & 0 & -\frac{1}{2} & 0 & -\frac{3}{2} \\ 1 & -\frac{1}{2} & 0 & -\frac{1}{2} & 1 \\ -\frac{1}{4} & -\frac{1}{4} & -\frac{1}{4} & \frac{1}{4} & \frac{1}{4} \end{pmatrix}$$

Therefore for every permutation P, which is always a product of the form (24) of the four permutations P_1, P_2, P_3, P_4, we get

$$C_{ij}^{P}=\sum_{lm\ldots r} C_{il}^{P_a}C_{lm}^{P_b}\ldots\ldots C_{rj}^{P_k}.$$

Then (22) can be written $h=\sum_{P}\sum_{\mathbf{K}}\sum_{ij}\mathfrak{g}_i'(\kappa, P)(-1)^P C_{ij}^P J_j(\kappa)$.

By putting $$g_j(\kappa)=\sum_{i,P}\mathfrak{g}'(\kappa, P)(-1)^P C_{ij}^P$$

one gets $$h=\sum_{\mathbf{K}}\sum_{j} g_j(\kappa)J_j(\kappa) \qquad \ldots\ldots (26)$$

and (23) gives $$g_j(\kappa)=g_j(-\kappa). \qquad \ldots\ldots (27)$$

This last relation will be studied in §7.

Changing the order of the particles in H only means 'changing the name' of the interaction constants g_j; thus H remains invariant.

§6. A REMARKABLE INTERACTION

Can we define an interaction which is independent of the order of the four ψ^K in H?

A permutation leaves H invariant:

$$h=\sum_{\mathbf{K}}\sum_{j} g_j(\kappa)J_j(\kappa)=\sum_{\mathbf{K}}\sum_{i} g_i'(\kappa)J_i'(\kappa) \quad \text{with} \quad J_i(\kappa, P)=J_i'(\kappa),$$

but changes the 'five vector' $\vec{g}(\kappa)$ into $\vec{g}'(\kappa)$ according to $\vec{g}=(-1)^P\tilde{C}^P.\vec{g}'$ because equation (25) gives $J_i'(\kappa)=\sum_j(-1)^P C_{ij}{}^P J_j(\kappa)$, so that one must have

$$h=\sum_{\mathbf{K}}\sum_{j} g_j(\kappa)J_j(\kappa)=\sum_{\mathbf{K}}\sum_{ij} g_i'(\kappa)(-1)^P C_{ij}{}^P J_j(\kappa),$$

which gives $\sum_i g_i'(-1)^P C_{ij}{}^P=g_j$ or $(-1)^P\vec{g}'.C^P=\vec{g}$ or $(-1)^P\tilde{C}^P.\vec{g}'=\vec{g}$.

The above question is thus reduced to this: are there common 'eigenvectors' to the twenty-four $(-1)^P\tilde{C}^P$ matrices? To answer this it is sufficient to look for the common 'eigenvectors' of $-\tilde{C}^{P_3}$ and $-\tilde{C}^{P_4}$, since the other $(-1)^P\tilde{C}^P$ are products of 1, $-\tilde{C}^{P_3}$ and $-\tilde{C}^{P_4}$.

One finds that *the only* common 'eigenvectors' are given by

$$g_2=g_3=0, \quad g_1=-g_4=g_5. \qquad \ldots\ldots (28\,a)$$

They correspond to the 'eigenvalue' +1. Therefore h is symmetrical for all the ψ^{K} (which anti-commute); this is easy to verify, for, starting from

$$h=\sum_{\kappa}\sum_{i}\bar{g}(\kappa)\sum_{P}J_i(\kappa, P)=\sum_{\kappa}\sum_{i}\bar{g}(\kappa)\sum_{j}(\sum_{P}(-1)^P C_{ij}{}^P)J_j(\kappa)=\sum_{\kappa}\sum_{ij}\bar{g}(\kappa)Z_{ij}J_j(\kappa),$$

with $Z=(1-C^{P_3})(1+C^{P_5}C^{P_4}+C^{P_4}C^{P_5})(1+C^{P_2})(1+C^{P_1})$, one finds

$$h=\sum_{\kappa}2(\bar{g}_1-4\bar{g}_4+\bar{g}_5)(J_1-J_4+J_5) \quad \text{or} \quad h=\sum_{\kappa}g_0(\kappa)[J_1(\kappa)-J_4(\kappa)+J_5(\kappa)]. \qquad \ldots\ldots(28\,b)$$

It is also easy to verify that there is no h completely antisymmetrical with respect to the ψ^{K} (which anti-commute) because

$$(1+C^{P_3})(1+C^{P_5}C^{P_4}+C^{P_4}C^{P_5})(1+C^{P_2})(1+C^{P_1})=0.$$

Has this remarkable interaction a physical meaning? This question has no meaning if H is only phenomenological (see introduction). However, the field theory allows us to assume a physically direct interaction between four particles (that would be unthinkable with only the classical notion of forces), and we have seen that the only direct interaction symmetrical with respect to the four particles is the remarkable one g_0 (see equation (28)).

Now, in a Dirac equation, it is well known that F_2 and F_3 correspond to electromagnetic interaction and the sign of the interaction constant (electric charge or magnetic moment) is changed by charge conjugation; F_1, F_4, F_5 would correspond to a non-electromagnetic interaction and the sign of the interaction constant (mesic charge (Okayama 1949) for instance) is not changed by charge conjugation; but the $J_i(\kappa)$, which are quadratic with respect to the F_i, are invariant by charge conjugation and $g_i(\kappa)=g_i(-\kappa)$. However, there is only one interaction built either with F_2, F_3 or F_1, F_4, F_5 independently of the order chosen for the ψ^{K} in writing h: it is the remarkable interaction g_0 built with the three non-magnetic operators.

The interaction g_0 has already been proposed by Critchfield (1943) and can be written as the determinant of the four components of the four ψ^{K}.

§ 7. CLASS OF REACTIONS WITH SAME $g(\kappa)$

A reaction between four particles is defined by (see Table 3) the values of the M_S and of the L_S of each particle ($S=1$ to 4).

The conservation of the electric charge requires

$$\sum_{(S)c}\mathrm{M}_S\mathrm{L}_S=0, \qquad \ldots\ldots(29)$$

where Σ means the sum over the charged particles only.

We have already seen (12) that

$$\mathrm{M}_S\mathrm{L}_S=\mathrm{K}_S, \qquad \ldots\ldots(30)$$

so (29) can be written

$$\sum_{(S)c}\mathrm{K}_S=0. \qquad \ldots\ldots(31)$$

This relation indicates the possible different values which can be taken for κ (κ_1, κ_2, κ_3, κ_4) and for $\vec{g}(\kappa)=\vec{g}(-\kappa)$ in H.

For example, in β-radioactivity the magnetic moment of the neutron is of negative sign; let m be the sign of the magnetic moment of the neutrino emitted in β^--decay. Then the reaction

$$\begin{array}{lcccccc} & & & \mathrm{N} & \mathrm{P} & \epsilon & \nu \\ (a)\ \mathrm{N}_- \rightarrow \mathrm{P}^+ + \epsilon^- + \nu_{\mathrm{m}} \text{ corresponds to} & \left\{\begin{array}{l}\mathrm{M}\\ \mathrm{L}\end{array}\right. & & \begin{array}{c}-\\-\end{array} & \begin{array}{c}+\\+\end{array} & \begin{array}{c}+\\-\end{array} & \begin{array}{c}+\\\mathrm{m}\end{array} \\ \text{and (28) gives for } \kappa & \kappa & & + & + & - & \mathrm{m} \end{array}$$

With four Dirac neutral particles there are of course $2^4 \times 2^4 = 256$ distinct possible reactions $\mathrm{M} = (\mathrm{M}_1, \mathrm{M}_2, \mathrm{M}_3, \mathrm{M}_4)$, $\mathrm{L} = (\mathrm{L}_1, \mathrm{L}_2, \mathrm{L}_3, \mathrm{L}_4)$. This number is different for other kinds of particles since the charged particles have to fulfil (29) and the Majorana particles have only one state L. The result is given in the fifth line of Table 1.

Table 1

No. of charged particles	0	0	0	0	0	2	2	2	4
No. of Dirac neutral particles	4	3	2	1	0	2	1	0	0
No. of Majorana neutral particles	0	1	2	3	4	0	1	2	0
No. of different $\vec{g}$ or classes	8	4	2	1	1	4	2	1	3
No. of different reactions	256	128	64	32	16	128	64	32	96
No. of reactions per class	32	32	32	32	16	32	32	32	32

This table refers only to the cases of four distinguishable particles.

When a reaction is realized in nature, a $\vec{g}(\kappa) = \vec{g}(-\kappa)$ must be given for describing it, and all the reactions which have the same $\pm\kappa = (\kappa_1, \kappa_2, \kappa_3, \kappa_4$ or $-\kappa_1, -\kappa_2, -\kappa_3, -\kappa_4)$ can be associated with this $\vec{g}$. The set of all reactions which can be described by the same $\vec{g}$ will be called a 'class'. Therefore the interaction Hamiltonian density which describes all the interactions of a class is (like (26), but without summation over κ)

$$h = \sum_j g_j(\kappa)[J_j(\kappa) + J_j(-\kappa)] = \vec{g} \cdot [\vec{J}(\kappa) + \vec{J}(-\kappa)].$$

For example, the reaction

(b) $\mathrm{N}_- + \nu_{-\mathrm{m}} \rightarrow \mathrm{P}^+ + \epsilon^-$ belongs to the same class of reactions as (a): $\kappa = (+, +, -, \mathrm{m})$, but the reaction

(c) $\mathrm{N}_- + \nu_{+\mathrm{m}} \rightarrow \mathrm{P}^+ + \epsilon^-$ belongs to another class: $\kappa(+, +, -, -\mathrm{m})$, unless the neutrino is a Majorana particle, when the two reactions would be identical, $\nu_{-\mathrm{m}} \equiv \nu_{\mathrm{m}}$.

This very simple remark will be useful later on.

For given kinds (charged, Dirac or Majorana neutral) of the four fermions the fourth line of Table 1 gives the number of different classes of reactions and the sixth line the number of reactions per class.

§8. STUDY OF ONE REACTION. DETERMINATION OF TRANSITION PROBABILITIES: SPIN AVERAGES

For this study it will be assumed that the transition can be studied by the Born approximation, i.e. the particles are described by plane waves.

The transition is given by $\mathrm{M} = (\mathrm{M}_1, \mathrm{M}_2, \mathrm{M}_3, \mathrm{M}_4)$ and $\mathrm{L} = (\mathrm{L}_1, \mathrm{L}_2, \mathrm{L}_3, \mathrm{L}_4)$; therefore κ is known since $\kappa_S = \mathrm{M}_S \mathrm{L}_S$. If H_{T} is the element of H which leads to the transition T, the probability per unit time of the transition is proportional to $|H_{\mathrm{T}}|^2$.

First case: the four particles are distinguishable.

From (8), (12), (17) and (26) one gets: $H_{\mathrm{T}}=\int_V h_{\mathrm{T}}(\mathbf{x})\,d\mathbf{x}$, i.e.

$$H_{\mathrm{T}}=\sum_{ia} g_i(\kappa)\epsilon_{ia}'u_{\mathrm{L}_1}{}^{(\mathrm{L}_1\mathrm{K}_1)}u_{\mathrm{L}_2}{}^{(\mathrm{L}_2\mathrm{K}_2)}u_{\mathrm{L}_3}{}^{(\mathrm{L}_3\mathrm{K}_3)}u_{\mathrm{L}_4}{}^{(\mathrm{L}_4\mathrm{K}_4)}$$

$$\times(a_1{}^{\mathrm{L}_1\mathrm{K}_1}F_{ia}a_2{}^{\mathrm{L}_2\mathrm{K}_2})(a_3{}^{\mathrm{L}_3\mathrm{K}_3}F_{ia}a_4{}^{\mathrm{L}_4\mathrm{K}_4})(V^{-\frac{1}{2}})^4\int_V[\exp\{-i(\sum_S \mathrm{K}_S\mathrm{L}_S\mathbf{k}_S).\mathbf{x}\}]\,d\mathbf{x}$$

where $\sum_S \mathrm{L}_S\mathrm{K}_S\mathbf{k}_S=\sum_S \mathrm{M}_S\mathbf{k}=0$ from the conservation of momentum. Therefore the integral is equal to V and

$$|H_{\mathrm{T}}|^2=H_{\mathrm{T}}{}^{\dagger}H_{\mathrm{T}}=\sum_{ia}\sum_{jb}V^{-2}g_ig_j\epsilon_{ia}'\epsilon_{jb}'U\,.\,A_{iajb} \qquad \ldots\ldots(32)$$

with $U=1$ if the transition is allowed, i.e. the particles to be absorbed are present and the states of the particles to be created are not occupied initially (see (11)).

$$A_{iajb}(\mathbf{k}_S,\sigma_S)=(a_2{}^{-\mathrm{M}_2}F_{ia}a_1{}^{-\mathrm{M}_1})(a_1{}^{\mathrm{M}_1}F_{jb}a_2{}^{\mathrm{M}_2})(a_4{}^{-\mathrm{M}_4}F_{ia}a_3{}^{-\mathrm{M}_3})(a_3{}^{\mathrm{M}_3}F_{jb}a_4{}^{\mathrm{M}_4}) \qquad \ldots\ldots(33)$$

where LK has been replaced by M because of (30).

However, experimental physicists do not usually distinguish between the states of spin of the particles. By summing over the different states of spin of the emitted particles and taking the average over the $\mathrm{n}=4\times 2^{-\frac{1}{2}\Sigma\mathrm{M}_S}$ initial states, which are not distinguished experimentally, one calculates:

$$\frac{1}{\mathrm{n}}\sum_{\sigma_S}|H_{\mathrm{T}}|^2=\frac{V^{-2}}{\mathrm{n}}\sum_{ia}\sum_{jb}g_ig_b\epsilon_{ia}'\epsilon_{jb}'\sum_{\sigma_S}A_{iajb} \qquad \ldots\ldots(34)$$

and (9) gives:

$$\sum_{\sigma_S}A=\mathrm{Trace}\,F_{ia}D_1(\mathrm{M}_1)F_{jb}D_2(-\mathrm{M}_2)\times\mathrm{Trace}\,F_{ia}D_3(\mathrm{M}_3)F_{jb}D_4(-\mathrm{M}_4) \qquad \ldots\ldots(35)$$

Because of the symmetry between 1, 2 and 3, 4 one finds that $\sum_{\sigma_S}|H_{\mathrm{T}}|^2$ is quadratic in the M_S and does not change when one changes all the M_S into $-\mathrm{M}_S$, so that the reversibility principle of microphysics is satisfied.

One sees that the probability of the reaction M, L depends only on the M_S; it is independent of the L_S: the formalism is completely symmetrical with respect to the charge conjugate states of the particles; therefore it is also independent of κ, the class of the interaction.

This shows that for the so-called 'allowed' transitions of the β-radioactivity, the life-time, the electron spectrum, etc. . . . are the same whether the neutrino is a Majorana or a Dirac particle.

Second case: some particles indistinguishable.

Firstly, let us say two particles are indistinguishable, and let us suppose them to be 0′ and 0″, i.e. $\mathrm{K}_{0'}=\mathrm{K}_{0''}$, $\mathrm{L}_{0'}=\mathrm{L}_{0''}$, $\mathrm{M}_{0'}=\mathrm{M}_{0''}$. So we get

$$\psi_{0'}{}^{\mathrm{K}_0}=\psi_{0''}{}^{\mathrm{K}_0}=\psi_0{}^{\mathrm{K}_0}=(2V)^{-\frac{1}{2}}\sum_{R=1}^{2}u_{\mathrm{L}_0}{}^{(\mathrm{M}_0)}(\mathbf{k}_R,\sigma_R)a^{\mathrm{M}_0}(\mathbf{k}_R,\sigma_R)\exp\{-\mathrm{M}_0 i\mathbf{k}_R.\mathbf{x}\} \qquad \ldots\ldots(36)$$

J_i has two ψ^{K} identical; therefore H is invariant with respect to their permutation, and it follows that H *is a function of only three independent constants* g_i.

Let us put $0'=3$, $0''=4$; noting that $[u_4^{(M)}(\mathbf{k},\sigma)]^2=0$ (see (14)), it follows from (34):

$$V\psi_3^{K_3}F_{ia}\psi_4^{K_4}=u_{L_0}^{(M_0)}(0')u_{L_0}^{(M_0)}(0'')\frac{a^{M_0}(0')}{\sqrt{2}}F_{ia}\frac{a^{M_0}(0'')}{\sqrt{2}}$$
$$+u_{L_0}^{(M_0)}(0'')u_{L_0}^{(M_0)}(0')\frac{a^{M_0}(0'')}{\sqrt{2}}F_{ia}\frac{a^{M_0}(0')}{\sqrt{2}}$$

or
$$V\psi_3^{K_3}F_{ia}\psi_4^{K_4}=u_{L_0}^{(M_0)}(0')u_{L_0}^{(M_0)}(0'')a^{M_0}(0')\left(\frac{F_{ia}-\tilde{F}_{ia}}{2}\right)a^{M_0}(0''),$$

and we see from (18) that $J_2=J_3=0$ since $\tilde{F}_{ia}=F_{ia}$ for $i=2$ or 3. In this case H depends only on g_1, g_4, g_5. By a permutation P the new g_i (let us call them g_i') are linear functions of the three g_1, g_4, g_5.

If there are three (or four) indistinguishable particles, it is easy to see that h only depends on one g, which defines the special interaction (28), $g_0=g_1=-g_4=g_5$.

It is noteworthy that the preceding conclusions are independent of the fact that the indistinguishable particles can be of Dirac's or Majorana's kind.

Of course if the states of two indistinguishable particles were identical ($\mathbf{k}_1=\mathbf{k}_2$, $\sigma_1=\sigma_2$) (13) would give $U=0$, therefore $H=0$: the formalism assumes Pauli's exclusion principle.

Table 2

	g_1^2	g_2^2	g_3^2	g_4^2	g_5^2	$2g_1g_2$	$2g_1g_3$	$2g_2g_3$	$2g_2g_4$	$2g_3g_4$	$2g_3g_5$	$2g_4g_5$
1	1	4	6	4	1							
$\mathbf{p}_1\cdot\mathbf{p}_2+\mathbf{p}_3\cdot\mathbf{p}_4$	−1		2		−1							
$\mathbf{p}_1\cdot\mathbf{p}_3+\mathbf{p}_2\cdot\mathbf{p}_4$		−2	−4	−2			1		−2		−1	
$\mathbf{p}_1\cdot\mathbf{p}_4+\mathbf{p}_2\cdot\mathbf{p}_3$		−2	−4	−2			−1		2		1	
$(\mathbf{p}_1\cdot\mathbf{p}_2)(\mathbf{p}_3\cdot\mathbf{p}_4)$	1		−2		1							
$(\mathbf{p}_1\cdot\mathbf{p}_3)(\mathbf{p}_2\cdot\mathbf{p}_4)$		2	4	2			−1		2		1	
$(\mathbf{p}_1\cdot\mathbf{p}_4)(\mathbf{p}_2\cdot\mathbf{p}_3)$		2	4	2			1		−2		−1	
$\mathbf{p}_1\cdot\mathbf{p}_2m_3m_4+\mathbf{p}_3\cdot\mathbf{p}_4m_1m_2$	1	−2		2	−1							
$\mathbf{p}_1\cdot\mathbf{p}_3m_2m_4+\mathbf{p}_2\cdot\mathbf{p}_4m_1m_3$						1		−3		−3		−1
$\mathbf{p}_1\cdot\mathbf{p}_4m_2m_3+\mathbf{p}_2\cdot\mathbf{p}_3m_1m_4$						−1		−3		3		−1
$m_1m_2+m_3m_4$	−1	2		−2	1							
$m_1m_3+m_2m_4$						−1		3		3		1
$m_1m_4+m_2m_3$						1		3		−3		1
$m_1m_2m_3m_4$	1	4	6	4	1							

The formula (32) can be very useful for calculations. With the notations $(\mathbf{k}_S/k_{0S})=\mathbf{p}_S$, $(\kappa_S/k_{0S})=m_S$ one has $D_S(\mathrm{M}_S)=\frac{1}{2}(1+\boldsymbol{\alpha}\cdot\mathbf{p}_S+\mathrm{M}_S\beta m_S)$.

The value of $\sum_{\sigma_S}|H_T|^2$ for $\mathrm{M}_1=\mathrm{M}_2=\mathrm{M}_3=\mathrm{M}_4=\pm1$, i.e.

$$\sum_{\sigma_S}|H_T|^2=V^{-2}\sum_{ia}\sum_{jb}g_ig_j\epsilon_{ia}'\epsilon_{jb}'\,\mathrm{Trace}\,F_{ia}D_1(+)F_{jb}D_2(-)\times\mathrm{Trace}\,F_{ia}D_3(+)F_{jb}D_4(-),$$

is given in Table 2. The coefficients of g_ig_j are functions of the fourteen quantities listed in the first column of the Table. The figures indicate how these functions are built up from the fourteen expressions, so that, e.g., the second column of this Table means that the coefficient of g_1^2 is

$$1-(\mathbf{p}_1\cdot\mathbf{p}_2+\mathbf{p}_3\cdot\mathbf{p}_4)+(\mathbf{p}_1\cdot\mathbf{p}_2)(\mathbf{p}_3\cdot\mathbf{p}_4)+\mathbf{p}_1\cdot\mathbf{p}_2m_3m_4$$
$$+\mathbf{p}_3\cdot\mathbf{p}_4m_1m_2-(m_1m_2+m_3m_4)+m_1m_2m_3m_4.$$

For the remarkable interaction $g_0 = g_1 = -g_4 = g_5$ one finds

$$\begin{aligned}\frac{V^{2}}{g_0^{2}}\sum_{\sigma_S}|H_{\mathrm{T}}|^2 = {} & 6+(m_1^2+m_2^2+m_3^2+m_4^2)-(m_1+m_2+m_3+m_4)^2+6m_1m_2m_3m_4 \\ & +2(\mathbf{p}_1\cdot\mathbf{p}_2m_3m_4+\mathbf{p}_3\cdot\mathbf{p}_4m_1m_2)+2(\mathbf{p}_1\cdot\mathbf{p}_3m_2m_4+\mathbf{p}_2\cdot\mathbf{p}_4m_1m_3) \\ & +2(\mathbf{p}_1\cdot\mathbf{p}_4m_2m_3+\mathbf{p}_2\cdot\mathbf{p}_3m_1m_4)+(\mathbf{p}_1^2+\mathbf{p}_2^2+\mathbf{p}_3^2+\mathbf{p}_4^2) \\ & -(\mathbf{p}_1+\mathbf{p}_2+\mathbf{p}_3+\mathbf{p}_4)^2+2[(\mathbf{p}_1\cdot\mathbf{p}_2)(\mathbf{p}_3\cdot\mathbf{p}_4)+(\mathbf{p}_1\cdot\mathbf{p}_3)(\mathbf{p}_2\cdot\mathbf{p}_4) \\ & \qquad\qquad +(\mathbf{p}_1\cdot\mathbf{p}_4)(\mathbf{p}_2\cdot\mathbf{p}_3)],\end{aligned}$$

that is, completely symmetrical in the four particles.

For another set of values of $\mathrm{M}=(\mathrm{M}_1, \mathrm{M}_2, \mathrm{M}_3, \mathrm{M}_4)$ one can use Table 2, replacing m_S by $\mathrm{M}_S m_S$.

This table depends of course on the F_{ia} chosen. F_{ia} is defined in (15) as a function of γ_μ. Below, the F_{ia} are given as a function of the α_k, β. The above calculations are only possible in the Majorana representation, unless $\mathrm{M}_1=-\mathrm{M}_2=\mathrm{M}_3=-\mathrm{M}_4$, when they are also possible in the Dirac representation. For the latter case the F used here are given as functions of Dirac's ρ_k and σ_k.

$$\begin{array}{lllllllll} F_1= & \beta & & & & & & =\rho_3 & \\ F_2= & \alpha_1 & \alpha_2 & \alpha_3 & [1] & & & =\rho_1\sigma_k & [1] \\ F_3= & -i\beta\alpha_2\alpha_3 & -i\beta\alpha_3\alpha_1 & -i\beta\alpha_1\alpha_2 & [-i\beta\alpha_1] & [-i\beta\alpha_2] & [-i\beta\alpha_3] & =\rho_3\sigma_k & [\rho_2\sigma_k] \\ F_4= & -i\alpha_2\alpha_3 & -i\alpha_3\alpha_1 & -i\alpha_1\alpha_2 & [-i\alpha_1\alpha_2\alpha_3] & & & =\sigma_k & [\rho_1] \\ F_5= & -\beta\alpha_1\alpha_2\alpha_3 & & & & & & =\rho_2 & \end{array}$$

(time components are given in brackets; the sign of the F_{ia} is immaterial). In Dirac's representation one must choose $\mathscr{F}_{ia}$ instead of F_{ia} in $\psi_S{}^{\mathrm{K}}F_{ia}\psi_{S'}{}^{\mathrm{K}'}$ with $C=\rho_2\sigma_2$ and

$$\begin{array}{lll} \mathscr{F}_{ia}=F_{ia} & \text{for} & \mathrm{K}=+1 \quad \mathrm{K}'=-1 \\ \mathscr{F}_{ia}=\tilde{C}F_{ia}C^{-1} & \text{for} & \mathrm{K}=-1 \quad \mathrm{K}'=+1 \\ \mathscr{F}_{ia}=F_{ia}C^{-1} & \text{for} & \mathrm{K}=+1 \quad \mathrm{K}'=+1 \\ \mathscr{F}_{ia}=\tilde{C}F_{ia} & \text{for} & \mathrm{K}=-1 \quad \mathrm{K}'=-1 \end{array}$$

§ 9. DIRAC'S HOLE THEORY

It is not possible to describe the Majorana neutral particles by Dirac's hole theory. If no such particles are considered, this theory is of course entirely equivalent to the formalism of charge conjugation but not so convenient. In this section we shall follow up in some detail this equivalence, which shows in particular that it does not matter which charge we attribute to the particle or to the hole.

We distinguish between the physical particle and the theoretical 'corpuscle'. Let us write the $\psi^{\mathrm{K}}(\mathbf{x})$ of one 'corpuscle' of electric charge $\boldsymbol{\epsilon}e$ (with $\boldsymbol{\epsilon}=\pm 1$) or (for a neutral particle) of magnetic moment $\boldsymbol{\epsilon}\mathfrak{m}$, of momentum $\mathfrak{k}$, of energy $\mathfrak{k}_0=\eta(\mathfrak{k}^2+\kappa^2)^{\frac{1}{2}}$ with $\eta=\pm 1$, as

$$\psi_\varrho{}^{\mathrm{K}}(\mathbf{x}) = V^{-\frac{1}{2}}u^{(\mathrm{K})}(\mathfrak{k},\sigma,\eta)a_\varrho{}^{\mathrm{K}}(\mathfrak{k},\sigma,\eta)\exp(-i\mathrm{K}\mathfrak{k}\,.\,\mathbf{x}). \qquad \ldots\ldots (37)$$

$N(\mathfrak{k},\sigma,\eta)=u^{\dagger}(\mathfrak{k},\sigma,\eta)u/(\mathfrak{k},\sigma,\eta)$ is the operator number of 'corpuscles' in the state $\mathfrak{k}, \sigma, \eta$. Physically this corresponds to

$$N'_{\epsilon\eta}(\mathbf{k},\sigma) = \begin{cases} N(\mathfrak{k},\sigma,\eta) & \text{for} \quad \eta=1 \\ 1-N(\mathfrak{k},\sigma,\eta) & \text{for} \quad \eta=-1. \end{cases}$$

$N'_{\epsilon\eta}(\mathbf{k}, \sigma)$ is the operator number of particles of charge $\eta\epsilon e$ (or magnetic moment $\eta\epsilon m$), of momentum $\mathbf{k} = \eta\mathfrak{k}$, in the state σ, since the vacuum is defined by $N(\mathfrak{k}, \sigma, \eta) = \frac{1}{2}(1 - \eta)$.

This leads to two difficulties:

(i) The operator $\zeta' = \Pi[1 - 2N(\mathfrak{k}, \sigma, \eta)]$ corresponding to ζ of § 2 is not so easily defined because now an infinite number of states is occupied. In a diagonal representation ζ' is of the form $(-1)^\infty$, which gives rise to additional mathematical difficulties.

Table 3. Table of the Dichotomic Variables used in this Paper

x	1	-1	Physical significance	Letters used	Definition
M	Emission	Absorption	of the particle		§ 1
$u^{(x)}$	$u^\dagger$	u	Hermitian conjugation	K, KL = M	(7)
u_x	u_+	u_-	$\left\{\text{The two charge conjugate states (sign of the charge or of the magnetic moment)}\right\}$	L	(8)
a^x, ψ^x	a^*, ψ^*	a, ψ	Complex conjugation	K, KL = M	(7)
$D(x)$	$\frac{1}{2}\left(1 + \frac{\boldsymbol{\alpha} . \mathbf{k} + \beta\kappa}{k_0}\right)$	$\frac{1}{2}\left(1 + \frac{\boldsymbol{\alpha} . \mathbf{k} - \beta\kappa}{k_0}\right)$		M	(6)
$\mathfrak{D}(x)$	$\frac{1}{2}\left(1 + \frac{\boldsymbol{\alpha} . \mathfrak{k} + \beta\kappa}{\mathfrak{k}_0}\right)$	$\frac{1}{2}\left(1 + \frac{\boldsymbol{\alpha} . \mathfrak{k} - \beta\kappa}{\mathfrak{k}_0}\right)$	$\mathfrak{D}(x) = D(\eta x)$	K	(40)
η			Sign of the energy of the corpuscle		§ 9
ϵ			Sign of the charge (or the magnetic moment) of the corpuscle		§ 9
σ			The two states of spin		§ 1
$(-1)^P$	For even	For odd	permutation P		§ 5
$\epsilon_{ia}{}^2$			In $F_{ia} = \epsilon_{ia}\gamma_4\gamma_{[ia]}$ for $F_{ia}{}^\dagger = F_{ia}$		(15)
$\epsilon_{ia}{}'$	Space	Time	components of the invariant $\psi_s{}^{\mathrm{K}} F_{ia} \psi_{s'}{}^{\mathrm{K}'}$		(17)
θ_i	Symmetrical	Antisymmetrical	F_{ia}; $\theta_i = -1, +1, +1, -1, -1$		(18)

(ii) The ψ^{K} used in h cannot be the sum of all the plane waves describing the 'corpuscles' (they are infinite in number), but contain only $u^{(\mathrm{K})} a_\varrho{}^{\mathrm{K}} \exp(-\mathrm{K} i \mathfrak{k} . \mathbf{x})$ for the 'corpuscles' which will be emitted or absorbed. Then the exclusion principle is not automatically satisfied. If there are indistinguishable particles—they correspond to indistinguishable corpuscles—one must symmetrize h with respect to the corresponding ψ^{K} (which anti-commute). This symmetrization for an expression like $\psi_S{}^{\mathrm{K}} F_{ia} \psi_{S'}{}^{\mathrm{K}'}$ is automatically carried out in the Heisenberg notation (Heisenberg 1934). One writes $\frac{1}{2}(\psi_S{}^{\mathrm{K}} F_{ia} \psi_{S'}{}^{\mathrm{K}'} - \theta_i \psi_{S'}{}^{\mathrm{K}'} F_{ia} \psi_S{}^{\mathrm{K}})$ instead of $\psi_S{}^{\mathrm{K}} F_{ia} \psi_{S'}{}^{\mathrm{K}'}$.

Otherwise we form h as in § 4 and get the same formula for $|H_{\mathrm{T}}|^2$ and A (see (32) and (33)).

For the study of a transition given by M and L (with $\sum\limits_{(S)c} \mathrm{M}_S \mathrm{L}_S = 0$) we have the two relations:

$$\mathrm{M}_S = \eta_S \mathrm{K}_S \qquad \ldots\ldots (38)$$

and

$$\mathrm{L}_S = \eta_S \boldsymbol{\epsilon}_S. \qquad \ldots\ldots (39)$$

Here a new situation arises in that it is not clear how the $\boldsymbol{\epsilon}_S$ (sign of the electric charge or the magnetic moment of the corpuscles) are determined. The question arises whether the $\boldsymbol{\epsilon}_S$ have a physical meaning or are arbitrary; it will be shown that they are arbitrary.

Let us therefore choose the $\boldsymbol{\epsilon}_S$ arbitrarily; for the study of the M, L reaction, (39) gives us the η_S and (38) the K_S. It is well known that the summations over the spin states are made by the projection operator defined by Casimir (1933):

$$\mathfrak{D}(x) = \tfrac{1}{2}\left(1 + \frac{\boldsymbol{\alpha}.\mathfrak{k} + x\beta\kappa}{\mathfrak{k}_0}\right) = \tfrac{1}{2}\left(1 + \frac{\boldsymbol{\alpha}.\mathbf{k} + x\eta\beta\kappa}{k_0}\right). \qquad \ldots\ldots (40)$$

One easily sees, in the Majorana representation, that

$$\mathfrak{D}^{\mathrm{K}}(x) = \mathfrak{D}(-\mathrm{K}x) = \tilde{\mathfrak{D}}(\mathrm{K}x) \qquad \ldots\ldots (41)$$

and from (9)

$$\mathfrak{D}(x) = D(\eta x). \qquad \ldots\ldots (42)$$

With the well-known properties $\mathfrak{D}^{\mathrm{K}}(\eta) a^{\mathrm{K}}(\mathfrak{k}, \sigma, \eta') = \delta_{\eta\eta'} a^{\mathrm{K}}(\mathfrak{k}, \sigma, \eta')$ one gets

$$\sum_{\sigma} a_{\mu}^{-\mathrm{K}}(\mathfrak{k}, \sigma, \eta) a_{\nu}^{\mathrm{K}}(\mathfrak{k}, \sigma, \eta) = [\tilde{\mathfrak{D}}^{\mathrm{K}}(+)]_{\mu\nu} = [D(\mathrm{K})]_{\mu\nu} \qquad \text{(cf. (41))}.$$

This formula is equivalent to (9). Therefore, by the same method, one gets, instead of (35),

$$\sum_{\sigma_S} A = \text{Trace } F_{ia} \mathfrak{D}(\mathrm{K}_1) F_{jb} \mathfrak{D}(-\mathrm{K}_2) \times \text{Trace } F_{ia} \mathfrak{D}(\mathrm{K}_3) F_{jb} \mathfrak{D}(-\mathrm{K}_4) \qquad \ldots\ldots (43)$$

and from (42) and (38) $\mathfrak{D}(\mathrm{K}) = D(\eta\mathrm{K}) = D(\mathrm{M})$; hence the formulae (35) and (43) are identical.

Thus $\sum\limits_{\sigma} |H_{\mathrm{T}}|^2$ depends only on M_S, and is independent of L_S (sign of the electric charge or of the magnetic moment of the particles), of η_S (sign of the energy of the 'corpuscles') and of $\boldsymbol{\epsilon}_S$ (sign of the electric charge or of the magnetic moment of the 'corpuscles')

Thus the $\boldsymbol{\epsilon}_S$ are completely arbitrary* and have no physical meaning. That shows the artificial aspect of the hole theory, which, however, is more customary and, therefore, more intuitive.

Moreover, this formulation does not contain the conservation of the electric charge. From (38), (39) and (29)

$$\sum_{(S)c} \mathrm{M}_S \mathrm{L}_S = \sum_{(S)c} (\mathrm{K}_S \eta_S)(\eta_S \boldsymbol{\epsilon}_S) = \sum_{(S)c} \mathrm{K}_S \boldsymbol{\epsilon}_S = 0,$$

but it has been seen that the $\boldsymbol{\epsilon}_S$ are arbitrary.

There are no rules like (31) for the choice of the K_S. The K_S are completely arbitrary (a transition between particles can be described by 16 different transitions between 'corpuscles'; but after their choice the $\boldsymbol{\epsilon}_S$ are determined, by (38) and (39), and give rise to a charge interpretation of the representation.

---

* In Tiomno and Wheeler's (1949) paper on the interaction μ, ϵ, ν, ν, the authors have had to choose a sign of the charge of the μ and ϵ corpuscles. This is only due to the fact that they have limited their choice of the Hamiltonian to the kind $h = g_i J_i(+, -, +, -) = g_i(\psi^* F_i \psi).(\psi^* F_i \psi)$, which is the simplest when one does not use the Majorana representation of Dirac's matrices (see p. 521).

II. THE DECAY OF THE μ-MESON

Some experimental results published in 1948 pointed to the decay of the μ-meson into more than two particles (Steinberger 1948, Hincks and Pontecorvo 1948). The similarity of this decay to a β-decay was immediately noticed (Klein 1948, Horowitz *et al.* 1948). The suggested scheme is $\mu^{\pm} \rightarrow \mu^0 + \epsilon^{\pm} + \nu$, where μ^0 is a neutral meson already known (Lattes, Occhialini and Powell 1947) from the π-meson decay: $\pi^{\pm} \rightarrow \mu^{\pm} + \lambda$, where λ is written for μ^0.

From the work of Part I it is easy to study this phenomenon.

§ 10. DECAY $\mu \rightarrow \lambda + \epsilon + \nu$

Here the Born approximation is used and the electromagnetic interactions are neglected (cf. Feer (1949) for photon production by charge acceleration). From the results of Part I one sees that it is not necessary to know whether μ^0 and ν are, independently, 'Dirac' or 'Majorana' neutral particles. The results are the same in any case.

Let us call the rest-masses, in energy units, of the corresponding particles $\mu, \lambda, \epsilon, \nu$ (with $\nu = 0$). The frame of reference will be used in which the μ-meson is at rest. Let us denote the momenta and the energies (in energy units) of the particles by $\mathbf{p}_\mu = 0$, $\mathbf{p}_\epsilon = \mathbf{p}$, $\mathbf{p}_\lambda$, $\mathbf{p}_\nu$; $E_\mu = \mu$, $E_\epsilon = E$, E_λ, $E_\nu = p_\nu$. The conservation law gives: $\mathbf{p} + \mathbf{p}_\lambda + \mathbf{p}_\nu = 0$, $\mu = E + E_\lambda + E_\nu = E_{\mathrm{t}}$ (total energy). Table 1 immediately gives $\sum_\sigma |H_{\mathrm{T}}|^2$ for this decay; we know that $\mathrm{M}_\mu = -1$, $\mathrm{M}_\lambda = \mathrm{M}_\epsilon = \mathrm{M}_\nu = 1$; the order chosen is $\lambda, \mu, \epsilon, \nu$ (corresponding to that usually chosen for β-decay: P, N, ϵ, ν). Then (33) gives* (the g_i have the dimensions of energy . volume)

$$\begin{aligned} V^2 \sum_\sigma |H_{\mathrm{T}}|^2 = {} & (g_1^2 + 4g_2^2 + 6g_3^2 + 4g_4^2 + g_5^2) - (g_1^2 - 2g_3^2 + g_5^2) \cdot \frac{\mathbf{p} \cdot \mathbf{p}_\nu}{E p_\nu} \\ & -2(g_2^2 + 2g_3^2 + g_4^2) \left(\frac{\mathbf{p}}{E} + \frac{\mathbf{p}_\nu}{p_\nu} \right) \cdot \frac{\mathbf{p}_\lambda}{E_\lambda} + 2(g_1 g_3 - 2g_2 g_4 + g_3 g_5) \left(\frac{\mathbf{p}}{E} - \frac{\mathbf{p}_\nu}{p_\nu} \right) \cdot \frac{\mathbf{p}_\lambda}{E_\lambda} \\ & + (g_1^2 - 2g_2^2 + 2g_4^2 - g_5^2) \frac{\lambda}{E_\lambda} \left(1 - \frac{\mathbf{p} \cdot \mathbf{p}_\nu}{E p_\nu} \right) \\ & + 2(-g_1 g_2 + 3g_2 g_3 + 3g_3 g_4 + g_4 g_5) \frac{\lambda}{E_\lambda} \frac{\epsilon}{E} \\ & + 2(-g_1 g_2 - 3g_2 g_3 + 3g_3 g_4 - g_4 g_5) \frac{\epsilon}{E} \left(1 - \frac{\mathbf{p}_\lambda \cdot \mathbf{p}_\nu}{E_\lambda p_\nu} \right). \qquad \ldots\ldots (44) \end{aligned}$$

We want to calculate the energy spectrum of the emitted electron. Let us denote the angle between $\mathbf{p}$ and $\mathbf{p}_\nu$ by θ and let $P(E)\,dE$ be the probability per unit of time of observing the electron from a disintegration with a total energy between E and $E + dE$. We have $\epsilon \leqslant E \leqslant W = (\mu^2 + \epsilon^2 - \lambda^2)/2\mu$,

$$P(E)\,dE = \frac{2\pi}{\hbar} \int_0^\pi \frac{V^2}{\mathrm{n}} \sum_\sigma |H_{\mathrm{T}}|^2 \frac{p^2\,dp \sin\theta\,d\theta}{(2\pi\hbar c)\sigma} p_\nu^2 \left(\frac{\partial p}{\partial E_{\mathrm{t}}} \right)_{E_{\mathrm{t}} = \mu} . 8\pi^2;$$

$\mathrm{n} = 2$ (see (34)); $p\,dp = E\,dE$;

$$p_\nu = \frac{\mu(W - E)}{\mu - E + p\cos\theta} \left(\frac{\partial p_\nu}{\partial E_{\mathrm{t}}} \right)_{E_{\mathrm{t}} = \mu} = \frac{(\mu - E)(\mu - E + p\cos\theta) - \mu(W - E)}{(\mu - E + p\cos\theta)^2}.$$

---

* This formula contains as special cases the expressions (8–12) of Tiomno and Wheeler (1949). One would therefore expect that our formulae (45) and (46) would include the corresponding formulae in that paper; unfortunately, a closer comparison reveals various discrepancies, which, however, has been cleared up in the course of a correspondence with Prof. Wheeler and Dr. Tiomno. It appears that many formulae as given in their excellent paper are marred by errors of transcription or by slight slips in calculations. They intend to publish a full list of these errata.

The calculation gives:

$$P(E)=\frac{(E^2-\epsilon^2)^{\frac{1}{2}}\mu^2(W-E)^2}{12\hbar(2\pi\hbar^2c^2)^3[\mu(W-E)+\frac{1}{2}\lambda^2]^3}$$

$$\times\left[\begin{array}{l}(g_1^2+g_2^2+6g_3^2+4g_4^5+g_5^2)E\{[3\mu(W-E)+E^2-\epsilon^2][2\mu(W-E)+3\lambda^2]+3\lambda^4\}\\ +(g_1^2-2g_3^2+g_5^2)(\mu-E)(E^2-\epsilon^2)[2\mu(W-E)+3\lambda^2]\\ +2(g_2^2+2g_3^2+g_4^2)\{E\mu(W-E)+(\mu-2E)(E^2-\epsilon^2)][2\mu(W-E)+3\lambda^2]\\ +4E\mu^2(W-E)^2\}+2(g_1g_3-2g_2g_4-g_3g_5)\{\mu[E(W-E)-(E^2-\epsilon^2)]\\ \times[2\mu(W-E)+3\lambda^2]+4E\mu^2(W-E)^2\}\\ +(g_1^2-2g_2^2+2g_4^2-g_5^2)6\lambda(\mu E-\epsilon^2)[\mu(W-E)+\frac{1}{2}\lambda^2]\\ +2(-g_1g_2+3g_2g_3+3g_3g_4+g_4g_5)6\lambda\epsilon(\mu-E)[\mu(W-E)+\frac{1}{2}\lambda^2]\\ -2(g_1g_2+3g_2g_3-3g_3g_4+g_4g_5)12\epsilon[\mu(W-E)+\frac{1}{2}\lambda^2]^2.\end{array}\right]$$

$$\ldots\ldots(45)$$

§ 11. DECAY $\mu^{\pm}\to\epsilon^{\pm}+2\nu$

During the last year the existence of the μ^0-meson has become doubtful, and some recent experimental data (Leighton, Anderson and Seriff 1949) show that $W=55$ MEV. i.e. about $\frac{1}{2}\,\mu$. Therefore the mass λ must be very small and the decay of the μ-meson into an electron and two neutrinos is very probable.

We must consider two cases:

(i) All neutrinos are Dirac neutral particles, and the two emitted neutrinos are distinguishable (their magnetic moments are of opposite sign). We can then obtain $\sum_{\sigma}|H_{\mathrm{T}}|^2$ and $P(E)$ by putting $\lambda=0$ in (44) and (45).

We get a simpler formula by choosing the order μ, ϵ, ν, ν (of course now the g_i are not the same as in (45)):

$$P(E)=\frac{(E^2-\epsilon^2)^{\frac{1}{2}}}{3\hbar(2\pi\hbar^2c^2)^3}\mu[3E(W-E)K_1+2(E^2-\epsilon^2)K_2+3\epsilon(W-E)K_3]. \quad\ldots\ldots(46)$$

with $K_1=g_1^2+2(g_2^2+g_3^2+g_4^2)+g_5^2$, $K_2=g_2^2+2g_3^2+g_4^2$, $K_3=g_1^2-2g_2^2+2g_4^2-g_5^2$. In the preliminary note (Michel 1949) that formula was incorrect (put $K_4=0$ and correct K_3), but the errors do not change the spectral distribution by an appreciable amount.

(ii) Either all the neutrinos are Majorana neutral particles or all the neutrinos are Dirac neutral particles, and the two emitted neutrinos have the same charge conjugate state (their magnetic moments have the same sign); in both cases the two emitted neutrinos are indistinguishable.

From Part I (§ 8, second case) we know that then we obtain the same result as above except that there is no interaction in g_2 and g_3 (in the formula (46) put $g_2=g_3=0$).

§ 12. COMPARISON WITH EXPERIMENTAL RESULTS

The term proportional to K_3 does not appreciably change the curve $P(E)$, and it is neglected in the Figure.

If τ is the mean life of the μ-meson (2·15 microseconds)

$$\tau\int_{\epsilon}^{W}P(E)\,dE=1. \quad\ldots\ldots(47)$$

It is already well known (Tiomno and Wheeler 1949, Horowitz *et al.* 1948) that the g_i are of the order of the Fermi constant ($\sim 10^{-49}$ erg. cm^3). The condition (47) gives us the scale for drawing the different curves which we want to compare.

Let us denote the curve $P(E)$ by P_i when only one $g_i \neq 0$ ($\mathsf{P}_1 = \mathsf{P}_5$ and $\mathsf{P}_2 = \mathsf{P}_4$). All the possible curves P have (for $0 \leqslant \rho \leqslant 1$) the shape

case (i) $\mathsf{P}_1(E) + \rho[\mathsf{P}_3(E) - \mathsf{P}_1(E)]$ and sweep the whole areas A and B

case (ii) $\mathsf{P}_1(E) + \rho[\mathsf{P}_2(E) - \mathsf{P}_1(E)]$ and sweep only the whole area B.

All the curves pass through the same point M.

The experimental curve and the expected statistical spread given by Leighton, Anderson and Seriff (1949, Figure 5) are plotted together. The curve P_0 corresponding to the remarkable interaction g_0 (see (28)) is also shown.

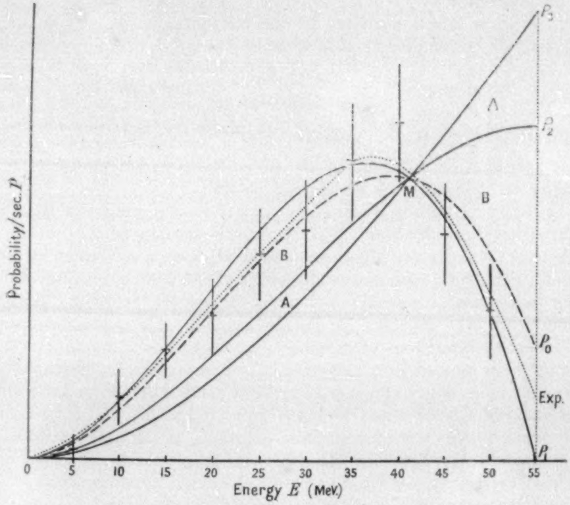

—— Theoretical curves $\mathsf{P}_1 \equiv \mathsf{P}_5$, $\mathsf{P}_2 \equiv \mathsf{P}_4$, P_3, boundaries of the A and B areas.

- - - - Theoretical curve P_0, remarkable interaction.

…… Experimental curve of Anderson *et al.*

The agreement is quite satisfactory and the experimental curve also passes through the point M.

There is thus strong evidence for the decay of the μ-meson into one electron and two neutrinos.* But, since the experimental curve falls in the B area, nothing can be said about the nature of the neutrinos; furthermore, the good fit of the theoretical curves with experimental results does not prove that a 'direct interaction' *necessarily* exists between μ-mesons, electrons and neutrinos.

---

* Of course this conclusion rests on the assumption that the μ-meson has a spin of one-half. It would be possible, as pointed out by J. Tiomno (*Phys. Rev.*, 1949, **76,** 856), to reproduce the experimental curve on the assumption of an integral spin for the μ-meson and one of the neutral particles.

§ 13. PROPERTIES OF THE NEUTRINO

(*a*) *Its magnetic moment.* From the theoretical point of view it is more exact to ask: is the neutrino a Dirac or a Majorana neutral particle ?

From the decay of the μ-meson it would have been possible to say that the neutrino is a Dirac particle if the experimental curve lay in the A area, but this is not the case. However, there is one phenomenon rather favourable to the hypothesis: the neutrino is a Majorana particle. This, as was shown by Furry (1939), is a double β-radioactivity without the emission of neutrinos. Recently experimental evidence for this phenomenon was published (Fireman 1949); it is the spontaneous decay

$$^{124}_{50}\mathrm{Sn} \rightarrow ^{124}_{52}\mathrm{Te} + 2\mathrm{e}^-.$$

No neutrinos are emitted, otherwise the lifetime would be 10^{10} times larger than the observed one.

Theoretically this is explained by the reactions: (*a*) $\mathrm{N}_- \rightarrow \mathrm{P}^+ + \epsilon^- + \nu_{\mathrm{m}}$ and (*c*) $\mathrm{N}_- + \nu_{\mathrm{m}} \rightarrow \mathrm{P}^+ + \epsilon^-$ in the following scheme:

$$\text{initial state} \rightarrow \begin{matrix}\text{intermediary}\\ \text{virtual state}\end{matrix} \rightarrow \text{final state}$$

$$N_{-1} + \mathrm{N}_{-2} \rightarrow \mathrm{P}_1{}^+ + \epsilon_1{}^- + \nu_{\mathrm{m}} + \mathrm{N}_{-2} \rightarrow \mathrm{P}_1{}^+ + \epsilon_1{}^- + \mathrm{P}_2{}^+ + \epsilon_2{}^-$$

but we have seen (§ 8) that the (*a*) and (*c*) reactions do not belong to the same 'class' unless the neutrino is a Majorana particle.

The simplest course is, therefore, to assume that the interaction Hamiltonian is reduced to terms corresponding to the single class embodying (*a*) and (*c*) when the neutrino is treated as a Majorana particle. However, one cannot exclude the possibility that the Hamiltonian would consist of two distinct $\vec{g}(\kappa)$ corresponding to the two classes involved in which neutrinos are Dirac particles. This possibility has been discussed by Touschek (1948); for ordinary β-decay this leads for each process to two competing transitions which differ only by the sign of the magnetic moment of the neutrino, of course without interference between them for such phenomena of first order in the $\vec{g}$. It may be observed, in particular, that if $\vec{g}(\kappa_1) = \vec{g}(\kappa_2)$ (the same $\vec{g}$ for both classes) this theory, which also maintains distinction between neutrinos and anti-neutrinos, is formally identical for all β-processes with that involving Majorana neutrinos.

Thus if the neutrino is a Majorana particle it has no electromagnetic interaction. The neutrino appears only in the spontaneous decay of elementary particles, and it is only required to preserve the conservation laws of energy, momentum and angular momentum. It therefore seems to be connected with the gravitational field; but perhaps not so simply as might be thought (Gamow and Teller 1937). The interaction between μ-meson, electron and neutrinos gives, in the second order, a very small interaction of infinite range between a μ-meson and an electron of the same charge. According to the calculation of Noma (1948), the static potential interaction is proportional to r^{-5}.

(*b*) *Its mass.* From the formulae (45) and (46) it appears that there is a large difference between the two cases $\lambda \neq 0$ and $\lambda = 0$. This is due to the fact that, in (45), $P(E)$ is proportional to $(W - E)^2$, but this factor, which disappears if $\lambda = 0$, would also have disappeared if $\nu \neq 0$ when $\lambda \neq 0$, and even if $\nu = \lambda \neq 0$, as in the well-known case of β-spectra the curve $\mathsf{P}(E, \nu) \rightarrow \mathsf{P}(E, 0)$ when $\nu \rightarrow 0$, although the same is not true for the derivative dP/dE. One cannot hope evidence of this kind will give an answer to the question: is the mass of the neutrino finite? Equation (48) gives a good example for the mass ϵ of the electron. The tangent of $\mathsf{P}(E)$ at the point $E=\epsilon$ is vertical when $\epsilon\neq 0$ and horizontal when $\epsilon=0$, but $\mathsf{P}(E,\epsilon)\rightarrow\mathsf{P}(E,0)$ continuously as $\epsilon\rightarrow 0$.

ACKNOWLEDGMENTS

The author wishes to thank Professor Rosenfeld for helpful advice and discussions. He is indebted to the French Service des Poudres for making possible his stay at Manchester University.

REFERENCES

Casimir, H., 1933, *Helv. Phys. Acta*, **6,** 287.
Critchfield, L., 1943, *Phys. Rev.*, **63,** 417.
Critchfield, L., and Wigner, E., 1941, *Phys. Rev.*, **60,** 412.
Feer, D. B., 1949, *Phys. Rev.*, **75,** 731.
Fierz, M., 1937, *Z. Phys.*, **104,** 553.
Fireman, E. L., 1949, *Phys. Rev.*, **75,** 323.
Furry, W. H., 1939, *Phys. Rev.*, **56,** 1185.
Gamow, G., and Teller, E., 1937, *Phys. Rev.*, **51,** 289.
Heisenberg, W., 1934, *Z. Phys.*, **90,** 209, and **92,** 692.
Hincks, E. P., and Pontecorvo, B., 1948, *Phys. Rev.*, **74,** 697.
Horowitz, J. J., Kofoed-Hansen, O., and Lindhard, J., 1948, *Phys. Rev.*, **74,** 713.
Klein, O., 1938, *J. Phys. Radium* (7), **9,** 1; 1948, *Nature, Lond.*, **161,** 897.
Kramers, H. A., 1937, *Proc. Acad. Sci., Amst.*, **40,** 814.
Lattes, C. M. G., Occhialini, G. P. S., and Powell, C. F., 1947, *Nature, Lond.*, **160,** 453.
Leighton, R. B., Anderson, C. D., and Seriff, A. J., 1949, *Phys. Rev.*, **75,** 1432.
Majorana, E., 1937, *Nuovo Cim.*, **14,** 171.
Michel, L., 1949, *Nature, Lond.*, **163,** 960.
Noma, S., 1948, *Prog. Theor. Phys.*, **3,** 54.
Okayama, T., 1949, *Phys. Rev.*, **75,** 300.
Pauli, W., 1936, *Ann. Inst. Henri Poincaré*, **6,** 109; 1941, *Rev. Mod. Phys.*, **13,** 203.
Racah, G., 1937, *Nuovo Cim.*, **14,** 322.
Speiser, A., 1945, *Die Theorie der Gruppen von endlicher Ordnung*, 3rd edition (New York: Dover Publications), p. 108.
Steinberger, J., 1948, *Phys. Rev.*, **74,** 500.
Tiomno, J., and Wheeler, J. A., 1949, *Rev. Mod. Phys.*, **21,** 141.
Touschek, B., 1948, *Z. Phys.*, **125,** 108.

Radioactive Dysprosium Isotopes

By F. D. S. BUTEMENT
Atomic Energy Research Establishment, Harwell, Berks.

MS. received 7th October 1949

ABSTRACT. A new isotope of dysprosium, identified as ^{166}Dy, has been studied. It has been shown that it is formed by thermal neutron capture in the 140 minute isomer of ^{165}Dy, the capture cross section being about 1,200 barns. It decays with a half-life of 82 hours and is the parent of 27 hour ^{166}Ho. It emits beta-particles, the energy of which was found by absorption in aluminium to be 0·22 Mev., and gamma rays of less than 50 kev. energy.

Another new isotope, ^{159}Dy, has been made both by slow neutron irradiation of dysprosium and by deuteron bombardment of terbium. It decays by orbital electron capture, with a half-life greater than 50 days. It will be described in a later paper.

---

§1. INTRODUCTION

THE stable isotopes of dysprosium are given in Table 1 (Inghram, Hayden and Hess 1949).

Table 1

Mass number	156	158	160	161	162	163	164
Abundance %	0·0524	0·0902	2·294	18·88	25·53	24·97	28·18

The only known radioactive isotope is ^{165}Dy (Seaborg and Perlman 1948, Table of Isotopes). The 1·25 minute isomer decays into the 140 minute beta-emitter, which decays to stable ^{165}Ho.

This paper discusses two new radioactive dysprosium isotopes found in neutron-activated dysprosium after the 140 minute activity has decayed. Their principal characteristics are summarized in Table 2.

Table 2

Assignment	Half-life	Radiation observed
^{166}Dy	82 hrs.	β, γ
^{159}Dy	>50 days	x-ray

The ^{159}Dy was also made by the reaction ^{159}Tb (d, 2n). Only ^{166}Dy is discussed here in detail: the other isotope will be dealt with in a later paper.

§2. SYMBOLS

$\lambda_1 = 0{\cdot}00845$ hr^{-1}, decay const. of 82 hour ^{166}Dy.
$\lambda_2 = 0{\cdot}0257$ hr^{-1}, ,, ,, ,, 27 hour ^{166}Ho.
$\lambda_3 = 0{\cdot}298$ hr^{-1}, ,, ,, ,, 140 minute ^{165}Dy.
$\lambda_4 = 33{\cdot}26$ hr^{-1}, ,, ,, ,, 1·25 minute ^{165}Dy.
t = time in hours after end of irradiation.
t' = irradiation time in hours.

§ 3. CHEMICAL IDENTIFICATION OF 82 HOUR DYSPROSIUM

Since the activities, other than ^{165}Dy, produced by slow neutron activation are all relatively weak, it is necessary to use extremely pure material. The dysprosium was purified either before or after activation by the technique of Ketelle and Boyd (1947), in which rare earths are eluted from a Dowex-50 resin ion-exchange column, in inverse order of their atomic numbers, a clear separation between adjacent rare earths being obtained.

30 mg. dysprosium oxide of over 99% purity was irradiated in the pile for 26 hours in a slow neutron flux of $3{\cdot}3 \times 10^{11}$ cm^{-2}sec^{-1}. After waiting two days for the intense ^{165}Dy activity to decay, the material was processed on the ion-exchange column. A Geiger counter and automatic recorder plotted the variation with time of the beta-activity of the elutriant, and six 20 ml. fractions of elutriant corresponding to the dysprosium 'peak' were collected and the dysprosium recovered by precipitation as oxalate and ignition to oxide. The beta-activities of the samples, eleven days after activation, and the weights of Dy_2O_3 are plotted as histograms in Figure 1. The correspondence shows that the activity is due to dysprosium. The subsequent decay of activity was the same for all fractions, the decay graph for the largest being given in Figure 2. After correction for a weak residual activity (^{159}Dy) of half-life >50 days, the main beta-activity showed, as the mean value for six samples, a half-life of 82 hours.

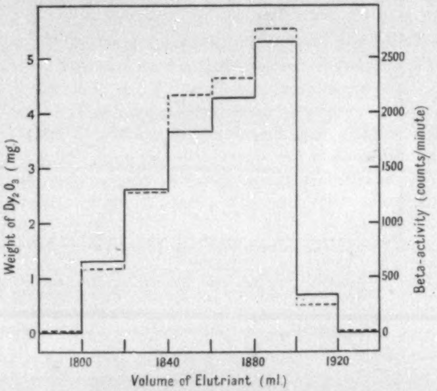

Figure 1. Dependence of activity (broken line) and weight (full line) of dysprosium oxide on volume of elutriant.

§ 4. GROWTH OF A 27 HOUR ACTIVITY FROM THE 82 HOUR DYSPROSIUM

In an experiment similar to the above, the ion-exchange purification of the dysprosium was completed within 36 hours of the end of the irradiation.

The change of activity during the next 320 hours was measured. Initially much of the activity was due to 140 minute ^{165}Dy, and the rate of decrease enabled an almost exact correction for this to be calculated. After the first day this correction becomes negligible. The corrected activity shows first a growth and ultimately a decay approximating to an 82 hour half-life (Figure 3). Assuming, on the basis of further evidence given below, that the process occurring is

$$^{166}\mathrm{Dy} \xrightarrow[82\ \mathrm{hr.}]{\beta} {}^{166}\mathrm{Ho} \xrightarrow[27\ \mathrm{hr.}]{\beta} {}^{166}\mathrm{Er}\ \text{(stable)},$$

the variation of total activity can be calculated. After the two activities had reached equilibrium, measurement of the absorption of the radiation in aluminium (§ 7) enabled an allowance for the absorption of the sample and counter window to be obtained by extrapolation. It was found that 0·91 of the ^{166}Dy beta-particles were transmitted. For ^{166}Ho 1·37 particles are counted per effective disintegration owing to the slight absorption of the 1·88 Mev. beta-particles and the additional presence of 70·5 kev. conversion electrons (Grant and Hill 1949). Hence the total activity counted should be proportional to

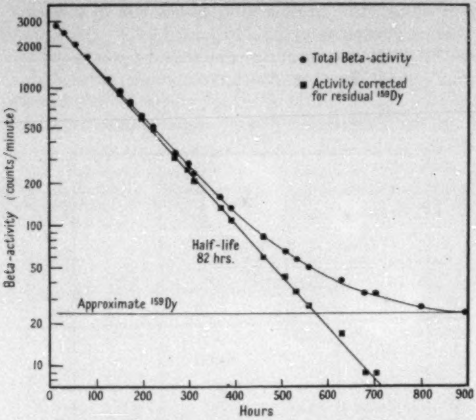

Figure 2. Beta-decay of equilibrium mixture of ^{166}Dy and ^{166}Ho.

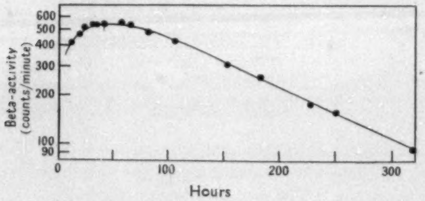

Figure 3. Experimental points and theoretical curve for growth of ^{166}Ho from ^{166}Dy.

$$0{\cdot}91\exp(-\lambda_1 t)+1{\cdot}37\frac{\lambda_2}{\lambda_2-\lambda_1}\{\exp(-\lambda_1 t)-\exp(-\lambda_2 t)\}.$$

A curve for the calculated activity can be made to fit the experimental points if suitably shifted parallel to the time axis to allow for the fact that the dysprosium initially contains a small indeterminate amount of holmium produced during its passage through the ion-exchange column.

§ 5. DEPENDENCE OF YIELD ON NEUTRON FLUX

A series of experiments indicated that the yield of the 82 hour activity for a 24 hours irradiation was approximately proportional to the square of the neutron flux. This indicates that the activity cannot be produced by capture of a single neutron, but must arise when some of the atoms of a radioactive Dy isotope, created by neutron capture, in turn capture a second neutron. The only instance for which this is possible is the chain

$$^{164}\mathrm{Dy}\,(\mathrm{n},\gamma)\longrightarrow{}^{165}\mathrm{Dy}\,(\mathrm{n},\gamma)\longrightarrow{}^{166}\mathrm{Dy}.$$

An appreciable yield is possible owing to the large cross section, 725 barns in natural Dy (Seren, Friedlander and Turkel 1947) of ^{164}Dy for thermal neutron capture.

To confirm this hypothesis and determine which of the two ^{165}Dy isomers captures the second neutron, samples of about one milligram of very pure Dy_2O_3 were irradiated in a slow neutron flux of $1{\cdot}06\times10^{12}$ cm^{-2} sec^{-1} for periods t' of 1, 2 and 4 hours. The samples were then chemically purified to remove possible contaminants other than rare earths, and mounted on counting discs.

The activities at $t=29$ and 45 hours were measured using a low geometrical counting efficiency. The large decrease in activity between these times is almost entirely due to decay of 140 minute ^{165}Dy, and when divided by the appropriate value of $1-\exp(-\lambda_3 t')$ gives the relative amounts of dysprosium in the samples.

The decay was followed for 18 days at a high geometrical counting efficiency, and the total activity of the 82 hour ^{166}Dy plus ^{166}Ho determined graphically at $t=240$ hours.

Neglecting trivial corrections for the time taken for the 1·25 minute ^{165}Dy to transform to its isomer, and for the decay of the 82 hour ^{166}Dy during the irradiation, the ^{166}Dy activity produced will be proportional to

$$\lambda t'+\exp(-\lambda t')-1,$$

in which $\lambda=$ either λ_3 or λ_4, according to which ^{165}Dy isomer is responsible for capture of the second neutron.

The method does not require a uniform distribution of samples on the counting discs or any accurate knowledge of the geometrical counting efficiency, or of the neutron flux.

The results (Table 3) show that the ^{166}Dy is formed by neutron capture mainly, if not entirely, by the 140 minute ^{165}Dy isomer.

Table 3

	Sample		
	I	II	III
a. Irradiation time, t' hours	1·00	2·00	4·00
b. Decrease in activity between $t=29$ and 45 hrs. (disintegrations per second)	12225	21767	22317
c. $1-\exp(-\lambda_3 t')$	0·258	0·449	0·676
d. Relative amounts of Dy $=b/c$	47380	48480	33010
e. ^{166}Dy, counts per min. at $t=240$ hrs.	46	180	380
f. Specific ^{166}Dy activity $=e/d$	0·000971	0·00371	0·0115
g. Relative f, Sample III $=1{\cdot}00$	0·082	0·31	1·00
Relative value $\lambda_3 t'+\exp(-\lambda_3 t')-1$, Sample III $=1{\cdot}00$	0·081	0·30	1·00
Relative value $\lambda_4 t'+\exp(-\lambda_4 t')-1$, Sample III $=1{\cdot}00$	0·24	0·50	1·00

§6. THERMAL NEUTRON ACTIVATION CROSS SECTION OF ^{165}DY

The capture cross section of the 140 minute ^{165}Dy isomer for slow pile neutrons was measured by the activation technique of Seren, Friedlander and Turkel (1947), and assuming their value of 725 barns for the cross section of ^{164}Dy, in natural Dy. Allowance was made for the growing concentration of ^{165}Dy during the irradiation.

The approximate value obtained was 1,200 barns. The error may be considerable if there is a strong resonance absorption of neutrons not of thermal energy.

§7. BETA-PARTICLE ENERGY

The usual technique of absorption measurement of the beta radiation in aluminium foils was used. The ^{166}Dy was virtually in equilibrium with the ^{166}Ho. Figure 4 shows the absorption curve and that of a pure ^{166}Ho sample. Evidently, allowing for a small tail due partly to X rays from the disintegration of ^{159}Dy contamination, all the beta radiation passing 50 mg.cm^{-2} of aluminium can be attributed to ^{166}Ho.

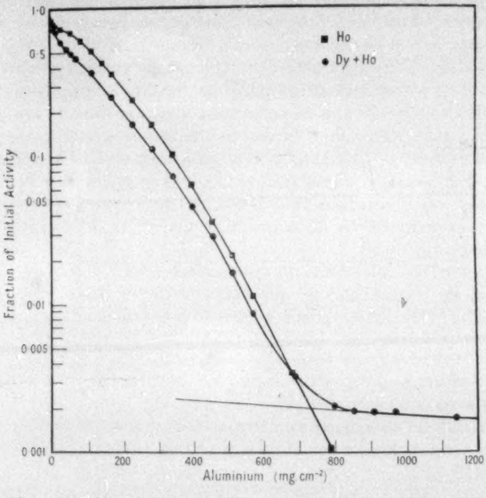

Figure 4. Absorption of beta radiation of ^{166}Dy in equilibrium with ^{166}Ho, and of pure ^{166}Ho.

Figure 5 shows the Ho curve fitted over the total activity between 50 and 200 mg.cm^{-2} of aluminium absorber. Subtraction of the Ho activity leaves a residue of 0·22 MEV. beta-particles (range 50 mg.cm^{-2} Al) due to ^{166}Dy.

§8. GAMMA RADIATION

The gamma radiation was studied by the usual technique of absorption measurements in aluminium, copper and lead. Similar measurements were also made on a pure sample of 27 hour ^{166}Ho, and used to calculate the correction to be subtracted on account of the holmium in equilibrium with the ^{166}Dy.

The dysprosium showed initially some hard gamma radiation with a half-life of approximately 42 hours, which may have been due to some unknown contamination. After 12 days the activity due to the 42 hour period had virtually disappeared. The decay of the x- and gamma radiation filtered through 1·14 gm. cm^{-2} of aluminium was then followed for a further 24 days. The decay curve could be analysed into an 82 hour period and a residual long-lived activity. Absorption measurements in copper indicated that the radiation from this long activity had an energy of approximately 45 kev. (this was probably due to x rays consequent to K-electron capture by ^{159}Dy). After correcting for this activity, the 82 hour ^{166}Dy gamma activity was still about three times as great as that calculated for the equilibrium amount of ^{166}Ho. It was concluded, therefore, that there is some gamma radiation due to ^{166}Dy, with energy less than 50 kev. An accurate determination could not be made owing to the low counting rate and the comparatively large corrections indicated above.

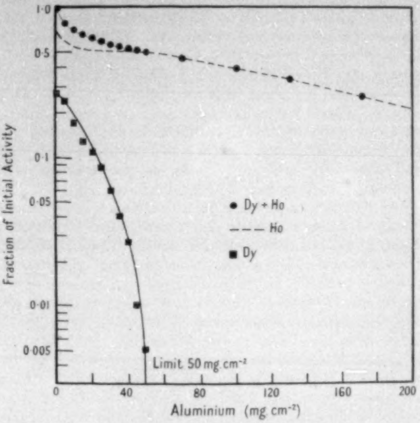

Figure 5. Absorption of ^{166}Dy beta radiation in aluminium.

§ 9. CONCLUSION

The capture cross section of the 140 minute isomer of ^{165}Dy for thermal neutrons is about 1,200 barns. The product, ^{166}Dy, decays wtih a half-life of 82 hours, and emits 0·22 Mev. beta-particles and low energy gamma-rays. It is the parent of 27 hour ^{166}Ho.

ACKNOWLEDGMENTS

Acknowledgment is made to the Director, Atomic Energy Research Establishment, for permission to publish these results, and to the Ministry of Supply for the grant of a Senior Harwell Research Fellowship.

REFERENCES

Grant, P. J., and Hill, J. M., 1949, *Nature, Lond.*, **163**, 524.
Inghram, M. G., Hayden, R. J., and Hess, D. C., 1949, *Phys. Rev.*, **75**, 693.
Ketelle, B. H., and Boyd, G. E., 1947, *J. Amer. Chem. Soc.*, **69**, 2800
Seaborg, G. T., and Perlman, I., 1948, *Rev. Mod. Phys.*, **20**, 585.
Seren, L., Friedlander, H. N., and Turkel, S. H., 1947, *Phys. Rev.*, **72**, 888.

LETTERS TO THE EDITOR

The Radioactivity of Fluorine 20

The beta and gamma radiation emitted by ^{20}F (half-life 12 seconds) has been studied by absorption, coincidence and spectrometer techniques. Previous work (Fowler, Delsasso and Lauritsen 1936, Bower and Burcham 1939, Curran and Strothers 1940) on this element led to the decay scheme shown in Figure 1 (*a*), in which a gamma-ray of energy 2·2 Mev. follows a simple beta-particle spectrum with an upper limit of 5·1 Mev., giving a total disintegration energy of 7·3 Mev.

The ^{20}F was produced by the ^{19}F(dp)^{20}F reaction, the deuteron beam being interrupted periodically to give convenient counting periods. The upper limit of the beta-particle spectrum was found to be 5·03 ± 0·05 Mev. by the spectrometer and 4·96 ± 0·08 Mev. by absorption in aluminium. Gamma-rays of 1·64 ± 0·05 Mev. and 2·45 ± 0·06 Mev. with an intensity ratio of (8·4 ± 2·6) to 1 were found by absorption of their secondary electrons in aluminium; the energy of the more intense radiation was also measured with the spectrometer and found to be 1·64 ± 0·02 Mev. No gamma-ray of about 600 kev., such as would be required by the decay scheme of Figure 1 (*a*), could be found with an intensity comparable with that of the 1·64 Mev. radiation either by absorption or spectrometer techniques.

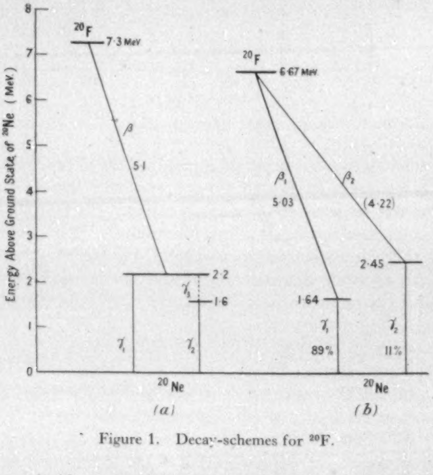

Figure 1. Decay-schemes for ^{20}F.

A beta-gamma coincidence experiment confirmed the earlier result (Curran and Strothers 1940) that the main beta-particle spectrum is linked with an excited state of ^{20}Ne. A quantitative gamma–gamma coincidence experiment gave a lower coincidence rate than required by the decay scheme of Figure 1 (*a*); the coincidences actually observed, after correcting for the chance rate, could have been due to bremsstrahlung.

These measurements suggest that the decay scheme of Figure 1 (*a*) should be replaced by that of Figure 1 (*b*). The total disintegration energy of 6·67 ± 0·05 Mev. leads to a mass of 20·00606 ± 0·00008 for ^{20}F, using the masses given by Rosenfeld (1948).

From an independent experiment on the energy release in the ^{19}F(dp)^{20}F reaction a mass of 20·00621 ± 0·00006 for ^{20}F was found, and the observations of Kinsey (private communication) on the energy of the capture gamma-radiation in the reaction ^{19}F(nγ)^{20}F give a mass of 20·00627 ± 0·00006. Both these values are based on a mass of 19·00444 ± 0·00004 for ^{19}F (Chao *et al.* 1949), which was deduced from recent measurements of the energy release in the reaction ^{19}F(pα)^{16}O* and the associated gamma-radiation; an average *Q*-value of 8·101 ± 0·030 Mev. was obtained for this reaction (Chao *et al.* 1949).

Cavendish Laboratory,
Cambridge.
Now at A.E.R.E. Harwell, Didcot, Berks.
9th February 1950.

J. V. JELLEY.

BOWER, J. C., and BURCHAM, W. E., 1939, *Proc. Roy .Soc.* A, **173**, 379.
CHAO, C. Y., TOLLESTRUP, A. V., FOWLER, W. A., and LAURITSEN, C. C., 1949, *Bull. Amer. Phys. Soc.*, **24**, No. 8, 11.
CURRAN, S. C., and STROTHERS, J. E., 1940, *Proc. Camb. Phil. Soc.*, **36**, 252.
FOWLER, W. A., DELSASSO, L. A., and LAURITSEN, C. C., 1936, *Phys. Rev.*, **49**, 561.
ROSENFELD, L., 1948, *Nuclear Forces* (Amsterdam : North-Holland Publishing Co.).

Proportional Counters in a Magnetic Field; an Investigation of the Nuclear Isomerism in ^{80}Br

Proportional counters have been used recently to measure low energy beta spectra and in other investigations of soft radiations (Curran, Angus and Cockcroft 1948, 1949, Kirkwood Pontecorvo and Hanna 1948, Hanna, Kirkwood and Pontecorvo 1949). It is obviously essential to the accuracy of these measurements that the great majority of electrons should spend all their energy in the counter. Angus *et al.* (1949) have used high gas pressures in a large diameter counter to reduce electron escape in their investigation of the spectrum of ^{14}C. Another method of reducing electron escape, which has not been investigated before, is to place the counter in a high magnetic field which coils up the electron track. The possibility that the multiplication properties of a proportional counter might be affected by the magnetic field could not be ignored, so the following experiment was performed to test this point. A small quantity of ^{37}A, whch decays by K-capture and gives an electron line at 2·8 kev., was placed inside a counter. The range of these electrons is very small, so there is virtually no escape from the counter, even without a magnetic field. The pulses from the counter were fed to a linear amplifier connected to a pulse analyser; pulse analyser runs were taken with the counter axis (*a*) parallel to, (*b*) perpendicular to, (*c*) outside a magnetic field of 7,500 gauss. The distributions obtained in these three cases were identical showing that this magnetic field has no effect on the counter multiplication. There are therefore no objections to the method on these grounds.

The possibilities of the magnetic field technique in reducing escape can be appreciated by inspection of Table 1, in which the radius of curvature ρ in a magnetic field of 7,500 gauss and the range in air of electrons are tabulated for various energies.

Table 1

Energy of electron (kev.)	50	100	500
Range in air at N.T.P. (cm.)	4	12	140
ρ in field of 7,500 gauss (cm.)	0·1	0·15	0·39

This method of reducing electron escape with a magnetic field has been tried out in an investigation of the isomerism of ^{80}Br which gives radiations of suitable energy.

It has already been established that ^{80}Br has a 4·4-hour isomer which decays into the 18 minute beta-active ground state with the emission of a 49 kev. gamma-ray and a 37 kev. gamma-ray in cascade (Grinberg and Roussinow 1940, Berthelot 1944). The 49 kev. gamma-ray is totally internally converted, the 37 kev. gamma-ray only partially. When a small quantity of ^{80}Br* (carrier free methyl-bromide (Glueckauf *et al.* 1949)) is introduced into the counter and the latter placed in a strong magnetic field, five distinct peaks in the pulse distribution would be expected at 37, 49, 62, 74 and 86 kev. The 49 and 37 kev. peaks are produced by the 49 kev. gamma-ray when the 37 kev. gamma-ray is unconverted and escapes from the counter. The vacancy left in the K-shell following internal conversion is filled in the case of the 49 kev. peak with emission of Auger electrons, in the case of the 37 kev. peak with emission of a 12 kev. bromine K x-ray, which escapes from the counter (so that only $49-12=37$ kev. are spent in the counter). The remaining three peaks are produced when both gamma-rays are internally converted; since they are emitted in cascade, their energies are added, and peaks are produced at $(49+37)=86$ kev., at $(49-12+37)$ and $(49+37-12)=74$ kev. and at $(49-12+37-12)=62$ kev.

The five peaks were in fact observed. Figure 1 shows the pulse distribution from ^{80}Br* measured with a five-channel pulse analyser (Cooke-Yarborough *et al.* 1950), curve A with the counter axis placed parallel to a magnetic field of 7,000 gauss, curve B without the magnetic field. These curves show very clearly the effect the magnetic field has in reducing electron escape. Curve C is the background distribution discussed below. The counter used was a 'Maze-type' proportional counter (Maze 1946), diameter 5 cm., active length 34 cm. filled to about 30 cm. pressure with a mixture of argon and carbon dioxide (9 parts to 1). It was calibrated with 20·2 kev. x-rays from a ^{103}Pd source, described in another publication (Rothwell and West 1950).

Figure 2 shows the pulse distribution from ^{80}Br* in presence of the magnetic field, in the same counter filled with krypton and CO_2 (66·5 cm. pressure of Kr, 4 cm. pressure of CO_2). The escape probability of the 12 kev. bromine K x-ray is 99% in the argon counter but only 45% in the krypton counter; it can be seen that the relative intensities of all the K-escape peaks (at 37, 62 and 74 kev.) have been reduced in this case.

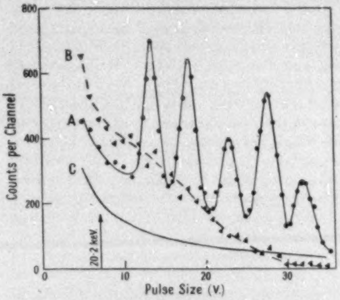

Figure 1. Pulse size distribution from ^{80}Br* in an argon filled counter.

Curve A: pulse distribution with counter in magnetic field of 7,000 gauss.

Curve B: pulse distribution without magnetic field.

Curve C: background from ^{82}Br (corrected for decay) in magnetic field of 7,000 gauss.

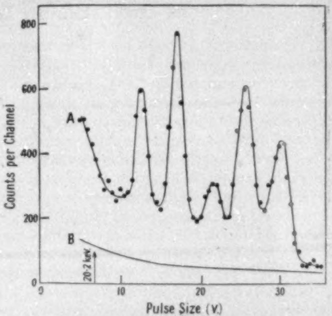

Figure 2. Pulse size distribution from ^{80}Br* in a krypton filled counter.

Curve A: pulse size distribution with counter in magnetic field of 7,000 gauss.

Curve B: background from ^{82}Br (corrected for decay).

It is possible to calculate the conversion coefficient of the 37 kev. gamma-ray from measurements of the relative intensities of the five peaks. The 49 kev. gamma-ray is totally converted (a point verified by the absence of a peak at $37-12=25$ kev.) so the conversion coefficient of the 37 kev. gamma ray is

$$\alpha_{37}=\frac{\text{Number of converted 37 kev. gamma-rays}}{\text{Number of unconverted 37 kev. gamma-rays}}=\frac{I_{62}+I_{74}+I_{86}}{I_{37}+I_{49}},$$

where I_{62} represents the intensity in the 62 kev. peak, etc.

Values of the conversion coefficient of the 37 kev. gamma-ray obtained in this way are given in Table 2 for various runs obtained with several different counter fillings and bromine samples.

The main source of error in these determinations arises from the background, which is composed partly of 34 hr. ^{82}Br which can be measured when the 4·4 hr. activity has decayed, and partly of the 18 min. ^{80}Br in equilibrium with the 4·4 hr. activity, which cannot be separated from it. Curve C, Figure 1, represents the 34 hr. background, corrected for decay. The conversion coefficients were evaluated : (i) taking a curve close to C as the background, (ii) taking a curve drawn close to the troughs between the peaks as the background.

There is a difference of about 14% between these two extreme values, and it is the mean which has been tabulated in each case in Table 1.

Berthelot, by coincidence absorption measurements, has obtained a value of 0·64 for the conversion coefficient of the 37 kev. gamma, and concludes that it is a magnetic dipole conversion. Segrè suggests from parity considerations that the transition is more likely to be electric dipole. The calculated conversion coefficients (Hebb and Nelson 1940) in these two cases are 0·60 (magnetic dipole) or 1·55 (electric dipole).

Table 2

	(1)	(2)	(3)	(4)	(5)	
Counter filling	A+CO_2	A+CO_2	A+CO_2	A+CO_2	Kr+CO_2	
Conversion coefficient	1·3	1·1	1·2	1·4	1·4	(average : 1·3)

Our value of 1·3 for the conversion coefficient proves that the transition is electric dipole rather than magnetic dipole.

We are grateful to Dr. B. Pontecorvo for valuable advice and assistance in this problem, and to Drs. W. D. Allen and R. H. V. M. Dawton for the use of a large electromagnet. The work was done in the Nuclear Physics Division at Harwell, and acknowledgment is made to Sir John Cockcroft, Director, A.E.R.E., for permission to publish these results.

Atomic Energy Research Establishment,
Harwell, Didcot, Berks.
10th February 1950.

P. Rothwell.
D. West.

Angus, J., Cockcroft, A. L., and Curran, S. C., 1949, *Phil. Mag.*, **40,** 522.
Berthelot, A., 1944, *Ann. Phys., Paris*, **19,** 219.
Cooke-Yarborough, E. H., Florida, C. D., Bradwell, J., and Howells, G. A., 1950, *J. Instn. Elect. Engrs.*, March issue.
Curran, S. C., Angus, J., and Cockcroft, A. L., 1948, *Nature, Lond.*, **162,** 302; 1949, *Phil. Mag.*, **40,** 36, 53, 305, 929.
Glueckauf, E., Jacobi, R. B., and Kitt, G. P., 1950, *J. Chem. Soc.*, Supplementary issue.
Grinberg, A. P., and Roussinow, L. I., 1940, *Phys. Rev.*, **58,** 181.
Hanna, G. C., Kirkwood, D. H. W., and Pontecorvo, B., 1949, *Phys. Rev.*, **75,** 985.
Hanna, G. C., and Pontecorvo, B., 1949, *Phys. Rev.*, **75,** 983.
Hebb, M. H., and Nelson, E., 1940 , *Phys. Rev.*, **58,** 486.
Kirkwood, D. H. W., Pontecorvo, B., and Hanna, G. C., 1948, *Phys. Rev.*, **74,** 497.
Maze, R., 1946, *J. Phys. Radium*, **6,** 164.
Pontecorvo, B., Kirkwood, D. H. W., and Hanna, G. C., 1949, *Phys. Rev.*, **75,** 982.
Rothwell, P., and West, D., 1950, *Proc. Phys. Soc.* A, **63,** 541.
Segrè, E., and Helmholz, A. C., 1949, *Rev. Mod. Phys.*, **21,** 271.

The Calibration of Proportional Counters with X-rays Produced by Radioactive Sources

In recent work (Kirkwood, Pontecorvo and Hanna 1948, Curran, Angus and Cockcroft 1948), the energy calibration of proportional counters has usually been carried out with x-rays from an x-ray tube. However, the size and the cost of an x-ray tube are often a disadvantage, particularly for use in mountain cosmic-ray laboratories and for work with magnetic fields similar to that described in another letter (Rothwell and West 1950). Alternative sources of x-rays which are cheap, compact, easily transportable and simple to use have been made from (*a*) long-lived radioactive isotopes which decay by K capture, and (*b*) thin foils bombarded with α-particles. Kirkwood *et al.* (1948) have used ^{37}A for calibration purposes, and Maeder (private communication) has used ^{55}Fe, but these are the only cases reported so far. A systematic investigation of these alternative sources has been carried out and is reported here.

(*a*) There are many long-lived K capture bodies among the unstable isotopes, but only those which can be prepared relatively free from long period β-activities are likely to be useful for calibration purposes. The K capture bodies listed in the Table were prepared by thermal neutron irradiation in the Harwell pile. Specific activities of a few in c/gm. were used.

Isotope	Half-period	Energy of K_α x-ray (kev.)	Isotope	Half-period	Energy of K_α x-ray (kev.)
$^{51}_{24}$Cr	26·5 days	5·0	$^{103}_{46}$Pd	17 days	20·2
$^{65}_{30}$Zn	250 days	8·1	$^{113}_{50}$Sn	105 days	24·2
$^{75}_{34}$Se	127 days	10·5	$^{169}_{70}$Yb	33 days	50·8

With the exception of ^{113}Sn they are all produced practically free from long period β-activity. In most cases a thin source was prepared by dissolving the irradiated element in acid and then evaporating a drop of solution on a mica foil. It was essential to use thin sources, otherwise the x-rays, which emerge only from a thin surface layer, are masked by the γ-rays from the body of the source which accompany the K-capture process. The sources were placed in contact with a thin window in the wall of a proportional counter containing argon and carbon dioxide. The counter pulses were amplified in a linear amplifier the output of which was fed into a pulse analyser. In Figure 1, curve A is the pulse analyser distribution obtained with a ^{65}Zn source and curve B is the distribution in the presence of a critical absorber (0·0005 in. nickel) which removes the K_β radiation. Since the K_β radiation is unresolved, however, the effect of the critical absorber is to reduce the width of the distribution slightly. The small peak on the left of the main peak is due to the escape of the K radiation of argon (2·9 kev.) from the counter. It is apparent from Figure 1 that ^{65}Zn gives an intense peak, free from background, which is very suitable for calibration. Similar distributions were obtained from ^{51}Cr and ^{75}Se. The energies of the radiations are given in the Table.

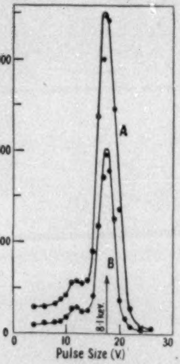

Figure 1. X-rays from ^{65}Zn source.
Curve A: without absorber.
Curve B: with critical absorber (0·0005″ nickel).

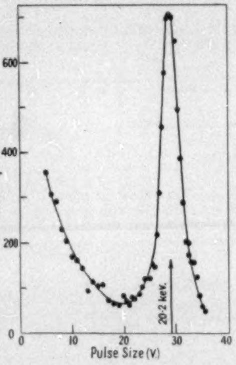

Figure 2. X-rays from ^{103}Pd source.

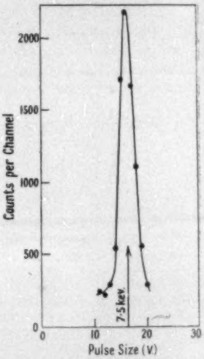

Figure 3. X-rays from nickel bombarded with polonium α-particles.

The distribution from ^{103}Pd is shown in Figure 2. The background is greater than in Figure 1 since there is a conversion electron from the isomeric transition in the daughter nucleus ^{103}Rh which can penetrate the counter window.

^{113}Sn gives a distribution similar to that from ^{103}Pd but with more background, due in this case to high energy β-rays.

^{169}Yb gives a distribution similar to that from ^{103}Pd. The probability of escape from the counter of the photoelectrons generated by the x-rays was small in all cases mentioned above.

Other possible isotopes which can be prepared by neutron irradiation are $^{71}_{32}$Ge and $^{153}_{64}$Gd.

(*b*) A second method of obtaining a convenient x-ray source depends upon the observation (see for example Curie and Joliot 1931) that characteristic x-radiation is emitted when α-particles are brought to rest in matter. These x-rays arise from direct ionization of K, L, M, etc. electrons during the slowing down of the α-particles.

Figure 3 shows the pulse distribution obtained by bombarding a nickel foil (0·0005 in. thick) with α-particles from 1 millicurie of polonium. The peak is at an energy equal to that of the K radiation of Ni (7·5 kev.). The intensity is sufficient for calibration purposes and the distribution is comparatively free from background. There is, however, a limit to the x-ray energy which can be excited by polonium α-particles. Simple considerations of conservation of momentum, taking account of the motion of the K electrons, sets this limit at an x-ray energy of about 14 kev. In fact, the most energetic x-rays that have been obtained in this way have an energy of about 12 kev. These come directly from the polonium source and are probably the L rays of either $_{82}$Pb or $_{84}$Po.

The production of x-rays by bombardment with β-particles was also tried but, except in the case of low energy x-rays, the results were unsatisfactory due to the presence of the continuous x-ray spectrum.

Atomic Energy Research Establishment,
Harwell, Didcot, Berks.
10th February 1950.

P. Rothwell.
D. West.

Curie, I., and Joliot, F., 1931, *J. Phys. Radium*, **2**, 20.
Curran, S. C., Angus, J., and Cockcroft, A. L., 1948, *Nature, Lond.*, **162**, 302.
Kirkwood, D. H. W., Pontecorvo, B., and Hanna, G. C., 1948, *Phys. Rev* **74**, 497.
Rothwell, P., and West, D., 1950, *Proc. Phys. Soc.* A, **63**, 539.

He_2^+ in the Helium Discharge

In a recent note on Biondi and Brown's (1949) measurement of recombination and mobility using a decaying R.F. discharge in helium, Bates (1950) has pointed out that the reaction

$$He^+ + 2He \rightarrow He_2^+ + He$$

should be responsible for populating the discharge almost entirely with the molecular ion, so that the measurements would refer to a dissociative recombination process and the mobility of He_2^+.

It has also been suggested by Meyerott (1944) that the discrepancy between Tyndall and Powell's (1931) value of the mobility of helium positive ions in helium and Massey and Mohr's (1934) calculated value (in which the effect of charge exchange is included) is due to the fact that the positive ions from the glow discharge employed by Tyndall and Powell were probably He_2^+. (If He^+ were present to the extent of 10% the curves should have revealed it.)

It is therefore of interest to determine experimentally the concentration ratio He_2^+/He^+ in the discharge in helium. The R.F. mass spectrometer probe (Boyd 1950) is particularly suitable in view of the short path length in the analyser (3 cm.). Since it is desired to make a study up to pressures as high as possible, a short path length is essential if attenuation of the He^+ beam by the reaction $He^+ + He \rightarrow He + He^+$ is to be kept small.

In the Table are given some preliminary measurements carried out on a hot (tungsten) cathode discharge 7 cm. in diameter. The probe was in the centre of the discharge distant 15 cm. from the anode and 20 cm. from the cathode. Even at these low pressures the molecular ion is predominant.

	Pressure (mm. Hg)	Discharge current (ma.)	He_2^+/He^+
Effect of pressure	0·047	100	4·7
	0·016	100	3·4
	0·006	100	2·7
	0·006	200	3·3*
Effect of current	0·016	20	2·3
	0·016	100	3·4
	0·016	200	[4·1]

The figure in brackets was obtained by extrapolation from the starred result.

The tendency of the ratio to increase with pressure shows that even at these pressures the three-body reaction is important and suggests that at the pressures used by Biondi and Brown and by Tyndall and Powell the ratio would be very large.

The reaction $He' + He \rightarrow He_2^+ + e$, where He′ denotes a helium atom in the (19·77 volt) metastable state, is also possible (Arnot and McEwen 1939) and may account for the lack of a more rapid rise with pressure. The increase in the collision rate as the gas temperature rises may account for the increase of the ratio with tube current. A comparison of helium with argon is of interest as no trace of a molecular ion of argon has been found in the course of work with the spectrometer probe.

R. L. F. Boyd,
I.C.I. Research Fellow.

Department of Mathematics,
University College, London.
27th February 1950.

Arnot, F. L., and McEwen, M. B., 1939, *Proc. Roy. Soc.* A, **171,** 106.
Bates, D. R., 1950, *Phys. Rev.*, **77,** in the press.
Biondi, M. A., and Brown, S. C., 1949, *Phys. Rev.*, **75,** 1700.
Boyd, R. L. F., 1950, *Nature, Lond.*, **165,** 142.
Massey, H. S. W., and Mohr, C. B. O., 1934, *Proc. Roy. Soc.* A, **144,** 188.
Meyerott, R., 1944, *Phys. Rev.*, **66,** 242.
Tyndall, A. M., and Powell, C. F., 1931, *Proc. Roy. Soc.* A, **134,** 125.

Bands of ZrF

The only compounds of zirconium for which a band system has so far been reported is ZrO. Among the compounds of the analogous element titanium, band systems due to TiCl and TiO have already been analysed. It is likely that the band systems due to TiCl and ZrF will be of the same type. Further, since zirconium occurs abundantly in stellar atmospheres, it seems possible that ZrF may also occur in these atmospheres in sufficient quantities to cause absorption. For this reason a study of the bands of ZrF has been made.

ZrF bands were observed from an ordinary low voltage arc with copper electrodes; the lower one had been shaped into a cylindrical cup supported on a neck (diameter approximately 1 mm.) to conserve heat. This was made the anode, and the anode cup filled with ZrF_4 (with impurities of KF and H_2O). The current was carefully maintained at a value where the temperature in the anode cup was sufficient only to melt ZrF_4 and not ignite it, for if the temperature rose above the oxidizing temperature of ZrF_4, rapid oxidation set in. Vapour of zirconium fluoride rising above the anode cup emitted bands considered to be ZrF, and these were photographed on a large Littrow spectrograph.

An attempt was made without success to vaporize and excite ZrF in a constricted quartz capillary of a high current discharge tube of the type used by Pearse and Gaydon (Pearse and Gaydon 1938). It appeared that ZrF_4 attacked quartz, for although bands due to SiF and SiO were manifestly strong, no trace of ZrF bands could be observed.

The following table gives the wavelengths of the band heads of ZrF thus observed. All these bands degrade towards the longer wavelength.

λ_{air}	I	ν_{vac}	λ_{air}	I	ν_{vac}
4897·25	0	20414·0	4926·88	4	20291·2
4897·88	0	20411·3	4932·11	5	20269·6
4899·24	0	20405·7	4933·38	4	20264·5
4906·18	2	20376·8	4933·95	4	20262·1
4911·37	2	20355·2	5026·15	0	19890·4*
4914·76	2	20341·2	5034·16	0	19858·8*
4916·33	3	20334·7	5044·08	1	19819·7
4920·22	2	20318·6	5052·27	2	19787·6
4921·58	5	20313·0	5061·18	3	19752·8

* Doubtful.

As will be evident from the record of the band heads of ZrF, it is difficult to find any simple relationship between them. It is even difficult to conclude whether any band heads other than those belonging to the (0, 0) band of the system have been recorded. The spectrum of ZrF should be of the same type as that of TiCl. The latter has been analysed by Parker and More (1937), who found six heads to each main band. This suggests that quite as complicated a spectrum should be expected for ZrF. It had further been suggested by Parker and More, that of the six band heads, only two formed in the main P_1 or P_2, branches, and the rest were either in Q or satellite branches. To support this hypothesis they postulated that the system involved a transition of the type $^2\Pi-{}^2\Delta$ or $^2\Delta-{}^2\Phi$. In the author's opinion, however, quartet states are more likely to be involved than doublets, since one would expect that the ground state of these molecules will be of quartet multiplicity. Let us suppose that in the formation of the molecule of ZrF one of the $(5s)^2$ electrons of the zirconium atom completes the outer shell of the fluorine atom. A zirconium atom deprived of one of its $(5s)^2$ electrons would resemble a singly ionized atom of zirconium, Zr^+, which is in a ^4F state. This shows that in ZrF, the total spin momentum

$$S=S_{\mathrm{Zr}}=3/2,$$

and therefore

$$\Sigma_{\mathrm{ZrF}}=S,\,(S-1),\,\ldots=3/2,\,1/2.$$

The combination of a zirconium and a fluorine atom in their ground states should give rise to both quartet and doublet states, but of these the quartet should lie the deeper, because of the assumed correspondence between the ground states of the molecule of ZrF and the singly ionized atom of zirconium.

The supposition, therefore, that quartet levels are involved in the band system of ZrF also provides some explanation of the complex structure of such spectra. For, if a transition of the type $^4\Pi-{}^4\Delta$ is supposed to be involved in this system, one would expect four strong Q heads, four strong R heads, and many weaker heads in satellite branches. This would certainly complicate the band structure, and make the analysis difficult unless several bands belonging to the same system, could be observed.

The author expresses his deep gratitude to Professor R. W. B. Pearse for valuable guidance throughout this work.

M. Afaf.

Department of Physics,
Imperial College of Science and Technology,
London, S.W.7.
8th February 1950.

Parker, A. H., and More, K. R., 1937, *Phys. Rev.*, **52,** 1150.
Pearse, R. W. B., and Gaydon, A. G., 1938, *Proc. Phys. Soc.*, **50,** 201.

CONTENTS FOR SECTION B

PAGE

Mr. G. **Bradfield.** Summarized Proceedings of Symposium on Applications of Ultrasonics 305

Mr. A. C. **Lynch.** Measurement of the Equivalent Electrical Circuit of a Piezoelectric Crystal 323

Dr. S. **Harper** and Prof. A. H. **Cottrell.** Surface Effects and the Plasticity of Zinc Crystals 331

Mr. H. L. **Wain** and Prof. A. H. **Cottrell.** Yield Points in Zinc Crystals . 339

Mr. L. M. T. **Hopkin.** A Simple Constant Stress Apparatus for Creep Testing. 346

Dr. G. L. J. **Bailey** and Mr. H. C. **Watkins.** Surface Tensions in the System Solid Copper–Molten Lead 350

Dr. K. M. **Greenland** and Mr. C. **Billington.** The Construction of Interference Filters for the Transmission of Light of Specified Wavelengths 359

Mr. D. R. **Barber.** Note on the Brightness Profile and Photometric Contrast of a Test-object having small Angular Dimensions and Silhouetted against the Twilight Sky 364

Letters to the Editor:

Dr. R. F. **Saxe** and Dr. J. B. **Higham.** The Measurement of Spark Channel Diameters 370

Mr. H. A. **Gebbie,** Mr. P. C. **Banbury** and Dr. C. A. **Hogarth.** Crystal Diode and Triode Action in Lead Sulphide 371

Reviews of Books 372

Contents for Section A 373

Abstracts for Section A 374

ABSTRACTS FOR SECTION B

Summarized Proceedings of Symposium on Applications of Ultrasonics, by G. **Bradfield.**

ABSTRACT. A symposium of the Acoustics Group of the Physical Society, held on 18th February 1949, surveyed recent advances in (*a*) the investigation of the fundamental structure of matter; (*b*) telecommunication and allied applications; (*c*) use of mechanical forces set up by intense waves.

In (*a*) derivation of elastic constants of matter was an important field especially as small samples such as single crystals could be used. Losses incurred in propagating waves were surveyed with the help of an electrical transmission line model and simple versions of this were established to represent relaxation phenomena based on Maxwell's hypothesis of shear elasticity as a time function and on Kneser's treatment of loss due to delay in a storage process. There was excellent agreement of the latter with recent results on acetic acid.

Available sources of ultrasonic power were surveyed and the importance of barium titanate as a powerful and strongly coupled piezoelectric transducer was emphasized.

An expression for the receiver/transmitter power ratio in telecommunications systems was examined for gaseous, liquid and solid media and, from available data, optimum frequencies for various ranges were deduced. These were found to be in accord with experience in echo-sounding, earth exploration and in propagation in metals.

Accounts were given of experience with flaw detectors and echo-sounding which showed that these were becoming important industrially and in navigation; work on blind aids was unpromising. Advances in timing and time delay devices were described.

There is a dearth of important industrial applications of the use of intense waves in spite of the interesting phenomena which have been demonstrated in the laboratory. The importance of the study of cavitation was pointed out. Results were discussed for killing

bacteria, disintegrating proteins, emulsifying, soldering aluminium and refining the crystalline structure in solidification of light alloys. Stress was laid on the wideness of the frequency spectrum over which these phenomena occurred and on the difficulties and importance of maintaining temperature constant and of measuring intensities during investigations.

Measurement of the Equivalent Electrical Circuit of a Piezoelectric Crystal, by A. C. LYNCH.

ABSTRACT. A new method for measuring the reactances in the circuit requires measurements of equivalent capacitance at several frequencies around that of resonance, preferably differing from the resonance frequency by from ½ to 5% ; the accuracy is unaffected by capacitance in parallel with that of the specimen. The measurements can be made with a suitably screened substitution Schering bridge ; it should be suitable for frequencies between about 50 and 600 kc/s., and the only unusual component needed for it is a variable condenser which can be read to 0·001 pF. If there are no unwanted modes of vibration, the equivalent circuit can be measured to within 0·1%.

The piezoelectric coefficient d is sometimes calculable from the equivalent circuit and the dimensions of the crystal, but there are difficulties which limit the accuracy of d to about ½%. Results obtained include, for example, d_{11} for quartz at 20° C. $=6{\cdot}9_5\times 10^8$ cm/E.S.U. of potential.

Surface Effects and the Plasticity of Zinc Crystals, by S. HARPER and A. H. COTTRELL.

ABSTRACT. The effects of various surface treatments on the plastic properties of zinc crystals are examined. Roscoe's observation of the hardening effect of a surface film of oxide is confirmed ; electrolytically polished specimens have critical shear stresses of about 33 gm.mm^{-2} whereas oxidized specimens have values up to 65 gm.mm^{-2}. Similar effects are observed on the rate of creep under constant stress. The Rehbinder effect—softening crystals by immersing them in paraffin and oleic acid—can be produced on oxidized specimens but not on others. Oxidized specimens do not respond instantly to immersion and the time of response is proportional to the viscosity of the liquid. It is suggested that the liquid penetrates the oxide film and reduces its ability to harden the metal; the action of the oxide film itself is not yet clear.

Yield Points in Zinc Crystals, by H. L. WAIN and A. H. COTTRELL.

ABSTRACT. It is shown that sharp yield points can be produced in crystals of zinc containing nitrogen. The gas is introduced in a preliminary melting operation, either by bubbling it through the metal or by allowing it to be absorbed from the atmosphere, using a flux to keep the surface clean. Strain ageing treatments are needed to develop the yield point clearly, but once it is developed it returns at the same level after each successive treatment at the same temperature. Ageing experiments at room temperature show that overstrained zinc crystals soften by recovery before the yield point returns; zinc differs from iron in this respect. General conditions for producing yield points in metals of common crystal structures are briefly discussed.

A Simple Constant Stress Apparatus for Creep Testing, by L. M. T. HOPKIN.

ABSTRACT. A simple device is described which can maintain the stress on a creep specimen constant to within 0·8% during uniform extensions up to 100%. The apparatus is suitable for slow rates of strain. Examples are given of creep curves obtained with this device from tests on lead and a lead–tin alloy extending to 1,000 and 400 hours respectively; good agreement with the Andrade creep equation is observed in both cases.

Surface Tensions in the System Solid Copper–Molten Lead, by G. L. J. Bailey and H. C. Watkins.

ABSTRACT. A method is described by which the surface tension of surfaces occurring in the systems copper–hydrogen or argon and copper–lead–hydrogen or argon is determined. At temperatures round 850° c., the surface tension between copper grains is 640 dyne/cm. and between copper and the equilibrium lead–copper liquid phase 340 dyne/cm. The surface tension of a copper–gas surface is the same whether the gas is hydrogen or argon, within the limits of precision of the experiment, and has the value 1,800 dyne/cm. When lead vapour is present in the gas atmosphere at a partial pressure of the order of 0·1 mm. Hg the surface tension of the copper–gas surface has the much lower value of 780 dyne/cm. It is suggested that the reduction is due to the adsorption of lead at the copper–gas surface. The failure of the liquid phase to exhibit a contact angle of zero against solid copper surfaces is thereby understood.

The Construction of Interference Filters for the Transmission of Light of Specified Wavelengths, by K. M. Greenland and C. Billington.

ABSTRACT. Optical interference filters are composed of thin films deposited on a glass base by volatilization in a high vacuum. The narrowness of the transmission bands characteristic of these filters demands a high degree of accuracy in the regulation of the thickness of the films if maximum transmission is to occur at a specified wavelength. A method of observing the optical thickness of transparent films during deposition is described, and it is concluded that its accuracy is sufficient, for instance, to enable the centre of a fourth-order transmission band to be placed within 20 A. of any wavelength in the visible spectrum.

Note on the Brightness Profile and Photometric Contrast of a Test-object having small Angular Dimensions and Silhouetted against the Twilight Sky, by D. R. Barber.

ABSTRACT. Microphotometry of photographs of distant objects with small angular subtense has shown that inaccurate results are obtained if the apparent contrast is calculated on the assumption of uniform sky brightness. No evidence was found of any edge effect due to inward small angle scatter.